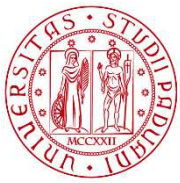

UNIVERSITÀ
DEGLI STUDI
DI PADOVA

Università degli Studi di Padova

Dipartimento di Scienze Biomediche

CORSO DI DOTTORATO DI RICERCA IN
SCIENZE BIOMEDICHE SPERIMENTALI

CICLO XXX

Role and regulation of the mitochondrial calcium uniporter (MCU) in cardiac adaptation to stresses

Tesi redatta con il contributo finanziario di Fondazione Cariparo

Coordinatore: Ch.mo Prof. Paolo Bernardi

Supervisore: Ch.mo Prof. Marco Mongillo

Co-Supervisore: Ch.ma Dott.ssa Tania Zaglia

Dottorando: Antonio Campo

Table of contents

ABBREVIATIONS

AAV	**A**deno-**a**ssociated **v**irus
Ab	**A**nti**b**ody
ACE	**A**ngiotensin **c**onverting **e**nzyme
Ad	**Ad**eno
ADP	**A**denosine 1,5, **di**ph**o**sphate
ANP	**A**trial **n**atriuretic **p**eptide
ANT	**A**denine **n**ucleotide **t**ranslocase
AP	**A**ction **p**otential
AR	**A**drenergic **r**eceptor
AR	**A**spect **r**atio
AT-1	**A**ngio**t**ensin II receptor **1**
ATII	**A**ngio**t**ensin **II**
ATP	**A**denosine1,4,5, **t**ris**p**hosphate
AV	**A**trio**v**entricular
BAPTA	1,2-**b**is(o-**a**mino**p**henoxy)ethane-N,N,N′,N′-**t**etra**a**cetic acid
BND	**B**uta**n**e**d**ione
BNP	**B**-type **n**atriuretic **p**eptide
BrdU	5-**Br**omo-2'-**d**eoxy**u**ridine
BSA	**B**ovine **s**erum **a**lbumin
CaM	**Ca**l**m**odulin
CaMKII	**Ca**$^{2+}$/cal**m**odulin-dependent protein **K**inase **II**
CFP	**C**yan **f**luorescent **p**rotein
CICR	**C**alcium-**i**nduced-**c**alcium **r**elease
CLB	**Cl**en**b**uterol
CM	**C**ardio**m**yocyte
CMV	**C**yto**m**egalo**v**irus
CPT-1	**C**arnitine **p**almytil **t**ransferase **1**
CPV	**C**ircularly **p**ermuted **v**enus
CRU	**C**alcium **r**elease **u**nit
CS	**C**ross **s**ectional

CsA	**C**yclo**s**porin **A**
CsH	**C**yclo**s**porin **H**
CTRL	**C**on**tr**o**l**
DAC	**D**ystrophin-**a**ssociated proteins **c**omplex
DAPI	4,6-**di**a**a**minidino-2-**p**heny**l**indole
DMEM	**D**ulbecco's **m**odified **e**agle **m**edium
DN	**D**ominant **n**egative
dNTP	**D**eoxy**n**ucleotide **t**ri-**p**hosphate
DTT	**D**i**t**hio**t**hreitol
ECC	**E**xcitation **c**ontraction **c**oupling
ECFP	**E**nhanced **c**yan **f**luorescent **p**rotein
ECG	**E**lectro**c**ardio**g**ram
ECM	**E**xtra**c**ellular **m**atrix
EDTA	**E**thilene**d**iamine**t**etra**a**cetic acid
EF	**E**jection **f**raction
EGFP	**E**nhanced **g**reen **f**luorescent **p**rotein
EGTA	**E**thylene **g**lycol **t**etra**a**cetic acid
EMRE	**E**ssential **M**CU **re**gulator
ER	**E**ndoplasmic **r**eticulum
ET-1	**E**ndothelin-**1**
FBS	**F**etal **b**ovine **s**erum
FCCP	**C**arbonyl **c**yanide-p-tri**f**luoromethoxy**p**henylhydrazone
FDM	**F**irst **d**ay **m**edium
FOXO	**Fo**rkhead bo**x** **O**
FPS	**F**rames **p**er **s**econd
FRET	**F**örster **r**esonance **e**nergy **t**ransfer
FS	**F**ractional **s**hortening
GC	**G**enome **c**opies
GECI	**G**enetically **e**ncoded **C**a^{2+} **i**ndicator
GFP	**G**reen **f**luorescent **p**rotein
GPCR	**G**-**p**rotein **c**oupled **r**eceptor
GRK2	**G** protein-coupled **r**eceptor **k**inase **2**
GSH	**G**lutathione (reduced form)

GSK3β	**G**lycogen **s**ynthase **k**inase **3β**
GSSG	**G**lutathione disulphide (oxidized form)
HBSS	**H**ank's **b**alanced **s**alt **s**olution
HE	**H**aematoxylin/**e**osin
HF	**H**eart **f**ailure
HRP	**H**orse **r**adish **p**eroxidase
HS	**H**orse **s**erum
HW/BW	**H**eart **w**eight/**b**ody **w**eight
I/R	**I**schemia/**r**eperfusion
ICEU	**I**ntracellular **e**nergy **u**nit
IF	**I**mmuno**f**luorescence
IMM	**I**nner **m**itochondrial **m**embrane
IMS	**I**nter **m**embrane **s**pace
IP	**I**ntra**p**eritoneal
IP3R	**I**nositol **tri**s**p**hosphate **r**eceptor
ITS	**I**nsulin **t**ransferrin **s**elenium
IV	**I**ntra**v**enous
IVS	**I**nter **v**entricular **s**eptum
JNK	C-**J**un **N**-terminal **k**inases
KD	**K**nock-**d**own
KO	**K**nock-**o**ut
LA	**L**eft **a**trium
LAD	**L**eft **a**nterior **d**escending (coronary artery)
lncRNA	**L**ong **n**on-**c**oding **RNA**
LTCC	**L**-**t**ype **c**alcium **c**hannel
LV	**L**eft **v**entricle
LVAD	**L**eft **v**entricle **a**ssist **d**evice
LVDV	**L**eft **v**entricle **d**iastolic **v**olume
LVID	**L**eft **v**entricle **i**nternal **d**iameter
LVPW	**L**eft **v**entricle **p**osterior **w**all
MAPK	**M**itogen-**a**ctivated **p**rotein **k**inase
MCU	**M**itochondrial **C**a^{2+} **u**niporter
MCUb	**M**itochondrial **C**a^{2+} **u**niporter **b**

MCUC	**MCU** **c**omplex
MCUR1	**M**itochondrial **C**a^{2+} **u**niporter **r**egulator **1**
MDR	**M**ulti **d**rug **r**esistance
Mef2	**M**yocyte **e**nhancer **f**actor-**2**
MEM	**M**inimal **e**ssential **m**edium
MHC	**M**yosin **h**eavy **c**hain
MI	**M**yocardial **i**nfarction
MICU1	**Mi**tochondrial **C**a^{2+} **u**ptake **1**
MICU2	**M**itochondrial **C**a^{2+} **u**ptake **2**
miR	**Mi**cro**R**NA
MOI	**M**ultiplicity **o**f **i**nfection
MOPS	4-**Mo**rpholine**p**ropane**s**ulfonic acid
MPTP	**M**itochondrial **p**ermeability **t**ransition **p**ore
NADH	Reduced **n**icotinamide **a**denine **d**inucleotide
NCM	**N**eonatal **c**ardiac **m**yocyte
NCS	**N**ewborn **c**alf **s**erum
NCX	**N**a^{+}/**C**a^{2+} e**x**changer
NE	**N**or**e**pinephrine
NEAA	**N**on **e**ssential **a**mino**a**cids
NFAT	**N**uclear **f**actor of **a**ctivated **T** cells
NF-Kb	**N**uclear **f**actor **k**appa-light-chain-enhancer of activated **B** cells
Nox-4	**N**ADPH **ox**idase **4**
O/N	**O**ver**n**ight
OCR	**O**xygen **c**onsumption **r**ate
OE	**O**ver**e**xpressing
OMM	**O**uter **m**itochondrial **m**embrane
OXPHOS	**Ox**idative **phos**phorylation
Pen/Strep	**Pen**icillin/**strep**tomycin
PBS	**P**hosphate **b**uffered **s**aline
PCR	**P**olymerase **c**hain **r**eaction
PCr	**P**hospho**cr**eatine
PDH	**P**yruvate **d**e**h**ydrogenase
PE	**P**henyl**e**phrine

PF	**P**urkinje **f**iber
PFA	**P**ara-**f**orm**a**ldehyde
PGC1α/β	**P**eroxisome proliferator-activated receptor **g**amma **c**o-activator 1-α/β
PI3K	**P**hospho**i**nositide **3**-**k**inase
PITA	**P**robability of **i**nteraction by **t**arget **a**ccessibility
PKA	**P**rotein **k**inase **A**
PKB	**P**rotein **k**inase **B**
PKC	**P**rotein **k**inase **C**
PLB	**P**hospho**l**am**b**an
PLC	**P**hospho**l**ipase **C**
PMCA	**P**lasma **m**embrane **C**a^{2+} **A**TPase
PTP	**P**ermeability **t**ransition **p**ore
PVDF	**P**oly**v**inyli**d**ene **f**luoride
RA	**R**ight **a**trium
RFP	**R**ed **f**luorescent **p**rotein
RNA	**R**ibo**n**ucleic **a**cid
ROI	**R**egion **o**f **i**nterest
ROS	**R**eactive **o**xygen **s**pecies
RT	**R**oom **t**emperature
RT-qPCR	**R**eal **t**ime **q**uantitative **PCR**
RV	**R**ight **v**entricle
RyR2	**Ry**anodine **r**eceptor **2**
SAN	**S**ino **a**trial **n**ode
SCF	**S**pontaneous **c**ontraction **f**requency
SDS	**S**odium **d**odecyl **s**ulphate
SEM	**S**tandard **e**rror of the **m**ean
SERCA	**S**arco-**e**ndoplasmic **r**eticulum **C**a^{2+} **A**TPase
shRNA	**S**hort **h**airpin **RNA**
SICM	**S**canning **i**on **c**onductance **m**icroscopy
SLC25a23	**S**o**l**ute **c**arrier **25a23**
SR	**S**arcoplasmic **r**eticulum
SRF	**S**erum **r**esponse **f**actor

TAC	**T**ransversal **a**ortic **c**onstriction
TBS	**T**ris **b**uffered **s**aline
TCA	**T**ri**c**arboxylic **a**cid cycle
TEM	**T**ransmission **e**lectron **m**icroscopy
TM	**T**rans**m**embrane
TMRM	**T**etra**m**ethyl**r**hodamine **m**ethyl ester
TN-C	Cardiac **t**ropo**n**in **C**
TNF-α	**T**umor **n**ecrosis **f**actor-**α**
TN-I	Cardiac **t**ropo**n**in **I**
TN-T	Cardiac **t**ropo**n**in **T**
TOM20	**T**ranslocase of **o**uter **m**embrane **20**
TTBS	**T**ween20-**t**ris **b**uffered **s**aline
UTR	**Un**t**r**anslated **r**egion
VDAC	**V**oltage-**d**ependent **a**nion **c**hannel
WB	**W**estern **b**lot
WGA	**W**heat **g**erm **a**gglutinin
WT	**W**ild **t**ype
YFP	**Y**ellow **f**luorescent **p**rotein
β- AR	**β**-**a**drenergic **r**eceptor

SUMMARY

Background.

From birth, throughout the entire lifespan, the myocardium is constituted by an almost fixed number of cardiomyocytes (CMs)[1]. Post-natal heart growth occurs through CM hypertrophy, and the cell achieves the adult phenotype through profound structural, functional and metabolic maturation. Once fully developed, the heart continuously adapts its performance and structure in response to the varying requests of the organism, elicited by changes in intrinsic and environmental conditions[2]. While acute stresses operate through reversible modulation of contractility, CMs subjected to prolonged increase in workload undergo complex structural remodelling, mostly occurring through further growth necessary to sustain the chronic elevation of mechanical load.

Depending on the nature, intensity and duration of the hypertrophying stimuli, cardiac remodelling may lead to either the so-called "physiologic" (i.e., in the athletic heart), or "pathologic" hypertrophy (i.e., in pressure overload), the latter resulting, with time, in cardiac dysfunction, heart failure (HF) and death. Although the cellular and clinical phenotypes of the two conditions are different, the common tenet is that, in the initial phases, they share the same adaptive mechanisms, including increased sarcomeric deposition and enhanced/preserved contractility, both of which require increased ATP supply[3]. Unsurprisingly, the regulation of mitochondrial function is a critical process for ATP production to match energetic demand during cell growth. Mitochondria are the CM powerhouse, and Ca^{2+} operates as a primary dynamic regulator of ATP production[4]. In CMs, Ca^{2+} influx into the mitochondrial matrix occurs during the systolic elevation in cytosolic Ca^{2+}, and is mediated by the recently identified mitochondrial Ca^{2+} uniporter complex (MCUC)[5,6]. Mitochondrial Ca^{2+} uptake is fundamental in the acute modulation of contractility during the fight-or-flight response triggered by β-adrenergic receptor (β-AR) activation. Consistently, deletion of MCU in mice impairs exercise capacity[7], and reduction of functioning MCU channels in sino-atrial node (SAN) cells or ventricular CMs, blunts the chronotropic or contractile response, respectively, to β-AR stimulation[8-11].

Whether changes in the expression of MCUC proteins take place during cardiac diseases and, conversely, the effect of modulating mitochondrial Ca^{2+} uptake on myocardial remodelling is, at present, not known.

Aims.

The aims of my PhD project were to:

Aim 1) identify the molecular mechanisms involved in the endogenous regulation of MCU;

Aim 2) determine whether MCU has a role in physiologic and pathologic cardiac remodelling;

Aim 3) develop an experimental model of cultured cardiomyocytes suited for the *in vitro* characterization of mitochondrial Ca^{2+} dynamics in prolonged observations.

Results.

1. Content of mitochondrial calcium uniporter (MCU) in cardiomyocytes is regulated by microRNA-1 in physiologic and pathologic hypertrophy.

In our preliminary experiments, we compared the protein levels of MCU in normal and hypertrophied hearts, and observed that changes in mitochondrial MCU protein density were not accompanied by parallel alteration in its transcriptional levels. This prompted us to investigate whether post-translational regulation of MCU might occur in myocardial remodelling. We thus focused on microRNAs (miRs), which are small, non-coding RNA sequences (18-25 nt) capable of finely tuning the expression of a variety of genes by interfering with either the stability or the translation of mRNA[12]. Growing evidence reveals the fundamental role of miRs in cardiac hypertrophy[13-19], and in other tissues, specific microRNAs have been shown to regulate MCU content.

We run a bioinformatics search using the probability of interaction by target accessibility (PITA) algorithm that identified several microRNAs predicted to target MCU 3'UTR (untranslated region). Among these, we focused on miR-1 for its muscle specific

expression, the critical role in the activation in cardiac hypertrophy[14,15], its conserved homology among species, and its specificity for MCU among MCUC members. Luciferase assay confirmed the prediction and identified the specific seed sequences on the MCU gene. Consistently, CMs expressing miR-1 showed decreased MCU protein content, with no alterations in mRNA expression, which resulted in significant reduction in mitochondrial Ca^{2+} uptake.

We thus investigated whether MCU content was modulated in hypertrophic conditions associated to changes in miR-1, including: i) post-natal development, ii) moderate exercise and iii) pressure overload.

By comparing neonatal and adult mouse hearts we observed that, in line with its role of repressor of fetal gene program, miR-1 expression increased during postnatal development and, coherently, MCU protein content decreased without alterations at transcriptional level. Moreover, this modulation was specific for MCU among the molecular components of MCUC, with the exceptions of mitochondrial calcium uniporter b (MCUb) mRNA, which increased.

We then investigated the miR-1/MCU axis, in murine and human heart models of physiologic and pathologic hypertrophy. Physiologic hypertrophy was obtained in mice with chronic exercise protocol, which caused enlargement in cardiac size, CM cross-sectional area, and a slight increase in contractility[20]. As compared to sedentary littermates, miR-1 expression level decreased and, consistently, MCU protein content increased.

Analysis of the uniporter complex biochemistry in hearts undergone pressure-overload through transverse aortic constriction (TAC) surgery demonstrated that during the initial, compensatory hypertrophy, characterized by modest CM growth with no contractile failure, changes in miR-1 and MCU were similar to those observed in hearts from exercised mice. Remarkably, the reciprocal miR-1 and MCU modulation occurred in a clinically relevant model of cardiac hypertrophy, as shown by the analysis of human heart biopsies obtained from healthy subjects and patients (age: 59 ± 13 years) with aortic stenosis-induced hypertrophy.

These results suggest that, regardless of the nature of the hypertrophic stimulus (physiologic or pathologic), the initial CM adaptation to increased heart work is

characterized by similar enhancement in the availability of uniporter-forming MCU molecules.

Given that similar changes in the miR1/MCU axis were detected both upon exercise and compensated pathologic hypertrophy, we made the hypothesis that a common regulatory mechanism may exist. We thus focused on the β-AR system, the primary physiologic mechanism engaged in response to increased heart load, a condition in common between exercise and TAC-induced pressure-overload. Activation of β-AR signalling leads to enhancement of cytosolic Ca^{2+} oscillations and mitochondrial Ca^{2+} uptake[21-23], and is involved in the parallel activation of hypertrophic pathways, such as the Akt-FOXO cascade[24]. Interestingly, miR-1 expression has been shown to depend on FOXO3a[25], suggesting that in conditions of chronic β-AR activation, the blockade of FOXO3a nuclear translocation may inhibit miR-1 increase. In support of this hypothesis, treatment of mice undergone TAC with the β1-blocker metoprolol ablated miR-1 repression and prevented accordingly the increase in MCU protein content.

Conclusions and future perspectives. Altogether, our data identifies miR-1 as a novel post-translational regulator of MCU, and supports that the miR-1/MCU axis is involved in physiologic and pathologic myocardial remodelling. Future experiments will be aimed at exploiting the mechanicism of miR-1 action on MCU, as well as understanding the complete signalling pathway involved in MCU modulation. Given that miRs are well-suited therapeutic targets, as they can easily be mimicked or antagonized pharmacologically (miR mimics or antagomiRs, respectively), even with target selectivity, our study of the miR-1/MCU axis may open to the refinement of the current therapeutic approaches to treat myocardial hypertrophy.

2. MCU participates to the myocardial adaptation to hypertrophic stimuli.

The observation that MCU protein content drops during long-term TAC, in which maladaptation occurs, suggested that MCU protein content fluctuates during pathologic hypertrophy. This led us to investigate whether MCU may have a role in myocardial remodelling caused by chronic increase in cardiac workload. To test this hypothesis, we sought to characterize functionally, biochemically, and morphologically the effect of modulating MCU expression level prior to exposing hearts to pressure overload through

TAC. To increase the insight on cellular signalling, we used adrenergic receptor agonists to study the effect of prolonged adrenergic stimulation in cultured CMs.

To study the role of MCU in cardiac adaptation to hypertrophy *in vivo*, we set up the conditions to modulate its expression by overexpressing (OE) and downregulating (knockdown, KD) MCU transcription using AAV9 injection, which efficiently transduced the gene in >70% of CMs using i.p. injection in 9 day old mice. In whole heart extracts, MCU downregulation resulted in a decrease of approximately 80 % of the protein level, while MCU overexpression determined a ten-fold increase in protein content. Altering MCU expression did not affect cardiac structure and performance at baseline, as assessed by echocardiography and standard histologic/morphologic analyses. However, in mice undergone TAC, MCU overexpression resulted in enhanced hypertrophy, as demonstrated by higher increase in cardiac mass, as compared to TAC-operated WT TAC (injected with AAV9-Empty vector). Interestingly, hypertrophic remodelling had characteristics similar to that of physiologic hypertrophy (i.e. increased capillary density, reduced fibrotic remodelling, and preserved cardiac contractility) also in the advanced stages of hypertrophy (i.e. 8 weeks). On the contrary, silenced mice subjected to TAC displayed a dramatic phenotype caused by the rapid appearance of severe maladaptive remodelling with typical hallmarks of dilated cardiomyopathy (Ejection Fraction, EF, %: Empty: 49.8 ± 5.1 *vs.* MCU OE: 54.5 ± 1.8 *vs.* MCU KD: 41.6 ± 5.4), including reduced capillary density, massive replacement fibrosis and decreased cardiac function. Altogether, these processes result in HF and increased susceptibility to sudden cardiac death already four weeks after TAC.

To gain insight on the molecular mechanism whereby changes in MCU impact on stress-induced CM growth, we used neonatal rat CMs in which MCU overexpression or downregulation were obtained with adenoviral vectors. We used FRET-based Ca^{2+} imaging in CMs expressing the mitochondrially-targeted sensor 4mtD3cpv. The measure of the kinetics of mitochondrial Ca^{2+} revealed that, as expected, MCU overexpression increased Ca^{2+} uptake (ΔR, %: MCU OE: 54.3 ± 3.3 *vs.* Empty: 26.0 ± 1.4), and conversely, MCU silencing decreased it (ΔR, %: MCU KD: 16.4 ± 1.5 *vs.* Empty: 26.0 ± 1.4). Interestingly, while MCU overexpression did not affect CM size and morphology at baseline, MCU KD cells displayed a significant increased area and disarranged sarcomeres. To mimic the increased sympathetic tone that characterises both physiologic

and pathologic hypertrophy, we treated CMs with the onset of both adrenergic agonist norepinephrine (NE). Interestingly, MCU OE cells had a significantly enhanced increase in cell size growth (Δ growth, %: Empty: 25.5 ± 2.1 *vs.* MCU OE: 52.1 ± 6.8). Conversely, MCU KD cells had a remarkably divergent phenotype, characterized by sarcomere disarray and activation of apoptosis. These data were intriguingly similar to the phenotype observed in MCU KD hearts developing dilated cardiomyopathy after TAC.

We thus analysed the effects of MCU modulation on a key Ca^{2+} dependent pathway central to hypertrophic signalling, by analysing the calcineurin/NFAT (CN/NFAT) pathway. Given the critical role of NFAT (nuclear factor of activated T cells) nuclear translocation in hypertrophy, we used fluorescence imaging in cells transfected with GFP-NFAT. Interestingly, nuclear translocation of NFAT was faster (starting already after 6-hours treatment) and more elevated in MCU OE than in control cells. Western blotting (WB) showed that CMs overexpressing MCU displayed phosphorylated Akt after β-AR and, strikingly, already at baseline. In line with this, MCU OE CMs had increased phosphorylation of the downstream target of Akt, GSK3β, which may explain the faster nuclear translocation of NFAT[26]. Interestingly the same biochemical pattern (increased p-Akt and p-GSK3β) was detected in the MCU OE hearts. We thus sought to determine the upstream mechanisms responsible for Akt phosphorylation, by focusing on the role of CaMKII, a critical mediator of CM hypertrophy[27]. Consistently, pharmacologic inhibition of CaMKII abolished the enhanced cell growth and the acceleration in NFAT nuclear translocation observed in MCU OE *vs.* control CM upon NE treatment.

Conclusions. At this point of the study, we can draw a number of conclusions regarding the role of MCU in myocardial remodelling. First, our studies show that increased heart workload, as achieved *in vivo* by TAC and mimicked in cells by NE treatment, is well tolerated when MCU levels are augmented by overexpression. Conversely, MCU downregulation leads, in the same conditions, to cell death and consistently faster maladaptive cellular and tissue remodelling. These data are well in accord with our preliminary observation that MCU content, increased in the compensated hypertrophy, decreases in the advanced remodelling associated to HF. Second, we have identified the β−AR/CaMKII/Akt cascade as a key signalling pathway involved in myocardial hypertrophy and dependent on MCU modulation. The question that remains open is how MCU modulation is mechanistically linked to CaMKII activity. Our working hypothesis

implicates the role of MCU on the regulation of mitochondrial ROS, which may affect in parallel Ca^{2+} release from sarcoplasmic reticulum (SR) (by oxidation of ryanodine receptor 2, RyR2) and CaMKII redox state (decreasing its Ca^{2+} dependency), which would converge in the enhanced activation of CaMKII dependent downstream effects.

3. *In vitro* maturation of cultured neonatal cardiomyocytes.

Primary neonatal CMs are a widely used cellular model in molecular cardiology, which can be maintained in culture for several days and is easily amenable to genetic manipulation[28]. However, this cell type has important functional and structural differences with the mature CMs. These differences range from the expression of different myosin isoforms (in the mouse, from β to α), necessary to maximize contractile performance, to changes in metabolism (switch from glucidic to oxidative metabolism), allowing increased ATP production to sustain higher consumption[29]. Importantly, postnatal cellular maturation involves structures that regulate Ca^{2+} dynamics[30]. In particular, in neonatal cells contraction is mostly due to Ca^{2+} entering through the plasmalemmal L-type Ca^{2+} channels (LTCC), directly triggering the activation of the sarcomeres, with little contribution from intracellular Ca^{2+} release from the immature SR stores. In contrast, in adult cells the plasma membrane has fully developed invaginations known as T-tubules which face the terminal SR cisternae, so that LTCC are in close juxtaposition to the Ca^{2+} Release Units (CRU) formed by the intracellular Ca^{2+} release channel, ryanodine receptor (RyR). Such arrangement allows few Ca^{2+} ions entering the cell to trigger release of further Ca^{2+} from the SR, in a process known as Ca^{2+}-Induced-Ca^{2+}-Release (CICR), which drives contraction. In parallel with the development of SR, the mitochondrial population enriches and interfibrillary mitochondria tether to the SR, in proximity to the CRUs, a condition in which the organelle is found within the confines of a high Ca^{2+} microdomain, fundamental to drive the ion into the mitochondrial matrix.

With these notions in mind, we sought to develop a protocol promoting maturation of neonatal CMs, thus obtaining a cellular model better suited to the study of subcellular Ca^{2+} handling in order to identify the mechanisms linking mitochondrial Ca^{2+} dynamics to hypertrophic remodelling.

To induce maturation of neonatal CMs, we modified the composition of the media traditionally used to maintain cells in culture. The cells were maintained in a medium containing MEM, penicillin/streptomycin (Pen/Strep), non-essential aminoacids, insulin, transferrin, sodium selenate (see *Table 1*). By removing serum from the culture medium, we could avoid cell proliferation and de-differentiation. In addition, we reduced glucose content and added vitamin co-factors and trophic hormones, such as insulin, to compensate the absence of mammalian serum. Furthermore, we improved the preparation purity by eliminating contaminating cardiac fibroblasts, which secrete growth factors and matrix components[31-34], promoting cell de-differentiation and hyperplastic growth. With these changes in the isolation conditions, we obtained a pure population of CMs that can be maintained in culture for several weeks, and after few days already acquired a different morphology, compared to those obtained with the more commonly used protocol. Indeed, microscopy imaging showed that the cells were larger, rectangular-shaped, with a regular perimeter, lacking the typical ramifications of neonatal CMs, and a higher long/short axis ratio. Moreover, we observed an increased area occupied by the contractile apparatus, which appeared more regularly displaced. Mitochondria appeared longitudinally displaced along and between the sarcomeres, similarly to adult cells. In addition, immunostaining of RyRs revealed that the protein appeared in clusters more regularly distributed, thus mimicking the phenotype observed in fully differentiated CMs and suggesting increased maturation of the SR. In line with this, we observed shorter and smaller Ca^{2+} sparks, which are elementary Ca^{2+} signalling events depending on RyR opening, thus supporting that the more organized RyR clusters formed functionally active CRU, alike those of more mature cells. Interestingly, cells were more receptive to adrenergic agonists, displaying a more pronounced growth by hypertrophy as compared to traditional neonatal CMs.

Conclusions. All the aforementioned aspects demonstrate that these cells may represent an *in vitro* model system well-suited to the study of Ca^{2+} dynamics and its relation with hypertrophic growth. Remarkably, these properties did not compromise the amenability for genetic manipulation, either via viral infection or transient plasmid transfection. Future experiment will aim at fully characterizing the Ca^{2+}-related structures, such as T-Tubules, as well as formation of dyads.

RIASSUNTO

Introduzione.

Dal momento della nascita, per tutta la durata della vita, il miocardio è costituito da un numero pressoché fisso di cardiomiociti (CM)[1]. Infatti, la crescita postnatale del cuore è di tipo ipertrofico, per cui lo sviluppo del cardiomiocita, anch'esso di tipo ipertrofico, avviene attraverso un profondo rimodellamento strutturale, funzionale e metabolico. Una volta raggiunto un completo sviluppo, il cuore adatta continuamente la sua contrattilità e struttura in base alle richieste perfusionali dell'organismo, che variano in base a fattori intrinseci ed ambientali[2]. Stimoli acuti determinano la modulazione della contrattilità, mentre stimoli cronici, che richiedono una *performance* elevata nel tempo, fanno sì che i cardiomiociti rimodellino la loro struttura, crescendo ulteriormente per sostenere l'aumentato carico meccanico.

In base a tipo, intensità e durata dello stimolo ipertrofico, il rimodellamento cardiaco può portare ad ipertrofia fisiologica (come nel caso del "cuore d'atleta") o patologica (ad esempio nel sovraccarico pressorio): in quest'ultimo caso, la crescita ipertrofica risulterà nel tempo in scompenso cardiaco, insufficienza cardiaca e morte. Nonostante i fenotipi cellulare e clinico siano distinti, il comune denominatore di queste condizioni è che, nelle fasi iniziali, i processi sono di tipo adattativo e comprendono la deposizione di nuovi sarcomeri nei cardiomiociti, per garantire una contrattilità migliorata o quanto meno preservata. Queste proprietà richiedono entrambe una maggiore produzione di ATP[3]. Non sorprende quindi il fatto che la regolazione della funzione mitocondriale sia un processo critico per la produzione di ATP, per soddisfare il fabbisogno energetico durante la crescita ipertrofica. I mitocondri sono la "centrale energetica" della cellula e la concentrazione di Ca^{2+} opera come un regolatore dinamico primario della produzione di ATP[4]. Nei cardiomiociti, l'influsso di Ca^{2+} nella matrice mitocondriale avviene durante l'aumento di Ca^{2+} sistolico ed è mediato dal complesso dell'uniporto mitocondriale per il calcio (MCUC), recentemente identificato[5,6].

L'*uptake* di Ca^{2+}mitocondriale è un processo fondamentale nella modulazione acuta della contrattilità durante la risposta "*fight-or-flight"* attivata dall'attivazione dei recettori β-adrenergici. A prova di ciò, la delezione di MCU nel modello murino diminuisce la

capacità d'esercizio[7], mentre la riduzione di MCU nelle cellule del nodo senoatriale o dei ventricoli riduce le risposte cronotropiche o contrattili, rispettivamente, indotte dalla stimolazione β-adrenergica[8-11] .

Al momento non è noto se avvengano cambi nell'espressione delle proteine formanti MCUC in diverse situazioni fisiopatologiche, così come non è noto l'effetto della modulazione dell'*uptake* di Ca^{2+} mitocondriale durante il rimodellamento cardiaco.

Obiettivi.

Su queste basi, gli obiettivi del mio progetto di dottorato sono:

1) Identificare i meccanismi molecolari coinvolti nella regolazione endogena di MCU;

2) Determinare se MCU ha un ruolo nel rimodellamento fisiologico e patologico del cuore;

3) Sviluppare un modello sperimentale di cardiomiociti isolati da cuori neonati per la caratterizzazione *in vitro* delle dinamiche del Ca^{2+}mitocondriale su tempi prolungati.

Risultati.

<u>1. Il contenuto dell'uniporto mitocondriale per il calcio (MCU) nei cardiomiociti è dinamicamente regolato da miR-1 nell'ipertrofia fisiologica e patologica.</u>

In esperimenti preliminari condotti nel nostro laboratorio, abbiamo confrontato i livelli proteici di MCU in cuori normali ed ipertrofici, ed abbiamo osservato che le variazioni nel contenuto proteico di MCU non erano accompagnate da variazioni in parallelo del suo trascritto. Ciò ci ha portato ad investigare se, nel rimodellamento cardiaco, potesse avvenire una regolazione post-trascrizionale di MCU. Ci siamo così focalizzati sui microRNA (miR), piccole sequenze non codificanti di RNA (18-25 nucleotidi) capaci di modulare finemente l'espressione di svariati geni, grazie all'interferenza con la stabilità o la traduzione dell'mRNA target[12]. Un numero crescente di evidenze rivela il ruolo fondamentale dei miRs nell'ipertrofia cardiaca e, in altri tessuti, è stato dimostrato come certi miR regolino il contenuto di MCU[13-19].

Tramite ricerca bioinformatica, abbiamo identificato diversi microRNA che potrebbero appaiarsi alla regione 3'UTR di MCU. Tra questi, ci siamo focalizzati su miR-1 per la sua espressione muscolo-specifica, il suo ruolo critico nell'ipertrofia cardiaca[14,15], la sua omologia conservata tra diverse specie e la specificità per MCU tra i membri del complesso MCUC. Il saggio di luciferasi ha confermato quanto predetto dalla bioinformatica ed ha permesso di identificare specifiche sequenze complementari sul gene di MCU. Consistentemente, cardiomiociti over-esprimenti miR-1 hanno mostrato un diminuito contenuto proteico di MCU senza alterazioni nel suo mRNA, risultando in una riduzione significativa nella capacità di importare Ca^{2+} nella matrice mitocondriale.

Quindi, abbiamo testato l'ipotesi che il contenuto di MCU fosse modulato in condizioni di ipertrofia associate a variazioni nell'espressione di miR-1, quali: i) lo sviluppo postnatale, ii) l'esercizio moderato, iii) il sovraccarico pressorio.

Confrontando cuori neonati ed adulti abbiamo osservato che l'espressione di miR-1 aumenta, in linea col suo ruolo di repressore del programma genico fetale. Questo calo di miR-1 è accompagnato da un aumento nel contenuto proteico di MCU senza che ne aumentasse il trascritto. Inoltre, abbiamo osservato come solo il contenuto di MCU vari, tra i vari membri del complesso, eccezion fatta per l'mRNA di MCUb, che aumenta.

Quindi, abbiamo analizzato l'asse miR-1/MCU in cuori ipertrofici murini e umani, con rimodellamenti sia fisiologici che patologici. Nei topi, l'ipertrofia fisiologica è stata indotta tramite protocollo di esercizio cronico, efficace nel determinare ingrandimento cardiaco, dei singoli cardiomiociti ed un aumento della contrattilità[35]. Il confronto coi cuori di topi sedentari ho dimostrato come il livello di miR-1 scenda nell'esercizio e, consistentemente, quello proteico di MCU salga.

L'analisi del complesso in cuori sottoposti a costrizione aortica ha dimostrato come, durante l'iniziale fase compensata, caratterizzata da crescita dei cardiomiociti senza scompenso, le variazioni di miR-1 e MCU rispecchino quelle osservate nei topi esercitati.

Inoltre, le reciproche variazioni di miR-1 e MCU accadono anche in un modello di ipertrofia di rilevanza clinica, come dimostrato dalle analisi di biopsie cardiache umane provenienti da donatori sani e pazienti (età: 59 ± 13 anni) con ipertrofia causata da stenosi aortica.

Questi risultati indicano che, indipendentemente dalla natura dello stimolo ipertrofico (fisiologico o ipertrofico), l'iniziale adattamento cardiaco all'aumentata richiesta contrattile è caratterizzato da analoghi aumenti nella disponibilità cellulare di MCU.

Viste le variazioni analoghe dell'asse miR-1/MCU riscontrate sia in ipertrofia indotta da esercizio che in quella compensata patologica, abbiamo ipotizzato che ci sia un meccanismo regolatorio comune. Ci siamo così focalizzati sul sistema β-adrenergico, il primo meccanismo fisiologico coinvolto nella risposta all'aumentato carico di lavoro, condizione che accomuna sia ipertrofia da esercizio che da costrizione aortica. L'attivazione del *signalling* β-adrenergico, infatti, determina aumento delle oscillazioni di Ca^{2+} citosolico e conseguentemente dell'*uptake* mitocondriale[21-23]. In parallelo, l'attivazione di queste cascate di segnale è coinvolta nell'attivazione di vie di segnale di ipertrofia come Akt-FOXO[24]. È interessante notare che l'espressione di miR-1, come è stato dimostrato, dipende da FOXO3a[25], indicando che, in condizioni di attivazione cronica dei recettori β-adrenergici, il blocco della traslocazione nucleare di FOXO3a potrebbe inibire l'aumento di miR-1. Per supportare questa ipotesi, abbiamo trattato topi sottoposti a costrizione aortica col β-bloccante metoprololo che, in linea con quanto ipotizzato, è stato in grado di abolire la repressione di miR-1 e di conseguenza l'aumento di MCU.

Conclusioni e prospettive future. Complessivamente, i nostri dati identificano miR-1 come un nuovo regolatore post-trascrizionale di MCU e supportano l'idea che l'asse miR-1/MCU sia coinvolto nel rimodellamento ipertrofico fisiologico e patologico. Esperimenti futuri mireranno ad approfondire il ruolo causale di miR-1 nella modulazione di MCU, ed a identificare la via molecolare coinvolta nel processo. Attualmente esistono *tools* farmacologici (quali *miR-mimics* o *antagomiRs*) in grado di interagire coi miR endogeni, antagonizzandoli o sostituendoli, modulando con efficacia e selettività l'espressione degli mRNA target. Su queste basi, il nostro studio sull'asse miR-1/MCU può aprire a nuove prospettive terapeutiche per trattare l'ipertrofia cardiaca.

2. MCU partecipa all'adattamento cardiaco a stimoli ipertrofici.

L'osservazione di come il contenuto di MCU cali durante la fase maladattativa dell'ipertrofia patologica, suggerisce che esso fluttui nelle varie fasi dell'ipertrofia.

Questa osservazione ci ha indotto a cercare di determinare se MCU potesse avere un ruolo attivo nel rimodellamento cardiaco. Per testare quest'ipotesi, abbiamo modulato il livello di MCU in topi successivamente sottoposti a sovraccarico pressorio. Inoltre, per avere dettagli meccanicistici sul *signalling* cellulare, abbiamo modulato l'espressione di MCU *in vitro*, e abbiamo studiato l'effetto della sua overespressione o silenziamento nella risposta ad incubazione cronica con agonisti adrenergici.

Per studiare il ruolo di MCU nell'adattamento cardiaco *in vivo*, abbiamo overespresso o silenziato l'uniporto mediante l'uso di vettori virali (AAV9). La modulazione di MCU, per sé, non ha alterato la struttura e la *performance* cardiaca. Tuttavia, quando abbiamo sottoposto gli animali a TAC, abbiamo osservato come l'overespressione di MCU comporti aumentata crescita ipertrofica, confrontando con animali WT allo stesso tempo dopo l'inizio della costrizione aortica. Inoltre, il rimodellamento nei topi overesprimenti ha caratteristiche simili a quello dell'ipertrofia fisiologica, quali aumentata densità capillare, scarsa fibrosi, funzionalità cardiaca preservata anche dopo 8 settimane di sovraccarico pressorio. Al contrario, il silenziamento di MCU ostacola l'adattamento cardiaco all'aumentata pressione, determinando un maladattamento prematuro, con caratteristiche tipiche della cardiomiopatia dilatativa, quali ridotta densità capillare, fibrosi diffusa ed inadeguata contrattilità. Queste caratteristiche hanno portato i topi MCU silenziati a sviluppare scompenso ed insufficienza cardiaca, ed a morire dopo solo 4 settimane dalla TAC.

Per approfondire i meccanismi molecolari mediante i quali MCU impatta nella crescita ipertrofica dei cardiomiociti, abbiamo overespresso o silenziato MCU in cardiomiociti neonatali di ratto. Tale procedura non ha alterato il potenziale di membrana dei mitocondri. Eseguendo esperimenti di *live imaging* delle dinamiche di Ca^{2+} mitocondriali con la sonda "mito-CaMeleon", abbiamo appurato come la modulazione di MCU risulti in aumentato o diminuito *uptake* di Ca^{2+} mitocondriale. Se da un lato l'over-espressione di MCU non determina alterazioni morfologiche in condizioni basali, cellule silenziate dimostrano dimensioni maggiori rispetto a cellule di controllo, con evidente alterazioni nella struttura sarcomerica. Per mimare l'iperattivazione del sistema nervoso simpatico che si riscontra nell'ipertrofia sia fisiologica che patologica, abbiamo incubato le cellule con norepinefrina. Anche in questo caso, l'overespressione di MCU aumenta la crescita ipertrofica, mentre il suo silenziamento ha un effetto opposto, contraddistinto da

compromissione dei sarcomeri ad attivazione di apoptosi, in evidente analogia ai dati ottenuti *in vivo*.

La via di segnale calcineurina/NFAT ha un ruolo conosciuto nell'ipertrofia cardiaca, e tale via è attivata da norepinefrina più velocemente nei CM MCU overesprimenti. Queste cellule, inoltre, mostrano una maggiore attivazione dell'asse Akt/GSK3β sia dopo norepinefrina che in basale, che potrebbe spiegare la maggior velocità di traslocazione nucleare di NFAT[26]. Akt, mediatore chiave di adattamento fisiologico all'ipertrofia cardiaca, è stato trovato attivato in condizioni basali anche in topi MCU overesprimenti: ciò potrebbe spiegare la loro migliore risposta a sovraccarico pressorio. Quindi, abbiamo voluto investigare i possibili attivatori di Akt e ci siamo focalizzati su CaMKII, un mediatore importante nell'ipertrofia cardiaca[27]. L'inibizione farmacologica di CaMKII ha ripristinato a livelli normali sia la crescita ipertrofica delle cellule MCU overesprimenti che l'accelerata traslocazione nucleare di NFAT, così come la fosforilazione basale di Akt.

Conclusioni. I nostri dati, ottenuti *in vitro* ed *in vivo*, indicano come MCU abbia un ruolo chiave nella crescita ipertrofica, e sia necessario per un rimodellamento di tipo adattativo. In modelli di ipertrofia cardiaca, come la TAC *in vivo* o l'incubazione con norepinefrina *in vitro*, abbiamo dimostrato come alti livelli di MCU favoriscano la crescita ipertrofica dei cardiomiociti e la *performance* contrattile del cuore; al contrario, il silenziamento di MCU provoca, nelle stesse condizioni, morte cellulare e conseguente precoce maladattamento cellulare e tissutale. Questi dati sono in accordo con le nostre osservazioni preliminari, che associano un aumento nel contenuto di MCU nelle fasi adattative dell'ipertrofia ed una riduzione dello stesso nelle fasi maladattive. Inoltre, abbiamo identificato la cascata di segnale β-adrenocettore/CaMKII/Akt come centrale nel rimodellamento ipertrofico, ed influenzata dal livello proteico di MCU. Il prossimo *step* sarà capire come le variazioni del contenuto di MCU impattino sull'attivita di CaMKII. Il modello da noi proposto prevede l'espressione di MCU come fattore coinvolto nella generazione di una piccola quantità di ROS mitocondriali, responsabili della pre-attivazione di CaMKII e della ossidazione RyR2, rendendolo *leaky*. Questo, assieme ad aumentato Ca^{2+} nel reticolo sarcoplasmatico, attiverebbe CaMKII.

3. Sviluppo di un protocollo di coltura che induca la maturazione di cardiomiociti neonatali *in vitro*

Le colture primarie di cardiomiociti neonatali sono un modello cellulare ampiamente utilizzato nella cardiologia molecolare, in quanto possono esser mantenuti in coltura per più giorni e sono facilmente manipolabili geneticamente[28]. Tuttavia, questo tipo cellulare ha importanti differenze funzionali e strutturali rispetto ai cardiomiociti adulti. Queste differenze vanno dall'espressione di diverse isoforme di miosina (nel topo, dalla β alla α), necessario per ottimizzare la *performance* contrattile, a cambi nel metabolismo (che passa da glucidico ad ossidativo), in modo da garantire maggior apporto di ATP in vista di un maggior consumo[29]. Inoltre, il processo di maturazione postnatale delle cellule comprende alterazioni nelle strutture coinvolte nelle dinamiche di Ca^{2+} [30]. In particolare, nelle cellule neonatali, la contrazione avviene principalmente grazie al Ca^{2+} che entra dai canali del Ca^{2+} di tipo L situati nella membrana citoplasmatica. Il Ca^{2+} che entra attiva direttamente i sarcomeri, con un minimo contributo del Ca^{2+} contenuto nelle vescicole che costituiscono un immaturo reticolo sarcoplasmatico. Al contrario, nelle cellule adulte la membrana plasmatica ha sviluppato una serie di invaginazioni note come tubuli T che penetrano nella cellula e giungono all'estremità del reticolo sarcoplasmatico, ora costituito dal tipico sistema di cisterne, cosicché i canali del Ca^{2+} di tipo L siano a stretto contatto coi RyR2, formando cosi le Unità deputate al Rilascio del Ca^{2+} (CRUs). Questa sofisticata struttura fa sì che le poche molecole di Ca^{2+} che entrano dai canali nei tubuli T possano scatenare il Rilascio di Ca^{2+} indotto dal Ca^{2+} (CICR), determinando l'uscita di un'ingente quantità di ione dal reticolo sarcoplasmatico.

Un altro importante cambiamento interessa i mitocondri che, se nel cardiomiocita neonatale occupano principalmente la zona perinucleare, in quello adulto si dispongono anche negli spazi sub-sarcolemmali ed inter-miofibrillari. In questi distretti, i mitocondri sono in prossimità del reticolo sarcoplasmatico, al quale possono ancorarsi fisicamente, trovandosi così in distretti cellulari caratterizzati da elevate concentrazioni di Ca^{2+}.

Tenendo a mente questi fattori, il nostro obiettivo è stato quello di sviluppare un protocollo che promuovesse la maturazione di cardiomiociti neonatali verso un fenotipo adulto, ottenendo così un modello sperimentale ottimale per lo studio delle dinamiche del

Ca^{2+} cellulare, ed identificare così i meccanismi che connettono il Ca^{2+} mitocondriale al rimodellamento ipertrofico.

Per indurre la maturazione dei cardiomiociti neonatali abbiamo modificato la composizione dei terreni di coltura tradizionalmente usati. Per mantenere le cellule ad una concentrazione di glucosio simile a quella fisiologica, abbiamo cambiato il costituente principale del terreno, passando da DMEM (Dulbecco's modified eagle medium) a MEM (minimum essential medium) e riducendo così la concentrazione da 25 mM a 5 mM, valore, quest'ultimo, paragonabile alla concentrazione fisiologica *in vivo*. Per ridurre la proliferazione dei fibroblasti, che tramite secrezione di fattori di crescita e componenti della matrice extracellulare determinerebbero de-differenziamento dei cardiomiociti[31-33], abbiamo fortemente ridotto il quantitativo di siero ed aggiunto un agente proliferativo (BrdU). Per compensare la rimozione del siero, abbiamo aggiunto co-fattori vitaminici ed ormoni trofici, come l'insulina. In tal modo abbiamo ottenuto una popolazione pura di cardiomiociti che può essere tenuta in coltura per più settimane, e che già dopo pochi giorni mostrano una morfologia diversa dalle cellule ottenute col protocollo tradizionale. Analisi alla microscopia hanno evidenziato come queste cellule siano più grandi, rettangolari con un asse maggiore ben distinto da un asse minore, ed un perimetro regolare senza le tipiche ramificazioni dei cardiomiociti immaturi neonatali. A livello subcellulare, abbiamo osservato una maggiore estensione dell'apparato contrattile, rivelatosi disposto in maniera più regolare. I mitocondri appaiono disposti longitudinalmente accanto e tra i sarcomeri, come nelle cellule adulte. Inoltre, l'immunofluorescenza per il recettore rianodinico ne ha evidenziato la presenza in *clusters*, distribuiti in maniera regolare, in analogia alla loro distribuzione in cellule mature, suggerendo così la presenza di un reticolo sarcoplasmatico maggiorente formato. Consistentemente con ciò, abbiamo osservato minori e più rapidi *Ca^{2+} sparks*, eventi elementari di dinamiche di calcio, determinati dall'apertura transiente di RyR. La minore frequenza ed entità di questi *sparks* suggerisce che i RyR disposti in maniera regolare in *clusters* determini la formazione di vere e proprie unità deputate al rilascio di calcio (Calcium Release Units, CRUs), strutture fondamentali nei cardiomiociti adulti. Infine, queste cellule han risposto maggiormente al trattamento con agonisti adrenergici, riportando una crescita ipertrofica maggiore rispetto a cellule neonatali tradizionali sottoposte allo stesso trattamento.

Conclusioni. Tutte queste caratteristiche sopracitate indicano come queste cellule possano rappresentare un modello *in vitro* adatto allo studio delle dinamiche di Ca^{2+} intracellulare, specialmente nel rimodellamento ipertrofico. È importante sottolineare come questo maggior grado di maturazione dei cardiomiociti neonatali non sia a discapito della capacità di manipolarli geneticamente, con tecniche di trasfezione od infezione. Esperimenti futuri cercheranno di caratterizzare a fondo le strutture coinvolte nelle dinamiche di calcio intracellulari, come ad esempio la formazione di Tubuli T ed il rapporto di questi con il reticolo sarcoplasmatico ed i mitocondri.

1. INTRODUCTION

1.1 The heart – Anatomy and histology

The heart is responsible for blood delivery to the entire body, to ensure continuous supply of oxygen and nutrients to all cells in the organism. The heart is divided into left and right sections each formed by one atrium and one ventricle, thus resulting in four chambers: *right atrium* (RA), *left atrium* (LA), *right ventricle* (RV), *left ventricle* (LV). Cardiac contraction and blood pumping can be physically described as originating from two pumps working in series, one deputed to oxygenation of the blood, the other aimed at delivering oxygenated blood to the peripheral tissues. Indeed, the right cardiac section pumps blood from the systemic veins to the pulmonary circulation, while the left section pumps the oxygenated blood from the pulmonary arteries to the systemic circulation. The left and right chambers are divided by two *septa:* the *interventricular septum* (IVS) separates left and right ventricles, the *interatrial septum* separates left from the right atria. Each atrium is connected to the corresponding ventricle through *atrioventricular* (AV) *valves* which allow unidirectional blood-flow from the atria to the ventricles (fig. 1).

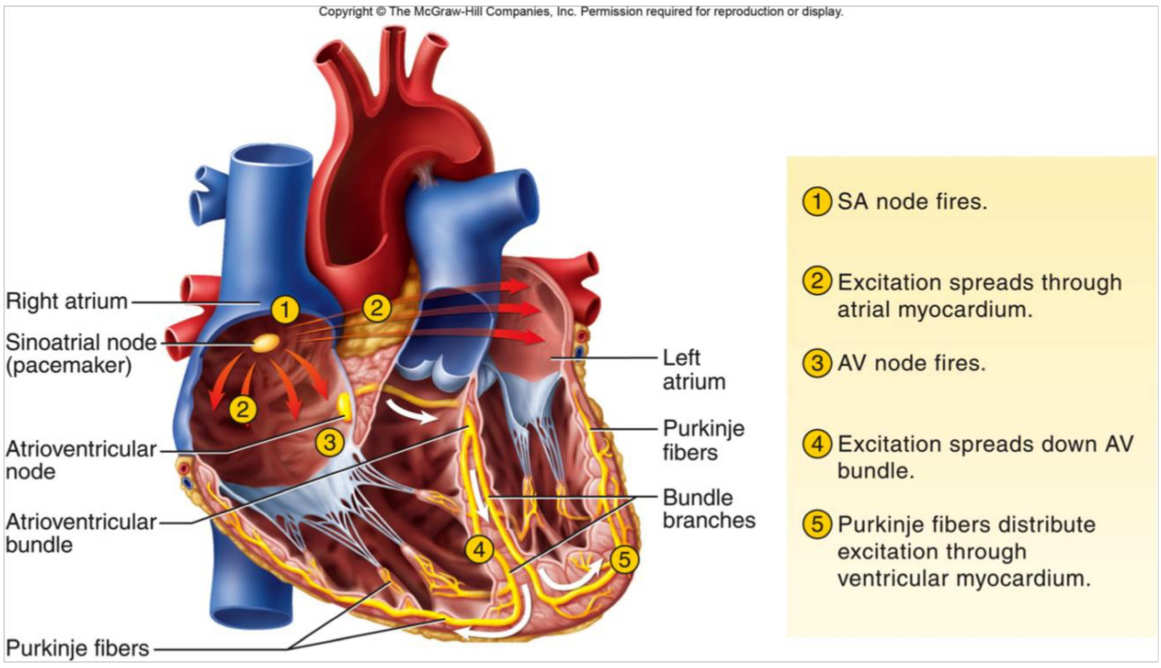

Figure 1. Heart anatomy.

The heart cycle is divided into two phases: the heart contraction (called "systole") and the subsequent heart relaxation (called "diastole"). Considering a normal heart rate around 75 beats per minute (bpm, source: American Heart Association, AHA), the human heart is required to contract billions of times during the average lifetime. This duty requires an anatomical structure tailored for efficient blood pumping and endowed with perfect synchronization of contraction and relaxation.

The cardiac walls are formed by three layers, here listed from the outer to the inner:

1. the *epicardium*;
2. the *myocardium*, the thicker cellular portion, responsible for the contractile activity;
3. the *endocardium*, that faces the lumen of the cardiac chambers.

The contractile cells of the heart are called *cardiomyocytes* and account for around 70% of the total cardiac volume. Cardiomyocytes can be classified in 2 subgroups:

1. *working cardiomyocytes*, that constitute the large majority and are responsible for mechanical contraction;
2. *cardiomyocytes of the conduction system*, including the nodal cells of the sino-atrial (SA) and the atrio-ventricular (AV) nodes, the His bundle cells, the left and right braches and the distal part the Purkinje fiber system (PFs)[36,37], all of which are responsible for the origin and propagation of electrical signals and synchronization of ventricular activity.

Cardiomyocytes are not the sole cellular components of the heart. Indeed, other cell types are abundantly represented, such as cardiac fibroblast (responsible for the formation and homeostasis of the extracellular matrix), endothelial cells (that constitute the highly organized vascular tree of the heart, which shows a "fractal" distribution[38]) and cardiac nerves, including intrinsic and extrinsic autonomic nerves. Cardiac contraction does not require nerve stimulation (contrarily to skeletal muscle, as described below), but relies on spontaneous automaticity. However, the heart is highly innervated by the autonomic nervous system[24] that continuously tunes the force and frequency of cardiac contraction. The autonomic nervous system is composed by parasympathetic and sympathetic systems, which exert opposite physiological functions. The parasympathetic component is responsible for the so-called *rest-and-digest* activity, and lowers the heart rate when the body is relaxed. Conversely, sympathetic innervation is responsible for the *fight-or-flight*

response, increasing heart rate and contraction force *via* the release of norepinephrine (NE), the main sympathetic neurotransmitter.

As previously said, the heartbeat does not require any nervous stimulation as a trigger, since the pumping activity is mediated by the perfectly synchronized electrical activation of the organ itself. Each heartbeat is, in fact, initiated by electrical impulses generated by spontaneously depolarizing cells that, altogether, constitute the sinoatrial node (SAN), the cardiac pacemaker. The electrical impulse is then propagated through the atria, and the depolarizing wave passes through the atrioventricular node (AVN), where it is slowed before entering the AV bundle, constituted by PFs. The entire system is known as His/Purkinje system, which allows rapid conduction of the electrical signal through the ventricular myocardium, thus allowing coordinated contraction of all cardiomyocytes[39].

1.2 Cardiomyocytes – structure and excitation-contraction coupling

The working cardiomyocytes (for simplicity, from now referred to as cardiomyocytes, CMs) are large muscular cells with a well-defined internal structure. Almost half of their volume (47%[40]) is occupied by contractile proteins, organized in crystal-like arrays of striated myofibrils. The remaining volume is occupied mainly by mitochondria (from 25% at birth to 35% in the adult[41]), as discussed in detail below.

Another key subcellular compartment is the sarcoplasmic reticulum (SR) that, although occupying only about 3.5% of the total volume, constitutes the main intracellular Ca^{2+} store and is crucial for CM contraction.

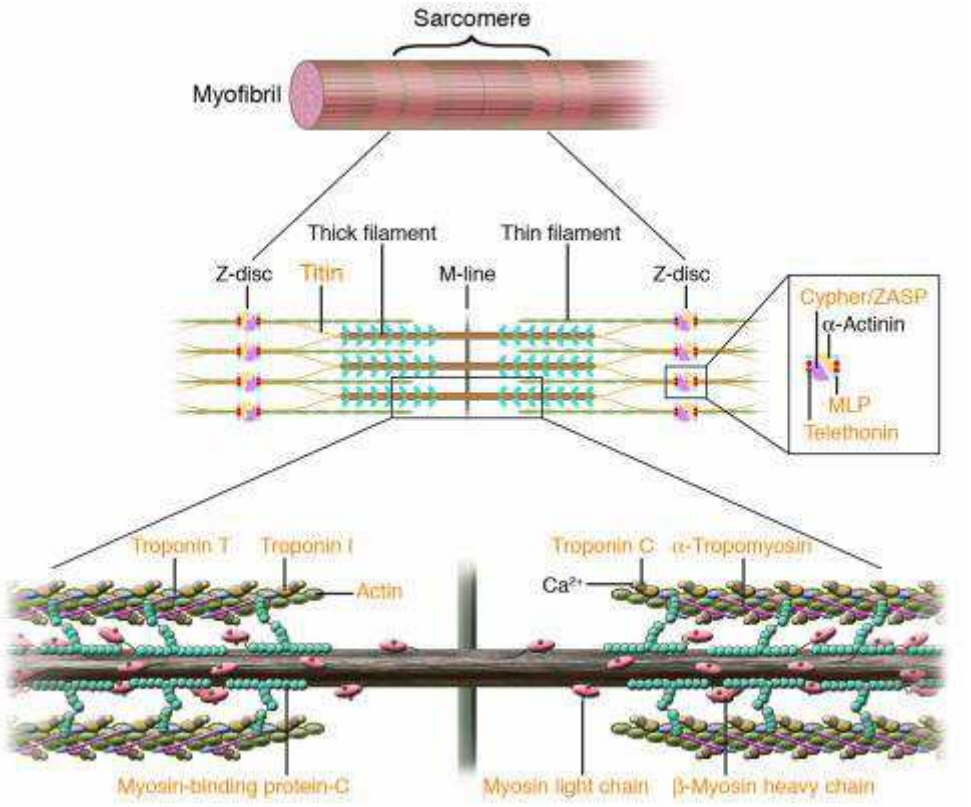

Figure 2. Sarcomere and troponin complex[42].

The contractile units in each CM, called sarcomeres, are formed by myofibrils, mainly composed by thin (actin) and thick (myosin) filaments, as shown in fig. 2. Each myosin molecule contains two heads with ATPase activity. In addition to actin, the thin filaments are composed of other interacting proteins: tropomyosin and troponins. Troponins are found in complex, and are located at regular intervals attached to tropomyosin. The troponin complex is represented by: troponin-T (TN-T), troponin-C (TN-C) and troponin-I (TN-I). Sarcomere shortening is enacted by the interaction between actin and myosin. When Ca^{2+} binds to TN-C, it induces a conformational change in the troponin complex proteins allowing the direct interaction between actin and myosin. TN-I exposes a site on the actin molecule that binds the myosin ATPase located on the myosin head. Such event results in ATP hydrolysis, which releases energy for the conformational change of the acto-myosin complex: the actin and myosin filaments slide along each other, thereby shortening the sarcomere length and thus inducing cell contraction.

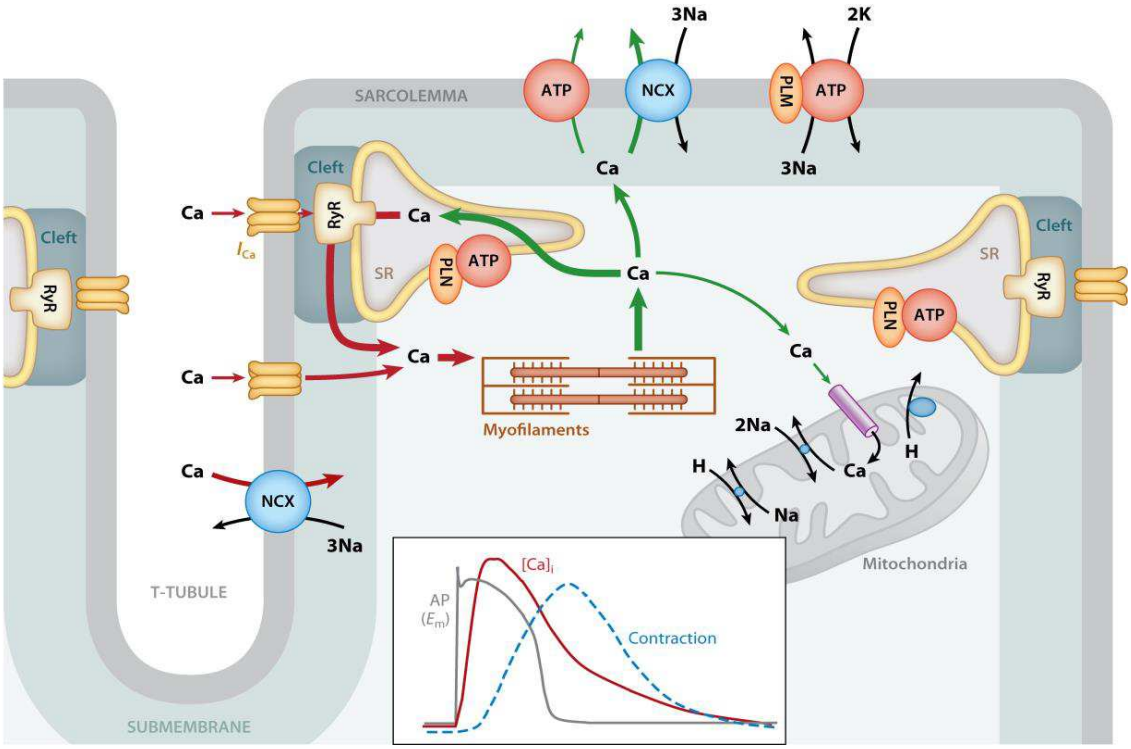

Figure 3. The role of Ca^{2+} in cardiomyocyte ECC. Ca^{2+} supply is indicated in red while Ca^{2+} removal in green[43].

The process initiating from the depolarizing wave, triggering an action potential (AP), and culminating in CM contraction, is called *Excitation-Contraction Coupling* (ECC)[44] and is represented in fig. 3. CM contraction is, in fact, triggered by an AP that induces opening of L-type Ca^{2+} channels (LTCC), located in the T-tubule plasma membrane. The resulting Ca^{2+} influx in the cytoplasm is responsible for the activation of Ryanodine Receptor-2 (RyR2) triggering a much larger release of Ca^{2+} from the sarcoplasmic reticulum (SR), the intracellular Ca^{2+} store. RyR2 Ca^{2+} channels are located in the SR membrane and open in response to elevations in submembrane [Ca^{2+}] achieved through LTCC. Ca^{2+} release from the SR is a passive flux that follows the concentration gradient, being $[Ca^{2+}]_{SR}$ several orders of magnitude larger than $[Ca^{2+}]_i$ in the cytosol, and is called *Ca^{2+}-induced-Ca^{2+}-release* (CICR)[45]. The elevated $[Ca^{2+}]_i$ in the cytosol allows the sarcomere shortening. Interestingly, the release of Ca^{2+} from the SR through a *single* RyR2 channel cluster does not cause a global increase in cytosolic Ca^{2+}, but generates individual "elementary" Ca^{2+} release events, known as *Ca^{2+} sparks*[46]. The features of these Ca^{2+} sparks, such as amplitude, duration and area, depend on RyRs, whose function is tightly regulated. Indeed, several proteins are known to bind the channels, mediating stabilization[47,48] or increasing flux (triadin, junction). Post-translational modifications of RyR2 also modulate channel activity: indeed, its phosphorylation, either by Ca^{2+}-

calmodulin dependent kinase II (CaMKII) or protein kinase A (PKA), increases the channel open probability and the resulting release of Ca^{2+}, participating to the mechanism of positive inotropy caused by β-adrenoceptor (β-AR) (sympathetic) stimulation[49].
The interaction between myosin and actin occurs as long as cytosolic Ca^{2+} concentration remains elevated. At the end of contraction, Ca^{2+} is then sequestered back into the SR by an ATP-dependent Ca^{2+} pump (sarco-endoplasmic reticulum Ca^{2+}-ATPase 2, SERCA2-A), thus lowering cytosolic [Ca^{2+}] and removing Ca^{2+} from TN-C. TN-I, thanks to the conformational change of the troponin complex induced by reduced intracellular [Ca^{2+}], is once again able to inhibit the actin-binding site on myosin, so that the initial sarcomere length is restored[50]. Ca^{2+} re-uptake, from the cytosol to the SR, is essential to restore the starting conditions before a new AP fires. In the adult CM, approximately 75-80% of cytosolic Ca^{2+} re-enters into the SR, the remaining is extruded from the cell *via* Na^{+}- Ca^{2+} Exchanger (NCX) (19-24%) or taken up by the mitochondria (1%)[41].

Ca^{2+} re-uptake from SR is mediated by SERCA, in an ATP-requiring process, as Ca^{2+} is transported against its concentration gradient. An essential regulator of SERCA2 is the interacting protein phospholamban (PLB), that keeps the pump in a low Ca^{2+} sensitivity state, thus slowing the re-uptake rate. Such inhibitory effect of PLB is reversed by its phosphorylation by PKA or CaMKII, whose effect is faster relaxation and increased SR load.

Ca^{2+} extrusion from the cell is primarily exerted by NCX, located on the plasma membrane. By transporting 3 Na^{+} across the membrane in exchange for a single Ca^{2+} ion, NCX is an electrogenic mechanism of efflux, that generates an inward depolarizing current consequent to Ca^{2+} efflux. This depolarizing current is usually small and impacts on the membrane potential only for few millivolts, however, in the failing heart, or during cytosolic Ca^{2+} overload, can cause dangerous arrhythmic phenomena[51].

Last but not least, 1% of total contractile Ca^{2+} enters the mitochondria. Mitochondrial Ca^{2+} uptake is mediated by a passive uniporter (MCU), whose molecular identity has been recently identified[5,6]. While in normal conditions the percentage of Ca^{2+} uptake seems not significant if compared to SERCA2 and NCX, the mitochondria have been shown to accumulate a large amount of Ca^{2+}, which is of particular interest in pathological Ca^{2+}-overloaded CMs, as discussed later.

1.3 Mitochondrial Ca^{2+} in cardiomyocyte homeostasis

Mitochondrial Ca^{2+} is a fundamental player in cardiac physiology, being involved in fundamental homeostatic processes, such as regulation of ATP production. The process by which mitochondrial Ca^{2+} regulates mitochondrial ATP production is usually referred as excitation-metabolism coupling, and is enacted through modulation of rate-limiting enzymes involved in pyruvate oxidation, tri-carboxylic acid (TCA) cycle and ATP synthesis (pyruvate dehydrogenase; isocitrate dehydrogenase and α-ketoglutarate dehydrogenase; ATP synthase, respectively).

ATP is essential, in CMs, both for shortening (occurring during systole) and for SERCA2-mediated replenishment of SR, with subsequent sarcomere relaxation, during diastole.

To give an idea, a single human heartbeat consumes about 300 mg of ATP distributed among the CMs; this means almost 1000 tons of ATP within human lifetime (calculated from[52]).

The classic view of mitochondria as "powerhouse of the cell" could not be more appropriate in the case of CMs, since almost all cytosolic ATP is provided by mitochondria. Indeed, in adult CMs, mitochondria account for more than 30% of total cell volume, thus resulting in the largest mitochondrial volume fraction among mammalian cell types[40]. However, recent evidence suggests that mitochondria in heart physiology not only provide chemical energy supply, but are also key modulators of electrophysiological and Ca^{2+} cycling properties, either directly through the activation of mitochondrial ion channels, or indirectly, by acting on ATP levels, redox state or signalling cascades[53,54].

The dark side of the coin is that mitochondrial Ca^{2+} overload has the potential to activate cellular death pathways: in fact, it has extensively been demonstrated that prolonged excessive [Ca^{2+}] into the mitochondrial matrix, opens the permeability transition pore (PTP) and activates cell apoptosis. Moreover, mitochondrial Ca^{2+} plays an important part in regulating the cellular redox state: Ca^{2+}-dependent activation of dehydrogenases involved in TCA cycle controls NADH production, which in turn impacts on cellular availability of anti-oxidative resources and on mitochondrial reactive oxygen species (ROS) production[55]. Thus, mitochondrial Ca^{2+} dynamics impact on several cellular pathways, related to cellular life and death.

While the outer mitochondrial membrane (OMM) is highly permeable to Ca^{2+} and other ions thanks to the voltage-dependent anion channel (VDAC), a porin ion channel; the

inner mitochondrial membrane (IMM) is relatively impermeable to Ca^{2+}. The biochemical properties of Ca^{2+} transport into the mitochondrial matrix were described long before the molecular identification of the proteins mediating it. Indeed, it was clear that Ca^{2+} flux only occurred in one direction (UNI-porter) and that the channel was passive, allowing Ca^{2+} entry only when the electrochemical gradient across the IMM is present. The uniporter has a low sensitivity to Ca^{2+}, meaning that it needs a large [Ca^{2+}] increase in order to open: this condition is made possible by the tethering of mitochondria to SR, at sites where, thanks to RyR2 (or, in analogy, inositol trisphosphate receptor (IP3R) in other cell types), Ca^{2+} flows out in the cytoplasm[56] generating a "high [Ca^{2+}] microdomain" close to the mitochondrial uptake sites. Several studies have reported that mitochondria are thus exploiting, for each systole, sufficient [Ca^{2+}] to induce mitochondrial Ca^{2+} uptake into the matrix[57].

1.4 The mitochondrial calcium uniporter (MCU)

While the observation that mitochondria are able to take up Ca^{2+} was performed decades ago[58], the molecular identification of the uptake machinery is still in progress. A great momentum was sparked in 2011 by the molecular identification of the mitochondrial Ca^{2+} uniporter MCU[5,6] which, together with several molecular partners, constitutes the soon defined mitochondrial Ca^{2+} uniporter complex (MCUC). The complex is a major pathway of mitochondrial Ca^{2+} influx into the matrix, a process driven by the mitochondrial membrane potential[59,60]. The MCUC consists in a 480 kDa multimeric channel, composed by pore-forming MCU subunits[5,6] and regulatory elements, namely MICU1 (mitochondrial Ca^{2+} uptake 1[61,62]), MICU2 (mitochondrial Ca^{2+} uptake 2[63]), EMRE (essential MCU regulator[64]), MCUb[65] and SLC25a23 (Solute Carrier 25a23[66]) (see fig.4).

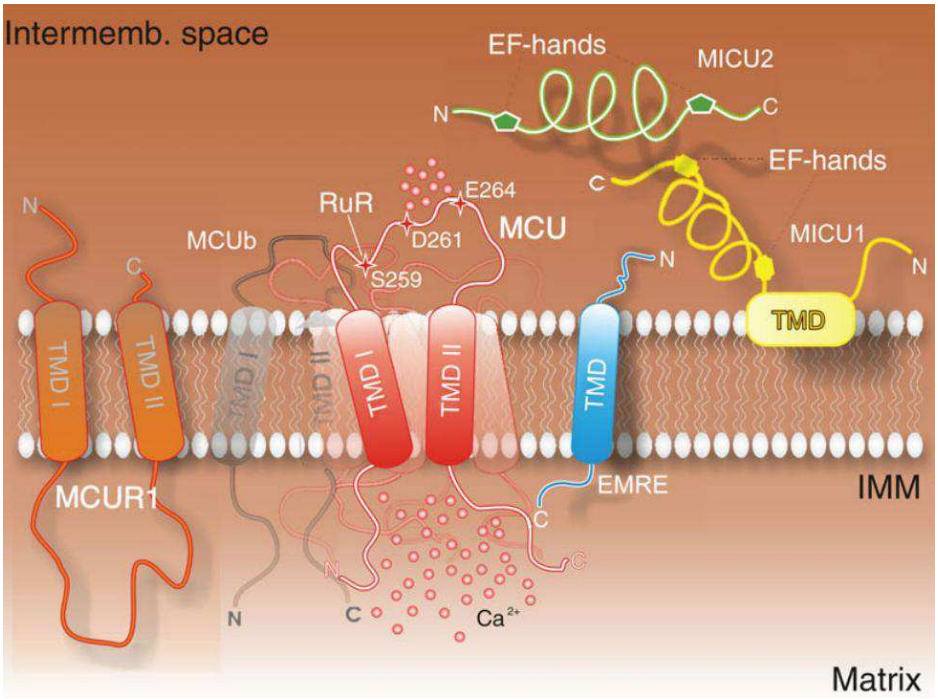

Figure 4. Mitochondrial Ca^{2+} uniporter complex[67].

MCU, a dual pass trans-membrane protein of the IMM, is central to the complex and oligomerizes to form the Ca^{2+} pore of MCUC. Its Ca^{2+} selectivity is granted by the "DIME motif", consisting in four highly-conserved D-I-M-E residues, located in a loop in the intermembrane space (IMS), linking the two transmembrane helices[68]. This motif contains the essential acidic residues critical for Ca^{2+} transport, as mutations at these sites inactivate the complex[6].

Recent evidence shows that the MCUC pore has a pentameric organization[69], in which the pore-forming subunits, MCU and MCUb, are associated to the regulatory proteins MICU1, MICU2, EMRE, SLC25a23.

MCUb is a MCU paralogue that, despite sharing high sequence similarity with MCU, lacks the acidic residues responsible for Ca^{2+} transfer, thus acting as an endogenous negative modulator of MCUC[65]. MICU1 and MICU2 (known as "MICUs") are Ca^{2+}-sensing proteins that modulate channel opening at low and high cytosolic Ca^{2+} concentrations[70]. EMRE regulates the complex assembly by linking MCU to MICUs[64]; moreover, recent studies suggest that EMRE can also serve as a matrix Ca^{2+} sensor[71]. Through its interaction with MCU and MICU1, the Mg-ATP/Pi transporter SLC25a23, located in the IMM, is thought to modulate Ca^{2+} influx. Finally, MCUR1 has also been proposed as a regulator of MCUC[62], by acting as scaffold and linking the complex to the respiratory chain[72], but this view has been challenged[73].

Interestingly, the molecular composition of the complex and the stoichiometry between its subunits, may vary between different tissues[74], thus adding complexity to the system and to the understanding of MCUC biology.

1.5 The biology of MCU *in vivo*

A high number of studies agrees on the pleiotropic effects of mitochondrial Ca^{2+}, in many essential aspects of cellular homeostasis. On these bases, one would expect genetic ablation of the MCU gene to be detrimental for so many functions at the level of a whole organism, to cause embryonic lethality during development.

The first MCU knockout (KO) mouse, however, "shocked" most of the scientists in the field: indeed, in 2013 Finkel and colleagues showed how MCU KO mouse (in which MCU gene was deleted in the whole body) was "safe and sound", and no signs of dysfunction in any organ were detected[7]. It is important to underline that these mice were generated in a mixed genetic background (CD1), since MCU deletion in pure genetic background such as C57BL/6 led to embryonic lethality. Despite the lack of Ca^{2+} uptake ability showed by the cells of CD1 mice, no animal phenotype was noted, except for overall limited size and decreased exercise capacity in MCU KO mice. Interestingly, MCU KO mitochondria were completely resistant to Ca^{2+} overload-induced mPTP opening and subsequent cell death[7]. Since Ca^{2+} overload is known to play an important role in ischemia/reperfusion (I/R) injury in the heart, MCU gene deletion was studied in such context, by using an *ex vivo* Langendorff model of I/R injury in wild type and MCU KO hearts. Surprisingly, MCU KO hearts were not protected to I/R injury and, moreover, the mPTP-inhibitor cyclosporin A (CsA) conferred significant protection in wild type hearts but not in MCU KO. A possible mPTP-independent pathway may explain the cell death occurring in MCU KO hearts, thus raising the questions of whether and how cell death signalling may be "reprogrammed" in a context of chronic MCU deficiency.

The same mouse strain was used in further studies[75], which focused on cardiac function. As shown by Holmstrom et al., despite MCU KO cardiac mitochondria displayed reduced matrix Ca^{2+} levels, basal cardiac function was unaltered in the adulthood and during ageing. Moreover, the absence of MCU did not affect whole cardiac physiology at baseline, or either upon pharmacologic stimuli (e.g. isoprenaline) or pressure-overload

(e.g. transversal aortic constriction, TAC) stimuli. This lack of both basal and stress-induced phenotypes was quite unexpected, given the numerous important roles played by mitochondrial Ca^{2+} in cardiac physiology[41].

In parallel with the study of MCU whole-body KO mice, another alternative approach was exploited: indeed, Wu and colleagues generated a CM-specific transgenic mouse model expressing a dominant negative MCU isoform, MCU D260Q E263Q (DN-MCU). This mouse model was generated in the same genetic background (C57BL/6 x CD1) of the constitutive MCU-KO model[11]. Beside constitutive MCU KO mouse (lacking the uniporter from birth), the authors also took advantage from a technique called "gene painting". In this work, they could selectively express DN-MCU in SAN cells of adult mice by conveying the exogenous DNA in a Poloxamer-constituted gel, and locally applying this mixture at the level of SAN. As expected, the expression of DN-MCU abolished mitochondrial Ca^{2+} uptake *in vivo* but, conversely to total-body MCU KO, both models (DN-MCU from birth and resulting from gene painting) showed a clear phenotype, since DN-MCU mice were unable to show the cardiac "fight-or-flight" response, and β-adrenergic stimulation with isoprenaline failed to induce heart rate acceleration[75]. Notably, β-AR stimulation determines $[Ca^{2+}]$mt increase which, in turn, enhances oxidative phosphorylation thus providing increased ATP to sustain the faster heartbeat. Indeed, while MCU appears to be dispensable for cardiac function at rest, under stress conditions, the MCU-dependent boost of ATP production is necessary to sustain the increased demand of SERCA pumps and the subsequent Ca^{2+} loading of SR in SAN pacemaker cells.

Similar results were found by Rasmussen and colleagues in another following study, conducted in mice expressing DN-MCU in the whole heart (αMHC x DN-MCU). Indeed, DN-MCU mice showed impaired performance at increasing workloads and higher oxygen consumption rate (OCR)[11]. Moreover, DN-MCU CMs showed higher diastolic cytosolic Ca^{2+}, due to reduced ATP availability and consequent SERCA efficiency[8]. The combination of these data pointed at a global cellular reprogramming, resulting from a broad transcriptional remodelling, aimed at extra-mitochondrially adapting cellular metabolism and Ca^{2+} handling. Interestingly, mitochondrial morphology, protein and DNA content were unaltered by MCU deletion, thus excluding a problem in the "energetic apparatus" structure, and pointing to its decreased efficiency. Similar to what

was reported in the whole-body MCU KO[7], phosphorylation of PDH was significantly increased, hence PDH was less active in absence of MCU. Despite DN-MCU hearts had a significantly reduced amount of ROS during I/R injury, MCU deletion did not reduce the infarct area following I/R, in line with previous observations in total body MCU KO mice[7].

In contrast to these models of constitutive MCU deletion or inhibition, a conditional KO mouse model was published concomitantly in Cell Reports by two different groups (Kwong et al., Luongo et al.,[9,10]). In these works, MCU was deleted in specific tissues by Cre-mediated recombinase. Interestingly, when these mice were crossed with mice constitutively expressing Cre recombinase (thus resulting in constitutive and not inducible MCU deletion), no homozygous MCU KO could be obtained due to embryonic lethality, thus confirming that MCU is required during development. When treated with tamoxifen, these mice displayed a decrease of about 80% of MCU at protein level, probably due to the mosaicism of Mer-Cre-Mer strain[76]. The functional consequence of such decrease in MCU content is a marked reduction of mitochondrial Ca^{2+} uptake which, however, did not result in significantly reduced matrix Ca^{2+} content. The authors suggest the existence of additional pathways of mitochondrial Ca^{2+} uptake different from the fast-entry mediated by MCU, that would contribute to slow Ca^{2+} entrance in mitochondrial matrix. Additionally, decreased mNCX levels were found, thus implying "intra-mitochondrial" compensatory mechanisms adjusting Ca^{2+} influx-efflux.

To assess I/R injury, the authors then performed a similar experiment performed in constitutive MCU KO mice. In contrast to the latter model, here, inducible MCU-KO mice were protected from injury, exhibiting reduced infarct size as compared to wild type littermates. The discrepancy between these positive results and the lack of protection seen in MCU KO or DN-MCU mice is currently unexplained.

Possibilities include technical differences such as differences in the model of I/R injury (e.g. *in vivo* LAD ligation as opposed to an *ex vivo* Langendorff model). Another plausible explanation would rely on the differences in the timing and duration of MCU deletion. In the MCU constitutive KO, the deletion of MCU was induced in adult mice, while in the MCU KO and DN-MCU mice, MCU activity was absent throughout development. This suggests that there might be important physiological differences between acute and chronic deletion of MCU. Indeed, MCU deletion in adult CMs did not affect basal respiration. However, when treated with isoproterenol, the absence of MCU

affected maximal oxygen consumption rates[10]. Moreover, when subjected to a classic model of pathologic hypertrophy (i.e. TAC), MCU conditional KO displayed similar damage as compared to WT hearts, consistent with data obtained in MCU constitutive KO mice[75]. Furthermore, when mice were challenged to sprint on a treadmill, MCU conditional KO mice needed more time to warm-up before reaching a running capacity comparable to littermates. These data suggest that adult cardiac-specific deletion of MCU impairs the ability of the heart to adapt to acute stresses, which require rapid increases in mitochondrial metabolism.

At the moment, a large consensus about MCU role in cardiac patho-physiology is still lacking, and the several studies conducted highlight different discrepancies among different mouse models, thus adding complexity to the study of the uniporter. Moreover, as mentioned above, MCU is the pore-forming subunit of MCUC and, interestingly, studies of the mitochondrial Ca^{2+} uniporter *in vivo* have comprised other components critical for its regulation. In particular, the impact of MICU's gatekeeping function on the uniporter *in vivo* is of great interest.
The first two studies investigating MICU1 deletion in mouse models were recently published[77,78]. In the first study, whole body deletion MICU1 resulted in complete perinatal lethality shortly after birth, presumably to phenomena linked to Ca^{2+}-overload[77]. In another background, homozygous deletion of MICU1 resulted in high but not total postnatal lethality. The rare surviving MICU1 KO mice initially exhibited a severe phenotype reminiscent of the alterations observed in patients with loss-of-function MICU1 mutations, which included abnormal mitochondrial morphology, decreased muscle ATP levels, elevated serum lactate, and neurological features such as ataxia[79]. In both studies, mitochondria isolated from these MICU1 KO mice exhibited increased Ca^{2+} uptake at low extramitochondrial Ca^{2+} concentrations, and in addition had elevated resting mitochondrial matrix Ca^{2+} levels.

Additional models and analysis are clearly required to understand the other components (e.g. EMRE, MICU2, etc.), as well as how all these components interact. The observation that the perinatal lethality induced by the absence of MICU1 may be rescued by heterozygous deletion of EMRE[78] suggests that the generation of additional mouse models will allow for insightful combinatorial models. Additional information is also needed to explain the clear distinction between acute and chronic effects of the deletion of

uniporter components. Indeed, some functional remodelling may occur following chronic MCU deletion to allows physiologic adaptation. In some ways, this may represent a form of retrograde signalling, by which a mitochondrial perturbation can ultimately result in nuclear transcriptional changes[80]. All these and other related questions suggest that further work has to be done, and the next studies may hopefully provide further insight into the *in vivo* role of the uniporter.

1.6 Cardiac postnatal development: structural and functional differences between neonatal and adult cardiomyocytes

In the very first weeks after birth, the heart undergoes dramatic changes depending on terminal differentiation of CMs, which lose the replicative capacity continuing their growth through physiological hypertrophy. In order to maximize their contractile performance, to fulfil the increasing perfusional demand of the growing organism, neonatal CMs face a profound process of maturation to the adult phenotype, characterized by alterations in sarcomeric structure, energetic metabolism and Ca^{2+} handling[29].

The hypertrophic process that leads neonatal CMs to acquire the size of adult cells includes synthesis and assembly of new sarcomeres, to maintain the contractile efficiency in a bigger cell. Concomitantly, several studies reported a switch in the expression of the two myosin isoforms: in mouse hearts, while neonatal cells predominantly express β-myosin, adult CMs express α-myosin[81]. Changes in the proportion of myosin heavy chain (MHC) isoforms seem to be directly related to the degree of mechanical performance and efficiency of the heart as it switches from fetal to postnatal circulation.

In the need of adapting cardiac performance to increasing perfusional requests, developing CMs tune their metabolism, increasing the efficiency of ATP production and its availability for contraction and relaxation.

Many studies[82] show that postnatal development of neonatal CMs (NCMs) is characterized by a switch from glycolic to oxidative metabolism. Indeed, if neonatal CMs mainly rely on glucose as main energetic source, up to 90% of ATP provided in adult CMs is obtained by oxidation of fatty acids. This process, triggered by the elevation of O_2 content, from uterus to external environment, ensures a higher efficiency of ATP production: in fact, if each glucose molecule yields 2 ATP molecules *via* anaerobic

glycolysis, the same amount of carbon atoms undergoing oxidative phosphorylation yield 36 ATP molecules.

Oxidative phosphorylation consists in sequential reduction-oxidation reactions, in which electrons flow from a donor to an acceptor molecule, such as oxygen, through energy-releasing processes. These reactions take place into mitochondria, where four enzymatic complexes that guide electron flow towards a fifth complex, known as ATP synthase, are localized in the inner mitochondrial membrane (IMM). Remarkably, this process also grants the maintenance of efficient mitochondrial homeostasis, as the concomitant proton exclusion from the mitochondrial matrix sustains the negative mitochondrial membrane potential.

Consistently with the increased energetic request and ATP production in adult CMs, compared to neonatal, a hallmark of CM postnatal development is represented by the increase in mitochondrial population (from 25% to 35%)[83].

Variations in mitochondria not only regard their quantity but, interestingly, their intracellular distribution: if neonatal cells display almost exclusively perinuclear mitochondria, in adult CMs at least three "sub-populations" can be distinguished, depending on their localization. Beside perinuclear mitochondria, also sub-sarcolemmal and inter-myofibrillar mitochondria can be observed. The formation of different mitochondrial sub-population is part of a more complex "cellular program" whose aim is the compartmentalization of intracellular signalling and optimization of energetic resources, acted primarily by the creation of specialized structure[83]. This sophisticated mechanism, which marks the development from immature to mature CM and includes cytoskeletal reorganization and formation of communication points between organelles, includes several players such as T-tubules, SR, myofibrils and, indeed, mitochondria.

With the purpose to minimize waste of ATP, in adult CMs, the players involved in its production and consumption are tightly coupled: indeed, mitochondria are found juxtaposed to myofibrils, SR, and sarcolemma. These complexes are called Intracellular Energy Units (ICEUs) and represent the basic organization pattern of energy metabolism in adult CMs. The metabolic feedback within the single ICEUs is acted by phosphoryl transfer pathways, such as creatine kinase (the predominant, in CMs), adenylate kinase and direct ADP/ATP channelling. These enzymes, especially creatine kinase, have been found to increase in protein content during cardiac development to adulthood[84]. In addition to the changes in cellular metabolism, CMs development is also accompanied to modifications in intracellular Ca^{2+} handling. During postnatal development the main

intracellular Ca^{2+} store, the SR, reaches its complete maturation and becomes central to the Ca^{2+} fluxes that accompany cardiac contractions. In CM of neonatal hearts, the SR is composed by several vesicles containing a limited amount of Ca^{2+} and, only in adult hearts, the SR is found in its typical structure made of well defined "cisternae". Moreover, the Ca^{2+}-related proteins (e.g. SERCA, PLB, RyR2) regulating the release and re-uptake of Ca^{2+} from the SR, and thus the oscillation of its cytoplasmic concentration in the adult hearts, are increasingly expressed and correctly placed in the SR membrane only during postnatal development. In addition, CMs develop T-tubules, which are membrane invaginations that regularly cross the cytoplasm from one cell side to the other. These peculiar structures are enriched in ion channels, including LTCC, which are positioned with their intracellular side facing the RyR2 Ca^{2+} release channel on the SR cisternae; the juxtaposed T-tubular and SR membrane form the so called "dyads"[85]. These morphological differences between the subcellular structures in neonatal *vs.* adult CMs carry important functional differences and thus, the mechanism of excitation-contraction coupling differs between neonatal and adult CMs. This is of particular interest and has to be considered in relation to the fact that NCMs are a widely used cellular model for the amenability to cell culture and genetic manipulation. Fetal and neonatal CMs have longer lasting contractions and their activation relies mostly on the influx of Ca^{2+} from the extracellular space. In such cells, Ca^{2+} cycle, including both the influx and the efflux of the ion, occurs across the plasma membrane and is accompanied by depolarizing currents. The entry of Ca^{2+} from the extracellular space is mediated, also in this case, by the L-type Ca^{2+} channels located in plasma membrane, however during diastole, Ca^{2+} is extruded from the CMs through the NCX and the Plasma Membrane Ca^{2+} Pump ATPase (PMCA)[86,87].

1.7 Myocardial hypertrophy

The fully developed heart is unable to regenerate, but cells retain a great plasticity, which allows adaptation to increased workload, caused either by pathological or physiological stimuli, with hypertrophic growth.

Depending on the type, strength and duration of stimuli, cardiac hypertrophy may classify as ***physiologic*** or ***pathologic***.

The former is characterized by normal or enhanced contractile function coupled with normal architecture and organization of cardiac structure[88]. The latter, contrarily, is characterized by CM death and fibrotic remodelling, resulting in reduced systolic and diastolic function, which eventually progress towards HF. The trigger events of remodelling are mechanical stress and neurohumoral stimulation that, combined, determine cellular responses including modulation of protein synthesis, gene expression and cell metabolism, which, altogether, orchestrate the development and progression of cardiac hypertrophy[89-91].

Hypertrophic remodelling may proceed with the deposition of new sarcomeres in series (eccentric remodelling) or parallel (concentric remodelling) (fig.5), reflecting on the LV volume, which increases or decreases, respectively.

Eccentric remodelling occurs in a context of volume overload and non-pathological eccentric hypertrophy shows increased ventricular volume with a coordinated growth in myocardial wall and septal thickness. In this condition, CMs grow both in length and width. Pathologic eccentric hypertrophy may be the consequence of post-ischemic or congenital dilated cardiomyopathies, and at the cellular level is characterize by increase in CM length and cell death.

Concentric hypertrophy determines reduced LV dimension, consequent to an increase in ventricular and septal wall thickness. CMs typically grow in thickness more than in length[90]. This condition may develop both in pathologic conditions, such as hypertension or valvular stenosis, and in non-pathologic conditions, such as particular kinds of physical exercise[92].

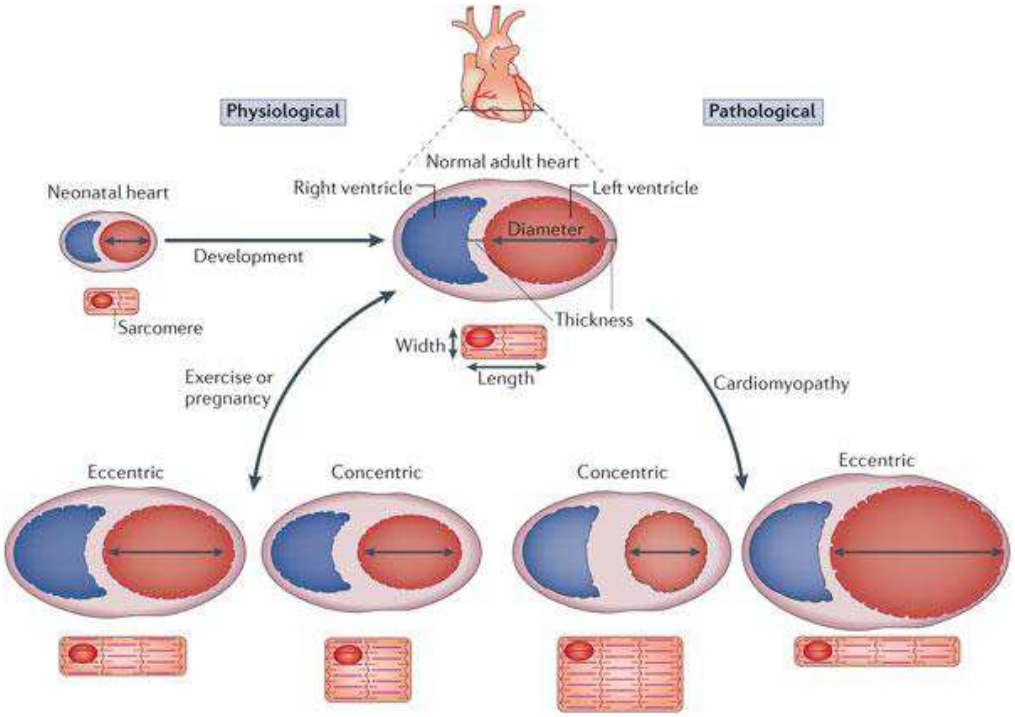

Figure 5. Cardiac hypertrophy geometries[90].

Physiologic cardiac hypertrophy

Physiologic cardiac hypertrophy is responsible for normal cardiac growth from birth to adulthood (process known as postnatal hypertrophy, a critical feature of cardiac postnatal development). Once fully developed, the heart can still physiologically grow in size: examples are the maternal cardiac hypertrophy during pregnancy, or the exercise-induced growth in athletes subjected to extreme and/or repetitive exercise.

Physiologic hypertrophy occurring in the adulthood is characterized by mild heart growth, consisting in 10-20% increase in heart weight/body weight ratio. In this condition, remodelling is fully reversible and, importantly, cardiac function is preserved or enhanced, to sustain increased perfusional demand: in the case of athlete's heart, echocardiography analyses showed improved systolic and diastolic function [93]. In conclusion, physiologic hypertrophy is likely to be harmless, and perhaps even beneficial, in healthy individuals, although pre-existing conditions, such as inherited cardiomyopathies, arrhythmogenic channelopathies or angiogenic imbalance, can promote disease and premature death in athletes and pregnant women[94,95].

In parallel to CM growth, enhancement of angiogenesis occurs in physiologic hypertrophy, to increase blood flow and myocardial supply of oxygen and nutrients to

sustain the higher energy consumption of enlarged cells[96]. In addition, CMs undergone physiologic hypertrophy show elevated efficiency in substrate utilization and ATP production rates through mitochondrial biogenesis and enhanced TCA cycle function[97,98].

The definition of physiologic hypertrophy relies on cardiac function and on the absence of markers of maladaptive cardiac remodelling, including the induction of the fetal gene programme[99,92], interstitial or replacement fibrosis, myofibroblast activation or inflammatory responses[92].

The triggers driving physiologic remodelling include biochemical signals and stretch-sensitive stimuli, which converge on complex and finely regulated intracellular signal transduction pathways, responsible for nuclear gene expression and in a wider context for the increase in protein synthesis. Among these pathways there are: PI3K-PTEN[100]; mTOR[101]; C/EBPβ[102]; ERK1/2[103,104]; AKT[32,34,90] (see fig.6). This latter, especially, will be discussed later (see *Results 3.2.11*).

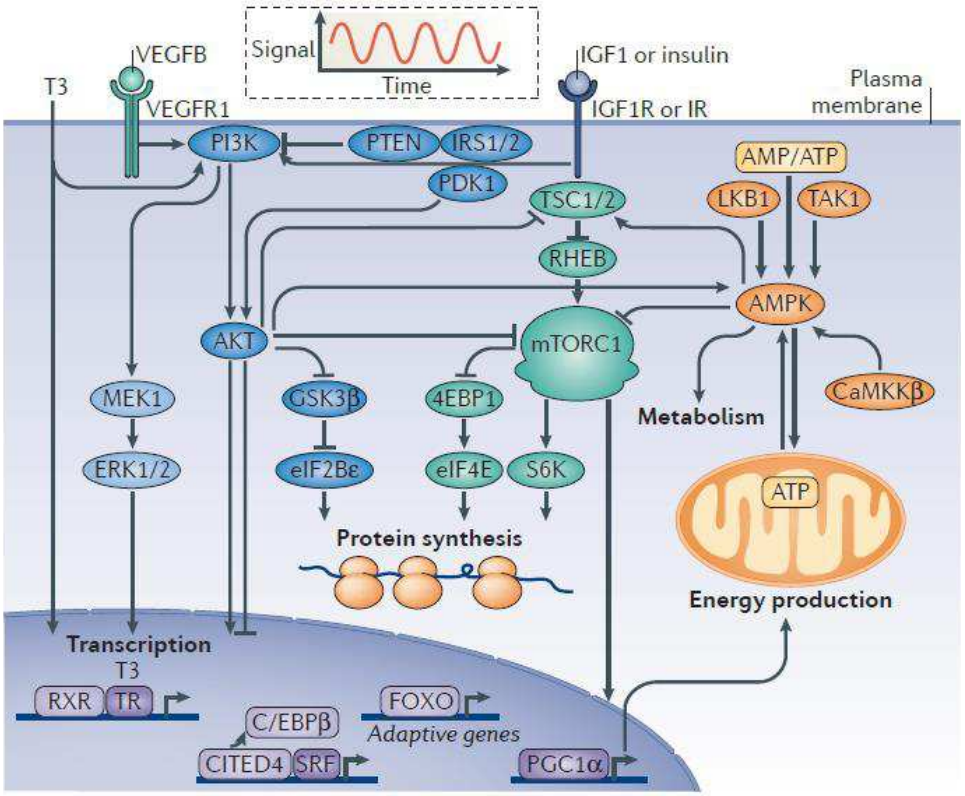

Figure 6. Signalling pathways involved in physiologic hypertrophy[90].

Pathologic cardiac hypertrophy.

Pathologic hypertrophy defines the myocardial remodelling elicited by adverse extrinsic and intrinsic stimuli, including conditions causing pressure-overload, e.g. outflow obstructions such as aortic stenosis or systemic hypertension; or volume overload, e.g.

aortic valve regurgitation. Additionally, other cardiac diseases, such as ischemia, myocardial infarction, atrial fibrillation, may be extrinsic pro-hypertrophic stimuli, as well as genetic mutations e.g. in sarcomeric proteins, causing familial myocardial hypertrophy.

Initially, hypertrophic growth is an adaptive response to maintain cardiac function: the enlargement of CMs and the formation of new sarcomeres aim to normalize wall stress and permit normal cardiac function at rest. This initial phase is clinically known as "compensated hypertrophy". However, opposite to the physiologic condition, the overloaded myocardium cannot maintain compensation and is destined to the progressive and irreversible decline of performance. This second phase, typical of pathologic hypertrophy, is referred as "maladaptive" remodelling, and characterizes the transition to HF, an end-stage condition in which the heart cannot sustain the metabolic demand of the organism. It is well established that pathologic hypertrophy is accompanied by alterations in Ca^{2+} handling, metabolism, increased cell death, fibrosis and impaired angiogenesis, but the molecular mechanisms responsible for the adaptive-to-maladaptive remodelling transition are up to date not fully understood.

In the failing heart, Ca^{2+} handling abnormalities contribute to contractile dysfunction[105]: impaired SERCA2a activity, caused from both the reduction of its expression and increased PLB phosphorylation, leads to reduction in SR Ca^{2+} load[106,107]. In addition, increased SR Ca^{2+} leak, through dysfunctional RyR2 (oxidized or hyperphosphorylated, as observed in human HF[108]), contributes to emptying the SR, worsening contractile dysfunction. Moreover, "leaky" RyR2 elevates cytosolic [Ca^{2+}], thus increasing incidence of arrhythmias[109,110]. Alterations in the complex cytoskeletal architecture impact on Ca^{2+} handling in failing CMs: T-tubules dysruption, occurring in HF, determines mislocalization of LTCCs, with consequent reduction in the efficacy of CICR[111,112].

Pathologic cardiac hypertrophy is associated with a metabolic change phenomenon known as "substrate switch", whereby CMs decrease the oxidation of fatty acids, favouring glucose utilization[113]. This change in substrate utilization is energetically unfavourable; given the different amount ATP produced by phosphorylative oxidation of fatty acids *vs.* glucose oxidation. In addition glucose oxidation is decreased because of uncoupling between glycolysis and glucose oxidation[114,115]. The net result of the uncoupling is a severe limitation in acetyl-coA availability for the TCA cycle to sustain

an adequate ATP production. The metabolic switch, from fatty acids to glucose, is thought to be more favourable in terms of oxygen consumption: indeed, each mole of glucose needs 6 moles of O_2, against 23 mol of O_2 to oxidize 1 mol of palmitate. Such oxygen-saving metabolic modification is important in the hypertrophic myocardial wall in which the increased thickness determines a situation of chronic hypoxia[116]. However, the increased energy demand during pathologic hypertrophy, not met by increased ATP production, causes the depletion of energy reserve compound, such as phosphocreatine (PCr)[117].

The chronic state of hypoxia, experienced by decompensating hypertrophic myocardium, is also determined by inadequate angiogenesis[118]. A correct supply of oxygen and nutrients is critical for myocardial hypertrophic adaptation, since angiogenesis disruption triggers adaptive-to-maladaptive transition[118,119] and, conversely, its stimulation during pressure overload prevents decompensation[116]. At a molecular level, the short action of Akt has been proposed as a beneficial effector for angiogenesis in myocardial hypertrophy[118].

Chronic hypoxia is one of the main causes of the cellular death observed in myocardial pathologic remodelling. As said before, CMs are terminally differentiated and thus unable to proliferate: it follows that dead CMs cannot be replaced by newly formed cells, but are replaced by fibrotic scars (see fig. 7). These non-cellular structures, composed by extra-cellular matrix (ECM) components, are the result of cardiac fibroblasts activation. Cardiac fibroblasts, the most prevalent non-myocyte cell of myocardium, are deputed to ECM synthesis and homeostasis, thus providing a functional mechanical and electrical scaffold for cardiac contraction[120]. During pathologic hypertrophy, a variety of stimuli are known to activate fibroblast, which replicate and trans-differentiate into myofibroblasts. The net result of this is abnormal collagen deposition in myocardial interstitium and fibrotic remodelling. Myocardial fibrosis is generally divided in “replacement fibrosis” or “interstitial fibrosis”: while the first event is triggered by CM death, and fibrotic scars serve as “patches” to fix the inhomogeneity in myocardial structure; the latter is due to aberrant cardiac fibroblast activation and myofibroblasts trans-differentiation between the CMs. In both cases, fibrotic scars do not conduct electric signals, hampering myocardial synchronous contraction and thereby constituting a pro-arrhythmogenic substrate[121].

Cardiac fibroblasts are not the only non-myocyte cellular population involved in pathologic hypertrophy: inflammatory cells, such as macrophages, are recruited at the level of injured myocardium, and contribute to the impending maladaptation. Several studies have reported increased levels, in failing hearts, of pro-inflammatory cytokines such as TNF-α, Toll-like receptors and interleukins, involved in contractile impairment, oxidative stress and fibrosis[33,122,123]. Interestingly, recent studies suggest an adaptive role for early short-term myocardial inflammation[123] although the chronic phenomenon is considered detrimental[124].

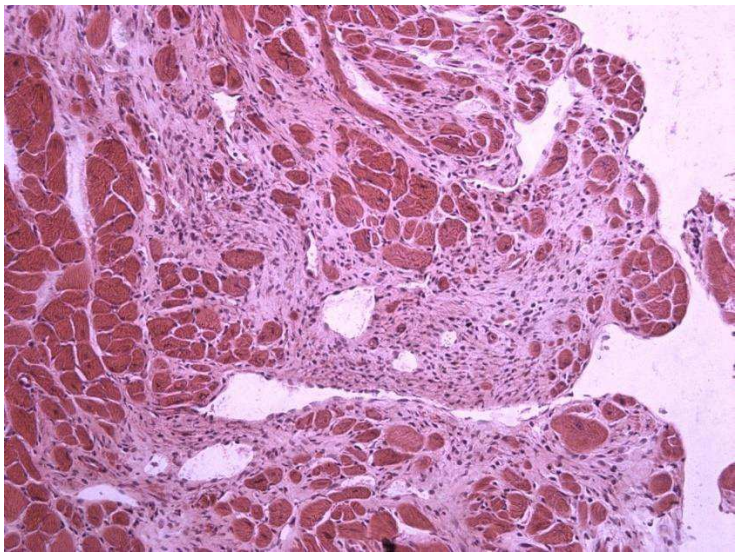

Figure 7. Fibrosis occurring in the myocardium of pressure-overloaded mice.

Myocardial maladaptation is accompanied by the re-induction of fetal genes not usually expressed by adult heart: increased transcript levels of atrial natriuretic peptide (ANP), B-type natriuretic peptide (BNP), α-skeletal actin have been found, accompanied, in the mouse, by α-to-β myosin switch.

Several molecular pathways have been correlated to pathologic hypertrophy (see fig.8). Signalling via G-protein coupled receptors (GPCR) pathways has been suggested as a main player involved in maladaptation. GPCRs are located in CMs membrane and interact with heterotrimeric G proteins, made up of three subunits: Gα, Gβ, Gγ. Gα includes Gαi, Gαs and Gαq, this latter isoform has been shown to play a major role in hypertrophy. A variety of molecules (e.g. angiotensin II, endothelin-1 and adrenergic agonists) bind to GPCRs, activating downstream signalling proteins, including phospholipase C (PLC), protein kinase A and C (PKA and PKC, respectively) and

mitogen-activated protein kinases (MAPKs)[92]. Interestingly, Gαq has also been associated to pathologic CaMKII signalling, as consequence of increased intracellular Ca^{2+} [27]. Interestingly, the sympathetic component of cardiac autonomic nervous system, leading to adrenergic receptor (AR) activation, has been linked to cardiac hypertrophy. ARs are activated by cathecolamines that relay the well-known "fight-or-flight" response. Chronic activation of β-ARs, especially, has been shown to trigger an initial adaptive mechanism to increased workload, since it increases contractility[125,126]. In time, however, ARs activation results in cardiac dysfunction and HF, associated with desensitization and downregulation of β-ARs[127]. Recent studies suggest that different AR isotypes play distinct roles in the response to pressure overload: β1- AR and β2-AR contribute to cardiac enlargement, α_{1B}-AR and β2-AR contribute to the transition to HF, and α_{1A}-AR may even play a protective role[125,128].

Other intracellular players associated to maladaptive remodelling are Ca^{2+}-dependent protein kinases. Among these, specific isoforms of PKC, such as PKCα and PKCβ, whose expression has been found to be elevated in human failing myocardium[129]. Genetic modulation of PKCα in mouse models, indeed, confirmed its implication in maladaptation: PKCα overexpression resulted in contractile dysfunction, while its deletion prevented this deleterious outcome[130]. Similar results were obtained with PKCβ[131].

Other Ca^{2+}-activated proteins proposed to play a role in development of cardiac hypertrophy and adverse remodelling are calcineurin and CaMKII. Calcineurin is a cytoplasmic phosphatase that, when activated by Ca^{2+}, dephosphorylates important transcription factors, such as NFAT. NFAT (Nuclear factor of activated T cells), when detached from phosphate-residues, migrates into the nucleus where activates pro-hypertrophic pathways, by acting on several hypertrophying genes such as Mef2 and GATAs. Calcineurin activity has been found elevated in hypertrophic and failing human hearts[132] and its genetic deletion in mouse prevented hypertrophic remodelling upon pressure-overload[133].

Ca^{2+}/calmodulin-dependent protein kinase II (CaMKII) is a kinase that, as the name suggests, is activated by high intracellular [Ca^{2+}]. CaMKII is a downstream effector of Gq signalling (which elevates intracellular [Ca^{2+}]) and it has been shown by several studies to

be critically implicated in cardiac remodelling and decompensation. Of the four isoforms (α, β, δ and γ) CaMKIIδ is the most abundantly expressed in the heart and its overexpression induces pathologic hypertrophy leading to HF[134]. Recently, it has been demonstrated that CaMKIIδ plays a role in mitochondrial dysfunction during HF, thus suggesting a CaMKII-mitochondria axis present, at least in pathology, in the heart[135]. Interestingly, the two aforementioned Ca^{2+}-related players, calcineurin and CaMKII, have been suggested to cross-talk during cardiac hypertrophy: the ablation of cardiac CaMKII in a condition of adrenergic-induced remodelling did not prevent cardiac growth, due to calcineurin-NFAT axis, but avoided the following maladaptation; thus suggesting that detrimental effects of calcineurin-NFAT may be due to CaMKII concomitant action[136].

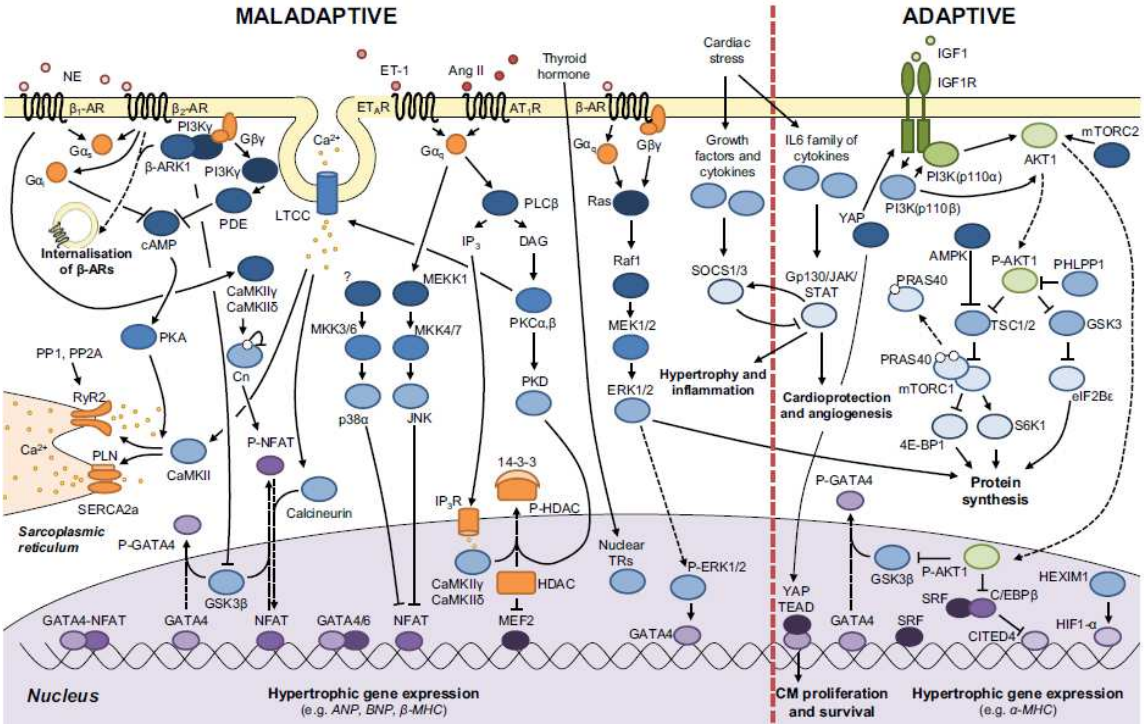

Figure 8. Schematic representation of signalling pathways involved in adaptive and maladaptive remodelling[137].

At the moment, therapies for pathologic hypertrophy and consequent HF are mainly pharmacological. Among these, the most used consist in ACE-inhibitors, β-blockers and AT1-antagonists ("sartans"), assisted by diuretics. The use of current pharmacological agents mentioned above largely slow down the progression of the disease; however, mortality remains high. The need to find new molecular targets drove the attention of researchers to focus on adaptive-to-maladaptive transition, in order to avoid decompensation and tackle HF before its onset. Currently, several approaches have been proposed: modulation of PI3K pathway[138,139], normalization of Ca^{2+} homeostasis by

SERCA2a modulation, (which, *via* exogenous expression, improved clinical signs of HF in patients[140]), interference with GRK2 (G protein-coupled receptor kinase 2, responsible for β-ARs internalization[141]), or inhibition of PKC, *via* ruboxistaurin[142], are few of the pharmacologic approaches being currently tested to treat myocardial hypertrophy.

Alternative approaches to treat maladaptive transition take advantage of RNA-based therapies (by using shRNA, lncRNA, microRNA) or, interestingly, of dietary supplementation (e.g. l-carnitine has been proposed as an useful tool to avoid ATP depletion in HF).

To conclude, mechanisms contributing to the development of cardiac hypertrophy are very complex, and the understanding of the key processes responsible for the transition to HF remains incomplete.

1.8 Mitochondria in cardiac hypertrophy

Given the close relationship between workload and energy demand, any form of cardiac hypertrophy will impact the energy generation by mitochondria, which are the key organelles for cellular ATP production. Apart from generating ~95% of the ATP used by the heart, cardiac mitochondria regulate Ca^{2+} homeostasis, participate in signalling, and in some instances trigger cell death[143].

Mitochondria generate energy by metabolizing dietary carbohydrates, lipids and amino acids. In the inner mitochondrial membrane (IMM), a series of metabolic pathways generate energy through oxidative phosphorylation (OXPHOS), in a process in which electrons are passed along mitochondrial carriers, cytochrome-c and ubiquinone. Finally, at the level of the V complex synthase, electrons reduce oxygen to water. Concomitantly to the electron flow, protons are pumped outside the IMM, thus generating an electrochemical gradient, whose energy is used then to produce ATP by ATP-synthase.
During pathologic cardiac hypertrophy, it has been reported[144] a decreased activity of the respiratory chain complexes, thus reducing maximal oxidative phosphorylation. Moreover, reduced activity of ETC complexes causes a decline in membrane potential, which impacts on ATP synthase activity and, eventually, on ATP production. With the concomitant accumulation of reducing equivalents from the TCA cycle, a dysfunctional

respiratory chain will lead to an impairment of oxidative phosphorylation resulting not only in decreased ATP production and redox imbalance because of changes in NAD^+/NADH, but also to increased levels of intracellular Ca^{2+} and increased generation of ROS. The complex I transfers electrons from NADH to ETC and constitutes the main site of electron leakage, thus significantly contributing to ROS formation. Apart from lower activity of ETC complexes, the mitochondrial defect could be caused by defective protein import into mitochondria and/or their assembly on complexes in the IMM, thus impairing cardiac oxidative phosphorylation[145,146].

Maintenance of normal cardiac contractility is correlated with the energy (ATP) generation inside the CM. Mitochondria normally generate energy by burning fatty acyl-coenzyme-A and pyruvate (fatty acid and carbohydrates metabolism, respectively). The heart is able to efficiently control ATP production by each substrate, which allows for optimized adaptation to changes in oxygen supply, substrate availability, and cardiac workload[147,148]. This reprogrammed substrate utilization is often associated with altered ATP yield: being fatty acids the most efficient in terms of ATP production, these substrates are the most used by adult CMs.

It has been described, however, a metabolic shift in substrate utilization during pathologic cardiac hypertrophy[147,149-151]: indeed, CMs utilize glucose instead of fatty acids. This point is still matter of debate: if there is a general consensus on a general decrease on fatty acids oxidation, a consequent increase in glucose oxidation is largely debated[114,152]. Up to date, researchers point at the possible uncoupling of glycolysis and glucose oxidation during hypertrophy[115,153] as one explanation.

The mechanism by which CMs maintain mitochondrial NADH levels in conditions of decreased glucose oxidation may rely on the introduction of carbo in Krebs cycle through anaplerotic reactions. In fact, hypertrophic hearts display anaplerotic flux into the Krebs cycle, but this flux bypasses the energy-yielding reactions and leads to a reduced energetic efficiency.

Therefore, the reprogrammed metabolism of the hypertrophied heart will impact overall ATP synthesis by oxidative phosphorylation[153] that, in the adult heart, as aforementioned, relies mainly on fatty acid metabolism. As stated above, cardiac tissue undergoes reprogramming, changing its preference for glucose metabolism with a concomitant decrease in fatty acid oxidation.

Many hypothesis on the molecular mechanisms whereby fatty acid oxidation decreases during hypertrophy have been made. The most important relies, in part, in the inhibition

of carnitine-palmitoyl transferase-1 (CPT-1), the rate-limiting enzyme for the entry and oxidation of fatty acids into mitochondria[154]. Additionally, a switch in the isoform of CPT-1, to mature to fetal one, characterised by lower shuttling efficiency, has been suggested[155]. Finally, lower levels of carnitine have been registered in HF, thus contributing to the diminished import of fatty acids into mitochondrial matrix by CPT-1 [156].

Beside ATP production, its correct consumption in the cytosol is important, in order to sustain the cardiac excitation-contraction-relaxation cycle. The adenine nucleotide translocator (ANT) is the protein responsible for the transfer of ATP from mitochondria to the cytosol.

Interestingly, ANT1 has been shown to be crucial for cardiac homeostasis: its deletion determined enlarged hearts[157], while its overexpression attenuates angiotensin-induced cardiac dysfunction[158]. Therefore, disturbances in ANT activity during hypertrophy would induce a lowering of ATP in the cytosol, thus prompting the "energy-starved heart" condition. This theory provides an additional link between the disturbed mitochondrial metabolism (production of ATP) to the mechanical dysfunction of the heart[159,160]. In agreement to this theory, ATP (mostly produced by mitochondria) is critical to compensate for the elevated cardiac demand during hypertrophy. Taking into account the previous findings, it appears that one of the primary contributors to cardiac hypertrophy is the defective ATP production brought by a low rate of fatty acid oxidation coupled with the low yield of ATP produced via glycolysis (see fig.9).

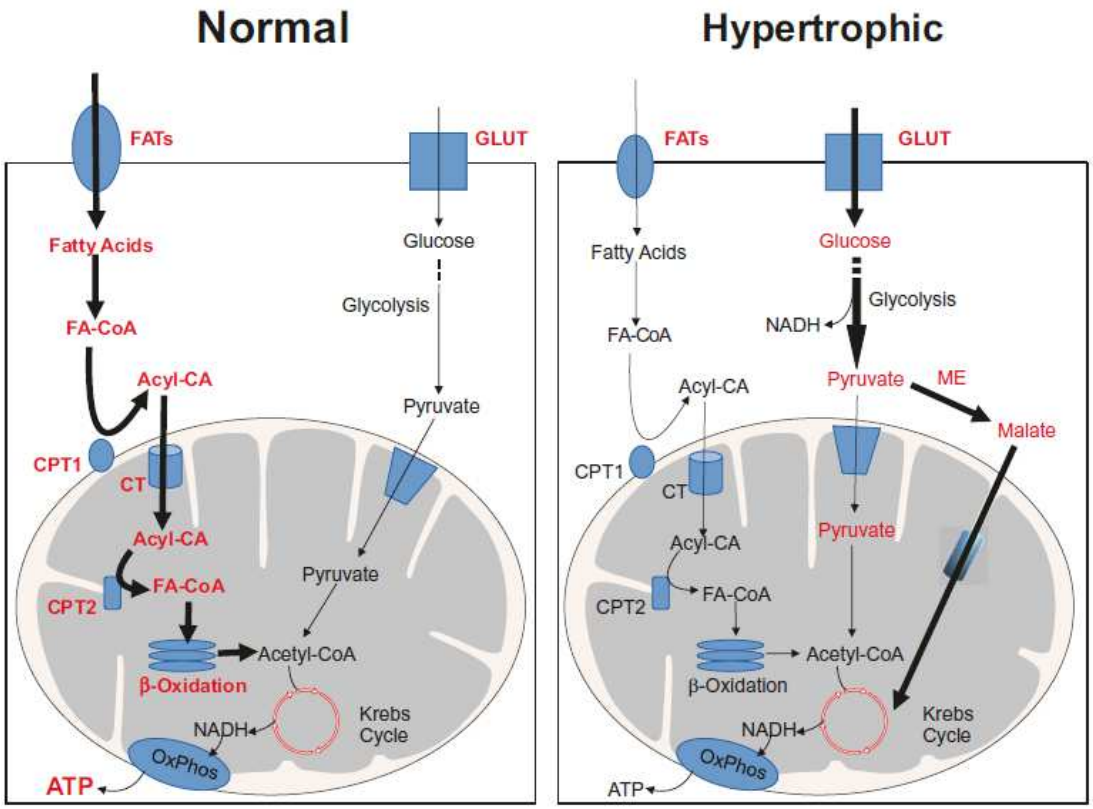

Figure 9. Metabolism in normal and hypertrophic heart[161].

Another important factor that impinges on deficient ATP content is the lowered mitochondrial content due to inappropriate mitogenesis. Mitochondrial biogenesis is a complex process triggered by variations in pre-existing mitochondria, which depends on mitochondrial DNA replication and on the synthesis, import and incorporation of lipids and proteins into the organelles structure. All these processes must be tightly coupled and regulated in order to meet the tissue requirements.

As shown by Spiegelmann and colleagues, the peroxisome proliferator-activated receptor gamma co-activator (PGC1-α) is a master regulator of mitochondrial biogenesis in mammals[162]. It is highly expressed, along with its homologous PGC1-β, in cardiac tissue and other tissues, all characterised by high oxidative capacity[163,164]. Interestingly, PGC-1α and PGC-1β have been found to be transcriptionally repressed during pressure overload-induced cardiac hypertrophy[165,166]. For this reason, the repression of PGC-1α and PGC-1β is regarded an important phenomenon responsible for driving the shift from fatty-acid oxidation towards glucose oxidation, which contributes to the impaired ATP production that characterizes maladaptive remodelling[167].

As aforementioned, mitochondria are the primary source of ROS production: in the organelle, indeed, leak of electrons from ETC (whose activity is decreased in maladaptive remodelling) or NADPH oxidase activity may determine addition of electrons to oxygen.
Mitochondrial damage seems to play a central role in the transition from hypertrophy to HF[168]. The mitochondrial ROS production, in fact, significantly influences the redox state of CMs.
Increased mitochondrial ROS have been found in a variety of cellular models of hypertrophy (stimulation with angiotensin II, endothelin-1, adrenergic agonists, TNF-α, mechanic stretch[169-172] while use of antioxidant compounds inhibited hypertrophic remodelling in pressure-overloaded mice[172,173].
The mitochondrial-isoform of NADPH oxidase, Nox-4 is upregulated during hypertrophy and is an important source of mitochondrial ROS in hypertrophying myocytes[174,175].
Moreover, growing evidence implicates redox-sensitive pathways in the development of cardiac hypertrophy either in response to neurohumoral stimuli or chronic pressure overload[176]. ROS can activate a variety of hypertrophic pathways including PKC[177], the MAPKs[178], p38[179], JNK[180], ERK1/2[181], PI3K[182], Akt[183] and NF-κB[184] (see fig.10).

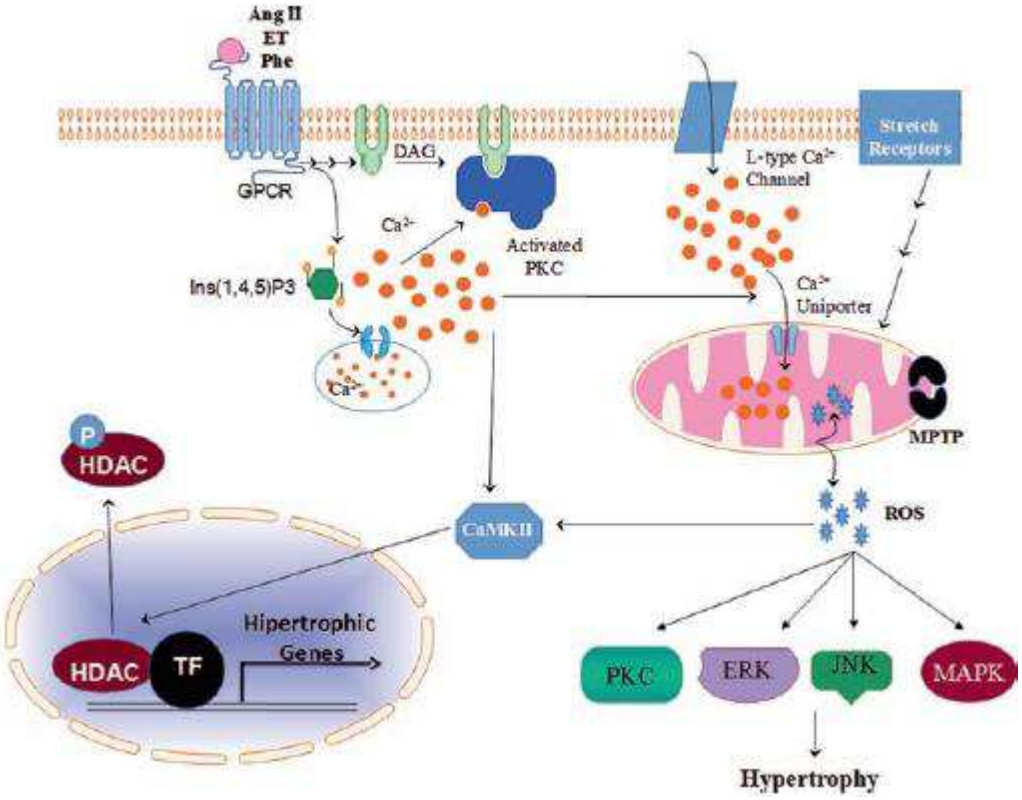

Figure 10. Hypertrophic oxidative signalling[161].

In cardiac hypertrophy, the reported Ca^{2+} accumulation may result in increased Ca^{2+}-dependent activation of intracellular pro-hypertrophic factors[185]. Moreover, the energetic unbalance and the decline in the transduction of protein involved in Ca^{2+} handling, determine a global Ca^{2+} dysregulation, which severely impairs cardiac contractility. In this context, the stress responses that determine the adaptive increased contractility induce amplified mitochondrial Ca^{2+} load and oxidative stress with consequent mitochondrial permeability transition pore (MPTP) opening[186].

Mitochondria are key players of Ca^{2+} signalling in CMs. Juxtaposition with the SR allows the rapid uptake of Ca^{2+} into mitochondria, where it leads to increased NADH production and upregulation of ATP production.

This cytosolic Ca^{2+} overload also determines increased mitochondrial Ca^{2+}, which in turns may trigger mtROS generation and opening of mitochondrial permeability transition pore (MPTP)[187]. This latter phenomenon, known as "permeability switch", determines the release of Ca^{2+} and apoptotic factors into the cytosol, resulting in cellular death and, ultimately, in HF. The concomitant oxidative stress, depletion of adenine nucleotide, and higher [Pi], are known to increase MPTP sensitivity to mitochondrial Ca^{2+} (fig.11).

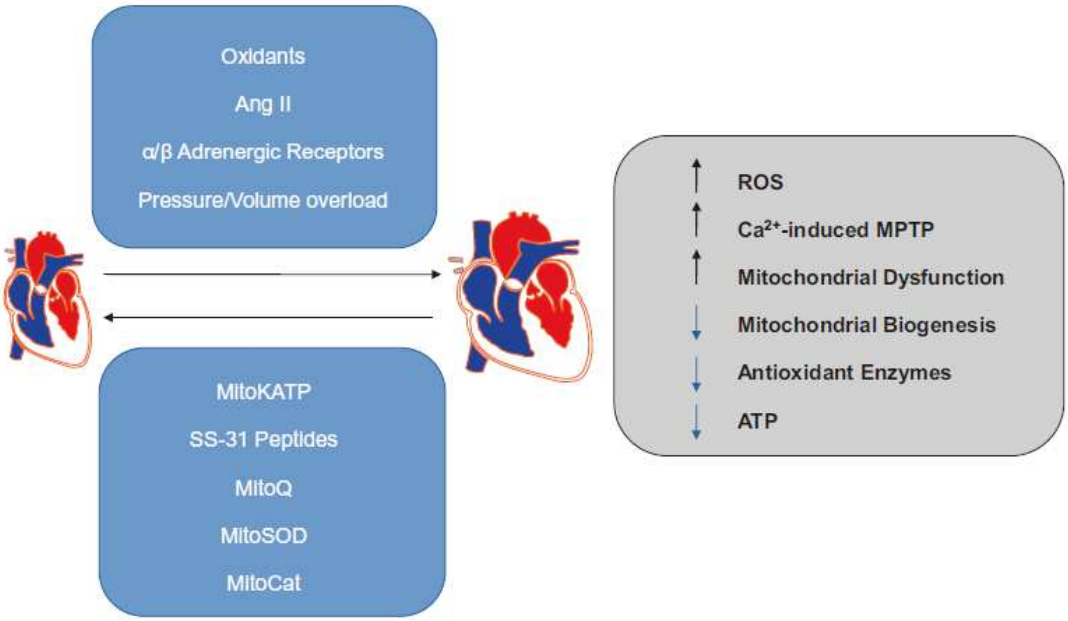

Figure 11. Summary of the mitochondrial dysfunction during cardiac hypertrophy[161].

2. AIMS OF THE THESIS

This thesis is organized as three different but interconnected stories, whose common ground is the study of MCU in the heart.

In detail, the aims of my PhD project were:

Aim 1) to identify the molecular mechanisms involved in the endogenous regulation of MCU;

Aim 2) to determine whether MCU has a role in physiologic and pathologic cardiac remodelling;

Aim 3) to develop an experimental model of cultured cardiomyocytes suited for the *in vitro* characterization of mitochondrial Ca^{2+} dynamics in prolonged observations.

3. RESULTS

The results section is divided into three main chapters, which present both published and unpublished data.

The first chapter, which data were recently published in PNAS[188], comprises the first of the projects covered in this thesis, whose aim was to identify the molecular mechanisms involved in the endogenous regulation of MCU (Aim 1, see *Aim of the thesis*). In *Appendix*, you can find attached the integral paper.

The second and third chapters contain unpublished data. In detail, the chapter "Results – II" (Aim 2, see *Aims of the thesis*) focuses on the role of MCU in cardiomyocyte adaptation to hypertrophic stimuli, a topic approached by using *in vivo* and *in vitro* experimental models. In this chapter, Aim 2 will be assessed (see *Aim of the thesis*). The chapter "Results – III" is more "methodological", and deals with the development of a cellular model of neonatal cardiomyocytes in which, by manipulating the culture conditions, we induced a pronounced maturation towards an adult phenotype (Aim 3, see *Aim of the thesis*).

At the end of each chapter, you can find the relative figures:

- Results 3.1: Content of mitochondrial calcium uniporter (MCU) in cardiomyocytes is regulated by microRNA-1 in physiologic and pathologic hypertrophy. (Fig. 1-8).
- Results 3.2: MCU participates to the myocardial adaptation to hypertrophic stimuli. (Fig. 9-19).
- Results 3.3: *In vitro* maturation of cultured neonatal cardiomyocytes. (Fig. 20-24).

3.1 RESULTS – I

The first part of the results showed in this PhD thesis, regards the identification of novel molecular modulators of MCU cardiomyocyte (CM) protein content. The rationale of this study was to understand whether in different cardiac conditions, whose common denominator was increased ATP demand, MCU mitochondrial density changed, and the molecular mediators responsible for such modulation.

At present, the transcriptional regulation of genes encoding the MCUC subunits is poorly understood, and whether changes in the expression of mitochondrial uniporter proteins take place during cardiac diseases have not been addressed. In intestinal epithelial cells, protein levels of MCU are regulated by the microRNA-25 (miR-25), and alterations in the miR-25/MCU axis are implicated in tumorigenesis[189]. This evidence highlights that post-translational modulation of MCUC protein levels, by microRNAs (miRs), may impact on cell trophism, reflected on the proliferative phenotype in epithelial cells. However, the comprehensive mechanisms underlying the miR role in MCU regulation in the heart remain elusive. MicroRNAs are small, non-coding RNA sequences (18-25 nt) capable of finely tuning the expression of a variety of genes, by interfering with either the mRNA stability or translation of target mRNA[12]. Among the few thousand different miRs identified so far, the miR-1/miR-133/miR-206 cluster, belonging to the same transcriptional units, has been largely recognized for their central regulatory role in muscle biology and are part of the so-called myomiRs, for their muscle-specific expression[190]. Post-translational control of protein expression by miRs has been shown to accompany the profound changes of CMs during post-natal development, and to allow the fully developed myocardium grow, in response to intrinsic or extrinsic hypertrophic stimuli[13].

Here, in light of the housekeeping function of metabolic adaptation during CM remodeling, we sought to determine whether myomiRs, involved in myocardial hypertrophy, could regulate the protein level of MCUC subunits, thus impinging on the molecular architecture and function of the uniporter complex.

3.1.1 MCU is a predicted target of the myomiR miR-1

To determine the potential role of miRs in cardiac MCU regulation, we performed a bioinformatic search using the probability of interaction by target accessibility (PITA) algorithm[191]. Among the microRNAs predicted to target the MCU 3'-untranslated region (UTR), we were intrigued by miR-1 and miR-206, as they belong to the family of the so-called 'myomiRs'. MiR-1 is the most abundant miR in the heart, is highly conserved among species (see Suppl. Fig. 1A in *Appendix*), and has previously been shown to regulate proteins involved in heart development and CM homeostasis[192]. MiR-206, on the other hand, is a skeletal muscle-specific microRNA[193] expressed at almost negligible levels in the heart. Interestingly, no targeting sites on the MCU mRNA were predicted for miR-133, which is co-expressed together with miR-1 by the same transcriptional unit[194,195] (see Suppl. Fig. 1B *in Appendix*). We thus focused on miR-1, which was found to potentially anneal with MCU mRNA in three putative sites, localized at the beginning (mmu: 86-108; hsa: 92-114 – site 1), and the end (mmu: 1706-1728; 1747-1769; hsa: 1780-1802; 1822-1844 – site 2 and 3, respectively) of the 3'UTR (**Fig. 1A**). Notably, the interaction site 1 is predicted also in the rat (rno: 96-118), suggesting strong evolutionary conservation (**Fig. 1B** and Suppl. Fig. 1C in *Appendix*). Given that mitochondrial Ca^{2+} uptake depends on the molecular architecture of the uniporter complex, we additionally searched whether miR-1 could potentially target other constituents of the complex. Interestingly, no targeting sites were found for MCUb, MICU2 and EMRE, and just a very weak-scored site resulted for the 3'UTR of the gatekeeper protein MICU1 (see Suppl. Fig. 1D in *Appendix*). We thus decided to keep our focus on the potential post-transcriptional regulation of the pore forming subunit MCU by miR-1, whose mechanism appears evolutionary conserved from rodents to humans.

3.1.2 MiR-1 represses MCU translation and reduces mitochondrial Ca^{2+} uptake in cardiomyocytes

To validate the *in silico* prediction, we developed a luciferase assay in which the Luc gene, fused to the MCU 3'UTR (psiCHECK-3'UTR-MCU), was transfected into HEK293T cells co-expressing miR-1 at increasing copy number. Consistent with the bioinformatic predictions, expression of miR-1 caused a dose-dependent reduction in

luciferase activity, while no effects were detected in cells transfected with the MCU-unrelated miR-199a, which served as negative control (**Fig. 1C**). To further our molecular insight, we constructed three mutant vectors (psi-CHECK.3'UTR-MCU-mut), each harbouring individual site-specific mutations to selectively ablate the predicted base pairing of miR-1 with its seed sequences in the 3'UTR-MCU sites. Notably, mutations of either site 1 or site 2 significantly blunted miR-1 dependent repression of luciferase activity (**Fig. 1D,E**), while no effects were obtained when site 3 was mutated (**Fig. 1F**). Collectively, these data demonstrate that miR-1 functionally interacts with the MCU 3'UTR, by specifically targeting both site 1 and site 2.

Interestingly, miR-1 targeting of MCU was confirmed by luciferase assay in HL-1 CMs (**Fig. 2A**). In such cardiac cell line, overexpression of miR-1 caused a marked reduction in MCU protein content, with no changes in the weakly predicted target MICU1, thus demonstrating that miR-1 is a selective negative regulator of MCU (**Fig. 2B**). In addition, such effect was not accompanied by changes in mRNA levels (**Fig. 2C**), indicating that miR-1 operates exclusively at the translational level, with no effects on mRNA stability. To functionally probe the effect of miR-1 on mitochondrial Ca^{2+} uptake, we monitored Ca^{2+} dynamics using fluorescence imaging in neonatal rat CMs transfected with the cytosolic or mitochondrial sensors CaMeleon D3cpV or 4mt-D3cpV, respectively. In cultured CMs, electrical pacing triggered rapid oscillations in cytoplasmic Ca^{2+} (see Suppl. Fig. 2 in *Appendix*) which caused its entry into the mitochondrial matrix. Consistent with the effects of miR-1 on MCU, its overexpression significantly reduced the amplitude of the steady-state mitochondrial Ca^{2+} level during pacing (CTRL: $\Delta R/R_0$: 42 ± 3 *vs.* miR-1: CTRL: $\Delta R/R_0$: 27 ± 3, in %) (**Fig. 3A-C**), with no significant effects on cytoplasmic Ca^{2+} dynamics (**Fig. 3D, E**)[196,197]. Altogether, these data support that, by reducing MCU levels, miR-1 directly affects the maximal capacity of mitochondria to take up Ca^{2+} during contraction. These results broaden the list of functions attributed to miR-1, extending its impact beyond the regulation of the hypertrophic gene program and excitation-contraction coupling, to include metabolism and ATP production, altogether processes deemed to change simultaneously during hypertrophic adaptation of CMs. On this basis, we next investigated the possibility that MCU levels may be modulated in hypertrophic conditions previously associated to changes in miR-1, elicited in response to either intrinsic or extrinsic factors, including: ***i)*** post-natal development, ***ii)*** moderate exercise and ***iii)*** pressure overload.

To test these hypotheses, we used molecular biology and biochemistry approaches to compare the miR-1 and MCU levels in a collection of tissue samples from human and experimental hearts before and after the onset of cardiac hypertrophy.

3.1.3 The miR-1/MCU axis during postnatal cardiac growth

Hypertrophic heart growth occurs throughout post-natal development to maintain cardiac size and performance adequate to the increasing perfusional demand of the body. In parallel to the increase in cell dimensions, post-natal CM growth is underlain by pronounced reshaping of the cellular architecture[198,199]. Such remodeling includes maturation of the sarcoplasmic reticulum (SR) and, remarkably, redistribution of mitochondria into the confines of the high-Ca^{2+} microdomains generated, during contraction, at the interface with the SR[199,200]. Whether the intrinsic properties of the Ca^{2+} uniporter complex adapt to the modified mitochondrial environment, along with CM maturation, has not been investigated. It has been demonstrated[201,202], and confirmed by us, that miR-1 levels increase during postnatal cardiac growth (**Fig. 4A**). In line with the role of miR-1 on MCU translation, mitochondrial MCU protein density decreased in adult, compared to neonatal hearts (3 mo. *vs*. P7 mice) (**Fig. 4B**), with no changes in its mRNA level (**Fig. 4C**). Notably, we did not observe significant changes in the transcriptional levels of the other MCUC components, with the exception of MCUb whose expression significantly increases during postnatal development (**Fig. 4C**). Remarkably, the reciprocal changes in miR-1 and MCU protein levels were similar during postnatal cardiac development in humans, as shown by the comparison of miR-1 and MCU levels in ventricular biopsies from neonatal and adult human hearts (**Fig. 4D-E**). Additionally, no changes in the expression of other human genes encoding the members of the uniporter complex, including MCUb, were detected (**Fig. 4F**). Taken together, these data demonstrate that changes in the molecular composition of the mitochondrial Ca^{2+} uptake complex, likely driven by the miR-1/MCU axis, take part to the plethora of structural and functional modifications of post-natal CM maturation.

3.1.4 The miR-1/MCU axis in physiologic and pathologic cardiac hypertrophy

Being an example of post-mitotic tissue, the adult myocardium is incapable of repairing tissue damage through cell division[203-205]. While such latter concept holds true, abundant clinical and preclinical evidence has demonstrated that, on the contrary, the heart is indeed highly dynamic, and fully developed CMs can grow further in response to stresses, such as increased mechanical workload. Differences in the nature, intensity and duration of the hypertrophying stimuli determine whether cardiac remodeling would progress towards either the so-called "physiologic" (i.e., in the athletic heart), or "pathologic" hypertrophy (i.e., in pressure overload), the latter resulting, with time, in cardiac dysfunction, heart failure (HF) and death. Although the cellular and clinical phenotypes of the two conditions are very different, the common tenet is that, in the initial phases, they share the same adaptive mechanisms, including increased sarcomeric deposition and enhanced/preserved contractility, both of which require increased ATP supply[206]. It follows that the regulation of mitochondrial function is a critical process for ATP production to match energetic demand during cell growth. With the notion that miR-1 is a repressor of the hypertrophic gene program[13,201], and based on our data showing the effect of miR-1 on the MCU levels, we analyzed in murine and human hearts, whether distinctive changes in the uniporter architecture may depend on physiologic *vs.* pathologic stimuli. To this end, two groups of mice were subjected to chronic running exercise and aortic coarctation, respectively.

The exercise protocol consisted in repeated running bouts of one hour/day for eight consecutive weeks[35], which caused an elevation in the maximal oxygen consumption (VO_{2max}), consistent with an increase in contractile performance, and accompanied, as expected, by a slight elevation in cardiac mass (heart weight/body weight, HW/BW, exercise: 5.5 ± 0.3 *vs.* sedentary: 4.6 ± 0.2, $*10^{-3}$) CM cross-sectional area (CM areas: exercise: 231 ± 6 *vs.* sedentary: 201 ± 5, in μm^2) (**Fig. 5A-D**). Exercised heart did not display changes in myocardial histology nor re-activation of the fetal gene program (**Fig. 5E** and Suppl. Fig. 3A in *Appendix*). In striking difference with the skeletal muscle, exercise dependent mitochondrial biogenesis was negligible in the heart. As previously demonstrated, miR-1 expression decreased in extracts from exercised hearts (**Fig. 5F**) and, in agreement with our findings (above), MCU protein levels increased (**Fig. 5G**). No

changes in the transcriptional level of the complex members genes were observed (**Fig. 5H**).

We thus analyzed the uniporter complex biochemistry in hearts harvested one week after the induction of ventricular pressure overload following trans-aortic constriction (TAC) surgery[207]. This condition corresponds to the initial, compensatory response to a hypertrophying stimulus and, in fact, elicits a modest CM growth with no contractile failure, and only limited signs of tissue damage (focal fibrosis) (**Fig. 6A-E**). Contrary to exercise hypertrophy, TAC hearts showed a significant increase in the expression levels of stress markers (see Suppl. Fig. 3B in *Appendix*). The changes in miR-1 and MCU were similar to those observed in hearts from exercised mice, with decreased miR-1 (**Fig. 6F**) and, accordingly, increased MCU content (**Fig. 6G**). These results suggest that, regardless of the nature of the hypertrophic stimulus (physiologic or pathologic), the initial CM adaptation to increased heart work is characterized by similar enhancement in the availability of uniporter-forming MCU molecules. Interestingly, while the transcriptional level of the MCU-related partners did not vary after exercise, in TAC hearts mRNA of the pore-inhibiting subunit MCUb was doubled compared to sham operated mice (**Fig. 6H**). To determine whether the reciprocal miR-1 and MCU modulation occurred in a clinically relevant model of cardiac hypertrophy, we analyzed human heart biopsies obtained from healthy subjects and patients (age: 59 ± 13 years) with myocardial hypertrophy due to aortic stenosis, undergone valve replacement surgery. This latter patient cohort had conserved ejection fraction (EF > 55%), and the expression of the fetal gene program only trended to be elevated (see Suppl. Fig. 4 in *Appendix*). Similar to the data obtained in the animal model, miR-1 level was generally decreased (**Fig. 7A**) and consistently, MCU content was augmented (**Fig. 7B**). Congruous with the results obtained in post-natal development of human hearts, no changes in the expression level of the other MCUC genes were detected (**Fig. 7C**).

3.1.5 The β-adrenergic receptor system participates to control the miR-1/MCU axis

Taken altogether, the results presented above demonstrate that reciprocal fluctuations of the miR-1 and MCU levels occur during physiologic (i.e. postnatal and exercise) and pathologic (i.e. pressure overload) cardiac hypertrophy, in both experimental models and

human hearts. Given that similar changes in the miR1/MCU axis occur, in the fully developed heart, upon exercise and in the initial phases of pathologic hypertrophy (**Fig. 8A**), we made the hypothesis that a common regulatory mechanism may exist. We thus focused on the cardiac β-AR system, which is the primary physiologic mechanism engaged in response to increased heart load, a condition in common between exercise and TAC-induced pressure overload. Activation of β-AR signaling leads to enhancement of cytosolic Ca^{2+} oscillations and mitochondrial Ca^{2+} uptake[208-210], and is involved in the parallel activation of pathways controlling cell growth, such as the Akt-FOXO cascade[24]. Interestingly, miR-1 expression has been shown to depend on FOXO3a[15], suggesting that in conditions of chronic β-AR activation, the blockade of FOXO3a nuclear translocation may inhibit miR-1 increase and, consequently, its repression of MCU translation. On these bases, we treated mice undergone TAC, a condition associated with increased cardiac sympathetic neuron activity, with the β1-blocker metoprolol. The efficacy of the treatment was confirmed by the inhibition of the TAC-induced reactivation of fetal genes (see Suppl. Fig.5 in *Appendix*). Interestingly, metoprolol treatment was not accompanied by miR-1 repression (**Fig. 8B**) and, accordingly, this prevented the increase in MCU protein content, which occurred in vehicle-treated, TAC mice (**Fig. 8C**). In addition, metoprolol treatment blunted the induction of MCUb transcription, presumably through a miR-1 independent mechanism, as the MCUb transcript is not targeted by miR-1 (**Fig. 8D**).

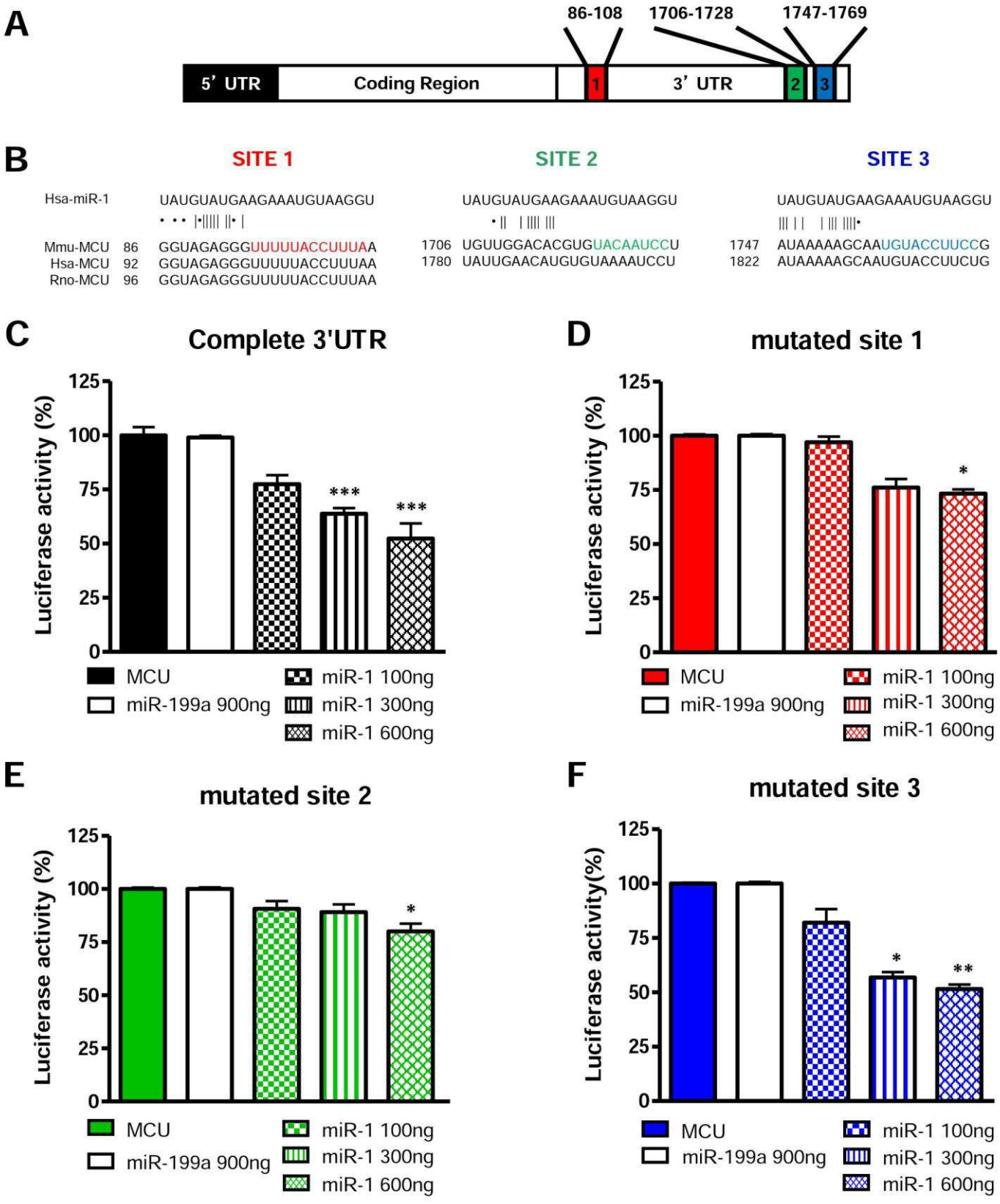

Fig. 1. Bioinformatic prediction and luciferase validation of miR-1 targeting of MCU mRNA. (A) Predicted interaction sites between miR-1 and the murine MCU 3'UTR region, revealing the three seed regions labeled 1-3. **(B)** Alignment of the miR-1 sequence with the seed regions in A, in mouse (Mmu), human (Hsa) and rat (Rno) showing that the seed region 1 is conserved among all these species. In the alignment, dots represent wobble pairs and lines represent base pairing. **(C-F)** Assessment of the effects of increasing doses of miR-1 on the bioluminescence of HEK293T cells transfected with a plasmid encoding Luciferase-flanking: **(C)** full length MCU 3'UTR, **(D)** site 1 mutant MCU 3' UTR, **(E)** site 2 mutant MCU 3' UTR, **(F)** site 3 mutant MCU 3' UTR. The non-interacting miR-199a was used as negative control. Luminescence values are normalized to those detected in cells transfected with the Luc construct, but not treated with miR. (*, $p<0.05$; **, $p<0.01$; ***, $p<0.001$; n=6 independent experiments).

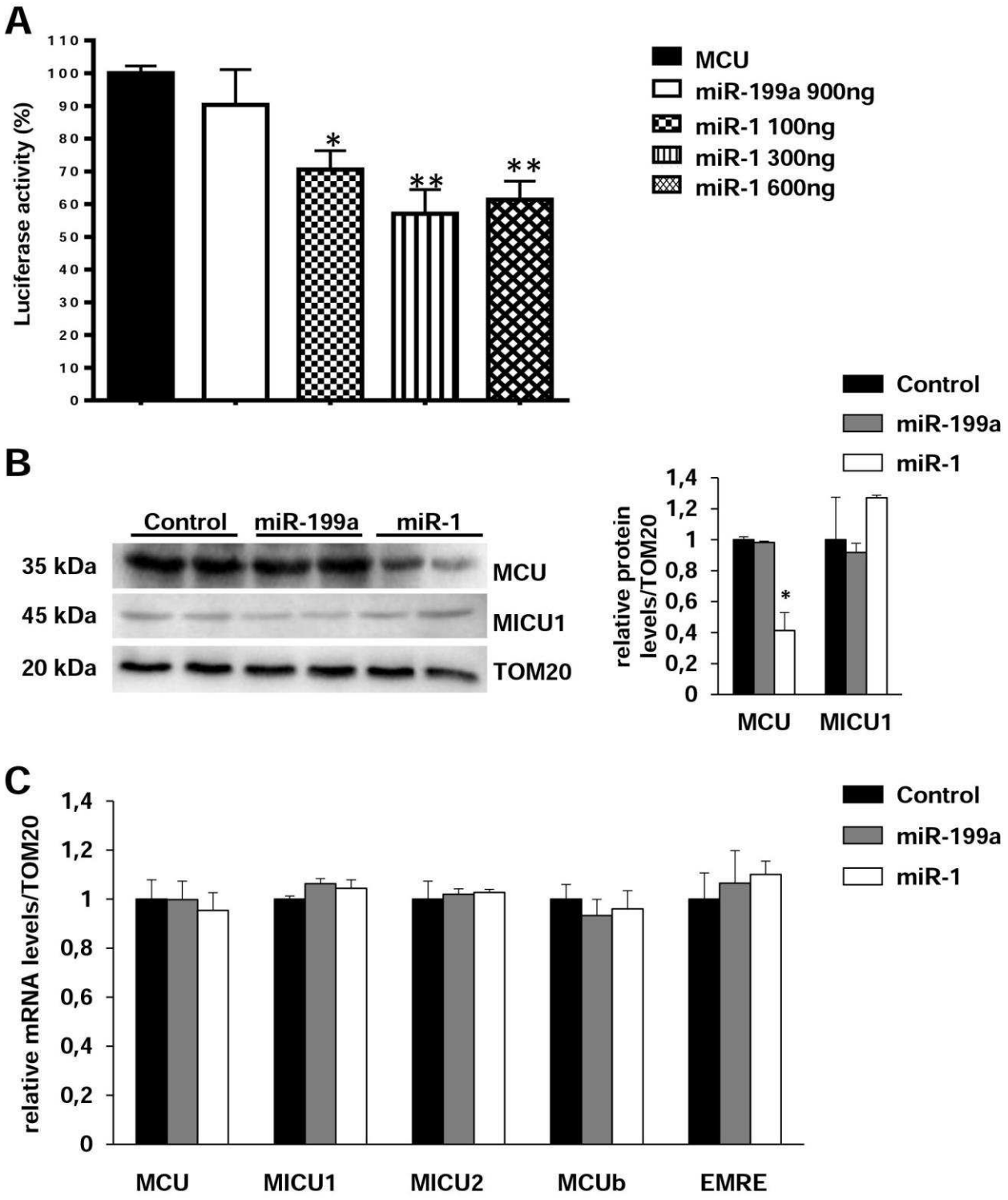

Fig. 2. *In vitro* regulation of MCU by miR-1 in HL1 cardiomyocytes. **(A)** Assessment of the effects of increasing doses of miR-1 on the bioluminescence of HL1 cardiomyocytes (CMs) transfected with a plasmid encoding Luciferase-flanking full length MCU 3'UTR. The non-interacting miR-199 was used as negative control. Luminescence values are normalized to those detected in cells transfected with the Luc construct, but not treated with miR. (**, $p<0.01$; ***, $p<0.001$; n=6 independent experiments). **(B)** Western blotting on protein extracts from control, miR-199a and miR-1 overexpressing HL1 CMs (left panel). TOM20 was used as mitochondrial protein loading control. Densitometry (right panel) shows a significant decrease in MCU protein content in miR-1 overexpressing cells. (*, $P<0.05$; n=6 samples for each study group). **(C)** RTqPCR analysis on extracts from control, miR-199 or miR-1 overexpressing HL1 cardiomyocytes. MCU mRNA levels were not affected by miR-1 expression. (n=6 samples for each group). In **(B-C)** miR-199a overexpression was performed as control.

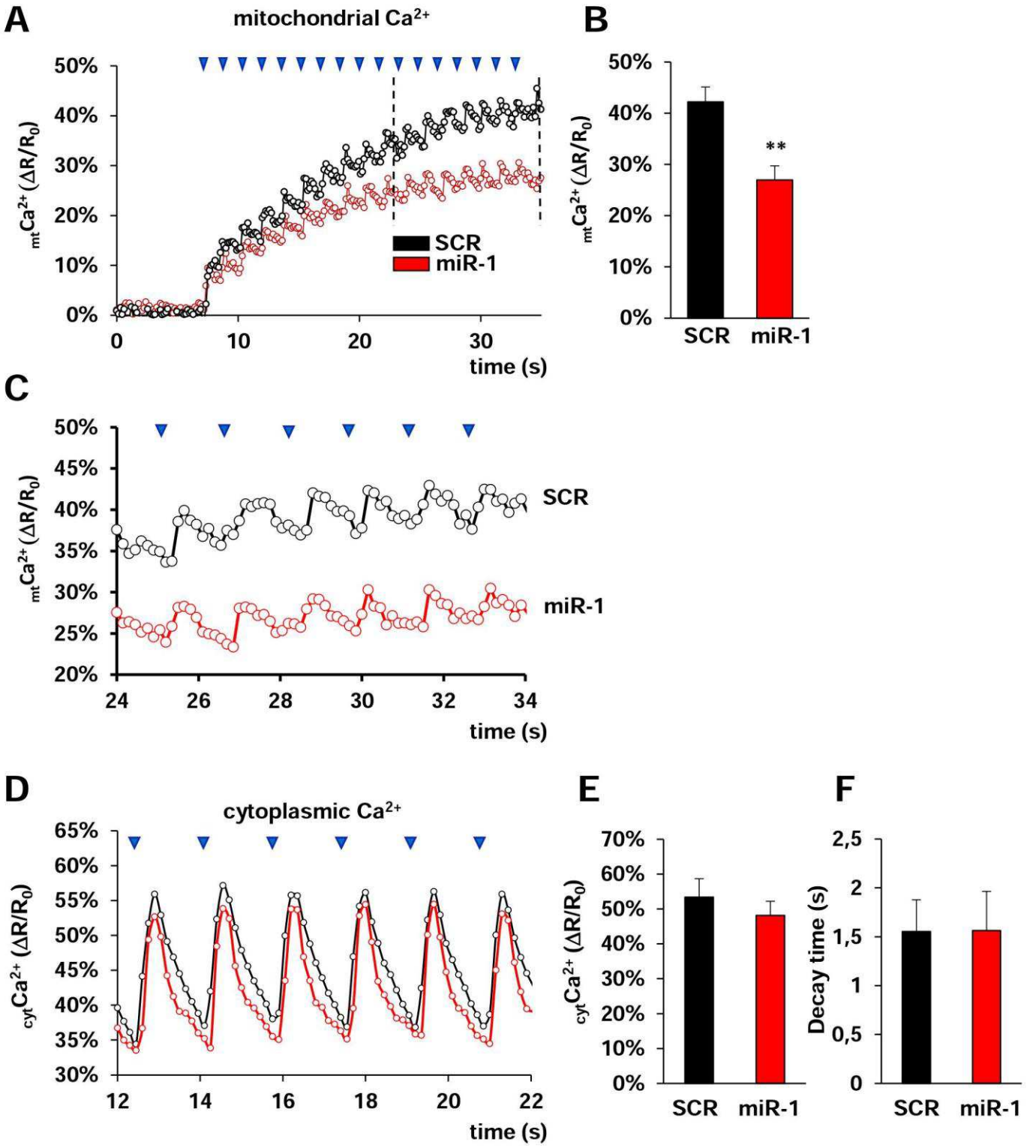

Fig. 3. MiR-1 over-expression reduces mitochondrial Ca^{2+} uptake in cultured neonatal cardiomyocytes. **(A)** Representative traces of mitochondrial Ca^{2+} uptake, measured with 4mt-D3cpV, in control (black trace) and miR-1 overexpressing (red trace) neonatal cardiomyocytes (CMs), electrically paced with field stimulation, at rates highlighted by the arrowheads. **(B)** Amplitude of the average mitochondrial Ca^{2+} level at steady state, in control (scramble, SCR) and miR-1 overexpressing CMs (**, $p<0.01$). (n= 40 CMs per group). **(C)** Magnification of the traces in panel **A**, showing mitochondrial Ca^{2+} uptake at steady state level. **(D)** Representative traces of cytosolic Ca^{2+} transients, measured with D3CPV, in control (black trace) and miR-1 overexpressing (red trace) neonatal CMs, electrically paced with field stimulation. Statistics of the amplitude **(E)** and kinetics **(F)** (decay time) of Ca^{2+} oscillations in miR-1 overexpressing and control cells. (n= 40 CMs per group).

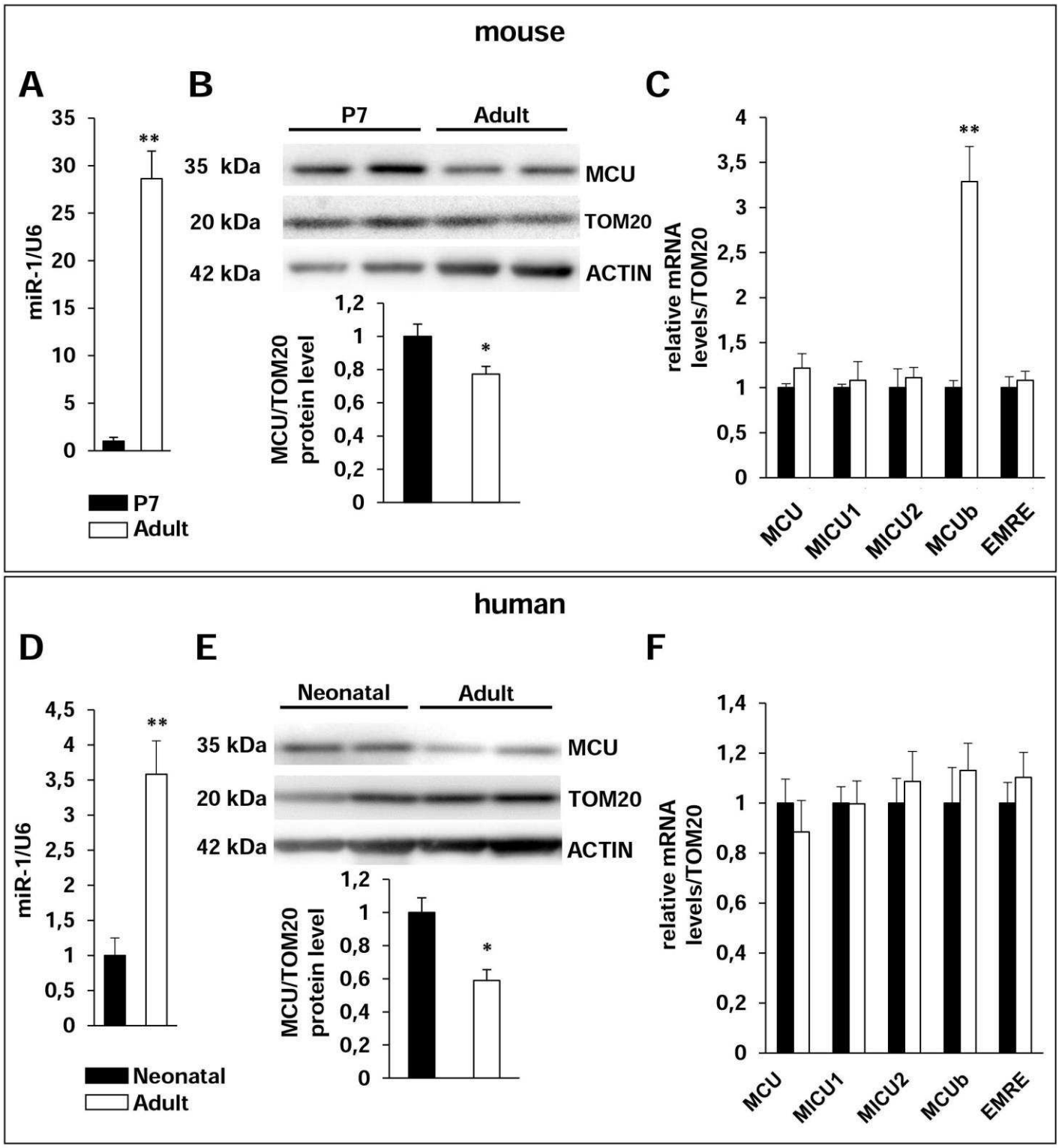

Fig. 4. Changes in mitochondrial MCU density during postnatal growth in mouse and human hearts. (**A**) MiR-1 expression was compared, by RTqPCR analysis, on extracts from neonatal (P7) *vs.* adult (3 mo.) mouse hearts. (n=6 mouse samples for each study group; **, p<0.01). **(B)** Western blotting (WB) on protein extracts from P7 and adult mouse hearts and relative densitometry showing a significant decrease in MCU protein content during postnatal heart development, (n=6 hearts for each study group; *, p<0.05). **(C)** RTqPCR analysis of the molecular components of the MCUC in extracts from P7 and adult mouse hearts (n=6 hearts for each group; **, p<0.01; *, p<0.05). **(D)** RTqPCR analysis of miR-1 expression in extracts from neonatal *vs.* adult human heart samples. (n=4 neonatal and 5 adult human heart samples; **, p<0.01). WB **(E)** and RTqPCR **(F)** on extracts from human heart samples showing mitochondrial MCU density and the expression levels of the molecular components of the uniporter complex in neonatal *vs.* adult subjects (n=6 neonatal and 4 adult heart samples; *, p<0.05). In both **(B)** and **(E)**, immunoreactivity for TOM20 was used as mitochondrial protein loading control, while that for actin was used as a whole-cell protein loading control.

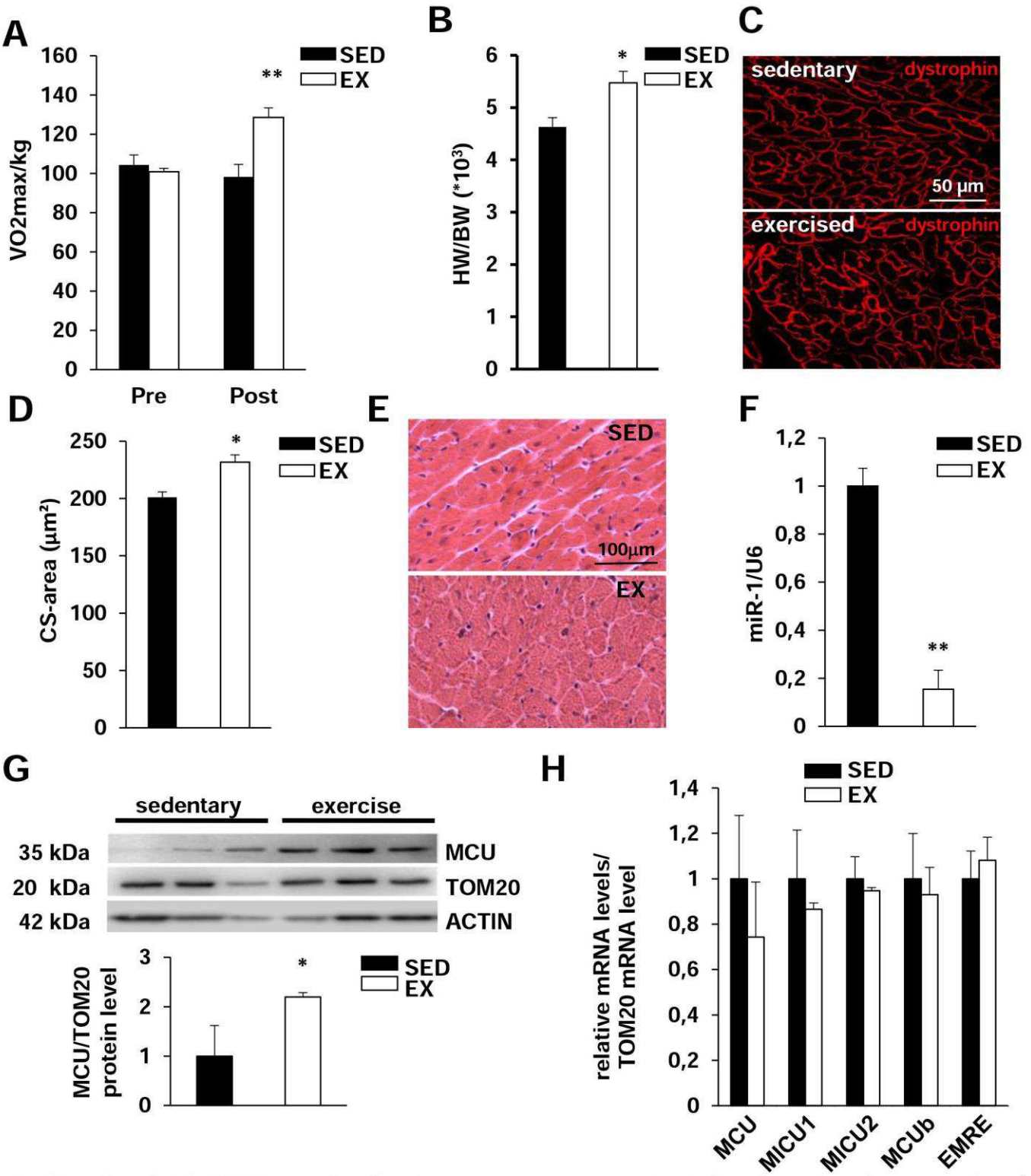

Fig. 5. Mitochondrial MCU protein density increases in exercise-induced cardiac hypertrophy. (A) Maximal oxygen uptake (VO_{2max}) from the sedentary (sed.) and exercised (ex.) mouse cohort before (pre) and after (post) the 8-week high intensity exercise training protocol. (n=6 mice for each study group; **, $p<0.01$). **(B)** Evaluation of Heart Weight-to-Body Weight ratio (HW/BW) in sed. and 8 weeks-ex. mice. (n=6 mice for each group; *, $p<0.05$). **(C)** H/E staining of heart sections from sed and ex. mice. Images are details from the LV showing the integrity of the myocardium. **(D)** Confocal IF analysis of LV sections from sed. and ex. mice, stained with anti-dystrophin. **(E)** Evaluation of LV CM CS areas in sed. *vs.* ex. mouse hearts. (n=500 CMs for each group; *, $p<0.05$). **(F)** MiR-1 expression was compared, by RTqPCR analysis, on LV heart extracts from sed. *vs.* ex. mice. (n=6 hearts for each study group; **, $p<0.01$). **(G)** WB on heart extracts from sed. and ex. mice, and relative densitometry showing an increase in mitochondrial MCU protein content. (n=6 hearts for each study group; **, $p<0.01$). Immunoreactivity for TOM20 was used as mitochondrial protein loading control, while that for actin was used as a whole-cell protein loading control. **(H)** RTqPCR on extracts from sed. *vs.* ex. hearts showing the expression levels of the members of MCUC. (n=6 hearts for each study group).

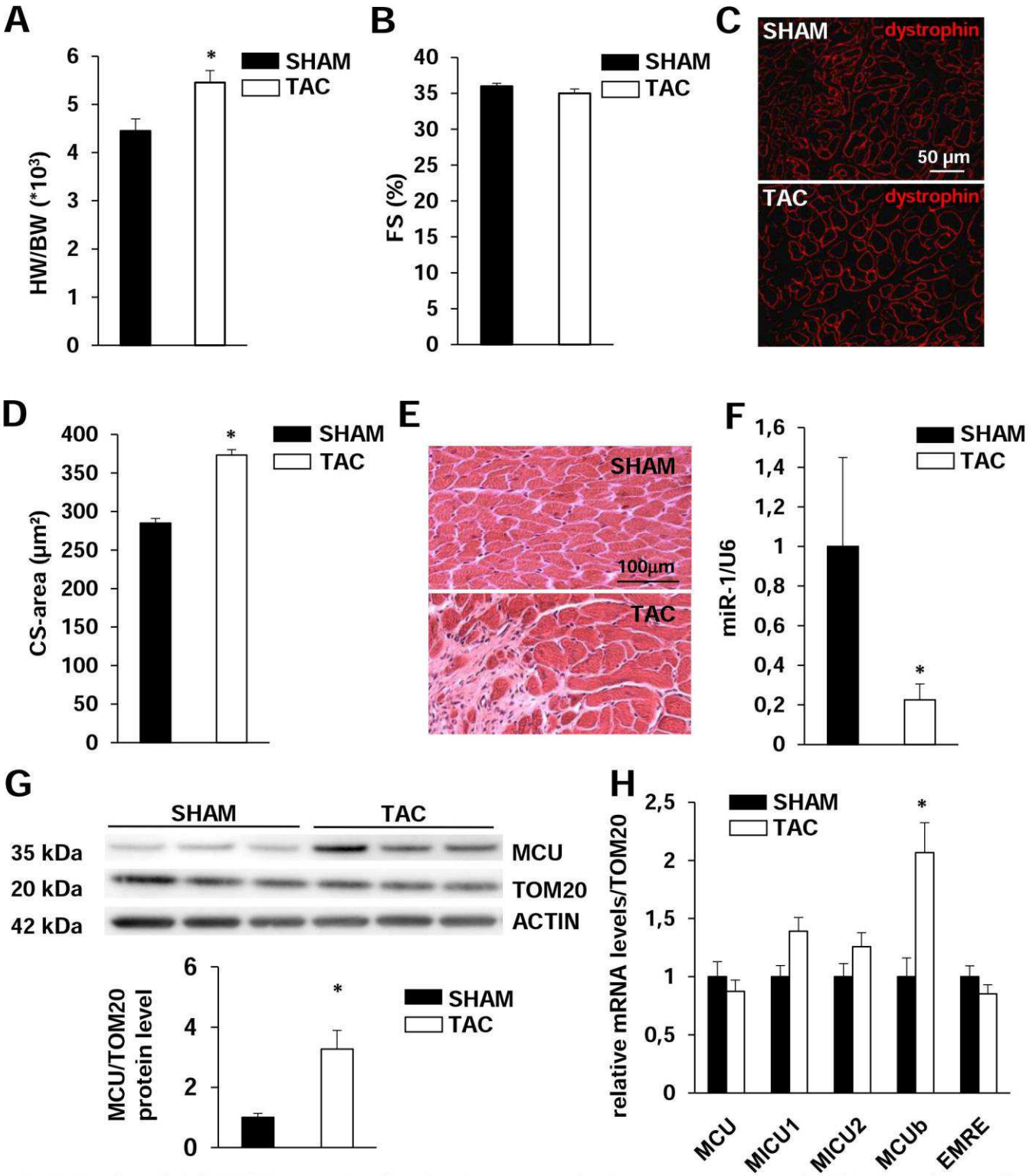

Fig. 6. Mitochondrial MCU protein density increases during pressure overload-induced cardiac hypertrophy in mouse hearts. **(A)** HW/BW and **(B)** Fractional Shortening (FS) in one-week sham-operated and TAC mice. (n=6 mice for each group; *, $p<0.05$). **(C)** H/E staining of heart sections from LV of sham and TAC mice. **(D)** Confocal IF analysis on heart sections from 1 week sham and TAC mice, stained withanti-dystrophin. Images are details from the left ventricle. **(E)** Evaluation of left ventricular cardiomyocyte cross-sectional areas in sham-operated *vs.* TAC mouse hearts. (n=500 CMs for each group; *, $p<0.05$). **(F)** MiR-1 expression level was compared, by RTqPCR analysis, on heart extracts from sham *vs.* TAC mice. (n=6 hearts for each study group; *, $p<0.05$). **(G)** WB on heart extracts from sham and TAC mice and relative densitometry showing an increase in mitochondrial MCU protein content, in TAC hearts. (n=6 hearts for each study group; *, $p<0.05$). Immunoreactivity for TOM20 was used as mitochondrial protein loading control, while that for actin was used as a whole-cell protein loading control. **(H)** RTqPCR on extracts from sham *vs.* TAC hearts showing the expression levels of the members of MCUC. The graph displays a significant increase in expression level of MCUb. (n=6 hearts for each study group, *, $p<0.05$).

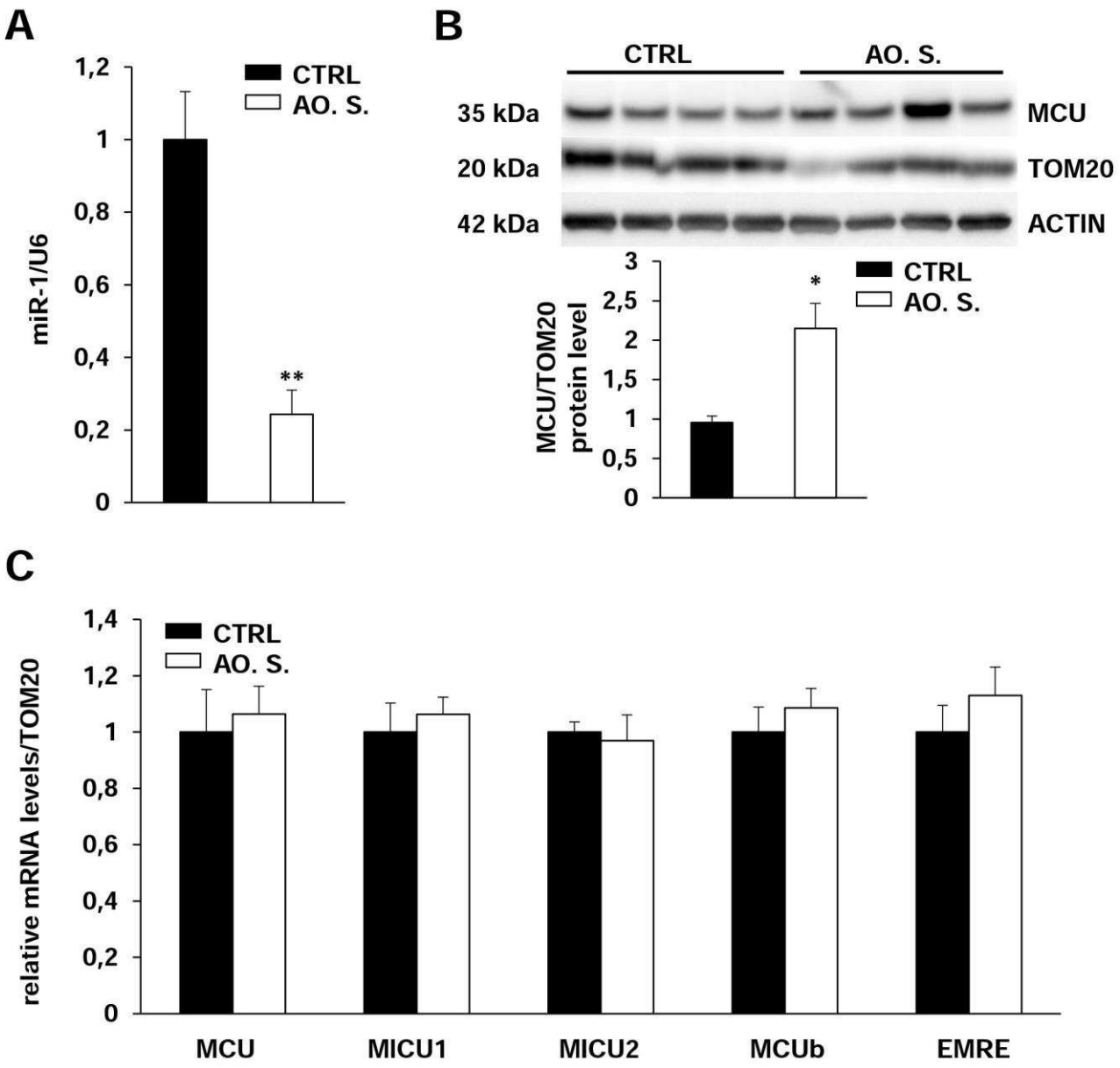

Fig. 7. Mitochondrial MCU protein density increases during pressure overload-induced cardiac hypertrophy in human hearts. **(A)** MiR-1 level assessed by RTqPCR in heart samples from healthy subjects (ctrl) and patients affected by aortic stenosis (Ao.S.). (n=5 control and 6 AoS hearts; **, $p<0.01$). **(B)** Western blotting on extracts from human heart samples from healthy subjects (ctrl) and patients affected by aortic stenosis (Ao.S.), and relative densitometry showing a significant increase in mitochondrial MCU protein content, in hypertrophic hearts. (n=5 CTRL and 6 Ao.S. hearts; *, $p<0.05$). Immunoreactivity for TOM20 was used as mitochondrial protein loading control, while that for actin was used as a whole-cell protein loading control. **(C)** RTqPCR on extracts from control and AoS hearts showing the expression levels of the members of the uniporter complex. (n=4 heart samples for each study group; *, $p<0.05$).

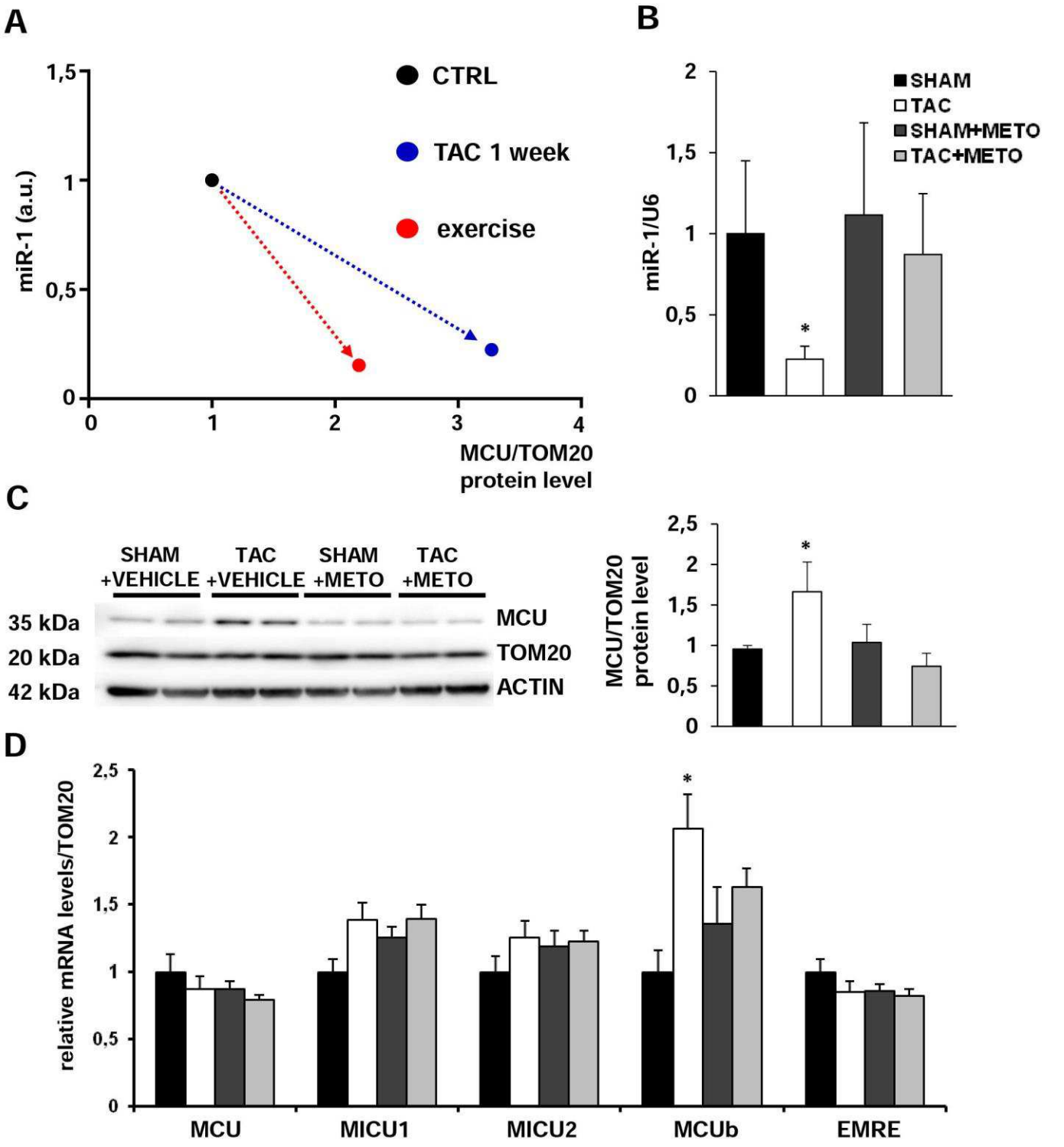

Fig. 8. The β1-AR blocker metoprolol counteracts changes in the miR1/MCU axis during pathologic cardiac hypertrophy. **(A)** Representative graph summarizing the variations of the miR1/MCU axis in exercise and pressure-overload heart hypertrophy, in experimental models. **(B)** RTqPCR analysis on heart extracts from sham-operated *vs.* TAC mice, either treated with the β1-receptor blocker metoprolol or with a vehicle control, to determine the expression level of miR-1. (n=6 hearts for each study group; *, $p<0.05$). **(C)** Western blotting on heart extracts from one-week sham-operated and TAC mice treated with metoprolol or vehicle and relative densitometry showing that metoprolol blunted TAC-dependent mitochondrial MCU increase. (n=6 hearts for each study group; *, $p<0.05$). Immunoreactivity for TOM20 was used as a mitochondrial protein loading control, while that for actin was used as a whole-cell protein loading control. **(D)** RTqPCR on extracts from sham-operated and TAC hearts, in both the metoprolol-treated or vehicle-treated groups, assessing the expression levels of the members of the uniporter complex. Note that metoprolol treatment blunted TAC-dependent MCUb transcriptional induction. (n=6 hearts for each group; *, $p<0.05$).

3.2 RESULTS – II

This second part of the results achieved during the PhD fellowship, stems from the observation that MCU is similarly up-regulated in both physiologic (e.g. exercise-induced) and pathologic (e.g. TAC-induced pressure overload) myocardial remodelling. At first sight, these results may detract from the importance of the uniporter as critical player in myocardial adaptation to hypertrophic stimuli. Indeed, the identical behaviour of MCU in physiologic and pathologic remodelling may offer unappealing immediate perspectives for MCU as a potential therapeutic target for treating maladaptive myocardial remodelling and its decline into HF. It has, however, to be noted that the hearts subjected to TAC were analysed one week after aortic constriction, a time point when hypertrophic remodelling is detectable, but cardiac function is unaffected, as assessed by echocardiographic and morphological analyses, indicating a fully compensated stage of hypertrophic cardiomyopathy (**Fig. 6A-E**). From the morphological and functional point of view, one week of TAC resulted in a cardiac phenotype similar to that resulting from chronic exercise: contractility was preserved (or even ameliorated, in the latter case), and no signs of cardiac maladaptation were detected. The results inform on the role of MCU in the early phase of adaptive hypertrophy. The role of MCU in more advanced phases of hypertrophy and in the transition of remodelling from adaptive-to-maladaptive was not initially addressed. To shed light on this subject, we decided to perform observations in a long-term TAC, until maladaptation occurred, and monitor MCU protein content.

3.2.1 MCU protein content is differently modulated in compensated and decompensated pathologic hypertrophy

To compare the MCU protein content in the adaptive and maladaptive phases of pathologic hypertrophy, we analysed hearts undergone surgical banding of the ascending aorta (see *Methods 5.1*), at different time points after surgery until 14 weeks, when overt maladaptation manifested with dilated cardiomyopathy and HF, as assessed by echocardiography.

Given that at the furthest time point after TAC, hearts were characterized by the presence of massive fibrotic scars, we analysed MCU content in isolated CMs to get rid of signals due to other cellular types present in damaged areas (fibroblasts, myofibroblasts, inflammatory cells).

The comparison between left ventricular CMs isolated from 14-week sham- and TAC-operated mice, showed that MCU protein content decreased in maladaptive hypertrophy, as shown in **Fig. 9A**. Although with the limit that at earlier time points after TAC the myocardial MCU content was evaluated in whole tissue lysates, this result suggests that the uniporter content in heart fluctuates during myocardial remodelling, with increases in the adaptive remodelling phase (i.e. early onset of pathologic or physiologic hypertrophy), followed by its decrease in maladaptation. Interestingly, while MCU expression in the early phases of hypertrophy mirrored the level of miR-1, this correlation failed in the failing myocardium, suggesting that other regulatory mechanisms may prevail over miR-1 in MCU modulation. What are the mechanisms responsible for MCU fluctuation during the onset of HF caused by prolonged pressure overload are unknown, and further research is required to address this issue, which carries relevant information for the understanding of cardiac pathophysiology.

3.2.2 MCU modulation in contraction-assisted human ventricles

To gain insight on MCU modulation in the human heart during maladaptation, we analysed myocardial samples from two patients undergone the implantation of a left ventricular assist device (LVAD) to support the failing heart function. As LVADs are normally used as a bridge to transplant, they offer the unique opportunity of analysing two large tissue biopsies, harvested respectively at the time of implant in the failing heart and at the time of heart explant for transplant surgery. This approach allowed comparing the myocardial biochemical parameters in the same heart prior to and after relief in cardiac workload, as provided by the assist device, thus significantly reducing the inter-individual variability. Heart biopsies were thus analysed using western blotting (WB) to assess MCU protein content, showing that in both patients analysed, MCU protein content strongly increased after LVAD implantation (**Fig. 9B**). This data suggested that the relief from mechanical stress, characterised by improved performance and reduction in workload, accompanies the concomitant up-regulation of MCU protein content. These

results would be in accord with a reduction in MCU content in the failing myocardium, especially when considering that the current literature suggests ventricular assistance to reduce the degree of cardiac failure[211].

In these advanced phases of HF, the modulation of MCU does not depend on miR-1 effect, since its expression does not significantly change from pre- and post-LVAD conditions. This preliminary result corroborates the idea that, during a condition of HF (such as at the moment of LVAD implantation or after long-term TAC), MCU levels are independent from miR-1, and the regulation of the protein is likely due to effect of other, yet to identify, mechanisms.

By combining the data achieved in murine models of compensated and decompensated pathologic hypertrophy, as well in pre- and post- LVAD human biopsies, the variations in MCU protein level can be interpolated along the different phases characterizing pathologic hypertrophic remodelling. During the early phases after TAC, in which the CMs grow and initially sustain the increased workload, MCU is up-regulated, with the contribution of the decrease in miR-1 levels. Subsequently, when maladaptation occurs, MCU expression dramatically decreases, and mechanisms different from post-translational regulation by miR-1 intervene. The drop in MCU levels is finally reversed upon partial recover from HF (after the aid of LVAD) (see fig.12, here below).

Figure 12. Schematic representation of MCU fluctuation during pathologic hypertrophy.

These experiments could not inform on whether these changes have a role in the pathophysiology of cardiac hypertrophy, or if they represent the secondary effect of altered heart mechanics or metabolism. Our subsequent experiments aimed at answering this riddle.

3.2.3 MCU modulation *in vivo*

To determine the effect of MCU modulation on cardiac remodelling, we sought to use viral transduction of AAV9 to overexpress or downregulate MCU in the heart. We set up three groups of mice, which were injected with AAV9-Empty (controls), AAV9-MCU-flag (causing MCU overexpression) or AAV9-shMCU-zGreen (causing MCU downregulation).

In the initial experiments, we evaluated the infection protocol better suited to obtain efficient viral transduction. To this aim, we compared the expression of the exogenous protein in adult mice injected at the concentration of $1 \cdot 10^{11}$ GC (genome copies). AAV9 was injected either in adult mice *via* tail vein (i.v.), or in neonatal mice *via* intraperitoneal (ip) at three different postnatal time points, namely: i) P2-P3 mice; ii) P5-P6 mice; iii) P9 mice. Morphological analyses were conducted after 21 days for the adult mice, or at 2 months of age for the neonates. IF combined with molecular and biochemical assays, allowed determine which of the three different approaches was the most efficient in inducing adequate MCU modulation.

As shown in **Fig. 10A**, AAVs are efficiently transduced in terminally differentiated cells, and in line with this, infection was more efficient in P9 mice, a time when virtually all CMs exit from the cell cycle. Similar results were obtained both with overexpressing (AAV9-MCU-flag) and silencing virus (AAV9-shMCU-zgreen). Overexpression and downregulation of MCU were confirmed both at mRNA and protein level, by real time-quantitative polymerase chain reaction (RT-qPCR) and western blotting (WB), respectively (**Fig. 10B-C**). In whole heart extracts, MCU downregulation resulted in a decrease of approximately 80 % of the protein level, while MCU overexpression determined a ten-fold increase in protein content. Thanks to the expression of flag-peptide fused to MCU in the overexpressing vector, and to the z-Green fluorescent protein expressed by the knockdown vector, infected CMs were easily detectable by immunofluorescence (IF) staining. Indeed, approximately 70% of CMs were expressing flag or z-Green, thus indicating efficient viral transduction. Conversely, injection in caudal vein in adult mice did not determine efficient viral transduction (approximately 25% ± 10% CMs infected, not shown).

Based on these results, for all *in vivo* experiments, we thus set up experimental groups consisting in P9 mice injected with AAV9-Empty, AAV9-MCU-flag and AAV9-shMCU-zGreen. Given the absence of phenotype induced by AAV9-Empty infection, we used this cohort of mice as control, and from now "Empty" will be synonym of "control" mice. MCU overexpressing and silenced (knockdown) mice, moreover, will be from now on referred as MCU OE and MCU KD mice, respectively.

Echocardiographic analyses, performed at various time points after MCU modulation, did not show any structural and functional alteration in either overexpressing or in silenced hearts, as compared to control (AAV9-Empty) and wild-type mice (EF, %: Empty: 59.1 ± 1.2 *vs.* MCU OE: 60.4 ± 2.6 *vs.* MCU KD: 61.8 ± 3.4) (**Fig. 10D**). The "heart-weight-to-body-weight" ratio (HW/BW) was not different in the three experimental groups (not shown), and haematoxylin/eosin (HE) staining on MCU OE, MCU KD and control heart sections did not show significant histological alterations (**Fig. 10E**).

While the non-uniform efficiency of viral transduction in all cardiac cells is a limitation of the use of virus-assisted gene modulation, it allowed comparing MCU overexpressing (flag-positive) or silenced (z-Green positive) CMs with normal ones in the same heart (**Fig. 10F**). The CM cross-sectional (CS) area of fluorescent and non-fluorescent CMs was thus measured in transversal cryosections of adult heart, by using wheat germ agglutinin (WGA) to mark cellular membranes and anti-flag or spontaneous green fluorescent protein (GFP) fluorescence to detect MCU overexpressing or silenced CMs, respectively. For each sample, three different 10 μm thick cryosections cut from the mid portion of the ventricles were analysed. For each cryosection, eight random fields were acquired with the confocal microscope, both from the left ventricle (LV) and the right ventricle (RV), and the cross-sectional CM area was measured using the image analysis software *Image J.* To avoid artefacts due to the different three-dimensional orientation of the CMs in the different myocardial regions, only the CMs with eccentricity index between 0.8 and 1 (considered transversal) were included in the analysis. CM size was unchanged between the three experimental conditions analysed (LV CMs area, μm^2: Empty: 200.2 ± 7.2 *vs.* MCU OE: 188.4 ± 12.0 *vs.* MCU KD: 206.9 ± 11.0) between the different cells, both using flag+ or z-Green+ compared to flag- or z-Green- in the same heart and AAV9-Empty infected hearts as controls (**Fig. 10G**). This data suggests that MCU modulation does not affect the gross CM morphology and function at baseline.

3.2.4 MCU protein content influences myocardial hypertrophic response to pressure-overload

To understand whether MCU could have a role in cardiac adaptation to stresses associated to increased energy demand, Empty, MCU OE or MCU KD adult (3 months-old) mice were subjected to TAC, as described in *Methods 5.1*. For each experimental group, relative sham-operated mice were used as controls of pressure-overload induced-hypertrophy. Echocardiographic analyses were performed every week after surgery, to non-invasively monitor cardiac functional and morphological indices.

In the early phases (i.e. 4 weeks) after pressure overload was set, MCU OE mice displayed a hypertrophic response comparable to that of Empty, with preserved or slightly more elevated contractile function (EF,%: Empty: 49.8 ± 5.1 *vs.* MCU OE: 54.5 ± 1.8) (**Fig. 11A-B**). At later time points, (i.e. 8 weeks) while control hearts showed decompensation with reduced contractile performance, MCU OE hearts had no signs of impairment of cardiac performance, with preserved contractility (**Fig. 11A-B**) (EF, %: Empty: 36.4 ± 1.2 *vs.* MCU OE: 58.2 ± 15.5), and increased LV thickness (**Fig. 11A** and **D**). Conversely, in MCU KD hearts, TAC caused contractile dysfunction already at the early time points (**Fig. 11A**), accompanied by reduced LV wall thickness, and significant increase in LV diastolic volume, indicating dilative remodelling of the heart (EF, %: MCU KD: 41.6 ± 5.4 *vs.* Empty: 49.8 ± 5.1) (**Fig. 11B-C**). More importantly, MCU KD mice died prematurely after 4 weeks of TAC. Heart samples from the mice undergone TAC and relative sham-operated controls were processed for immunohistochemistry and molecular analyses (see *Methods 5.2*). Cryosections were stained with H/E to visualize myocardial structure and the degree of fibrosis. In line with the echocardiographic results, MCU OE hearts showed increased thickness of IVS and LV, as compared to time-matched pressure-overloaded controls which, after 8 weeks of TAC, tended to show decompensatory mechanisms which included decreased contractility and pronounced fibrosis, as shown by collagen I immunostaining (**Fig. 12A**). Conversely, MCU KD hearts displayed dilative remodelling, whose hallmarks are thin LV wall and increased LV chamber diameter (**Fig. 11D**). Moreover, myocardial structure was inhomogeneous, as massive fibrotic replacement was evident already after 4 weeks of TAC.

3.2.5 MCU modulation impacts on myocardial vascular adaptation to pressure overload-induced hypertrophy

It is well agreed that during the initial compensatory phase of TAC-induced hypertrophy, angiogenesis sustains CM function and growth by maintaining unaltered oxygen and nutrient supply to the working CMs. With time, the increased wall thickness and the presence of fibrotic scars hamper angiogenesis causing, subsequently, chronic hypoxia, increasing cellular death rate, additional fibrotic replacement and contractile dysfunction. Therefore, the correct ratio between capillaries and CMs is a simple but meaningful parameter to estimate the state of myocardial hypertrophic remodelling.

Briefly, different cryosections from sham- and TAC-operated Empty, MCU OE and MCU KD hearts were stained with an antibody against dystrophin, to mark CM membranes, and isolectin, to mark capillaries (**Fig. 12B, *left panel***). The same strategies used to evaluate CM cross-sectional (CS) areas (see *Results 3.2.3*) were used to assess the capillaries/CM ratio. Sample images were acquired at confocal microscope and analysed with the tool "cell counter" of *Image J* to measure the capillary/CM ratio. Sham controls, in all the three groups, showed a ratio of about 1.4 capillaries per CM. Pressure overload determined, in Empty mice, a time-dependent decrease of vascularization density 8 weeks after TAC (capillaries/CM: sham: 1.39 ± 0.12 *vs*. TAC 4 weeks: 1.30 ± 0.04 *vs*. TAC 8 weeks: 1.00 ± 0.03). Interestingly, pressure-overload did not affect significantly the capillary/CM ratio in MCU OE hearts, thus suggesting adequate oxygen supply to the overloaded CMs (capillaries/CM: sham: 1.38 ± 0.10 *vs*. TAC 4 weeks: 1.27 ± 0.00 *vs*. TAC 8 weeks: 1.19 ± 0.02). On the other hand, MCU KD myocardium displayed impaired capillaries/CMs ratio already after 4 weeks of TAC, representing therefore a likely mechanism reducing nutrient and oxygen supply to the myocardium and contributing to CM death, contractile impairment and, ultimately, HF (capillaries/CM: sham: 1.22 ± 0.13 *vs*. TAC 4 weeks: 0.98 ± 0.11) (**Fig. 12B, *right panel***).

3.2.6 MCU modulation affects cardiomyocyte hypertrophic growth upon pressure-overload

To assess whether MCU expression level impacts on CM growth upon pressure-overload, the mean CM cross-sectional areas were measured in cryosections stained for IF with

anti-dystrophin or agglutinin, to mark cell membranes. The comparison between the mean area of CMs in sham and TAC mice confirmed that aortic banding increased the cross-sectional CM area of about 30% at the 4 weeks time point (Δ growth, %: 31.0 ± 4.8). Interestingly, MCU OE cells had a much more pronounced response than controls with average increase in cell size of about 60% (Δ growth, %: 63.5 ± 6.6). Interestingly, but due to mechanisms yet unexplained which may involve paracrine effects, flag-negative CMs in MCU OE hearts, which have not been transduced with the MCU OE virus, displayed an increase in the mean area comparable to flag-positive cells.

Conversely, comparison between the cross-sectional area of zGreen positive cells (expressing, therefore, AAV9-shMCU) in sham and TAC hearts, did not show significant cell enlargement, suggesting that MCU silencing impairs the CM adaptation increased workload through hypertrophy (Δ growth, %: 9.15 ± 8.1) (**Fig. 12C**). This effect is attributable to the reduced expression level of MCU, since zGreen negative cells in silenced hearts showed normal hypertrophic growth, of about 30% (data not shown). The different cell size was reflected upon the LV thickness, as shown in **Fig. 12D**.

Altogether, the results of our experiments show that MCU modulation affects myocardial adaptation to hypertrophy. In details, MCU overexpression determines amplified CM growth in a context of adaptive hypertrophy, characterized by preserved contractility and vasculature. On the other hand, MCU silencing resulted in decompensated hypertrophy, with frustrated hypertrophic response, LV dilatation, inadequate angiogenesis and massive fibrosis.

To understand the molecular mechanisms whereby MCU modulation affects myocardial adaptation to pro-hypertrophic stimuli, we sought to dissect hypertrophic signalling pathways *in vitro* in cultured CMs.

3.2.7 MCU can be efficiently modulated *in vitro*

Neonatal ventricular cardiomyocytes (NCMs) were infected with adenoviruses, coding either MCU-flag or the shRNA against MCU (sh-MCU, Vector BioLabs) (see *Methods* 5.*3* and *Table 3.3*) to achieve overexpression or downregulation of MCU, respectively. As control, the non-coding viral vector Ad-Empty virus was used, and from now on Ad-

Empty cells will be considered as controls. For both overexpression and downregulation experiments, the dose/effect relationship of viral treatment was determined, by analysing cell viability and morphology, sarcomeric and mitochondrial structure. No effects were detected at concentrations lower than MOI 5 (multiplicity of infection) for Ad-MCU-flag and MOI 25 for Ad-shMCU. MCU overexpression with higher MOI (MOI 50 and 100) caused cellular death, which was attributable to the higher exposure to mitochondrial Ca^{2+} overload due to MCU, since the same concentration of Empty virus used as control did not cause any effect (**Fig. 13A**). Analogously, MCU downregulation with MOI 50 and MOI 100 lead to increased cell death, presumably due to altered Ca^{2+} dynamics.

Efficient MCU modulation (both overexpression and downregulation) was verified at transcriptional and translational level, using RT-qPCR and WB, respectively (**Fig. 13B-C**). Moreover, the flag-peptide attached to MCU gene encoded by the overexpressing virus allowed to identify, with IF, the overexpressing CMs, which represented normally more than 90% of the cells plated.

In MCU overexpressing (MCU OE) CMs, we analyzed the protein level of MCU partners and while no variations could be observed in MICU1 and MICU2, MCUb level was markedly increased (**Fig. 13D**). Although the mechanism of regulation of MCUb is undetermined, it would be sensible if its upregulation depended on mitochondrial Ca^{2+} overload, given its inhibitory function on the process. However, such evidence of the cross-regulation between MCU and MCUb was somewhat surprising given the current evidence, confirmed also by our own assessments (**Fig. 13E**), indicating that MCUb levels decreased upon increasing MCU expression in HEK-293 and HeLa cells.[64] While this data is in overt contrast with the results obtained in CMs, it has to be taken into account that intracellular Ca^{2+} homeostasis in HEK and HeLa cells differs substantially from that of CMs. In this latter cell type, cytoplasmic [Ca^{2+}] oscillates rhythmically from values close to 100 nm to around 1 μM and this process is accompanied by beat-to-beat Ca^{2+} uptake in mitochondria. It is therefore plausible that the risk of mitochondrial Ca^{2+} overload is very elevated and that the cell has compensatory mechanisms opposing it. The analyses of the protein levels of MCU partners in MCU silenced (MCU KD) cells are in progress.

3.2.8 MCU modulation affects cardiomyocyte Ca^{2+} dynamics and morphology *in vitro*

To assess the effect of MCU modulation on the mitochondrial Ca^{2+} uptake capacity, we performed live imaging experiments of mitochondrial Ca^{2+} dynamics. To this purpose, MCU OE, MCU KD or Empty CMs were transfected to express the mitochondria-targeted Ca^{2+} sensor 4mtD3CPV (mito-CaMeleon). As expected, MCU overexpression significantly increased the amplitude and speed of the steady-state mitochondrial Ca^{2+} level, while its downregulation reduced it (amplitude, measured as $\Delta R/R_0$, %: Empty: 25.9 ± 1.4 *vs.* MCU OE: 54.3 ± 3.3 *vs.* MCU KD: 16.4 ± 1.5; speed, measured as time to plateau in seconds, Empty: 15.5 ± 5.8 *vs.* MCU OE: 9.7 ± 4.1 *vs.* MCU KD: 19.3 ± 1.56) (**Fig. 14A**).

Given that the Ca^{2+} affinity of 4mtD3CPV causes poor sensitivity at $[Ca^{2+}]$ ~100 nM, we used the high-affinity Ca^{2+} probe 2mtGCaMP6, to estimate the basal mitochondrial Ca^{2+} level in MCU OE or MCU KD CMs. Interestingly, MCU OE CMs displayed increased matrix Ca^{2+} content, at baseline. Conversely, MCU KD CMs showed a trend towards reduced Ca^{2+} content, though short of statistical significance (ratio 490/410: Empty: 4.88 ± 0.55 *vs.* MCU OE: 9.25 ± 2.88 *vs.* MCU KD: 3.51 ± 0.66) (**Fig. 14B**).

These findings were attributable to alteration in the properties of the mitochondrial Ca^{2+} transport mechanism, as the kinetics and peak amplitude of pacing-induced cytoplasmic Ca^{2+} transients, which would serve as Ca^{2+} input to mitochondrial uptake, were identical in Empty, MCU OE and MCU KD cells, as assessed with the fluorescent dye FLUO-4 (F_{max}/F_0, normalized on Empty CMs: MCU OE: 1.01 ± 0.07 *vs.* MCU KD: 1.01 ± 0.01) (**Fig. 14C**).

Given that FLUO-4 is a Ca^{2+} dye based on detection of single emission wavelength, it is not suited for the detection of differences in the resting Ca^{2+} level. For this purpose, in a subset of experiments, we used the ratiometric indicator FURA-2. In these experiments, no differences in the resting mitochondrial Ca^{2+} levels could be appreciated between cells in the different groups (data not shown).

To address whether the changes in mitochondrial Ca^{2+} uptake could impact on the structure of CM contractile apparatus, we acquired confocal IF images of MCU OE, MCU KD and Empty cells, immunostained for α-actinin and for the mitochondrial

marker TOM20. The images were analysed to determine CM area, sarcomeric organization and the morphology of mitochondria.

While non-significant differences were observed in the size of Empty *vs.* MCU OE cells, we observed a significant increase in the area of MCU KD CMs, accompanied by a disarrangement of the sarcomere, which was not observed in the overexpressing cells (CMs area, μm^2: Empty: 1013.65 ± 39.6 *vs.* MCU OE: 1092.35 ± 36.5 *vs.* MCU KD: 1356.42 ± 73.66).

While MCU overexpression did not alter mitochondrial morphology, number and area, as assessed by transmission electron microscopy (TEM) analysis, a trend to smaller mitochondria was observed in MCU KD cells (mitochondrial area, μm^2: Empty: 0.39 ± 0.03, MCU OE: 0.45 ± 0.03, MCU KD: 0.32 ± 0.02) (**Fig. 14D**). This result, at the moment falls short of statistical significance due to low number of samples analysed, is object of further investigations.

The mitochondrial physiology in MCU OE, MCU KD and Empty cells, was further evaluated with live imaging of TMRM fluorescence. This mitochondria-specific lipophilic dye accumulates in the organelle depending on the membrane potential, and is thus a commonly used tool to assess this parameter (see *Methods 5.5*). After incubation with TMRM in the imaging solution (see *Table 1*) supplemented with cyclosporin H (to prevent active extrusion of the probe, see *Methods 5.5*), CMs were imaged with an inverted fluorescence microscope (Olympus IX-81). The inhibition of ATP synthase, with oligomycin, did not alter mitochondrial capacity to preserve $\Delta\psi_m$ in either MCU overexpressing, silenced or Empty CMs. FCCP addition, to dissipate $\Delta\psi_m$ and induce TMRM extrusion from mitochondria, had the same effect on ΔF in the three experimental groups (**Fig. 14E**).

All these data combined, suggest that MCU modulation in neonatal CMs alters mitochondrial capacity to take up Ca^{2+} upon electrical pacing, which is accompanied by alterations in mitochondria morphology, cell size and structural organization.

3.2.9 MCU expression level influences cardiomyocytes hypertrophic response upon chronic adrenergic stimulation.

Our previous *in vivo* data, presented above, suggested an involvement of MCU in CM adaptation to hypertrophic stimuli. One of the main pathways activated during pressure-overload and central to CM hypertrophic remodelling is the β-adrenergic stimulation operated by sympathetic neurons.

To understand whether MCU may have a role in CM growth elicited by pro-hypertrophic stimuli, we subjected MC OE, MCU KD and Empty cells to continuous adrenergic stimulation, by incubating cultured CMs, previously infected with the MCU-modulating viruses, with norepinephrine (NE, 100 nM) for 72 hours. At the end of treatment, cells were fixed and processed and immunostained for the sarcomeric protein α-actinin and flag-peptide (in MCU OE CMs). Morphometric analyses were then performed to measure mean cellular area and displacement of the contractile apparatus (see *Methods 5.3*) (**Fig. 15A**). Consistent with the results obtained *in vivo* in pressure-overloaded hearts, NE determined very different responses in MCU OE, MCU KD and Empty CMs. The increase in cell size elicited by NE in MCU OE cells was almost doubled when compared to the effect of the drug in Empty cells (Δ growth, %: Empty: 25.5 ± 2.1 *vs*. MCU OE: 52.1 ± 6.8) and, consistent with the data obtained in murine hearts, growth was blunted in MCU KD CMs (Δ growth, %: 4.8 ± 0.7) (**Fig. 15B**). Interestingly, MCU KD cells displayed, after chronic adrenergic stimulation, worsened sarcomeric disarrangement (**Fig. 15A**) and positivity to anti-cleaved-caspase 3 antibody (**Fig. 15C**), the latter event supporting the increased apoptosis rate in these conditions. Impaired cell growth and cell death in response to adrenergic stimulation replicated *in vitro* the consequence of TAC in MCU KD hearts featuring maladaptive dilative remodelling (**Fig. 11-12).**

To address the mechanisms whereby changes in MCU content modulate CM hypertrophic responses to adrenergic stimulation, we focused on molecular pathways downstream of β-AR, involved in cell growth and potentially affected by alterations in mitochondrial Ca^{2+} uptake. We initially focused on the amplified hypertrophic response occurring in MCU OE cells.

Since NE can activate both α- and β-ARs (both β1 and β2 isoforms), all expressed by cultured CMs, we decided to discriminate the molecular players upstream to the MCU-dependent trophic response of CMs.

To this purpose, Empty and MCU OE cultured CMs underwent prolonged stimulation with the selective AR agonists. In detail, phenylephrine (PE, 100 μM) was used to activate α-ARs, while clenbuterol (10 μM) was chosen as β2-AR agonist. Both treatments, that lasted three consecutive days as above, led to a hypertrophic remodelling, which was more pronounced with PE than CLB. Interestingly, with both compounds, the degree of growth was identical in Empty and MCU overexpressing cells (CLB-induced Δ growth, (%): Empty: 35.0 ± 4.8; MCU OE: 30.1 ± 6.1; PE-induced Δ growth, %: Empty: 66.0 ± 5.4 *vs*. MCU OE: 62.0 ± 5.9). This data combined with the fact that NE has a higher affinity for β1-AR, suggest that the increased hypertrophic response occurring in MCU OE CMs during chronic adrenergic stimulation is presumably mediated by β1-AR (**Fig. 15D-E**).

3.2.10 MCU overexpression accelerates norepinephrine-induced NFAT nuclear translocation

The *in vitro* system allows monitoring and interfering with several molecular pathways involved in cardiac hypertrophy. To understand how MCU overexpression determines amplified hypertrophy, we aimed at dissect the signals controlling cellular growth and we initially focused on the calcineurin/NFAT pathway.

Calcineurin is a well-known Ca^{2+}/calmodulin-dependent phosphatase, which dephosphorylates transcription factors involved in cell growth, triggering their nuclear translocation and activation. A main target of calcineurin is NFAT (Nuclear Factor of Activated T cells) which, upon activation and nuclear translocation, promotes the transcription of several hypertrophying genes, including GATA and Mef2[212]. This pathway resulted fundamental in mediating cardiac hypertrophy in our Empty and MCU OE CMs, since the inhibition of calcineurin, achieved *in vitro* with either cyclosporin A (1 mM) or FK506 (100 μM), completely inhibited the NE-dependent increase in CM size, in both experimental groups (**Fig. 16A**).

To monitor the activation state of the calcineurin/NFAT pathway, MCU OE and Empty CMs were transfected with a plasmid encoding a green fluorescent-protein (GFP) tagged chimaera of the cardiac isoform c3 of NFAT (eGFP-NFATc3). This allowed dynamic tracking of NFAT using fluorescence microscopy, to follow its localization and movement from the cytosolic (inactive, dephosphorylated form) to the nuclear (active, phosphorylated form) compartment (**Fig. 16B**).
After transfection and expression of the eGFP-NFATc3, CMs were incubated with NE for 6 or 24 hours. These time points were chosen to investigate the early events that precede the effective hypertrophic remodelling, being calcineurin-NFAT an initial step of adrenergic-induced cellular growth. After the incubation with NE, cells were fixed and processed with α-actinin, (to discriminate CMs from contaminating fibroblasts) and DAPI (to co-localize nuclear NFAT green signal and nucleus). Two-hundred cells were counted for each coverslip for each time point, and divided in nuclear *vs*. cytosolic eGFP-NFATc3 fluorescent signal. The analysis showed that at the beginning of the experiment (prior to adrenergic stimulation), the percentage of cells displaying a nuclear localization of NFAT was equal in both experimental groups (CMs with nuclear NFAT, %: Empty: 3 ± 3 *vs*. MCU OE: 5 ± 2).

Interestingly, the percentage of nuclear-GFP positive cells increased after 24 hours of chronic adrenergic stimulation, especially in MCU OE cells (CMs with nuclear NFAT, %: Empty: 45 ± 5 *vs*. MCU OE: 71 ± 5). Strikingly, MCU OE CMs displayed a high percentage of cells with activated NFAT already after 6 hours of NE treatment, while Empty cells did not (CMs with nuclear NFAT, %: Empty: 15 ± 8 *vs*. MCU OE: 57 ± 13) (**Fig. 16C**). Both Empty and MCU OE CMs were also treated with the calcineurin inhibitors CsA and FK506, as negative control. In these conditions, as expected, NE treatment did not elicit NFAT nuclear translocation, (not shown).

These data suggest that MCU overexpression facilitates activation of calcineurin-NFAT pathway, which is activated more promptly upon NE stimulation.

3.2.11 MCU modulation affects the Akt/GSK3β signalling pathway

To gain further insights on the molecular mechanisms causing enhanced hypertrophy in MCU OE cells, additional molecular pathways were assessed. Whole cell protein extracts from Empty and MCU OE CM, treated with NE or vehicle, were analysed by WB to assess the state of activation of Akt and GSK3β. Recently, it has been demonstrated that adrenergic agonists can potentiate insulin-mediated Akt activation and, interestingly, may also activate the kinase also in absence of growth factors[213]. GSK3β is a downstream target of Akt, which has been shown in the heart, restrains pro-hypertrophic gene expression, including NFAT[26]. Antibodies specific for the phosphorylated form of the proteins were thus used in combination with total anti-Akt and anti-GSK3β to estimate the phosphorylated fraction of these key mediators of protein synthesis, central to the cardiac hypertrophic response.

As showed in **Fig. 17A**, WB revealed that prolonged incubation with NE significantly increased the phospho-Akt/Akt ratio, which was significantly higher in MCU OE cells, compared to Empty CMs. This change was accompanied by an increase in the phosphorylation of GSK3β. Strikingly, activation of this signalling pathway was detected even at baseline in MCU OE cells which, in fact, had higher phospho-Akt/total AKT and phospho-GSK3β/total-GSK3β ratios compared to Empty cells (**Fig. 17B-C**). In basal conditions, the increased phosphorylation of the Akt was not accompanied by an increased activation of the Akt downstream target S6, thus indicating no activation of protein synthesis, a result in line with the evidence that MCU OE cells were similar in size with the control ones. Increased phosphorylation of S6 was observed in MCU OE cells *vs*. Empty, upon NE stimulation (data not shown). Interestingly, the same biochemical profile was observed in MCU OE hearts (**Fig. 17D**), and may fit well with the enhanced adaptive response of MCU OE hearts to TAC (see *Results 3.2.4*). Whether increased Akt phosphorylation occurs upon TAC is, at the time being, unknown and will be object of our future evaluations.

These data suggest that Akt/GSK3β axis is activated in MCU OE CMs already in baseline conditions, and that this may account for the amplified remodelling occurring upon β-adrenergic stimulation by NE, as the stimulus impinges on the same signalling pathway.

3.2.12 MCU modulation affects the CaMKII signalling pathway

The following step, to explain the increased propensity of MCU OE CMs to grow upon adrenergic stimulation, was to identify the molecular upstream modulators responsible for Akt phosphorylation. Among the numerous signalling pathways activated downstream β-ARs, the Ca^{2+}/calmodulin dependent kinase II (CaMKII) plays a key role in mediating responses to adrenergic activation in the heart[27]. To understand whether CaMKII may be implicated in the amplified NE-induced CM hypertrophy, occurring in MCU OE cells, we used pharmacological CaMKII inhibitors in NE-treated CMs. First, we performed WB analyses to assess the phosphorylation state of Akt in CMs at baseline. In this preliminary experiment, cells were treated with KN93 (CaMKII inhibitor) or KN92 (inactive analogue) for 72 hours (both at the concentration of 1 μM). As shown in **Fig. 18A**, treatment of cells with the CaMKII inhibitor KN93 reduced the increased Akt phosphorylation observed in MCU OE CMs, while KN92 had no effects. This data suggests that CaMKII may directly account for basal phosphorylation of AKT in MCU OE CMs.

Being CaMKII involved in Akt phosphorylation, and this latter possibly contributing to accelerated NFAT nuclear translocation in MCU OE CMs upon NE incubation, we monitored NFAT pathway upon KN93 pre-treatment. As mentioned above (see *Results 3.2.10*), cells were transfected with eGFP-NFATc3 and incubated with CaMKII inhibitor for 48 hours. Then, the pro-hypertrophic treatment (NE 100 nM, 6h) was started. While KN92 did not affect the dynamics of NE-dependent NFAT nuclear translocation both in Empty and MCU OE cells, KN93 completely inhibited the NE-dependent accelerated NFAT nuclear translocation occurring in MCU OE cells. Indeed, it restored the percentage of cells displaying nuclear-translocated NFAT to values comparable to those described for Empty cells in basal conditions (**Fig. 18B**).
As an additional readout to test the effects of CaMKII inhibition, we measured CM areas after chronic NE-stimulation. In line with our previous results, immunostaining and morphometric analyses showed that NE successfully induced hypertrophy in KN93 treated Empty and MCU OE CMs, but totally blunted the increased cell growth described in MCU OE cells, as the two experimental groups provided similar responses to NE (Δ growth, %: Empty: 24.1 ± 4.2 *vs.* MCU OE: 23.8 ± 3.6) (**Fig. 18C**).

This result suggests that CaMKII is involved and has a key role in the amplified hypertrophic response, which characterizes MCU OE cells upon β1-AR stimulation. The experiments suggest that CaMKII participates in the phosphorylation of Akt at baseline, this latter being involved in GSK3β inhibition and consequent removal of a constitutive brake to NFAT pro-hypertrophic effects, elicited by calcineurin.

3.2.13 MCU overexpressing cardiomyocytes display increased sarcoplasmic reticulum Ca^{2+} content and mitochondrial ROS production

Given that the amplified hypertrophic response to NE observed in MCU OE CMs depends on CaMKII, we sought to identify the mechanisms whereby increased MCU content would enhance CaMKII activation. We thus explored two distinct pathways converging on CaMKII activation: on the one hand, we sought to determine whether higher input to the conventional route of activation, implying Ca^{2+}-dependent phosphorylation by calmodulin, could be enhanced by MCU overexpression; on the other, given that CaMKII oxidation, as elicited by increased reactive oxygen species (ROS) has been reported to decrease Ca^{2+}-dependency of CaMKII[214,215], we aimed to measure whether increased MCU content could impact on ROS production.

To this aim, we deepened Ca^{2+} imaging experiments by measuring the second messenger dynamics in the SR, to address the hypothesis that MCU overexpression might increase Ca^{2+} available for CaMKII activation. The rationale of this hypothesis is based on the observation that MCU deletion affects SR Ca^{2+} content[8], by reducing the amount of ATP available for SERCA pumps to take up cytosolic Ca^{2+}. Therefore, we used the genetically encoded SR-targeted sensor D4ER to measure SR Ca^{2+} during cell pacing, and its total content by inducing its depletion with the acute treatment with caffeine (10 mM). Whereas pacing-induced SR Ca^{2+} transients did not differ significantly between Empty and MCU OE CMs, caffeine elicited a much higher fluorescence change in the latter group (ΔR,%: Empty: 11.7 ± 1.1 *vs.* MCU OE: 17.5 ± 1.4) (**Fig. 19A**), indicating that MCU overexpression increased SR Ca^{2+} content. This finding would support that increased Ca^{2+} availability to CaMKII would be subsequent to MCU overexpression, and facilitate the kinase activation upon NE treatment, leading to the downstream effects described above and culminating in enhanced hypertrophy.

Based on the evidence that the oxidation of the two methionine residues (M281 and M282) predisposes CaMKII to Ca^{2+}-independent activity or even leads to self-activation of the kinase[214,215], we next assessed whether increased ROS production occurred in MCU OE CMs.

We thus sought to measure mitochondrial ROS using the genetically-encoded ratiometric probe roGFP1 ratio (see *Methods 5.5* and *Table 3*). The experiments were performed in three experimental groups at baseline, with no adrenergic stimulation, 48 hours after viral infection. As shown in **Fig. 19B**, adenoviral infection *per se* does not induce mitochondrial ROS production, as emerging from the comparison between Empty and not-treated (NT) cells. Moreover, our preliminary data suggests that this MCU OE CMs have a trend to increased mitochondrial ROS. Such small "physiological" increase in ROS production may cooperate in CaMKII oxidation. The oxidative state of CaMKII is going to be assessed by WB in extracts from cultured CMs, as well as from intact hearts.

The hypothesis by which a slight increase in ROS production would contribute to CaMKII activation in MCU OE CMs was corroborated by an additional preliminary experiment in which blunting ROS production, by cell treatment with the anti-oxidant vitamin E, significantly reduced (approximately of 40%) the percentage of MCU OE cells displaying nuclear translocated NFAT at 6 hours upon NE treatment (**Fig. 19C**).

This second set of data suggests the existence of a molecular mechanism, implicated in CM adaptation to hypertrophic stimuli, which is affected by the amount of MCU protein content.

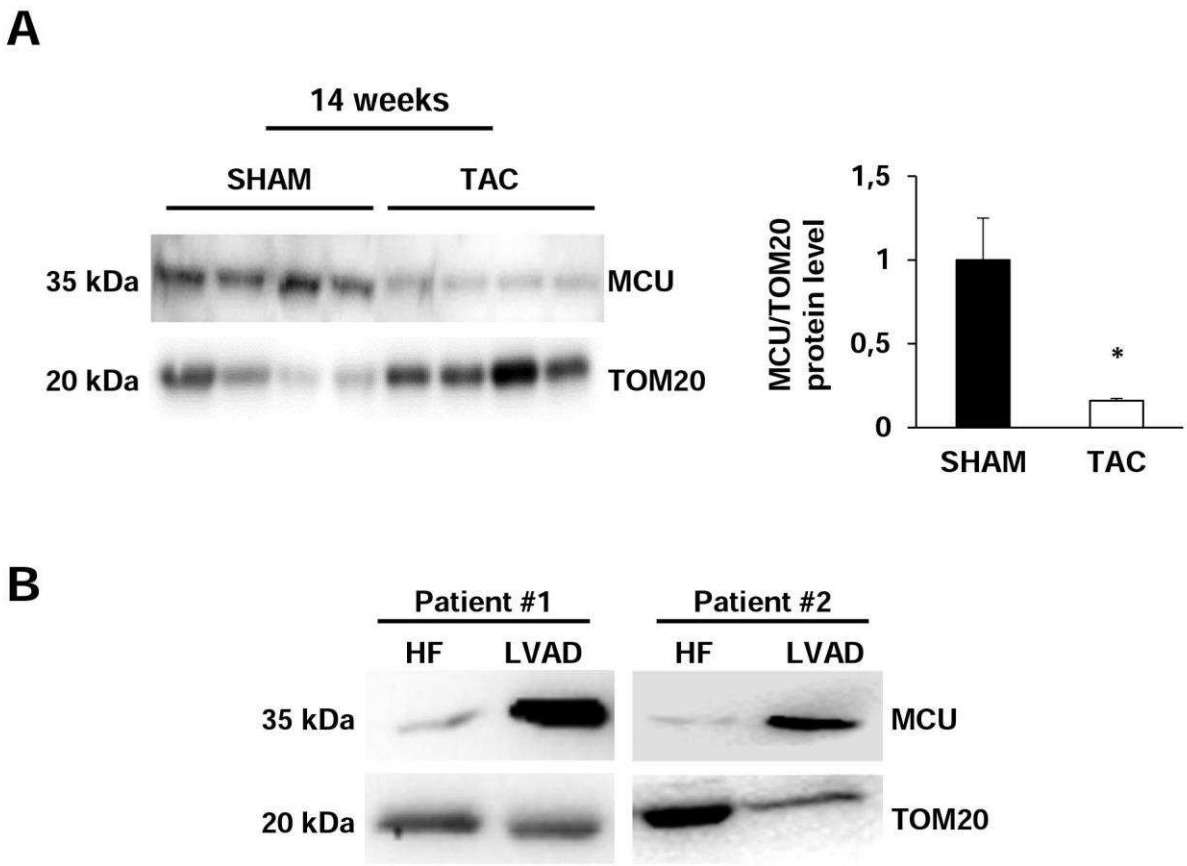

Fig. 9. MCU is differently modulated in adaptive and maladaptive hypertrophy. (A) MCU protein content, assessed by WB analysis, in LV cardiomyocytes isolated from SHAM- and TAC-operated mice 14 weeks after surgery (left panel) and relative densitometry (right panel). **(B)** MCU protein content measured in human myocardial samples obtained from two different patients. The samples were harvested both pre- and post- LVAD implantation, hence in a situation of heart failure (pre-) and in a partially relieved condition (post-). Both the human samples show that MCU protein content increases during myocardial assisted-recovery. In both **A** and **B**, TOM20 was used as mitochondrial protein loading control. (n= 4 mice for each group in **A**, 2 patients in **B**. *, $p<0.05$).

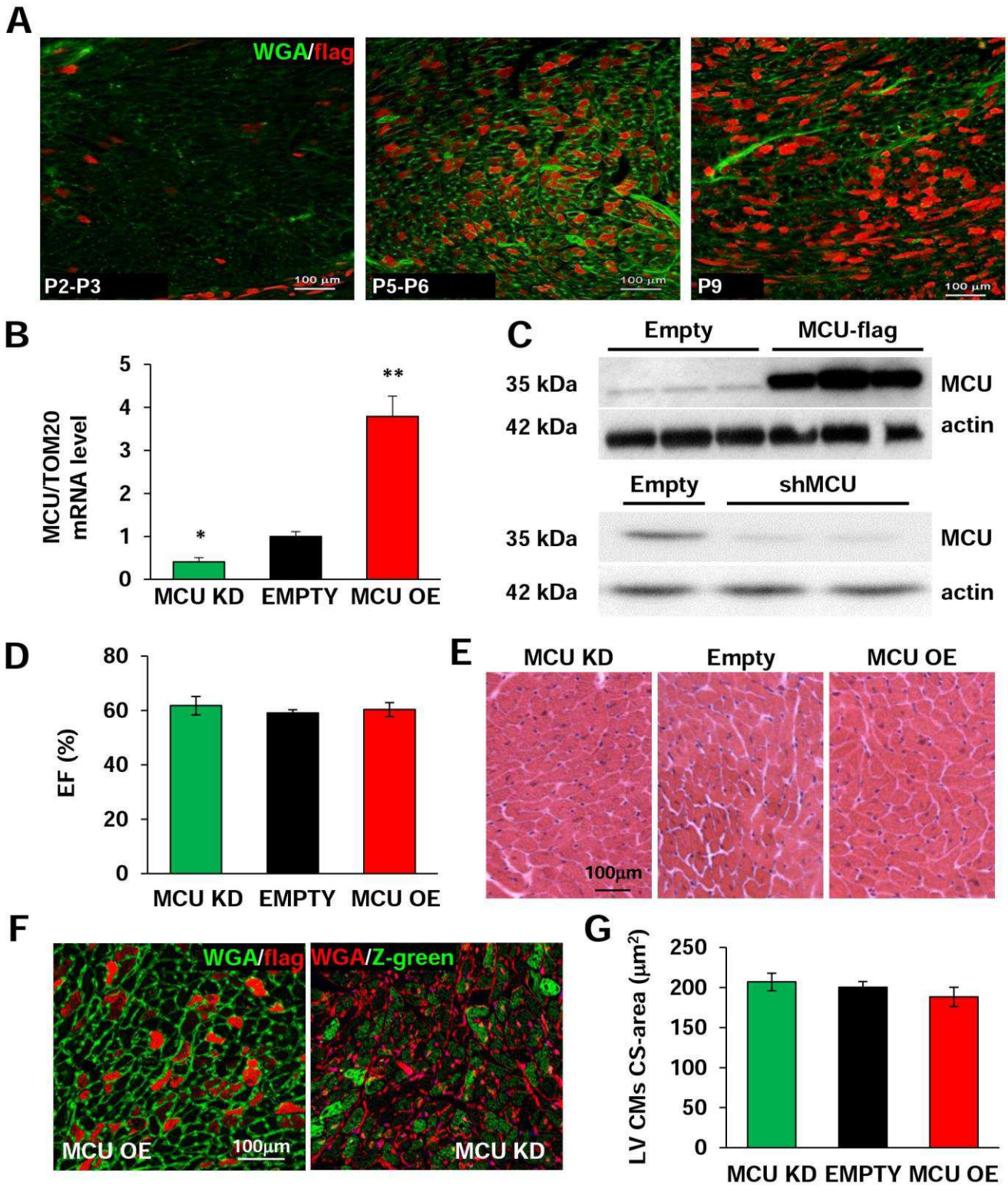

Fig. 10. MCU can be modulated *in vivo*. **(A)** Confocal IF analysis on heart cryosections from adult mice injected, at different time points after birth, with AAV9-MCU-flag. Sections were co-stained with an antibody to flag and wheat germ agglutinin (WGA). **(B-C)** RTqPCR **(B)** and WB **(C)** analysis on mRNA and protein heart extracts, from mice infected with AAV9-Empty, AAV9-MCU-flag (MCU OE) and AAV9-shMCU-zGreen (MCU KD), respectively. Immunoreactivity for actin was used as a whole-cell protein loading control. (n=6 mice for each study group, *, $p < 0.05$; **, $p < 0.01$.) **(D)** Echocardiographic evaluation of the Ejection Fraction (EF) in Empty, MCU OE, MCU KD mice, at baseline. **(E)** Haematoxylin/Eosin staining on left ventricle (LV) cryosections from Empty, MCU OE, MCU KD mice. **(F)** Confocal IF analysis on cryosections from MCU OE and MCU KD mice, stained with WGA to mark CM membranes. MCU OE hearts were also incubated with an antibody to flag. MCU KD CMs were identified by z-Green expression. Images are details of the LV. **(G)** Evaluation of CM cross-sectional areas in Empty, MCU KD and MCU OE hearts. (n=200 CMs for each study group).

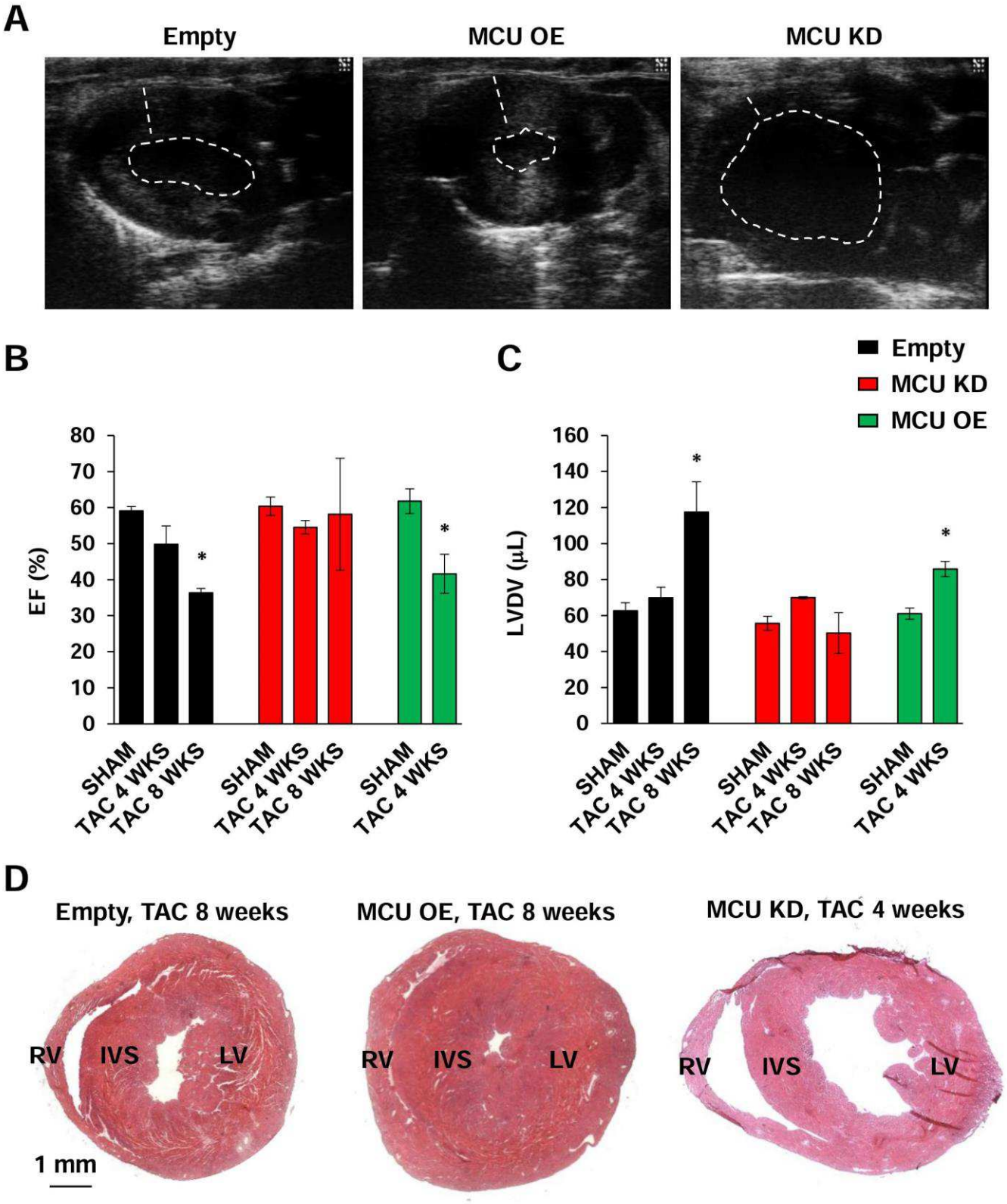

Fig. 11. MCU affects heart response to pressure overload. (A) LV long-axis echocardiographic view of Empty, MCU OE, MCU KD mouse hearts. Dashed lines delineate the LV chamber and evidence the wall thickness. **(B-C)** Evaluation, by echocardiographic analysis, of the Ejection Fraction (EF) and the Left Ventricle Diastolic Volume (LVDV), of 4- and 8-weeks sham-operated and TAC Empty, MCU OE and MCU KD mice. (n= 7 mice for each study group; *, $p < 0.05$). **(D)** Haematoxylin/eosin staining on heart sections from Empty, MCU OE and MCU KD TAC mice. (RV, right ventricle; IVS, interventricular septum; LV, left ventricle.)

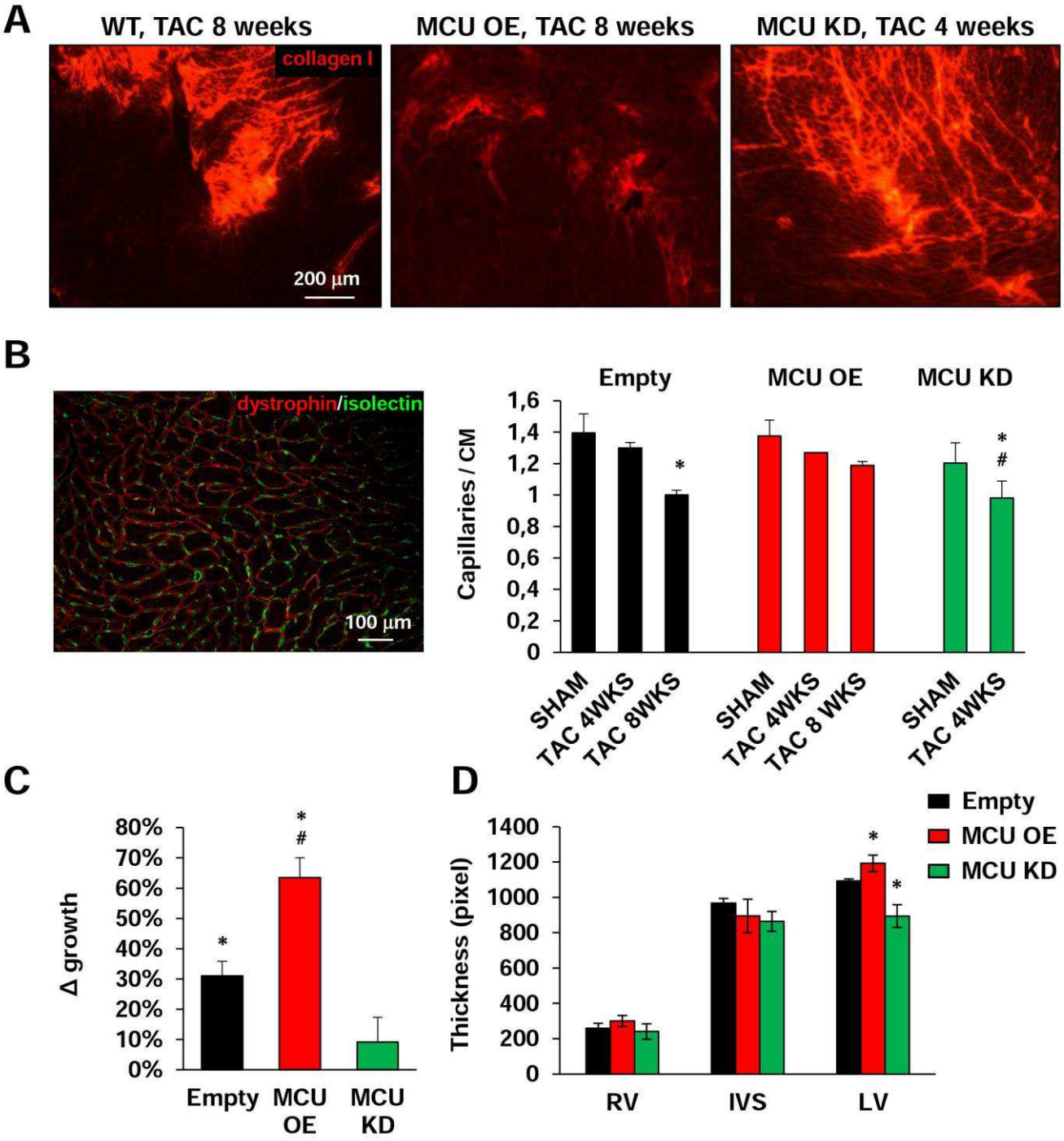

Fig. 12. MCU affects heart remodelling upon pressure-overload. (A) Immunofluorescence analysis on heart sections from Empty, MCU OE and KD TAC mice stained with an antibody to collagen I. **(B)** Immunofluorescence analysis on heart sections from Empty, MCU OE and MCU KD TAC mice co-stained with an antibody to dystrophin and FITC-conjugated isolectin (left panel). On the right, quantification of capillaries/CM ratio on sham-operated and TAC MCU OE, MCU KD and Empty mice (n=7 mice for each study per group; *, $p < 0.05$). **(C)** Percentage of CM growth in 4 weeks Empty, MCU OE, MCU KD TAC mouse hearts. The values were compared to those obtained in sham-operated littermates. In **(B)** and **(C)**, * is referred to group-matched sham, # is referred to 4 weeks TAC Empty. (n=200 CMs for each study group; *, $p < 0.05$). **(D)** Average thickness, measured transversally, of Right Ventricle (RV), Inter-Ventricular Septum (IS) and Left Ventricle (LV), in heart sections from 4 weeks Empty, MCU OE and MCU KD TAC mice. (n=24 heart sections from 4 different mice for each group; *, $p < 0.05$.

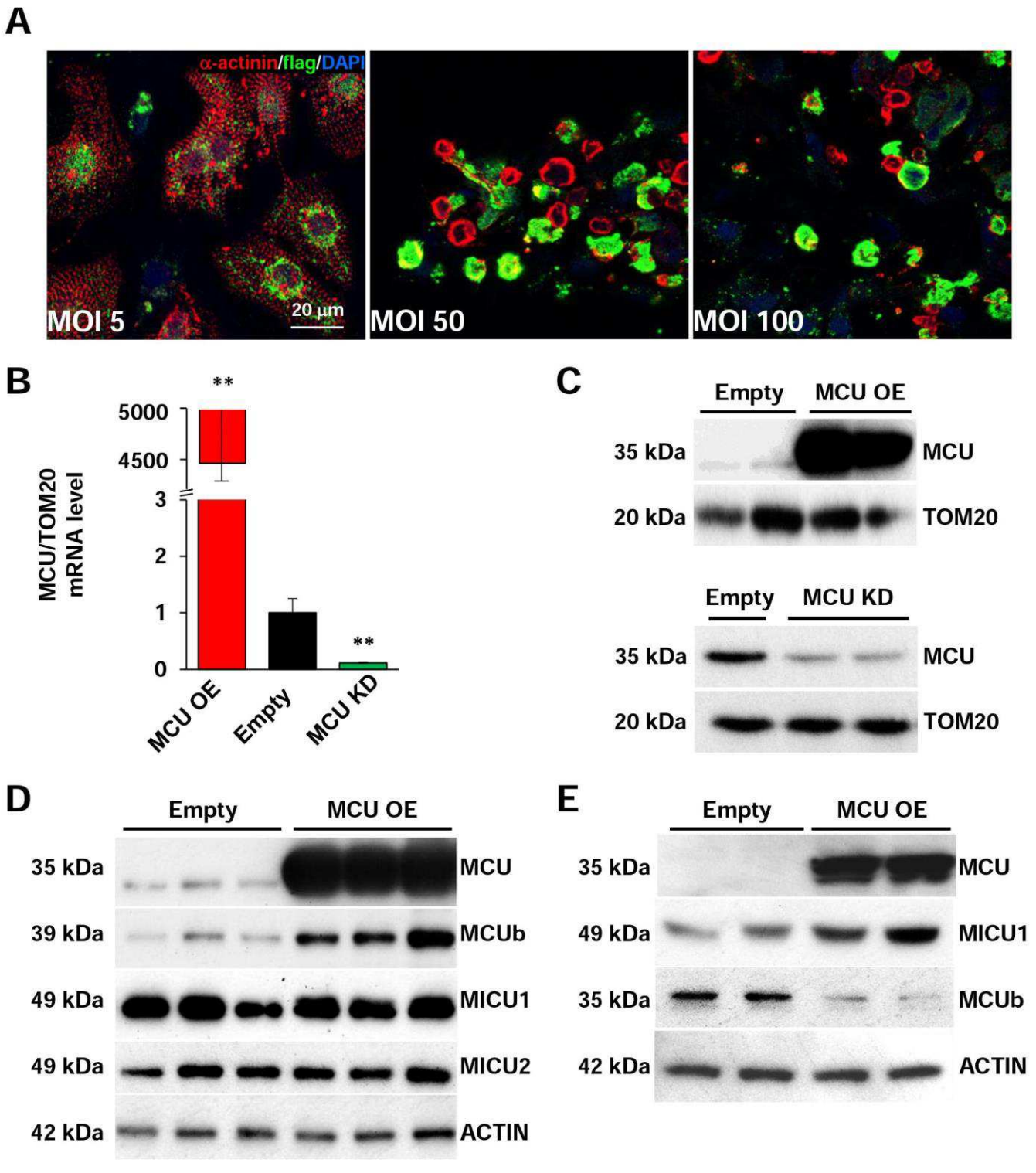

Fig. 13. MCU can be modulated *in vitro.*

(A) Confocal IF analysis on cultured rat neonatal CMs, infected with Ad-MCU-flag at different MOIs (5, 10 and 50), co-stained with antibodies to flag (green) and α-actinin (red). Nuclei were counterstained with DAPI (blue). **(B)** RTqPCR and **(C)** WB analysis of mRNA and protein extracts from MCU OE, Empty and MCU KD CMs. In **(B)** MCU mRNA levels were normalized to TOM20. (n= 6 samples for each group; **, $p < 0.01$). In **(C)** immunostaining with TOM20 was used to ensure equal mitochondrial protein loading. **(D-E)** WB analysis on protein extracts from MCU OE and Empty CMs **(D)** and control and MCU OE HEK293 cells **(E)**. The protein content of MCU and its partners was evaluated. Immunostaining with actin was used to ensure equal protein loading. (In **(C-E)**, n= 6 samples for each study group).

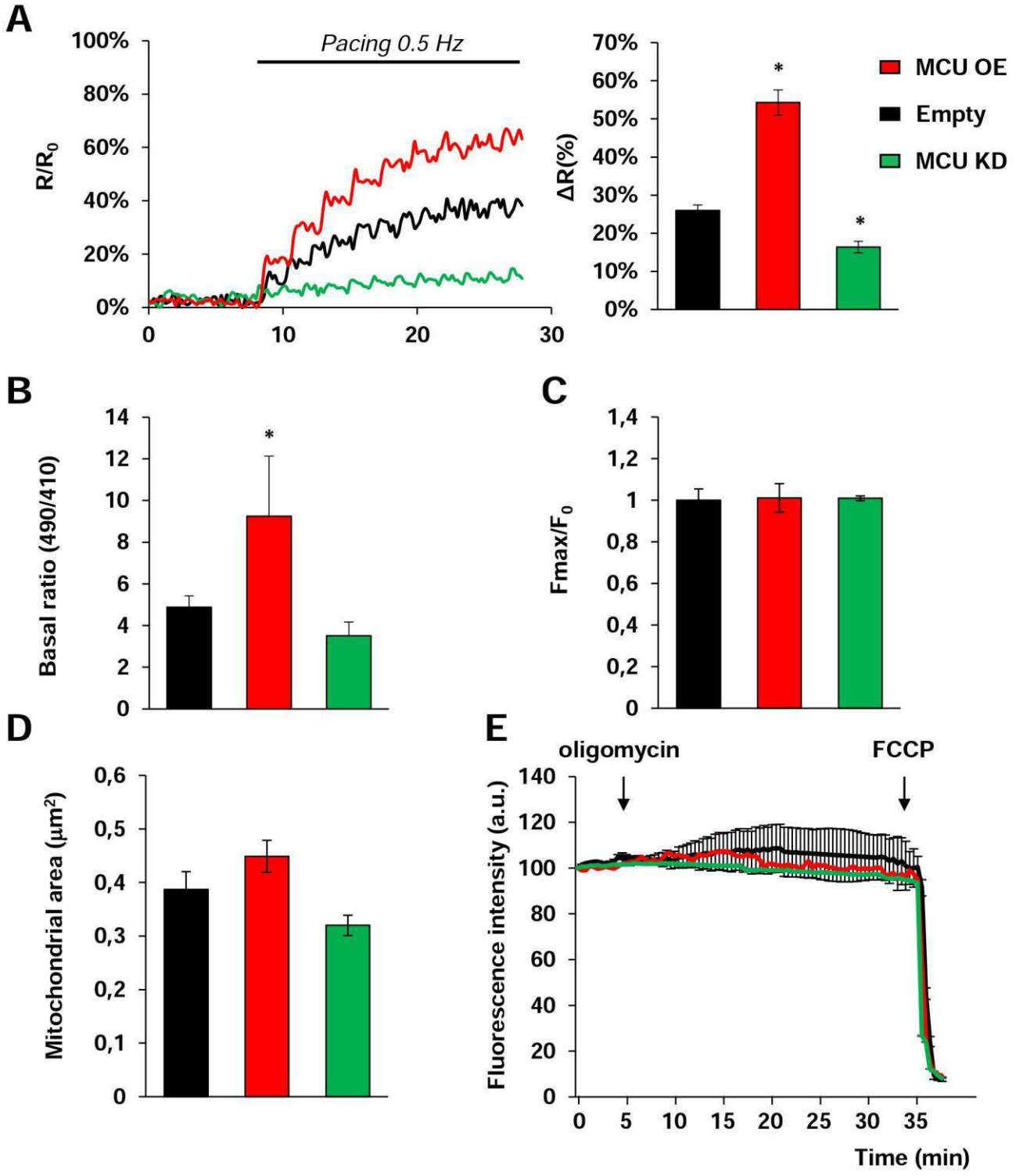

Fig. 14. MCU modulation does not affect cardiomyocytes homeostasis at baseline.
(A) Live imaging of mitochondrial Ca^{2+} uptake measured, during electric stimulation, in MCU OE, MCU KD and Empty CMs, transfected with mito-cameleon. The left panel shows a representative trace of $mtCa^{2+}$ dynamics showing that MCU OE CMs reached a higher steady-state Ca^{2+} level in shorter time compared to controls. Conversely, in MCU KD cells an opposite behaviour was observed. The right panel shows statistics of the average steady-state Ca^{2+} level in the three experimental groups. (n=45 cells per group; *, $p<0.05$). **(B)** Relative mitochondrial Ca^{2+} content, measured in baseline conditions with the high-affinity ratiometric probe 2mtGcaMP6, showing the highest Ca^{2+} levels in MCU OE CMs. (n=40 cells per group; *, $p<0.05$). **(C)** Histogram representing the average peak amplitude of cytosolic Ca^{2+} transients measured as F_{max}/F_0 in FLUO-4AM loaded CMs. (n=30 cells per group). **(D)** Measurement of mitochondrial mean area, measured in TEM images, in the three experimental groups. (n=20 mitochondria per group). **(E)** Imaging analysis of mitochondrial membrane potential, measured using TMRM in Empty, MCU OE, MCU KD CMs (n=20 cells per group).

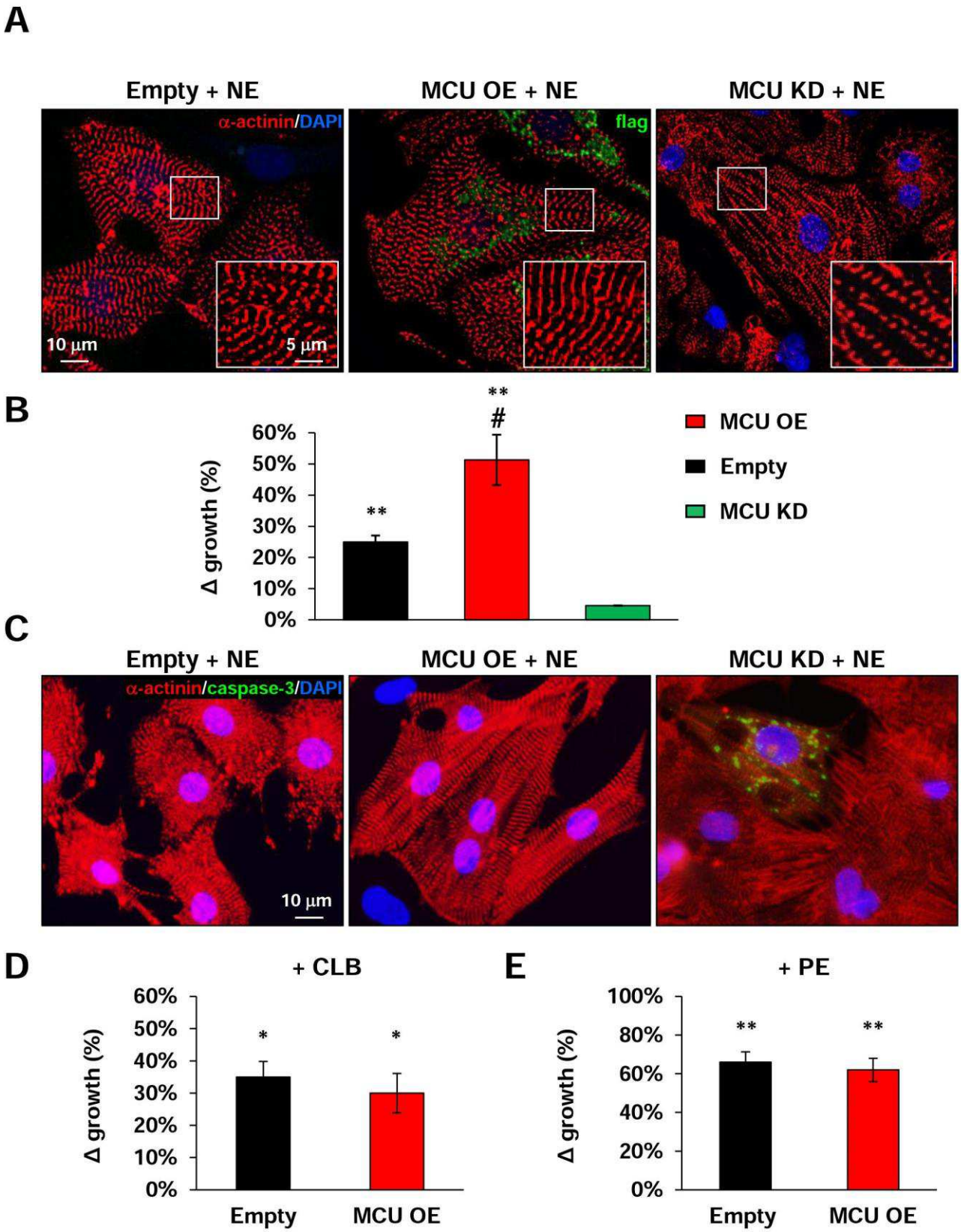

Fig. 15. MCU protein content affects cardiomyocyte hypertrophic response.
(A) Confocal IF analysis on cultured Empty, MCU OE and MCU KD CMs treated with NE (100 nM, 72h), stained with an antibody to α-actinin (red) and flag (green for MCU-OE). Nuclei were counterstained with DAPI (blue). **(B)** Percentage of CM growth measured in Empty, MCU OE and MCU KD CMs chronically treated with NE. Cell areas were compared with those of group-matched non-treated (NT) CMs. (n= 400 CMs per group, 3 replicates. **, $p < 0.01$). **(C)** Confocal IF analysis on cultured Empty, MCU OE and MCU KD CMs treated with NE (100 nM, 72h), co-stained with antibodies to α-actinin (red) and caspase-3. Nuclei were counterstained with DAPI (blue). **(D-E)** Percentage of cell growth occuring in Ad-Empty and MCU-OE CMs induced by treatment with clenbuterol **(D)** or phenylephrine (PE) **(E)**. (n= 400 CMs per group, 3 replicates. *, $p < 0.05$; **, $p < 0.01$). In **(B)** and **(D)**, * is referred to group-matched NT, # is referred to NE/CLB/PE-treated Empty CMs.

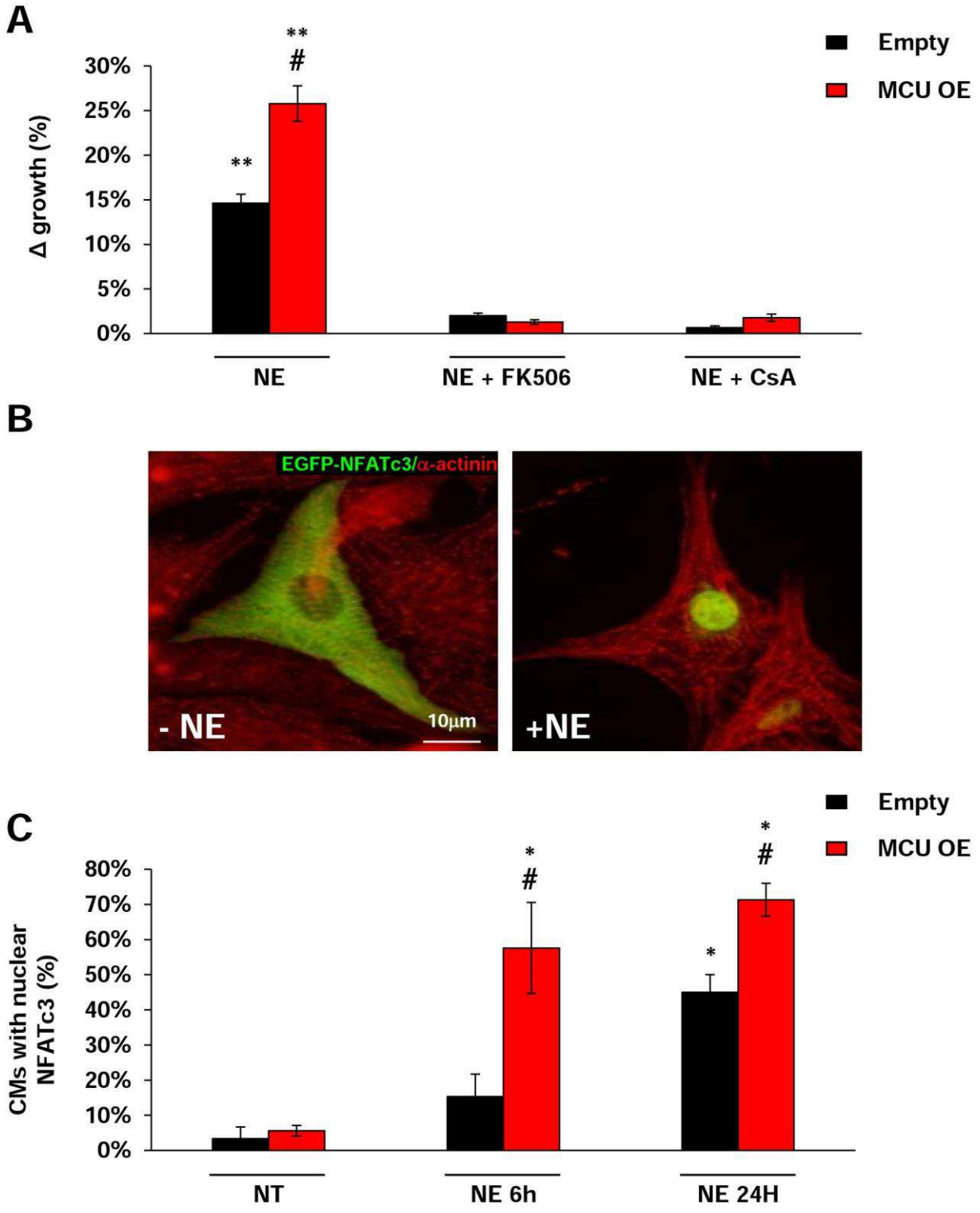

Fig. 16. MCU overexpression accelerates NE-induced calcineurin-mediated NFAT nuclear translocation.

(A) Percentage of cell growth in Empty and MCU-OE CMs, treated with NE in the absence or presence of the calcineurin inhibitors, cyclosporin A and FK506. (n=200 cells for each study group; **, $p < 0.01$). **(B)** IF analysis on control CMs transfected with EGFP-NFATc3 and treated with NE for 24 hours. Cells were stained with an antibody against α-actinin (red). The GFP signal localized in cytoplasm at baseline (left), while nuclear translocation occurs upon adrenergic stimulation (right). **(C)** Percentage of Ad-Empty and MCU-OE CMs showing EGFP-NFATc3 nuclear translocation, measured at baseline and at different time points after NE treatment (6 and 24 h). (n=200 CMs per group, *, $p < 0.05$). In **(A)** and **(C)**, * is referred to group-matched NT; # is referred to time-matched NE-treated Empty CMs).

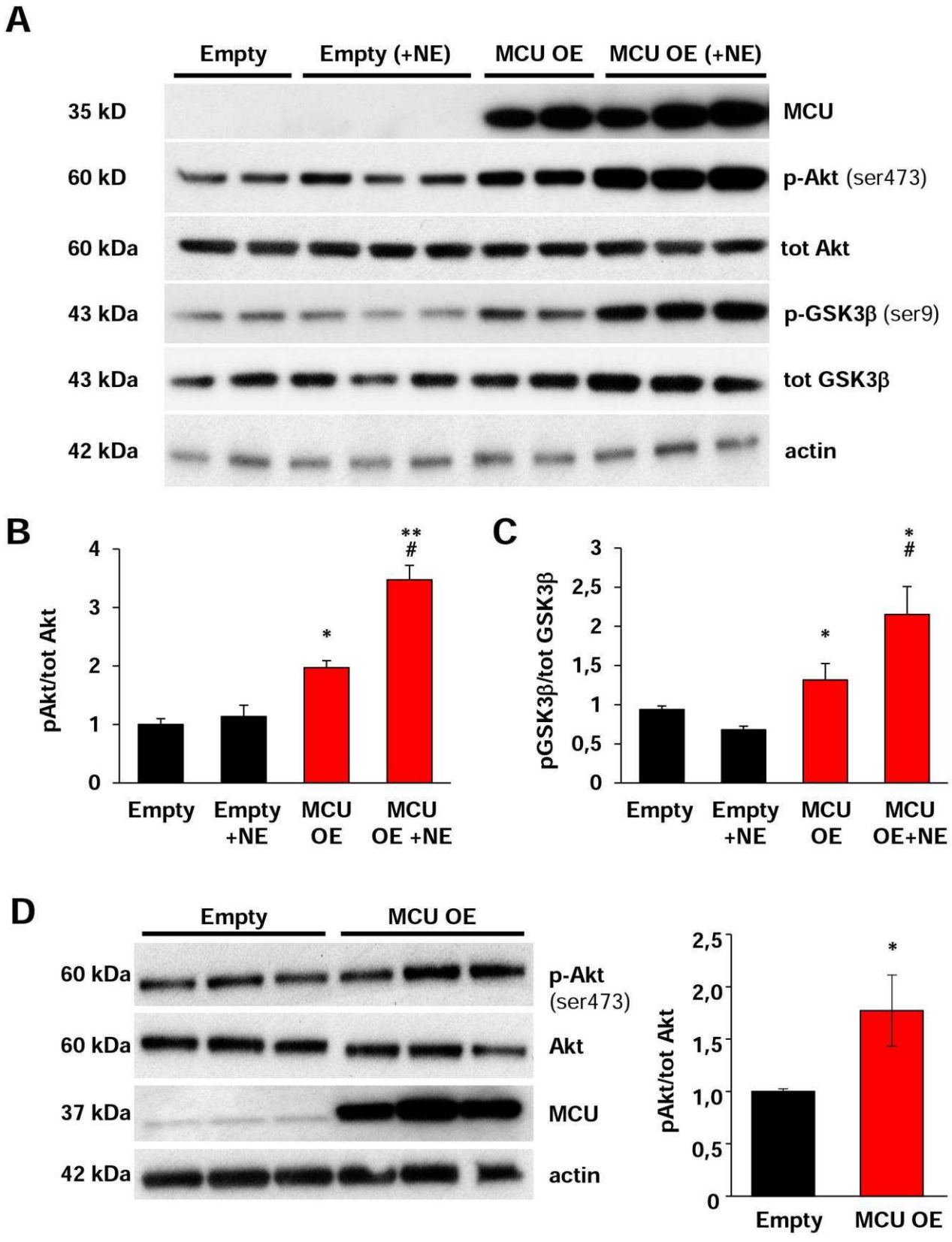

Fig. 17. MCU overexpression induces phosphorylation of Akt and GSK3b in basal conditions.
(A) WB analysis on protein extracts from Empty and MCU OE CMs, both not-treated (NT) and NE-treated (NE for 72 hours). Immunostaining with actin was used to ensure equal protein loading. **(B-C)** Densitometry analysis of the WB shown in **(A)**. (n=6 samples per group. *, $p<0.05$). **(D)** WB on protein extracts from control (AAV9-Empty) and MCU OE mice at baseline (left). The right panel shows the densitometry for p-Akt normalized on total-Akt. (n= 6 hearts rfor each group; 3 replicates. *, $p<0.05$. * is referred to Empty NT cells or control mice, # is referred to group-matched NT cells.)

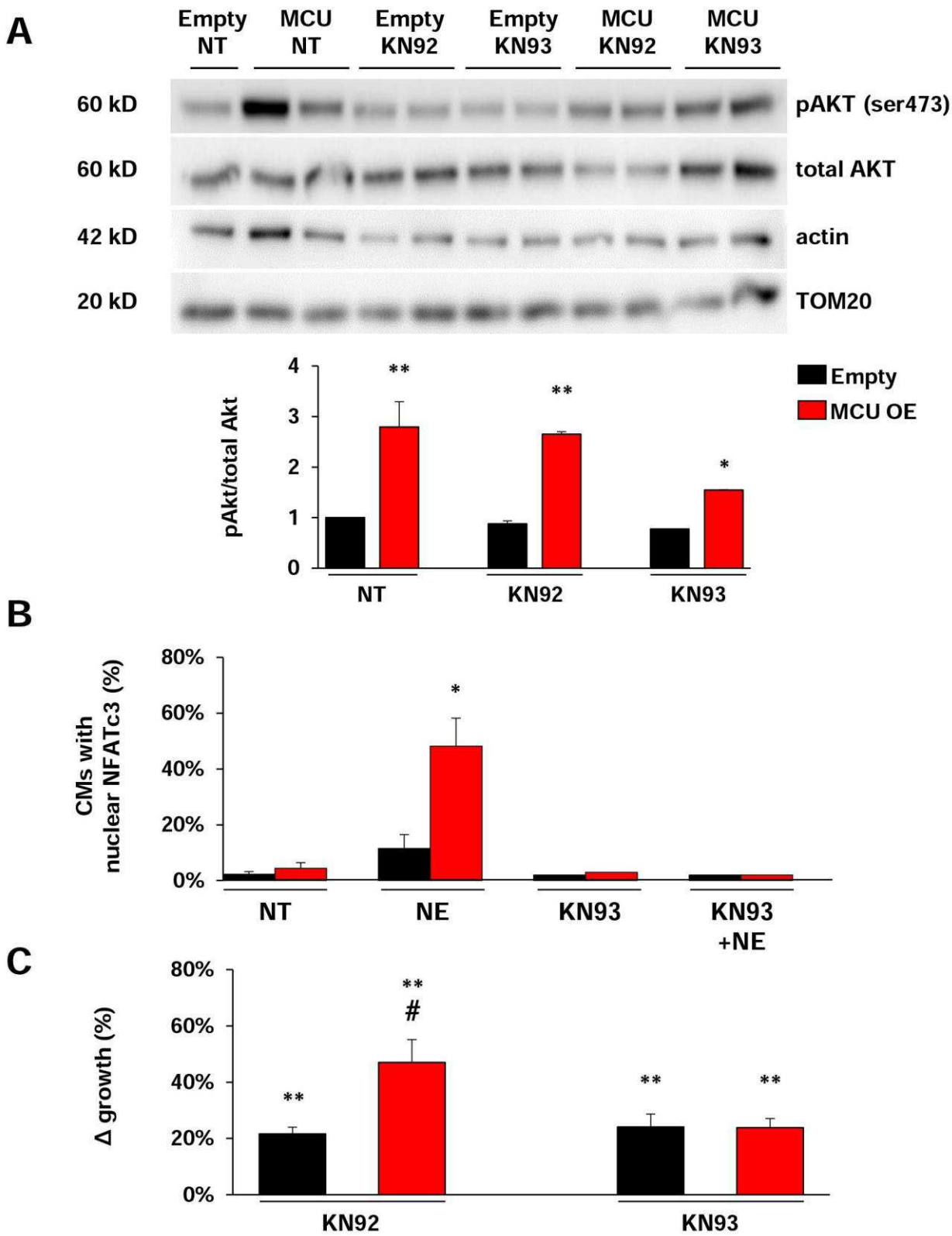

Fig. 18. CaMKII is involved in the amplified NE–induced hypertrophy of MCU overexpressing cardiomyocytes. (A) WB analysis (top panel) on protein extracts from Empty and MCU OE CMs not-treated (NT), treated with NE concomitantly with CaMKII inhibitor KN93 or with the inactive peptide KN92, to assess the activation state of Akt-GSK3β pathway upon CaMKII inhibition. The bottom panel shows the relative densitometry. (n= 6 samples for each group; *, $p < 0.05$; **, $p < 0.01$). **(B)** Percentage of Empty and MCU OE CMs showing nuclear localization of EGFP-NFATc3, both at baseline or after 6 h of NE treatment, both in the absence and the presence of KN93. (n=200 CMs in 2 replicates. *, $p < 0.05$). **(C)** Percentage of NE-induced growth in Empty and MCU OE CMs treated with KN93 or KN92, compared to group-matched cells treated with KN93 or KN92 in absence of NE (n= 300 CMs in 2 replicates for **(C)**. **, $p < 0.01$). In **(C)**, * is referred to group-matched NT CMs, # is referred to Empty NE-treated CMs.)

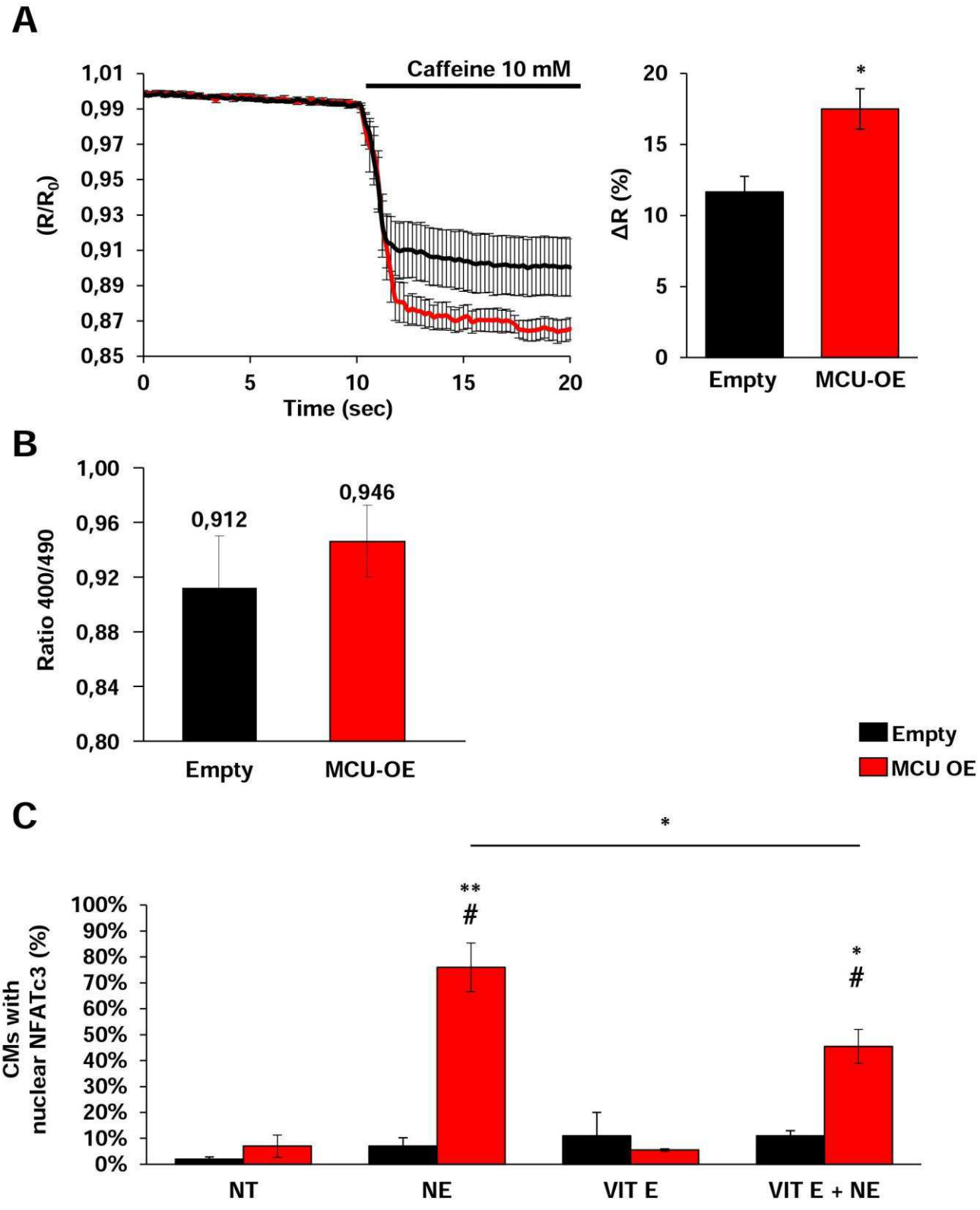

Fig. 19. MCU overexpressing CMs display increased SR Ca^{2+} content and mitochondrial ROS. (A) Representative trace of Ca^{2+} imaging experiment in cells transfected with the SR-targeted Ca^{2+} probe D4ER. SR Ca^{2+} content was estimated upon caffeine treatment in MCU OE and control cells. Right panel shows quantification of flurescence changes upon caffeine. (n=40 cells per group; *, $p<0.05$). **(B)** Mitochondrial ROS measurement in Empty and MCU OE cells, measured with roGFP1. (n=30 cells per group). **(C)** Evaluation of the percentage of control and MCU OE CMs displaying NFAT nuclear translocation, upon NE treatment both in the absence and presence of the antioxidant Vitamin E pre-treatment. (n=200 CMs per group. *, $p<0.05$; **, $p<0.01$). * refers to group-matched NT CMs, # is referred to treatment-matched Empty CMs.

3.3 RESULTS - III

To gain insights on the molecular mechanisms whereby MCU modulation impacts on CM hypertrophic remodelling, we performed several *in vitro* experiments (see *Results 3.2*), based on the use of cultured isolated cardiomyocytes (CMs), a commonly used model in experimental molecular cardiology[28,30]. Cardiac cells obtained from adult hearts are the ideal experimental model as they represent *in vitro* the cell type replicating more closely the phenotype of CMs in the intact heart. Nevertheless, technical and biological issues, such as the difficult procedure to isolate adult CMs and, more importantly, the short time in which cells can be maintained in culture, are the main limitations to the use of this cell type. CMs obtained from neonatal hearts are well-suited to be maintained in culture and amenable to genetic manipulation, but they display an immature phenotype with different electro-physiological, functional and structural properties as compared to adult CMs (see *Introduction 1.6*).

Moreover, mitochondria in CMs are strategically positioned in "hot spots" for Ca^{2+} signalling, such as in the proximity of ATP production and consumption sites (e.g. SR and myofibrils). In light of the role of Ca^{2+} in mitochondrial bioenergetics, and given the peculiarities of uptake kinetics, the location of mitochondria is pivotal in understanding the data obtained from experiments performed in cultured neonatal CMs. The completely different intracellular architecture shown by neonatal *vs*. adult CMs results in non-comparable environmental conditions in which mitochondria experience different kinds of Ca^{2+} handling. This is a major caveat in the use of neonatal CMs as an experimental tool for the study of the biology of mitochondrial Ca^{2+} uniporter, in favour of adult CM, which display greatly specialized Ca^{2+}-related intracellular structures.

On these basis, we sought to optimize the culture conditions with the aim to promote the maturation of neonatal CMs in order to preserve neonatal cellular plasticity in a more reliable and translatable cellular model which would ideally replicate some of the characteristics of the cells isolated from adult hearts.

This property would be crucial, for the reasons described above, for a correct study and interpretation of MCU role in CM homeostasis.

3.3.1 *In vitro* cardiomyocytes maturation: choosing the right medium

To develop a new protocol able to induce maturation of neonatal CMs, we focused on the composition of the media, maintaining the traditionally used technique to isolate cells from neonatal rat hearts (as described in *Methods 5.3*). For the complete description and comparison of the different *media* used in this project, see *Table 1*.

Differently from *Standard* medium, which is constituted mainly by DMEM (Dulbecco's Modified Eagle Medium), our *New* medium is based on MEM (Minimum Essential Medium). The lower glucose content (5 mM *vs.* 25 mM) led us to choose MEM as mainly constituent of both first and second day medium, to maintain cells in a glucose concentration similar to the physiologic[57] (see *Introduction 1.6*).

Considering the fact that fetal serum tends to maintain cells in an undifferentiated state, we thus focused our attention on this component of the *media*, and therefore we decided to lower the total serum content in both first and second day medium (from 15% in *Standard* medium to 10% v/v in *New* medium, from 5.5% to 0%, respectively). Additionally, we replaced horse serum (HS) with fetal bovine serum (FBS), thus reducing the quantity of nutrients and growth factors. On the other hand, we decided to add a combination of growth factors typically used in adult CMs culture, such as insulin, transferrin and sodium selenate, known to preserve and enhance sarcomere arrangement of the cells.

By using morphologic, morphometric and biochemical analyses, we thus assessed the effect of these modifications of culture conditions (from *Standard* to *New* protocol) on the cellular phenotype.

3.3.2 Reduction of proliferating fibroblasts and increase of cardiomyocyte purity in culture

Although the standard procedure to obtain neonatal CMs includes manoeuvres to increase the preparation purity and increase the fraction of CMs, among the several cell population present in the tissue fragments, a small amount of cells able to divide inevitably contaminates the preparation, especially in prolonged term cultures. Cardiac fibroblasts that are not perfectly removed during preparation have the potential to do this and, upon differentiation into myofibroblast, increase collagen synthesis and secretion, and establish

direct cell-cell coupling with CM. Both the direct interaction and the paracrine communication with CMs has the potential to induce CM de-differentiation[31-34].

With this in mind, we thus aimed at minimizing the stimuli that would promote fibroblast growth, which was already decreased by the reduction of glucose and the removal of serum in the culture medium, by adding from the first day after cell separation, the anti-proliferative agent bromodeoxyuridine (5-Bromo-2'-deoxyuridine, BrdU). BrdU is a thymidine-analogue that, once incorporated into newly synthetized DNA, inhibits cellular cell replication. Its effect on CM is negligible, given the very low mitotic index of these cells in culture.

To assess the percentage of contaminating fibroblasts and, therefore, the purity of *Standard vs. New* CMs culture, IF analysis was performed. By doing a double staining with an antibody specific for the sarcomeric protein α-actinin coupled with the nuclear marker DAPI, we could identify the CM fraction (positive for α-actinin) from the other cells present in the culture (positive to DNA-intercalated DAPI). Confocal microscopy analysis showed that the non-CM cellular population was significantly decreased in cultures obtained following the treatment with BrdU (CM fraction in *New* protocol, %: 85 ± 5 *vs. Standard* protocol: 65 ± 8) (**Fig. 20A**).

To investigate the effect of this treatment at different time points after cell plating, equal number of cells were plated at the same density in *Standard vs. New* medium and, after 5 days, fixed and processed for WB. Immunoreactivity for α-actinin and SERCA-2A resulted significantly increased in *New* neonatal CMs, as compared to *Standard* CMs, thus suggesting, *via* biochemical analysis, the higher percentage of CMs, per culture, in the newly developed protocol (**Fig. 20B**).

These data suggest that the addition of anti-proliferative agents in the culture medium is useful to reduce the number of proliferating cardiac fibroblasts in culture, thus enhancing CM purity in culture and, at the same time, lowering the de-differentiative effect that fibroblast have on cultured CMs.

3.3.3 Morphologic and morphometric characterization of cultured cardiomyocytes

To perform morphologic and morphometric analyses, we next fixed the cells and immuno-stained them with an antibody specific for α–actinin, a sarcomeric protein, which allowed the analysis of size and shape of *Standard vs. New* CMs.

The most evident difference between the two conditions regarded the size and shape of CMs, which showed a more regular and compact morphology, with a homogeneous distribution along the coverslip with the *New* culture conditions. Conversely, CMs cultured with the traditional protocol tended to clusterize and displayed several ramifications that resulted in an irregular shape (**Fig. 21A**). These initial qualitative observations were followed by quantitative analyses, performed on fixed samples processed for IF, imaged with confocal microscopy and analysed using *Image J* (see *Methods 5.3*).The measurement of the mean cellular area showed that the CMs cultured following the *New* protocol were bigger, as compared to CMs cultured with the *Standard* protocol (CMs area, μm^2: *Standard*: 800.8 ± 28.2 *vs. New*: 1017.9 ± 25.7) (**Fig. 21B**).

Once fully developed, the adult CM is characterized by a compact cylindrical shape and, when isolated and plated, it adheres to the coverslip displaying a regular-rectangular shape, with an evident major axis and the absence of invaginations (**Fig. 21A, right image**). To determine if the *New* protocol affected CMs morphology, we analysed the confocal images with specific plugins running in *Image J*, to evaluate several *shape factors*, including: *i) Aspect Ratio*, *ii) Roundness, iii) Solidity.* As reference, we performed the same analysis on isolated adult CMs.

i) Aspect Ratio (AR). This parameter is the ratio between the long and short axis of the cell. The ratio is highest in rod-shaped cells, such as isolated adult CMs. The analysis, performed in *Standard, New* neonatal and adult CMs, revealed that neonatal CMs cultured following the *New* protocol showed higher AR, with values close to those of adult CMs than that of *Standard* neonatal cells (**Fig. 21C**).

ii) Roundness. This coefficient is an index of the circumference-like shape of the cell. The mathematic formula is: $4*area/\pi*major\ axis^2$. Contrarily to AR, this parameter was chosen as indicator of less differentiated cells. The measurements performed showed that *Standard* neonatal CMs had higher roundness as compared to *New* neonatal CMs thus suggesting that, this latter cell type was more differentiated than the former. Consistently, adult CMs had the lowest roundness parameter, being mature (**Fig. 21D**).

iii) Solidity. This parameter represents the ratio between the total cellular and the convex area, being this latter the area of the polygon that best fits in. Solidity indicates the degree of regularity of the perimeter. A regular perimeter, determined by absence of invaginations and ramifications, is typical of adult mature CMs. Analysis of solidity showed higher values for *New* neonatal CMs as compared to *Standard* CMs, thus

indicating a more regular and mature shape in the cells cultured following the newly developed protocol (**Fig. 21E**).

Globally this set of data demonstrates, with unbiased quantification methods, that, compared to *Standard* protocol for neonatal CMs preparation, the *New* conditions yield more elongated cells, with regular membranes, and allow obtain a morphologic phenotype more closely resembling that of CMs isolated from the adult heart.

3.3.4 Analysis of sarcomere structure on cultured cardiomyocytes

The regular organization of contractile units in sequentially displaced sarcomeres is a hallmark of mature CMs. In the cells obtained from neonatal hearts, sarcomeres are not fully developed yet, and distribute roughly radially along the multiple cell membrane elongations, which may co-exist in multiple directions.

To determine whether the *New* protocol may promote sarcomeric organization, we evaluated the distribution profile of α–actinin in cultured CMs. The images of CMs incubated with anti-α–actinin antibody were acquired at high detail with confocal microscope, and analysed with *Image J* (**Fig. 22A**). The degree of organization of α–actinin was estimated by fluorescence measurement along a hand-traced line paralleling the cellular major axis. The graphs in **Fig. 22B** represent the *plot* of fluorescence intensity *profile*: as intensity of the fluorescence is proportional to immunoreactivity, intensity peaks are located in correspondence of Z-lines delimiting the sarcomere. While the fluorescence intensity profile observed in *Standard* neonatal CMs was irregular, in both peak intensity and frequency, *New* neonatal CMs showed increased organization and the peaks of fluorescence intensity were at a regular distance (about 1.6 ± 0.07 μm). The analysis on adult CMs demonstrated perfect repetition of fluorescence peaks, detected at the regular distance of 1.8 ± 0.04 μm.

These data suggest that the *New* protocol promotes, in neonatal CMs, the organization of contractile apparatus, hallmark of mature adult CMs.

3.3.5 Analysis of mitochondria on cultured cardiomyocytes

As previously described, one important difference between neonatal and adult CMs is represented by the displacement of the mitochondrial population. Indeed, neonatal mitochondria are almost exclusively found in the perinuclear region; conversely, the mitochondrial network observed in adult CMs shows three well-defined sub-populations: perinuclear, inter-myofibrillar, subsarcolemmal.

We thus decided to investigate mitochondrial distribution by performing morphological analyses, using confocal microscopy. IF staining performed on neonatal CMs cultured with the *Standard* and *New* protocol revealed that TOM20 signal, a protein found in the OMM, was different in the two experimental models. In *Standard* neonatal CMs, mitochondria were found in the typical perinuclear distribution, while *New* CMs showed mitochondria well positioned throughout the cell, in peripheral as well as inter-myofibrillar and subsarcolemmal regions (**Fig. 23A**).

Additionally, TEM images were analysed. Interestingly, *New* CMs displayed a higher organized structure, with mitochondria tightly placed along sarcomeres and SR cisternae. In line with this, mitochondria occupied a percentage of the total cellular area that was higher in *New* CMs (area mito/total area, %: *Standard*: 14.3 ± 3.8 *vs*. *New*: 21.3 ± 2.1). Moreover, a light increase of electron density, which did not reach statistical significance, suggested a more developed OXPHOS machinery (**Fig. 23C-D**). Interestingly, preliminary observations suggested also the existence of T-tubules, which are absent in CM cultured in *Standard* conditions (**Fig. 23B**). These preliminary observations are now object of further investigations, to achieve statistical power.

3.3.6 Characterization of spontaneous contraction frequency and RyR2 distribution on neonatal cultured cardiomyocytes

During de-differentiation, cultured neonatal ventricular CMs express an electro-physiological phenotype similar to SAN pacemaker cells[85], showing spontaneous rhythmic depolarizations. Conversely, working CMs isolated from adult hearts do not show spontaneous activity and only contract in response to electrical depolarization. Spontaneous contraction frequency (SCF) represents therefore an indicative parameter of the maturation state of neonatal CMs. To measure SCF in *Standard vs. New* CMs, cells

were placed on the stage of a bright field microscope (Olympus CK30), where short movies (1 minute) were recorded and contractions determined by analysis of the digital sequences. The analysis of SCF in *Standard vs. New* CMs showed that, after 5 days of culture, *Standard* CMs spontaneously contract, synchronously within the single clusters, at a higher frequency than *New* CMs (SCF, Hz: *Standard* CMs: 0.45 ± 0.07 *vs*. *New* CMs: 0.02 ± 0.01) (**Fig. 24A**).

Among the molecular components involved in the modulation of spontaneous contractions and in CICR, RyR2 has a key role. During postnatal development, RyR2 expression increases and the protein achieves its mature distribution appearing in clusters localized along lines parallel to Z-bands in correspondence to the terminal SR cisternae[216]. To analyse RyR2 expression and distribution in *New* neonatal CMs, immunofluorescence analysis was performed. Image analysis showed that *New* CMs had a significatively increased RyR2 signal, which clustered in a similar fashion to that of adult cells (**Fig. 24B**). The correct localization and clustering of RyRs, typical of adult CMs, is essential for the formation of Ca^{2+} Release Units (CRUs), which are responsible for the small spontaneous diastolic Ca^{2+} release events, causing the localized and transient Ca^{2+} elevation known as "spark". These phenomena are detectable in cultured CMs loaded with Ca^{2+} probes in live imaging experiments with microscopes endowed with high-temporal and spatial resolution[85,216]. The magnitude and duration of Ca^{2+} sparks depend on RyR2 distribution as more organized CRUs determine faster and smaller Ca^{2+} sparks. The comparison of amplitude and speed of Ca^{2+} sparks was performed in FLUO-4 loaded CMs, obtained using either *Standard* or *New* protocols, and significant differences between the behaviours of the two populations was observed. Whereas *Standard* cardiomyocytes showed large prolonged macro-sparks and travelling Ca^{2+}, *New* CMs displayed short lasting and small Ca^{2+} sparks, similar to those recorded in isolated adult CMs (**Fig. 24C**).

This functional aspect suggests a more "mature" RyR2 expression and localization in neonatal CMs cultured with our *"newly"* developed protocol.

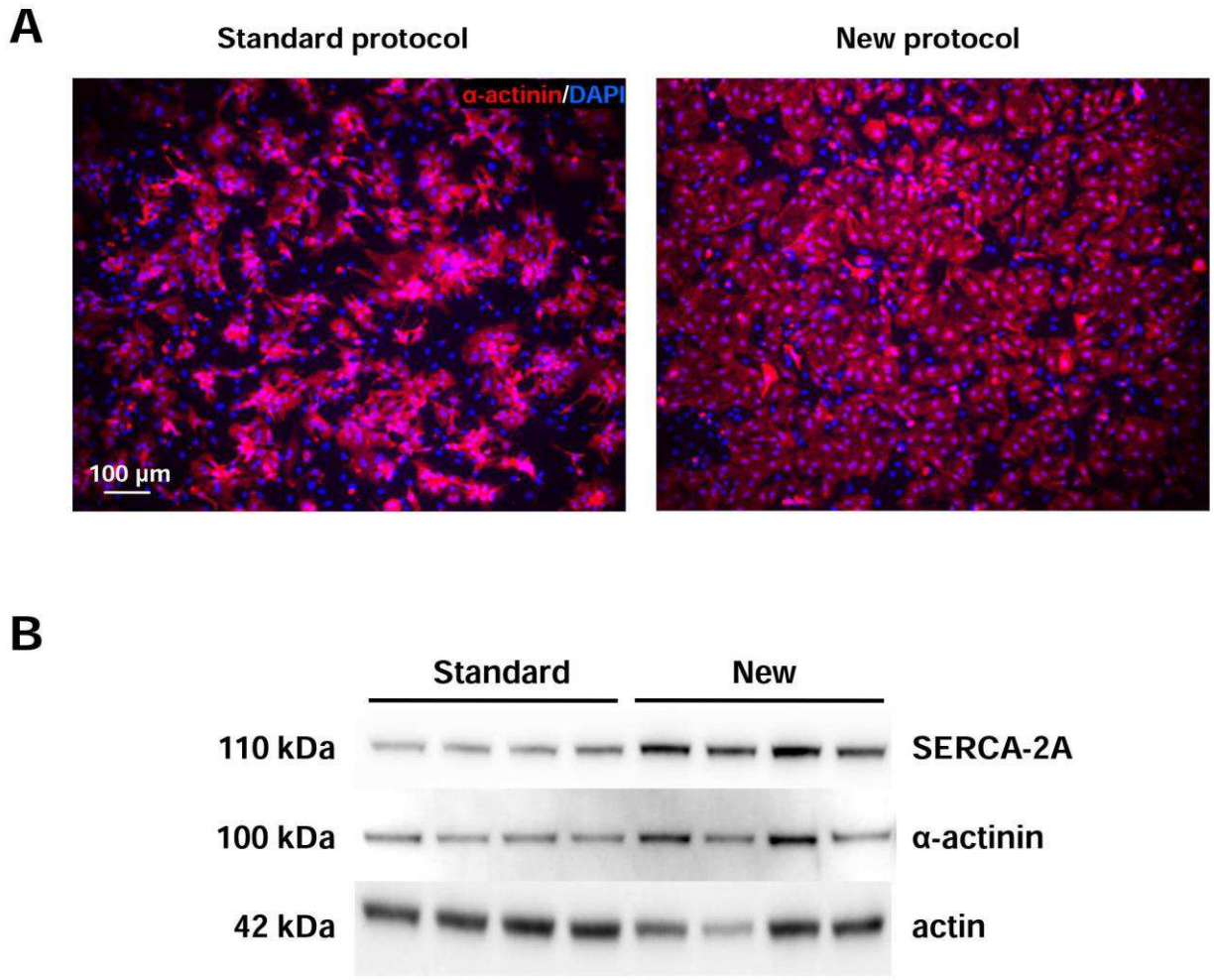

Fig. 20. Establishment of a novel protocol to increase the purity of cultured neonatal cardiomyocytes.

(A) IF analysis on rat neonatal CMs cultured with the *Standard* (left panel) and the *New* protocol (right panel). Cells were stained with an antibody to α-actinin. Nuclei were counterstained with DAPI. This procedure allowed to estimate the percentage of "non-cardiomyocyte" nuclei among the total cells in the coverslip, thus providing a percentage of CM purity. **(B)** WB analysis on protein extracts from CMs cultured with the *Standard vs. New* protocol. Actin was used as whole-cell protein loading control. (n= 3 replicates).

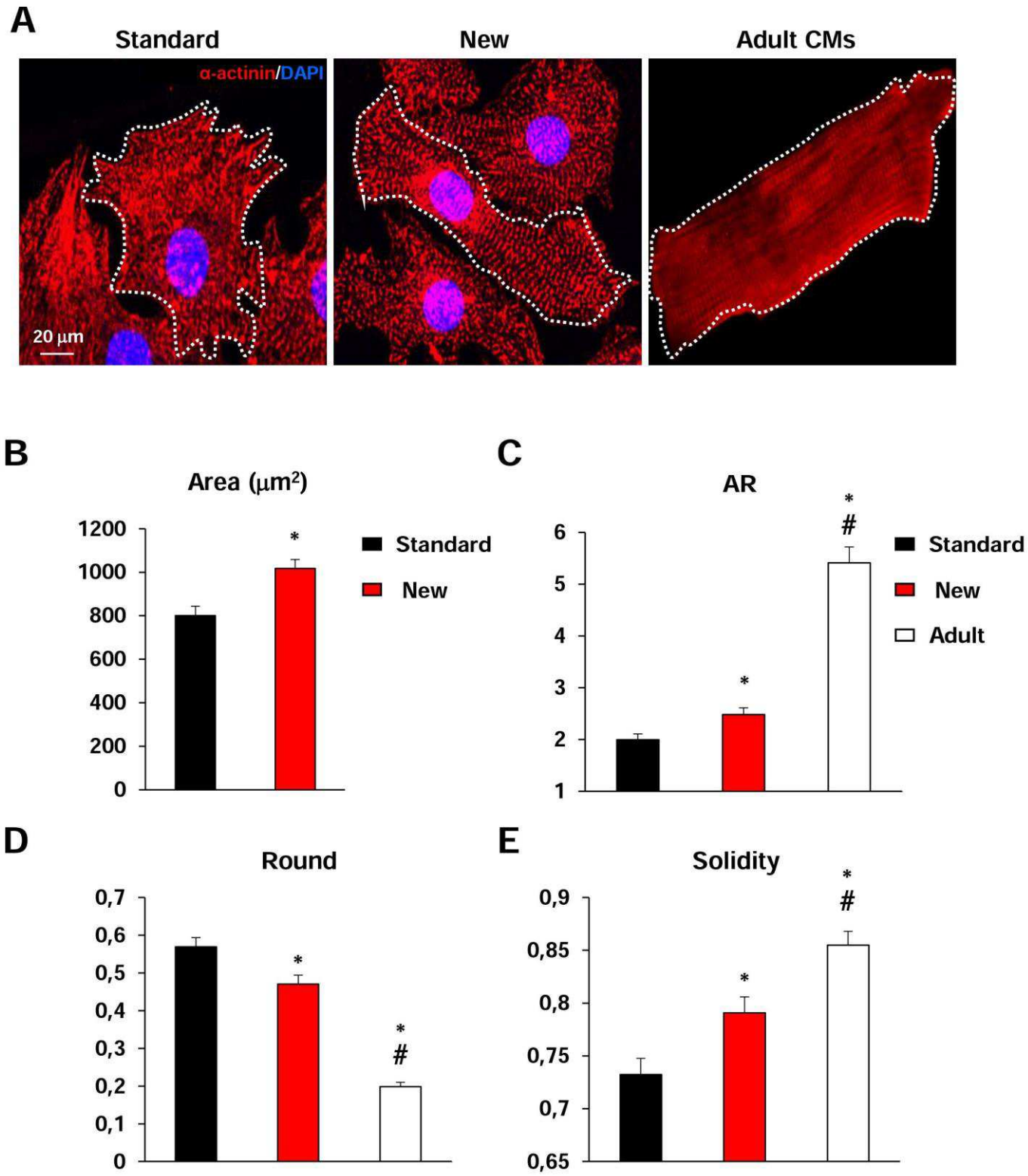

Fig. 21. Neonatal cardiomyocytes cultured with the novel protocol are more similar in shape to adult cells. (A) Confocal IF analysis on cultured rat neonatal CMs processed with the *Standard* (left) and *New* (right) protocols, as well as freshly isolated rat adult CMs. Cells were stained with an antibody to α-actinin. Nuclei were counterstained with DAPI. The white lines delineate the cellular profile. **(B)** Evaluation of cell area measured in neonatal CMs cultured with *Standard* and *New* protocol. **(C-E)** Morphometrical analyses (Aspect Ratio, AR, Round, Solidity) performed on neonatal CMs cultured with the *Standard* protocol (black bars) *vs.* the *New* protocol (red bars) *vs.* adult CMs (white bars). (n=100 CMs per group, 3 cultures. *, $p<0.05$; **, $p<0.01$. * is referred to *Standard* CMs, # is referred to *New* neonatal CMs).

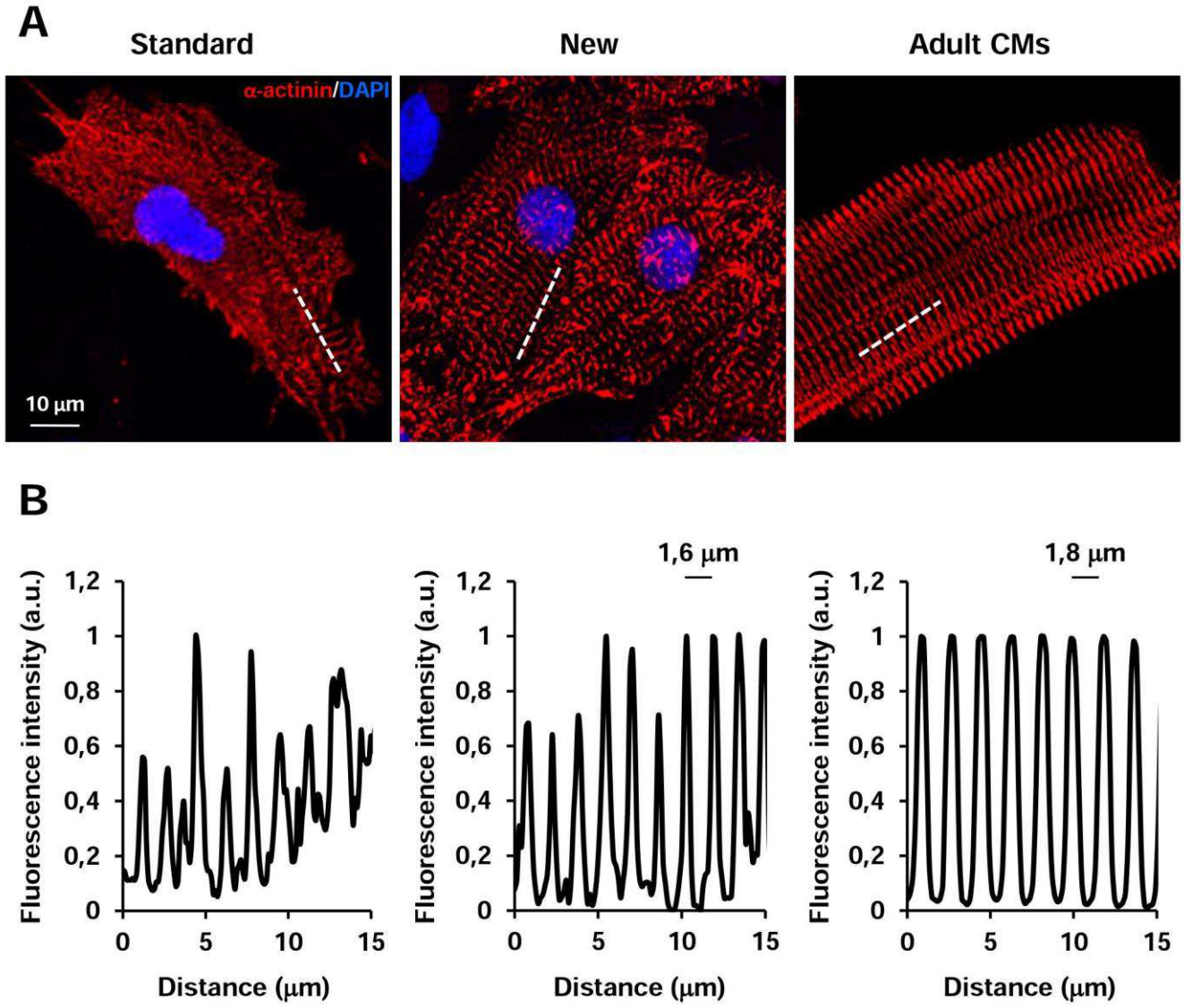

Fig. 22. Neonatal cardiomyocytes cultured with the novel protocol display higher sarcomeric organization. (A) Confocal IF analysis on neonatal CMs cultured with *Standard* or *New* protocols, as well as adult CMs, all stained with an antibody to α-actinin, to mark sarcomeric structure. **(B)** Fluorescence intensity analysis ("plot profile") of sarcomeric α-actinin signal along the dashed line in (A) showed a more regular signal in *New* CMs compared to *Standard* ones, resembling the perfectly-localized signal detected in adult CMs. (n= 10 CMs per group).

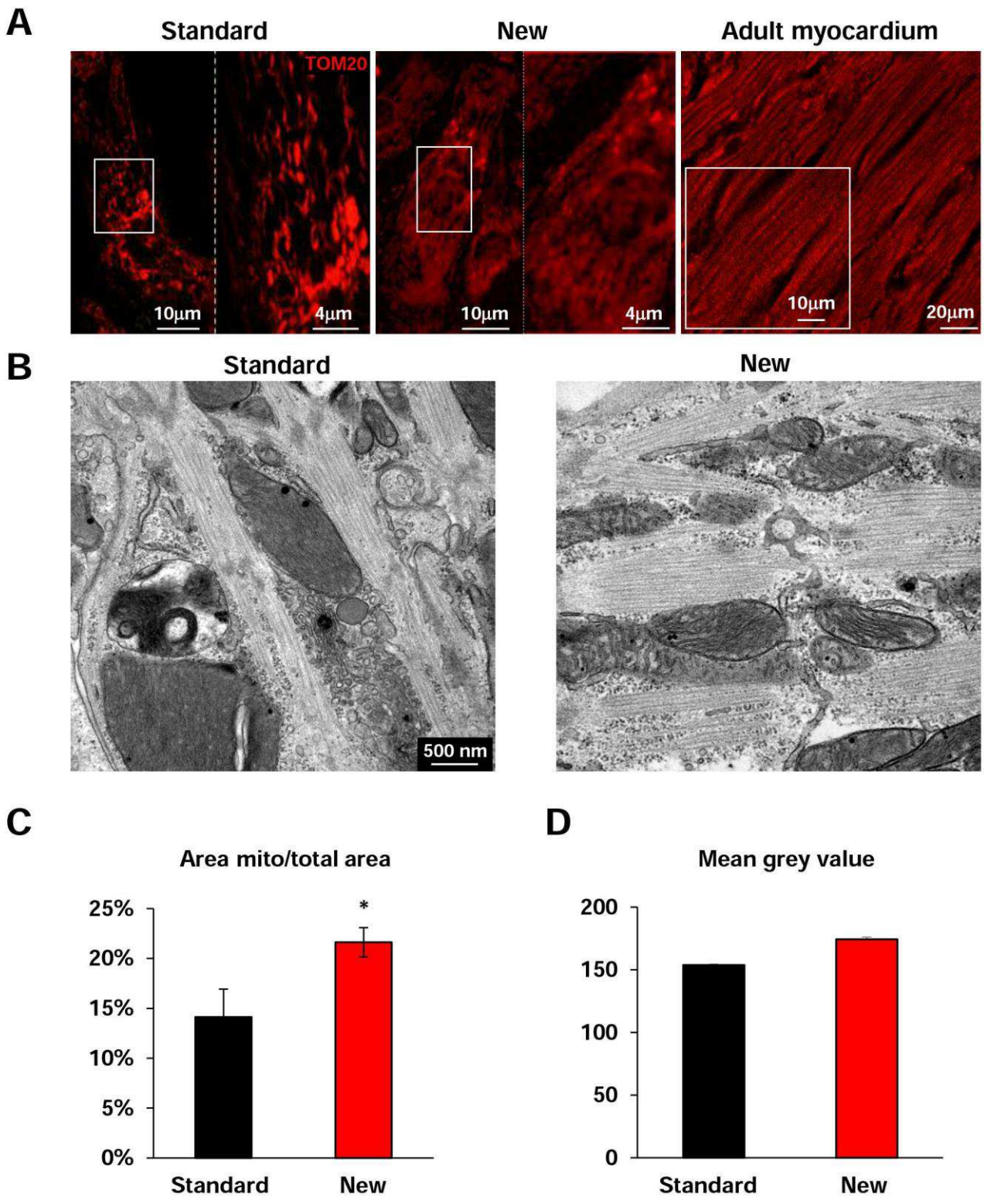

Fig. 23. Neonatal cardiomyocytes cultured with the novel protocol display increased ultrastructural organization. (A) Confocal IF analysis on neonatal CMs cultured with *Standard* or *New* protocols, as well as on heart cryosection, all stained with an antibody to TOM20, to detect mitochondria. **(B)** Transmission Electron Microscopy (TEM) analyses performed on *Standard* and *New* neonatal cultured CMs. **(C)** Measurement of the ratio between the area occupied by mitochondria and the total cellular area in *Standard* and *New* CMs. **(D)** Mean grey value in *Standard* and *New* CMs , index of ETC complexes-derived electron density. (n=20 CMs per condition; *, $p<0.05$).

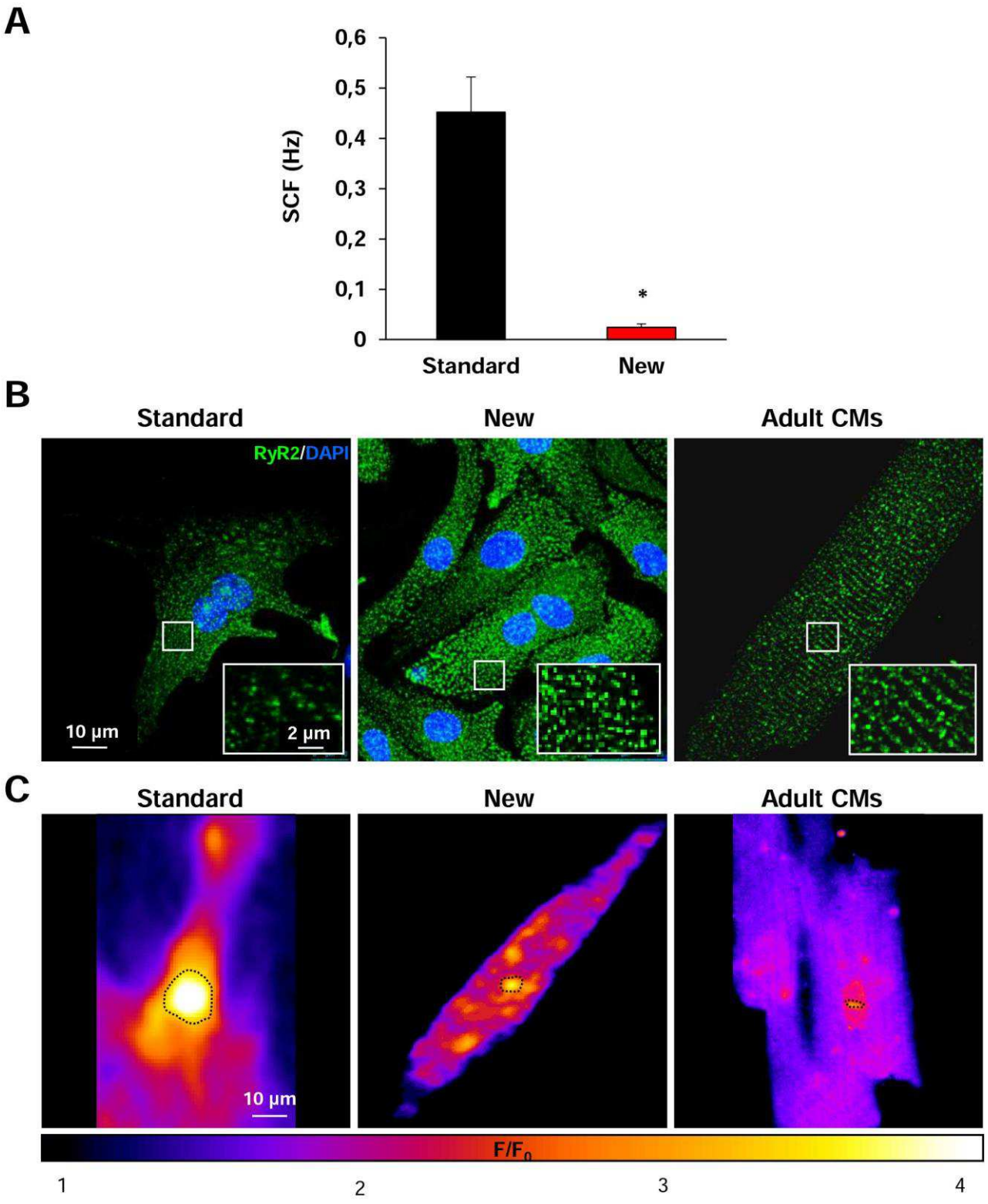

Fig. 24. Neonatal cardiomyocytes cultured with the novel protocol display descreaed spontaneous contraction frequency and improved RyR2 distribution.
(A) Quantification of spontaneous contraction frequency (SCF) in *Standard* and *New* neonatal CMs, measured both at bright field and with real-time imaging of Ca^{2+} dynamics. (n=20 CMs per group, *. P<0.05) **(B)** Confocal IF analysis on neonatal CMs cultured with *Standard* or *New* protocols, as well as adult CMs, all stained with an antibody to RyR2. **(C)** Live imaging of Ca^{2+} sparks in neonatal CMs cultured with *Standard* or *New* protocols and adult CMs revealed more frequent events in *Standard* CMs as compared with *New* and adult CMs. Dashed black lines represent the amplitude of a single Ca^{2+} spark, much bigger in *Standard* CMs.

4. DISCUSSION AND FUTURE PERSPECTIVES

Matching energy production and cellular metabolic request is essential in cardiomyocytes (CMs), which are high-energy consuming cells, subjected to variable ATP consumption rates mainly depending on cardiac contractile load. Intracellular Ca^{2+} is a central mediator of contraction/metabolism coupling, as during the same heart cycle it modulates contraction on one hand and enters mitochondria stimulating ATP production, on the other[4]. Given that the heart is continuously subjected to acute and chronic inputs, resulting, respectively, in enhancement of contractility or stimulation of cell growth, both of which associated with increased energy demand, one would expect modulation of the mitochondrial Ca^{2+} uptake machinery to be a central need for adequate metabolic adaptation. Up to now, however, studies focusing on MCU (by itself or along with the multimolecular complex MCUC) fail to produce consensus about its role in cardiac pathophysiology and the mechanisms responsible for MCU and partners regulation are still largely unknown.

The observation that, during hypertrophic growth, MCU protein content increases with no alterations in mRNA transcription, led us to hypothesize that the protein expression could be regulated by some post-transcriptional mechanism. We thus focused on the role of microRNAs, which have been shown to play important roles in cardiac homeostasis.

In the first part of the thesis, we discovered that the 3'UTR region of MCU is a target of miR-1, a well-characterized modulator of protein expression in the heart, and that this modulation is evolutionarily conserved in many species, including mice and humans. Interestingly, miR-1 action is very specific for MCU among the MCUC components, and its activity is thus expected to modify the complex stoichiometry. According to current biophysical models of mitochondrial Ca^{2+} uptake, by selectively reducing MCU copy number within the complex, miR-1 would decrease mitochondrial ability to take up Ca^{2+} both directly and by the enhanced influence of the inhibitory MCU paralogue MCUb.

Our initial study demonstrated that the mitochondrial content of MCU increases in the compensatory phase of hypertrophy, reflecting the decrease in miR-1 expression. Interestingly, in advanced hypertrophy, this correlation does not play a major role, as MCU content decreases independently from miR-1 changes. Such observation supports

that miR-1 dependent regulation of the Ca^{2+} uniporter only has a rather limited range of action. This seems sensible, given that profound modifications in protein content would more easily be elicited by transcriptional rather than post-transcriptional effects. Together with the observation that miR-1 is a microRNA central to the regulation of cardiac plasticity, our findings prompt the speculation that in the early hypertrophic phase, fine tuning of MCU content is part of a wide spectrum of structural, metabolic and mechanical changes. This is further supported by the observation that, in the advanced, maladaptive phase of myocardial hypertrophy, the inverse relation between miR-1 and MCU is not preserved, with the latter decreasing when compared to its levels in the earlier phases of compensated remodelling, independently from miR-1.

These results clearly demonstrate that at least two classes of mechanisms modulate MCU during heart adaptation to chronic mechanical and metabolic stresses, both in preclinical, and more interestingly, in human hearts. While one such mechanism is represented by post-translational control by miR, the other(s) are yet to be uncovered.

These results opened the question on whether MCU *per se* has a role in myocardial adaptation in conditions promoting hypertrophy. This question, guiding the second part of the thesis is, at the time being, object of several parallel studies using different model systems, which failed to provide consensual answer, as discussed in detail in the introduction (see *Introduction 1.5*). We thus decided to approach this problem by using viral transduction in mice, to modulate (by either overexpressing or downregulating) MCU content in fully developed hearts, prior to exposing them to pressure overload.

Strikingly, MCU overexpression or downregulation determined two divergent fates upon TAC surgery. While MCU overexpressing (MCU OE) hearts had a prolonged compensated phase of hypertrophic response, with preserved contractility and cardiac structure, MCU knocked down (MCU KD) hearts suffered from precocious maladaptive remodelling. These results strongly support that MCU is beneficial for CMs to tolerate increased workload, and are in line with the evidence that increased mitochondrial Ca^{2+} enhances ATP synthesis, which is in turn required to sustain the increase cardiac work during pressure-overload[11]. Although this data adds another piece to the rather confounding puzzle picturing the role of MCU in cardiac homeostasis, the differences in the approach used to modulate MCU content offer possible explanations. For instance, while in constitutive KO mice, MCU is ablated from birth, and in conditional KOs, MCU

is totally ablated at a given time point during adult life, MCU silencing viral transduction has a "softer" effect of reducing MCU levels within a rather limited range. Based on the results of the experiments in murine or human hearts subjected to TAC, such degree of protein content change mimics more closely the pathophysiological situation. To gain insight into the mechanisms linking MCU to CM hypertrophy, we analysed in parallel the effects of its modulation in cultured cells, undergone prolonged adrenergic stimulation to mimic the effects of the enhanced sympathetic neuron activation occurring during pressure-overload. In strict similarity to what happens *in vivo,* MCU OE CMs had more pronounced hypertrophy and preserved cell morphology when treated with NE, compared to controls; conversely, MCU KD CMs replicated the *in vivo* phenotype showing sarcomere disarrangement and lethal growth. The *in vitro* system offered the possibility to dissect the molecular players responsible for such behaviour. The investigations described here were mostly focused on the effects of MCU overexpression. Based on the combined results from Ca^{2+} imaging, molecular and biochemical analyses, we demonstrated the involvement of CaMKII, Akt, GSK3β, and CN/NFAT signalling pathways in the response to adrenergic stimulation. These molecular mediators may be linked to MCU overexpression by the working model whereby: i) MCU overexpression determines a slight increase in mitochondrial ROS production, causing CaMKII oxidation, which has been shown to increase its Ca^{2+} sensitivity; ii) the increased SR Ca^{2+} content, fuelled by higher ATP synthesis, reflects on Ca^{2+} availability for CaMKII activation; iii) oxidized CaMKII, by phosphorylating Akt would inhibit GSK3β, thus relieving the block of CN/NFAT signalling. Altogether, these effects may precondition the pro-hypertrophic signalling pathway, thus amplifying the response to hypertrophic stimuli impinging on the same route, such as NE/β-AR activation.

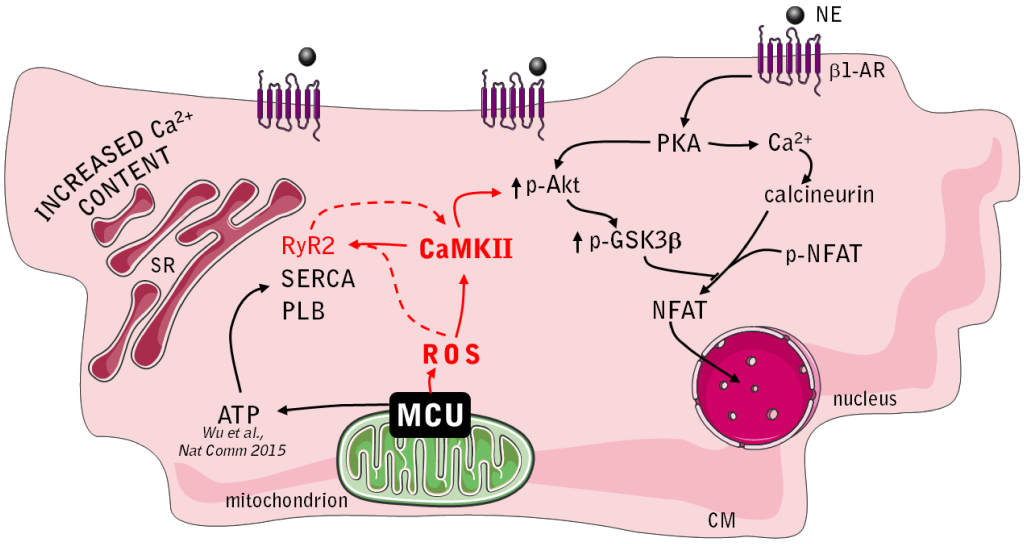

Figure 13. Our working hypothesis. As shown, we hypothesize that MCU overexpression leads to increased ATP production[11], thus enhancing SERCA activity and increasing SR Ca^{2+} content. Concomitantly, MCU overexpression determines increased ROS production, which oxidize CaMKII and RyR2, this latter object of CaMKII phosphorylation. Increased SR Ca^{2+} activates CaMKII, which phosphorylates and activates Akt, resulting in phosphorylation and inhibition of GSK3β. Upon β1-AR stimulation, the canonical PKA/Ca^{2+} activated pathway calcineurin/NFAT, therefore, is accelerated because of the absence of the constitutive inhibition by GSK3β.

In essence, our *in vitro* and *in vivo* models identify MCU overexpression as protective, and we may speculate that some concurrent factors may determine its beneficial effects. These include Akt activation, increased ATP availability (shown by Wu et al., still not proven by us), and finally, the hormetic effect of the MCU-dependent moderate elevation in ROS, altogether fulfilling the increased metabolic requests occurring in expanding CMs.

In parallel, on-going experiments are aiming at understanding how MCU knockdown determines maladaptation to adrenergic stimulation and precocious HF in TAC-mice.

The identification of the mechanisms by which MCU impacts on myocardial remodelling is of great relevance for the refinement of the understanding of cardiac pathophysiology. In addition, having uncovered a novel pathway tuning MCU content via miR-1, opens to the potential therapeutic use of antagomiRs or miR-mimics for MCU modulation in cardiovascular therapy.

5. METHODS

5.1 *In vivo* procedures

All experimental procedures were performed according to the European Commission guidelines and have been approved by the local ethical committee and the Italian authority (Ministero della Salute), in compliance of Italian Animal Welfare Law (Law n. 116/1992 and subsequent modifications).
In this thesis, the *in vivo* experiments were performed on C57BL/6J male mice (all from Charles River, Milan, Italy). The *in vitro* experiments were performed by isolating CMs from neonatal (P0-P3) Sprague-Dawley rats.

Viral infection of neonatal mice

MCU overexpression and downregulation were achieved *via* intraperitoneal injection of adeno-associated viral (AAV) vectors coding for MCU-flag or sh-MCU-zgreen (pZacf-U6-MCU-ZsGreen, Vector BioLabs), respectively, in P9 male mice. A Hamilton syringe equipped with 35 gauge needle was used to inject $1*10^{11}$ GC (genome copies) of the viral agents. A non-coding virus (AAV-Empty) was used as control. All AAVs used are serotype 9, known in literature as the most cardio-specific serotype available[217].

Echocardiography

Echocardiography is a non-invasive diagnostic technique based on the application of ultrasound. Pulses of ultrasound are sent to the heart by a transducer, and their echo is recorded by the detector. The machine used is Vevo 2100™ (VisualSonics, Toronto, Canada), equipped with 30 MHz transducer (see fig.14). To perform echocardiography, mice were anesthetized with isoflurane (3% v/v in O_2 for the induction of anesthesia, 1.5% for maintenance). During the analysis, temperature, respiration rate and ECG were constantly monitored. Two-dimensional cine loops with frame rates of 200 frames per second of a long-axis view and a short-axis view at proximal, mid, and apical level of the LV were recorded. Interventricular septum (IVS) and LV posterior wall (LVPW)

thicknesses, LV internal diameter (LVID) and maximal LV length were measured in systole (s) and in diastole (d) from the long axis B-mode image, according to standard procedures. Ejection fraction (EF) was determined by the following formula: Simp EF (%) = 100xSimp Systolic Volume (SV)/ Simp LV volume; d. Echocardiographic image acquisition and analysis were performed by a single operator, blinded to the mouse phenotype.

Figure 14. Echocardiograph Vevo 2100™ (VisualSonics, Toronto, Canada).

Transverse aortic constriction (TAC)

Adult (3 months) male mice were anesthetized with Zoletil (15mg/gr, i.p.) and placed in a supine position under the dissecting microscope. Animals were intubated using a 24G needle, and ventilated (tidal volume 0.4 ml, 120 strokes/min) with an artificial ventilator

(SAR-830). The chest cavity was entered in the second intercostal space at the left upper sternal border through a small incision, and aortic constriction was performed by tying a 7-0 nylon suture ligature against a 27-gauge needle to yield a narrowing 0.4 mm in diameter when the needle was removed and a reproducible transverse aortic constriction (TAC) of 65-70%. Body temperature was constantly monitored during the entire experiment. Mice were sacrificed and hearts were removed after 1, 4, 8 and 14 weeks after surgery.

Treadmill exercise

Adult (3 months) were trained on a treadmill chamber (Harvard Apparatus) for 60 minutes/day, 5 days/week, for 8 consecutive weeks (see fig.15). In detail, after acclimation to the treadmill, mice started to warm up at 10cm/sec increasing the running speed with 2cm/sec every 2 minutes until 18cm/sec was reached. Afterwards, high-intensity aerobic interval training was performed, alternating between 4 minutes of maximal speed and 2 minutes of slow speed for a total of 10 repetitions. To determine maximal oxygen uptake (VO_2max), mice ran a ramp protocol until exhaustion on a customized treadmill in a metabolic chamber.

Figure 15. Mice during endurance training on the treadmill chamber (Harvard Apparatus).

5.2 *Ex vivo* procedures

Selection and use of human samples.

Patients with aortic stenosis who underwent aortic valve replacement were recruited retrospectively from the biobank of the University Hospital of Verona, Division of Cardiac Surgery, Verona, Italy. Approval for studies on human tissue samples was obtained from the Ethical Committee of the University Hospital of Verona. Each patient gave written informed consent. Septal specimens were collected from five healthy donor hearts rejected for transplantation, and included as controls (experimental protocols approved by the ethical committee of Careggi University-Hospital (2006/0024713; renewed May 2009). Neonatal heart biopsies were obtained as routine procedure during cardiac surgery for correction of non-hypertrophying congenital cardiomyopathies in patients from 4 to 48 months. This procedure was communicated to the Nucleo di Valutazione della Ricerca Clinica, Az. Ospedaliera di Padova, for approval. All samples were anonymous to the investigators, and no details on the anagraphical and clinical data were available to the researchers. Samples were used in accordance to the directives of the national committee of Bioethics and the Recommendation R(06)l on research on biologica1 materials of human origin of the European Commission (15/03/2006)

Heart harvesting and processing

Mice were sacrificed by cervical dislocation and hearts were quickly harvested and cut in two portions transversally. Large arteries and veins were carefully removed and hearts were cleaned from blood clots and weighted with a precision balance. If necessary, the lower portion of the heart (apex) was snap-frozen in liquid nitrogen to perform biochemical analysis, while for histological analysis the base was fixed to preserve structural integrity (with 1% PFA in PBS 1X, see *Table 1*). Fixation was performed at room temperature for 15 minutes, followed by three washes of 5 minutes with PBS 1X. Hearts were then dehydrated by overnight 4°C incubation in sucrose 30% (w/v in distilled water). The following day, hearts were embedded in OCT freezing medium (Optimal Cutting Temperature, Kaltec) and carefully frozen in liquid nitrogen vapour. Frozen samples were stored at -80°C.

Immunofluorescence staining on heart samples

Frozen hearts were cut in 10 μm slices using a cryostat (LEICA CM1850) and placed on superfrost glass slides (Vetrotecnica) maintained at -80°C until use.
The day of immunofluorescence staining, slides with cryosections were allowed to equilibrate at room temperature for 10 minutes. Then slices were encircled with DAKO Pen (DAKO) and rehydrated for 10 minutes in PBS 1X. After rehydration, sections were incubated with the primary antibody diluted in PBS 1X supplemented with 1% BSA and 0.5% Triton-X. The incubation was performed overnight at 4°C in a humidified chamber to prevent samples drying.
The following day, slices were washed 3 times with PBS 1X before incubation with the secondary antibody, which was performed at 37°C for 30 minutes, diluting the antibody in PBS 1X supplemented with 1% BSA. Three additional washes were performed at the end of the staining, before mounting the slides with the mounting medium (elvanol).

Haematoxylin and eosin staining

Haematoxylin-eosin (HE) staining on cryosections is a standard histological protocol to evaluate tissue morphology. Heart cryosections were stained with the HE kit (Bio-Optica) following manufacturer's instructions. Briefly, after a 30 seconds treatment with haematoxylin, cryosections were washed to remove the excess of reagent, then 10 seconds in the toning solution allowed haematoxylin to reach its blue-violet coloration. Three additional washes were performed before incubation with eosin that was maintained for 1 minute. Washout of the excess reagent was carefully performed, then slices were dehydrated in 2 steps: 95% EtOH for 5 seconds, 100% EtOH for 2 minutes and 100% xylene for 5 minutes. Final mounting was perfomed with Eukitt (SIGMA-Aldrich), a mounting medium based on xylene.

Confocal microscopy

Samples were imaged using a confocal microscope (Leica TCS SP5, Leica microsystems, Germany) equipped with 40X, 1.4NA and 63x, 1.4NA oil immersion objectives. The microscope is equipped with four different laser lines for excitation (405 nm, 488 nm, 561 nm and 633 nm) and three tunable emission filters. Images were digitally acquired and

stored in a PC station, and analysis was performed using the image analysis software ImageJ (Wayne Rasband, NIH, Bethesda, USA).

5.3 *In vitro* procedures

Neonatal cardiomyocyte culture

Neonatal cardiomyocyte (NCM) culture is a well-established cellular method to investigate signalling pathways and ion homeostasis in cardiac cells. NCMs were prepared from newborn (P1-P3) rat hearts. Rats were sacrificed by cervical dislocation and hearts quickly removed. Atria were carefully excised, then ventricles were collected in a 50 mL tube half-filled with ice-cold ADS buffer (see *Table 1*). Under a sterile hood, ventricles were washed to remove excess of blood then minced in a 10 cm petri dish, placed on ice, in 5 mL of ADS in order to obtain heart fragments around 1 mm^3. Ventricles mechanically minced were then transferred to a 50 mL sterile tube with a 5 mm magnetic stir bar. ADS Buffer was completely removed and replaced with 6 mL of Digestion Buffer (see *Table 1*) and positioned on a magnetic stirrer inside a water-bath at 37°C. The first cycle of 10 minutes allows to remove damaged cells so the supernatant was discarded at the end of this time. Another 6 mL of Digestion Buffer were added to the heart pieces for 20 minutes always at 37°C on a stirrer. The supernatant of this cycle was then transferred to a 15 mL tube containing 1 mL of Horse Serum in order to block the enzymatic activity then centrifuged at 1250 rpm for 5 minutes. The supernatant was removed and cells were resuspended in 2.5 mL of first day medium (see *Table 1*) and maintained in the incubator until the digestion cycles were completed.
Non-digested heart pieces repeated the digestion step previously described; usually a total of 5-6 cycles are required to complete the enzymatic digestion of 10 hearts. At the end of the digestion cycles, isolated cells from the different cycles were mixed and seeded in a 10 cm tissue culture dish (BD Falcon) and maintained in the incubator at 37°C for 1 hour. This step is named “pre-plating” and allows to separate CMs from cardiac fibroblasts that are characterized by faster adhesion to the dish. After the pre-plating step, cells in suspension were collected in a new 50 mL tube. The total number of cells obtained was determined diluting cells in 0.2% Trypan Blue and counting viable cells in a Bürker chamber. CMs were then plated on laminin-coated glass coverslips (1.8 μg/100 mm^2) at a density of 470 cells/mm^2 for live imaging and immunofluorescence analysis while for

protein and RNA extraction the density was raised to 550 cells/mm^2. Twenty-four hours after plating, the medium was removed, cells washed twice with ADS Buffer, to remove dead cells, and incubated with second day medium (see *Table 1*).

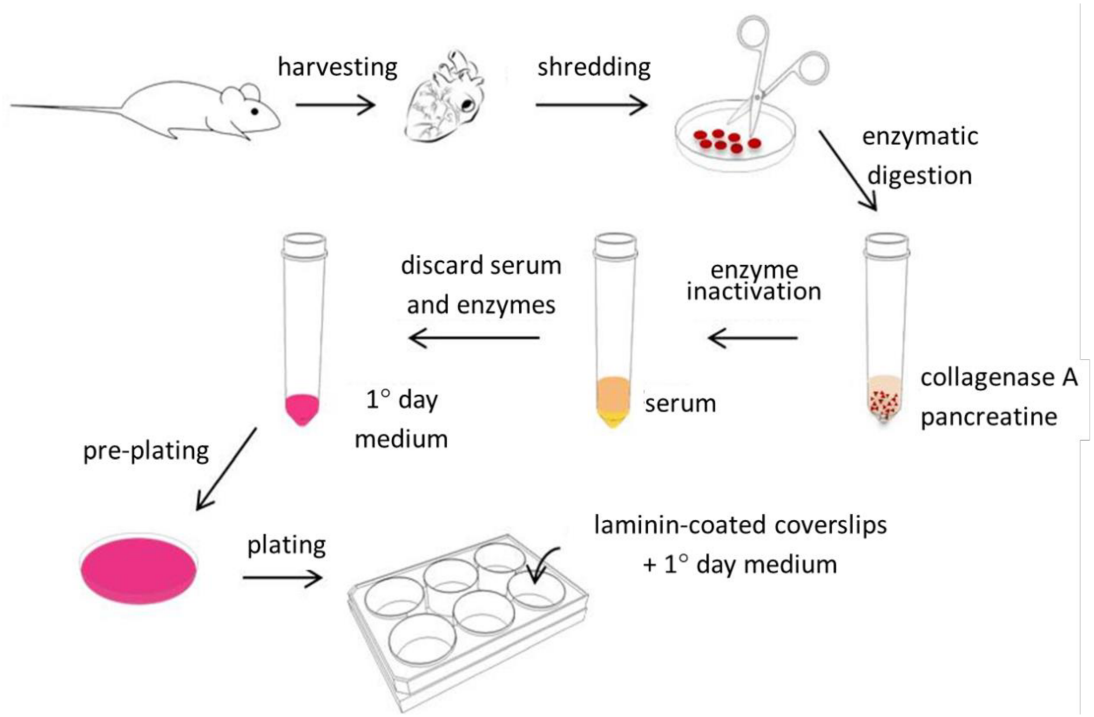

Figure 16. Schematic representation of neonatal ventricular CMs isolation and culture.

Adult cardiomyocytes isolation

To isolate adult CMs, the usual technique used is the enzymatic dissociation by retrograde coronary perfusion (commonly known as "Langendorff" technique). Briefly, adult mice were anesthetized with zoletil (1.5 mg/kg) and treated with the anti-coagulant eparin (2500 units). After sacrifice, chest was open and heart was removed, along with lungs and thymus and quickly placed in cold Perfusion Buffer (see *Table 1*). After lungs and thymus removal, pulmonary artery was cut and aorta cannulated with 4 Franch cannula-needle plugged to perfusion apparatus. The first perfusion made with 25 mL of Perfusion Buffer, was followed by a second perfusion with 12.5 mL of Perfusion Buffer supplemented with collagenase B and 25μM Ca^{2+}, thus resulting in ECM digestion. Finally, digested-heart was perfused with 15 mL of Perfusion Buffer added with the fetal bovine serum (FBS, 10%) to inactivate collagenases, at increased Ca^{2+} concentration (100 μM). Then, heart was removed from the apparatus and mechanically minced with scissors in Perfusion Buffer, and cells were filtered with cheese-cloth and collected in a conical tube. The

product obtained was gradually exposed to increasing Ca^{2+} concentration (250 μM, 500 μM, 1 mM), to avoid sudden Ca^{2+} overload during plating. Finally, CMs were plated in laminin-coated coverslips.

HEK-293T cell line

Human Embrionic Kidney cells (HEK-293T) were maintained in Standard Medium in T25 or T75 flasks (Corning) and split at around 80% confluence. Before cells splitting, culture medium was removed and cells were washed twice with PBS 1X to eliminate dead cells and serum. Then 1 mL of 0.25% Trypsin with EDTA was added and incubated for 3 minutes at 37°C. Trypsinization was blocked adding 3 mL of Standard Medium (Table 1). Cells in suspension were spun at 1250 rpm for 5 minutes and resuspended in fresh medium. For cell line expansion, a dilution 1:10 was plated in a T75 flask, whereas for experiments cells were seeded at a density around 125 cells/mm^2.

HL-1 cell line

HL-1 cells were kindly provided by Dr. W. Claycomb and cultured in Claycomb medium (Sigma) with 10% FBS (Sigma), 100 U/ml penicillin, 0.1 mg/ml streptomycin (Euroclone), 1% ultraglutamine 1 (Lonza), and 0.1M norepirephrine (Sigma) in a gelatin/fibronectin pre-coated flask. The maintenance in culture was performed as for HEK293T cells.

Immunofluorescence analysis on cultured cells

Cells seeded on coverslips were fixed with formaldehyde 3.7% in PBS (v/v, SIGMA-Aldrich) for 30 minutes at 4°C and washed 3 times for 10 minutes in PBS 1X. As first step, cells were permeabilized with PBS 1X supplemented with BSA 1% and Triton-X 0.1% for 5 minutes at room temperature, then washed 3 times with PBS 1X for 5 minutes. Cells were then incubated with the primary antibody (or antibodies if multiple staining is required) in PBS 1X-BSA 1% for 2 hours at 37°C in a humidified chamber. At the end of the incubation with the primary antibody, cells were washed 3 times for 5 minutes, then incubated with the secondary antibody in PBS 1X-BSA 1% for 30 minutes at 37°C. If

two secondary antibodies were required, this last step was repeated using the other secondary antibody. The sequence was decided in order to reduce the risk of cross-reactivity between the secondary antibodies. When secondary antibodies incubation was concluded, cells were washed 3 times with PBS 1X for 5 minutes. Then nuclei were stained with DAPI (1:5000, v/v in PBS 1X) for 5 minutes at room temperature. Finally, the coverslips were mounted with elvanol over a glass slide (Vetrotecnica).

Transient transfection in cell lines and cardiomyocytes

Transfection is a process that allows to introduce an exogenous sequence of DNA into the cell. The method used for cell lines and CMs takes advantage of liposomes that fuse with the external membrane and let the DNA enter inside the cell. This leads to a transient perturbation of the plasma membrane, so the adequate transfection protocol must be adapted to the specific target cell type.

HEK-293T and HL-1 cells underwent the same transfection protocol, different from transfection of NCMs.

HEK-293T or HL-1 cells were seeded with a density of 100 cells/mm^2 in a 6-well plate (BD Falcon) the day before transfection. The day of transfection, two mix were prepared in separated polystyrene tubes following manufacturer's instructions: 5 µL of Lipofectamine (Life Technologies) were diluted in 245 µL of M199 (Life Technologies) and 3 µg of DNA were diluted in a total volume of 250 µL (quantities reported refer to a single well). Dilutions were left for 5 minutes at room temperature and then mixed together for additional 20 minutes always at room temperature. In the meanwhile, cells were washed twice with PBS 1X and maintained in 500 µL of M199. Finally, 500 µL of the previously prepared mixture of transfection were added to the cells and left in the incubator for 5 hours. At the end of this incubation period, transfection solution was replaced with standard culture medium. With this protocol usually cells express the exogenous plasmid were more than the 80%.

NCMs are more sensitive to liposomal transfection so both the quantities and the timing were modified and set up in the lab.

Transfection was performed the day of culture preparation. Before seeding the cells, two solutions were prepared in polystyrene tubes. One solution contains Lipofectamine (2µL + 73µl of OptiMEM), the other contains the DNA (2 µg in 75 µL of OptiMEM). As for

cell lines, the 2 solutions were left for 5 minutes at room temperature, then put together for additional 20 minutes. After this period, 150 μL of the mixture were laid on coated 24 mm coverslips and left for additional 20 minutes. Finally cells were seeded over this mixture in their medium and left overnight to allow adhesion. The day after cells were washed twice and first day medium was replaced with second day medium. Depending on the experiment, different plasmids were used in this thesis and are listed in *Table 3*.

Adenoviral infection in cell lines and cardiomyocytes

Transient transfection with Lipofectamine reaches a percentage of transfected cells that is extremely variable among different cell types. An alternative method to achieve DNA manipulation consists in viral infection. Cultured cells were infected with adenoviral vectors (serotype 5) coding for the protein of interest 24 hours after plating. Different concentrations were tested (multiplicity of infection, MOI) to assess the lowest dose of virus in order to modulate MCU protein content without detrimental effects to the cells due to viral exposure. Viral vectors were diluted in culture medium and removed after 24 hours. The viral vectors used for modulating MCU were Ad-MCU-flag (obtained starting from the plasmid), Ad-shMCU (Ad-U6-rm-MCU-shRNA, Vector Biolabs) (see *Table 3*). and Ad-Empty, consisting in the viral vector without coding DNA, used as control (kindly provided by Dott. Daniele Catalucci).

Luciferase assay

The luciferase reporter assay is a commonly used tool to study gene expression at the transcriptional level. To assess the downregulation of MCU by miR-1, the murine MCU 3'UTR was cloned into psiCHECK-TM2 vector (Promega) using the In-fusion HD Cloning Plus kit (Clontech). The miR-1 mature sequence was cloned in pcDNA6.2-GW/EmGFP-miR vector according to manufacturer's procedure (Invitrogen). 1.5 x 10^5 HEK293T or HL1 cells were co-transfected with psiCHECK-3'UTR-MCU and pcDNA6.2-GW/EmGFP-miR-1. Forty-eight hours after transfection, the luciferase activity was detected using a luminometer (Synergy 4, BioTek, USA). To further confirm the specific targeting of the 3'UTR of MCU, site-directed mutagenesis were performed at predicted sites using the QuikChange Site-Directed Mutagenesis Kit (Stratagene) following the manufacturer's instructions.

Pharmacological stimulation of NCMs

In this thesis, neonatal CMs were treated with adrenergic agonists, as pro-hypertrophic agents, CaMKII and calcineurin inhibitors, or the antioxidant vitamin E .
All the compounds used were dissolved following the manufacturer's instructions, and then diluted in the second day medium.
In the experiment of hypertrophic growth, cells were treated from the third day of culture for three consecutive days with norepinephrine, phenylephrine or clenbuterol. For all the conditions, medium containing the stimulus was changed daily. The concentrations used were the following:

- Norepinephrine (NE): 100 nM;
- Phenylephrine (PE): 100 μM;
- Clenbuterol (CLB): 10 μM.

In this experiment, pro-hypertrophic mediators were inhibited for the whole duration of the adrenergic stimulation. To this purpose, we used KN93 (1 μM) as CaMKII inhibitor and cyclosporin A (1 mM) and FK506 (500 nM) as calcineurin inhibitors. All the inhibitors were used concomitantly with pro-hypertrophic stimuli and added to the medium. The inactive peptide, KN92, was used as control at the same concentration of the active-analogous.

In the experiment of NFAT nuclear translocation, cells were incubated with norepinephrine at the same time (third day) and at the same concentration (100 nM), but only for six hours. CaMKII inhibitor KN93 (and its relative control KN92, both 1 μM) was pre-incubated for 48 hours before adrenergic stimulation. Calcineurin inhibitors cyclosporin A and FK506 (1 mM and 100 μM, respectively) were equally effective in preventing NE-induced NFAT nuclear translocation both in pre-incubated CMs (48 hours before NE) and in CMs administered with CsA/FK506 contemporarily with NE. The antioxidant vitamin E (100 nM) was added to the medium 48 hours before adrenergic stimulation.

After all the experiments, CMs were either fixed and processed for immunofluorescence, or processed for protein and RNA extraction.

Morphometric analyses

NCMs, after fixation, were processed by immunofluorescence and the images acquired with the chosen microscope. Images were analysed by using the software *ImageJ* and the shape descriptors tool provided. Different morphological parameters were considered:
1) mean CM area;
2) ratio between area occupied by sarcomeres and total cellular area;
3) Aspect ratio (major axis/minor axis);
4) Roundness (4*area/π* major axis^2; this coefficient is an index of the circumference-like shape of the cell);
5) Solidity (effective area/convex area; being "convex area" the area of the polygon that best fits in);
6) Plot profile (analysis of the intensity of fluorescence/pixel along a determined segment).

For every experiment, five to twelve images were acquired and analysed. As for the "Development of a model of mature neonatal cardiomyocytes" project, both the type of CMs (*"Standard" vs. "New"*) were compared to isolated adult CMs, whose data were already available in this lab.

Sample preparation for *in vitro* transmission electron microscopy (TEM)

For *in vitro* TEM, cells were seeded directly on the plastic of 6-well plates, previously laminin-coated. Samples were fixed by using a solution of 0.1M sodium cacodylate supplemented with 2.5% glutaraldehyde, at pH 7.2 for 40 minutes at 4°C and washed twice for 30 minutes with 0.2M sucrose, 0.1M sodium cacodylate at pH 7.2 maintaining cells on ice. After fixation, samples were processed in the TEM facility at the Department of Biology, University of Padova. Post-fixation was done in 1% osmium tetroxide, 0.1 M sodium cacodylate, pH 7.2 for 2 hours at 4°C. Samples were then dehydrated in alcoholic solutions containing increasing ethanol concentration (50% for 15 minutes, 70% for 30 minutes, 90% for 30 minutes and 100% for 90 minutes), incubated with propylene oxide for 45 minutes and embedded in epoxy resin. Resin embedding was performed with three successive 45 minutes incubations with different solutions of acetone/resin (2:1, 1:1 and 1:2) and incubating cells with 100% resin for 1 hour. Then fresh resin was added. Polymerization was

performed with 3 repeated 24 hours incubations at 37°C, 45°C and 60°C. The resin was extracted from the wells and sections were cut, stained with 1% toluidine blue and observed at the light microscope. Sections of selected fields were stained with uranyl acetate, 50% ethanol and Reynolds lead citrate and examined with a FEI Tecnai 12 electron microscope.

5.4 Molecular and biochemical analyses

RT-qPCR

To evaluate the mRNA expression levels of different genes, RT-qPCR analysis was performed in both murine and human samples.

RNA isolation from both frozen tissue and cultured cells was performed using the SV total RNA isolation kit (Promega, Z3100) accordingly to the manufacturer's instructions.

Frozen tissue pieces of approximately the same size were immerged in 175 µl of RNA Lysis Buffer, previously supplemented with β-mercaptoethanol, and homogenized using Tissue Lyser (Qiagen) at 30 Hz for 1 minute. 350 µL of RNA Dilution Buffer were then added and mixed by inverting the tube few times. The tubes were centrifuged for 10 minutes, to remove undesired material, and the cleared lysate was transferred into a new tube. To optimize the binding of the RNA to the column, 200 µL of 95% Ethanol were added, mixed thoroughly and transferred to the Spin Basket Assembly. A centrifugation of 1 minute allowed the binding to the column, then a passage with 600 µL of RNA Wash Solution was performed. To obtain a pure extraction of RNA, 50 µL of DNase incubation mix were added to the membrane and incubated for 15 minutes at room temperature. To stop the enzyme, 200 µL of DNase Stop Solution were addend and the column centrifuged for 1 minute in order to discard the flow-through. An additional wash was then performed. To elute the RNA, 70 µL of RNase-Free Water were added to the membrane. After 1 minute of centrifugation the RNA is collected in the tube.

The RNA extracted was quantified using the NanoDrop (ThermoScientific), as described for DNA. RNA purification, quantification and retro-transcription were performed on the same day in order to minimize the RNA degradation.

Single-strand cDNA was synthesized following manufacturer's instruction for SuperScript III (Life Technologies). The retro-transcription "preparation mix" (see *Table*

1) was prepared for each sample and put in autoclaved 0.2 µL tubes. After an incubation at 65°C for 5 minutes the samples were left in ice of 2 minutes then spin down. Another mix containing the enzyme used to perform the retro-transcription was prepared than added to the "preparation mix" (see *Table 1*).
The program set in the Thermocycler to perform the retro-transcription consisted in three steps:

25 °C	5 min
50 °C	60 min
70 °C	15 min

RT-qPCR analysis was performed using a C1000 Thermal Cycler BioRad coupled with a GeneAmp 7500 Sequence Detection System by Nicola Pianca (PhD).
To evaluate differences in gene expression, the relative quantification using the ΔΔct method was adopted, normalizing to the internal reference of TOM20. The reference gene adopted was selected among those used in the literature selecting the more stable in our experimental conditions.

Protein expression analysis

Protein expression in the samples was analysed by western blotting (WB), in whole cell or tissue protein extracts from mouse and rat hearts, or cultured cardiomyocytes NCMs.
For WB we used murine samples as well as human samples.

Protein extraction

Tissues from mice and rats were frozen in liquid nitrogen immediately after removal from the animals. Frozen tissue pieces of approximately the same size were immerged in 400 µl of Lysis Buffer (see *Table 1*) and homogenized using Tissue Lyser (Qiagen) at 30 Hz for 1 minute. Tissue lysates were incubated for 1h at 4°C then centrifuged at 12000 rpm (10000g) for 15 min at 4°C. Pellet was discarded and the supernatants were collected in new 1.5 mL tubes, then denaturated in a thermo mixer (10 min. at 70°C and 1250 rpm). Protein quantification was performed using the Bradford assay subsequently validated with a blue coomassie staining. Protein extracts were then aliquoted and stored at -80°C.
To obtain protein extracts from cells, NCMs were washed with cold PBS 1X then incubated with 150 µL of RIPA Buffer for 1 minute. Cells were scraped from the plate

and lysates were collected in 1.5 mL tubes. To complete protein extraction the subsequent steps were the same as for tissue lysates.

SDS-PAGE

The electrophoresis is used to separate molecules depending on their different molecular weights. To this purpose, 20 μg to 60 μg of protein extracts were prepared in Loading Buffer (Table 1) and denaturated at 70°C and 1250 rpm for 10 min. Electrophoresis was performed with gels purchased by Life Technologies (4-12% gradient) and MOPS was used as running buffer at 130 mV. SeeBlue Plus2 was the protein weight standard adopted. All the chemicals are from Life Technologies. Running time was adjusted depending on the molecular weight of the protein of interest.

Coomassie Brilliant Blue

SimplyBlue™ SafeStain (Life Technologies) was used to stain protein samples after electrophoresis. This staining allows to evaluate the quality of the extracted protein (single bands reflect good protein extract without signs of protein degradation) and control the calibration of different samples.

Briefly, gels were incubated for 30 minutes, with Simply Blue dye, at room temperature in constant shaking. Gels were then incubated with Fixing Solution (Table 1) for 30 minutes at room temperature to fix the dye; then gels were incubated for 1 hour up to few days with Destaining Solution (Table 1) at room temperature to remove the excess of dye from the gel and clearly visualize the protein bands.

Immunoblotting

Proteins were then transferred on a methanol-activated PVDF membrane (GE Healthcare, 0.2 μm porosity) by using Transfer Buffer at 4°C, 400 mA for 90 minutes. After the transfer, membranes were usually stained with red ponceau dye (SIGMA-Aldrich) to check the transfer efficiency and quality.

Membranes were saturated in 0.1% TTBS supplemented with 5% milk for at least 1 hour at room temperature, to reduce the non-specific binding of the primary antibody to the membrane. The antibodies used in this PhD thesis are reported in the Table 3 at the end of this chapter, and were incubated on a shaker. After incubation with the primary antibody, membranes were washed with 0.1% TTBS 3 times for 10 minutes. The adequate HRP conjugated secondary antibody was incubated for 90 minutes at room temperature; other

3 washes were then performed. Finally, for the detection we used a chemiluminescent substrate (ECL Plus, Pierce) that produces light when combined with the enzyme. The device used for chemiluminescence detection was ImageQuant Las 4000 mini (GE Healthcare).

5.5 Live imaging

Genetically Encoded Ca^{2+} Indicators (GECIs)

There are two main categories of GECIs: those based on Föster Resonance Energy Transfer (FRET) and those adopting circularly permuted GFP[218-220].

The former category takes advantage of FRET that describes the energy transfer occurring between two fluorophores with one functioning as energy donor having the emission spectrum overlapping with the second, working as energy acceptor. The resonant transfer is efficient only when the two chromophores (donor and acceptor, respectively) are close one another (the efficiency is inversely proportional to the sixth power or the distance).

The latter category consists of single wavelength sensors constituted by circularly permuted GFPs.

FRET measurements of cytosolic, mitochondrial and SR Ca^{2+}

To measure cytosolic, mitochondrial and SR Ca^{2+}, genetically-encoded and targeted sensors of the CaMeleon family[221,222] have become a gold standard. The cytosolic and mitochondrial sensors used in this PhD thesis to measure Ca^{2+} have the same molecular components. The SR sensor has a slight difference in acceptor chromophore (citrine instead of CPV) (see fig.17).

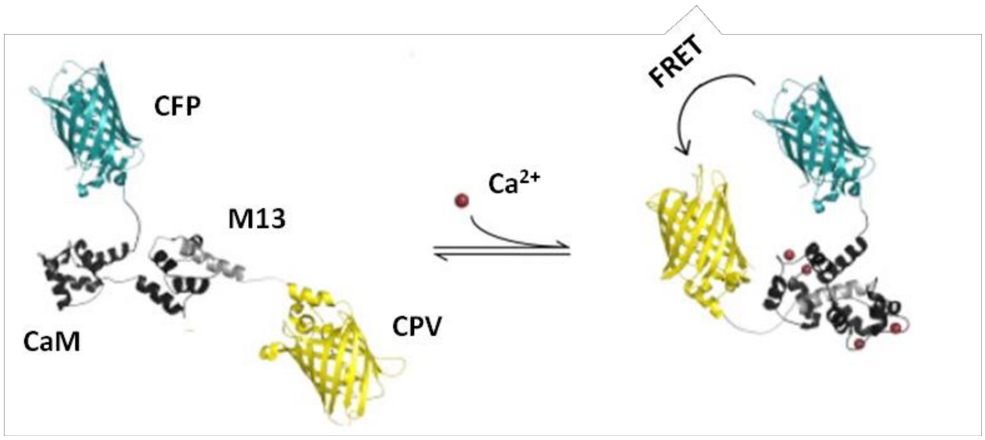

Figure 17. Schematic representation of CaMeleon conformational modification upon Ca^{2+} binding. Modified from[223]

The two chromophores, a CFP (Cyan Fluorescent Protein, donor) and a CPV (Circularly Permuted Venus, acceptor), are linked through Calmodulin (CaM) and a Ca^{2+} dependent CaM-binding peptide M13, fused together (D3 component). Ca^{2+} binding to M13 enables CaM to wrap around the M13 peptide, thus shortening the distance between the chromophores and enhancing FRET efficiency. From a practical point of view the ratio between the fluorescence emitted by the acceptor and the donor (upon excitation of the latter) is proportional to the Ca^{2+} concentration[221].

Technique: FRET experiments on neonatal CMs were all performed on an inverted fluorescence microscope Olympus IX50 equipped with a Nikon 40X oil immersion objective. The light source used was either a Xenon Arc Lamp or a LED (Thorlabs, 410 nm), depending on speed and light power needed for the experiments. FRET sensors were excited with a bandpass filter 430/25 nm, then, emitted fluorescence was split with a dichroic mirror and acquired simultaneously at 530 nm (YFP) and 480 nm (CFP) in two portions of the camera (Hamamatsu), shown in fig. 18.
The acquisition system of the microscope is synchronized with shutter movement or LED activation by the software Roboscope (kindly provided by Prof. Fabio Mammano). The exposure time was set at 150-200 ms to obtain a good signal-to-noise ratio.

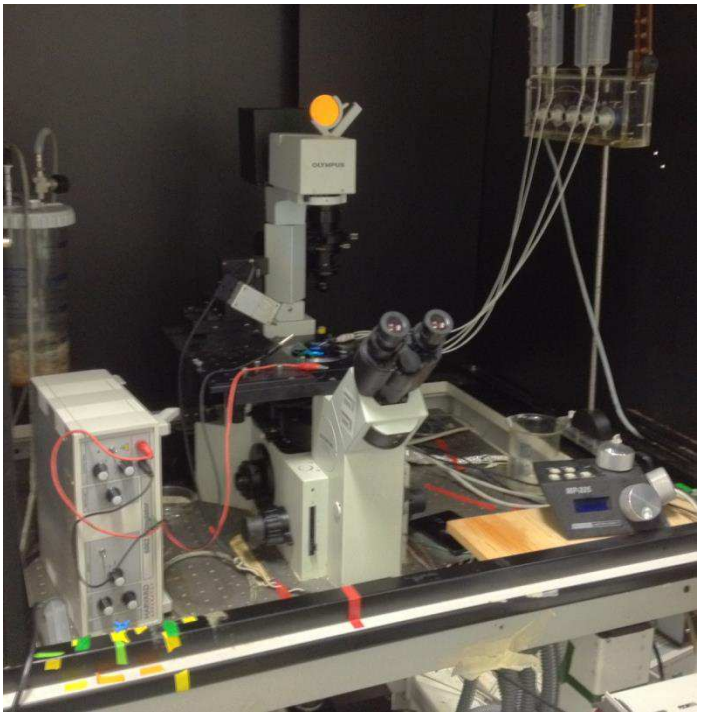

Figure 18. FRET-imaging setup at VIMM.

Neonatal rat CMs seeded on round coverslips (VWR) and transfected at least 48 hours prior to experiments were washed twice with NCMs imaging solution (see *Table 1*) and mounted on the imaging chamber.

To stimulate electrically the CMs, the 6002 Stimulator (Harvard Apparatus) was connected to the chamber conceived for pacing. Electrical squared pulses, 5 ms long, were given at different frequency controlled in remote.

FRET-based mitochondrial Ca^{2+} uptake measurement

To measure mitochondrial Ca^{2+} uptake upon electrical field stimulation, isolated CMs were transfected with a plasmid coding for 4mtD3CPV, commonly known as "mito-CaMeleon" (see *Table 3*). This probe has a specificity for mitochondria thanks to the expression, fused to the protein, of 29 aminoacids of N-terminus of human COX subunit 8a.

To reach an adequate signal-to-noise ratio in both CFP and YFP emission channels, the exposure time adopted was 150-200 ms, conditions that, unfortunately, cause a partial loss of fast and compartmentalized Ca^{2+} events. The dissociation constant (K_d) of 4mtD3CPV is, as reported in literature, of 760 nM [Ca^{2+}] (67).

A standard protocol of NCMs stimulation consists in electrical pacing at variable frequencies. When resting NCMs were forced to contract at a given frequency (usually 0.5 or 1 Hz) they showed Ca^{2+} transients in response to the stimulation, but also an increase in the basal Ca^{2+} level up to a plateau state.

Concerning mitochondrial Ca^{2+} uptake, it has to be considered that, whether mitochondria respond to cytosolic fluctuations in a beat-to-beat fashion or acting as low-pass filters is still matter of debate[224]. Pieces of evidence in both directions, or to support a combination of the two models, can be found in the literature[23,225]. In our experiments on NCMs, shown here below, we observed that mitochondria are able to take up Ca^{2+} responding to acute cytosolic elevations, both in the case of spontaneous activity, electrical pacing or agonist stimulation (caffeine for example). In the meantime, mitochondria are also able to accumulate Ca^{2+} up to a plateau level, corresponding to elevated frequency and fusion of subsequent transients.

FRET-based cytosolic Ca^{2+} measurement

One of the chosen approaches to monitor cytoplasmic Ca^{2+} dynamics, was to take advantage of D3CPV, known as CaMeleon, developed by Tsien's Lab[226]. The affinity of this probe is of Kd= 0.6 μM[227]. In cytosolic Ca^{2+} dynamics experiment, CMs were electrically paced to induce depolarization-induced transients. When resting NCMs were forced to contract at a given frequency (usually 0.5 or 1 Hz) they showed Ca^{2+} transients in response to the stimulation, but also an increase in the basal Ca^{2+} level up to a plateau state.

FRET-based sarcoplasmic reticulum Ca^{2+} measurement

To evaluate SR Ca^{2+} content and dynamics, we took advantage of the SR-targeted CaMeleon D4ER[228]. This sensor locates in the main intracellular Ca^{2+} store thanks to the signal sequence of human calreticulin (MLLPVLLLGLLGAAAD), fused to ECFP; whilst ER retention sequence (KDEL) is attached to the C-terminus of citrine. Although CPV increases the dynamic range of CaMeleon by approximately five-fold[229], citrine has been chosen as acceptor because of the better ER localization.

To evaluate SR Ca^{2+} dynamics content and dynamics, cells were both electrically stimulated at different frequencies and acutely treated with RyR2 agonists, such as caffeine (10 mM).

GCaMP sensors

In addition to CaMeleon indicators, other methods to record Ca^{2+} signals have been used. GCaMP sensors are single wavelength Ca^{2+} indicators based on circularly permuted GFP. They always maintain the CaM and M13 domains that wrap in presence of Ca^{2+}, however these two peptides are fused in such way that they can alter GFP conformation until Ca^{2+} binds, causing a large increase in fluorescence emission intensity (see fig. 19).

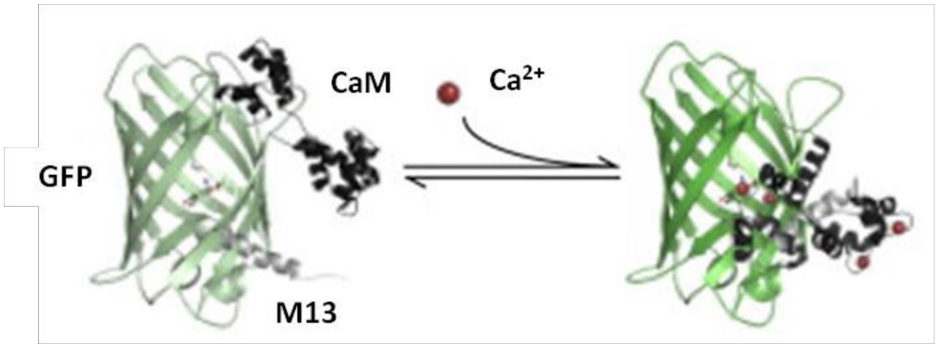

Figure 19. GCaMP schematic representation. Modified from [223].

As reported in several neuroscience experiments[219,230], the advantage of this sensor is that it can report very rapid Ca^{2+} events, if compared to FRET-based sensors. In fact, GCaMP6 has a higher affinity as compared to CaMeleons (K_d = 167 nM)[70]. The high affinity, combined with low exposure required, allow to acquire subcellular cytosolic Ca^{2+} events, otherwise not visible with D3CPV. This property is particularly relevant in the mitochondria-targeted variant, since the Kd is in the range of resting mitochondrial Ca^{2+} concentration implying, then, that under large cytosolic Ca^{2+} elevations, the mitochondrial sensor may saturate. Nevertheless, mitochondrial 2mtGCaMP6 is useful in light of estimating basal mitochondrial Ca^{2+} content, rather than evaluating mitochondrial Ca^{2+} dynamics.

GCaMP mitochondrial Ca^{2+} dynamics

In order to test resting $[Ca^{2+}]$mt with high sensitivity, we took advantage of mitochondrial-targeted variant of the last-generation GCaMP probe[231], generated by Rizzuto's lab[70]. A useful property of 2mtGCaMP6 is its isosbestic point in the excitation spectrum: excitation at 410 nm leads to $[Ca^{2+}]$ not dependent fluorescence emission, while excitation at 474 nm depends on $[Ca^{2+}]$. As a consequence, the ratio between 474 and 410 nm excitation wavelengths is proportional to $[Ca^{2+}]$ and independent of probe expression.

Technique: The microscope adopted for 2mtGCaMP6 experiments is the same used for FRET experiments, Olympus IX81 equipped with a Nikon 40X oil immersion objective. This imaging setup has been used for 2mtGCaMP6 experiments on neonatal CMs adopting the transfection and electrical pacing protocols described for CaMeleons. These sensors were excited at 474 nm and 410 nm wavelengths and emission acquired through a 525/30 filter. Exposure time was set at 50-100 ms to reach an adequate signal to noise ratio.

Ca^{2+}-sensitive dyes

The first and still the most amenable tools used to detect in real time Ca^{2+} dynamics in living cells are chemical compounds that, upon binding of Ca^{2+}, are able to emit fluorescence if excited at a certain wavelength. On this thesis, two dyes were used for cytosolic Ca^{2+} imaging: FLUO-4 AM and FURA-2 AM.

FLUO-4 AM is an evolution of the previous Ca^{2+} indicator, the BAPTA-derived FLUO-3, whose chlorine residues were replaced by fluorine, thus resulting in enhanced fluorescence emission. FLUO-4 is a single wavelength probe that, when excited at 488 nm by argon laser, emits a bright fluorescence at 516 nm. This dye, being cell-impermeable, is commonly used as non-fluorescent acetoxymethyl ester (AM) which, once entered the cell, is cleaved by endogenous esterases giving the free fluorescent FLUO-4, now trapped in the cytosol.

FURA-2 AM is an aminopolycarboxylic acid that binds intracellular Ca^{2+}, thus acting as a Ca^{2+} sensor. The main advantage of this probe is that it is ratiometric: in fact, FURA-2

can be excited both at 340 nm and at 380 nm of light, and the ratio of the emissions is directly related to the intracellular Ca^{2+}. This useful property allows to get rid of confounding variables, such as unequal dye loading, bleaching and focal-plane shift: the ratio, indeed, does not depend on the absolute intensity of the two signal, both detected at 510 nm but determined by different wavelengths of excitation. Also FURA-2, like FLUO-4, is frequently used as acetoxymethyl ester (AM), to allow its entrance inside the cell.

Technique: The microscope adopted for FLUO-4 AM experiments is an inverted confocal spinning disk microscope (Perkin Elmer Ultraview).

The light source consists of lasers as for confocal microscopy, but the spinning disk confocal microscope collects multiple points in parallel rather than scanning a single point at a time, lowering light power on the sample and increasing acquisition speed.

The set up installed at VIMM is equipped with two lasers (488 nm and 570 nm) and with a Nikon oil immersion 60X, 1.4 NA objective.

FLUO-4AM was dissolved at the concentration of 2.5 μM in Pluronic F-127 in proportion 1:2. Upon proper Fluo-4AM mixing with Pluronic F-127, NCMs imaging solution, supplemented with 10uM sulphinil pyrazone (SP), was added and thoroughly mixed to hamper precipitation of the dye. Then, CMs were loaded in the cell culture incubator (37°C, 5% CO_2 and controlled humidity). After incubation, two washes were performed in NCMS imaging solution (supplemented with SP 10 μM), and then cells were placed in imaging chambers. Cytosolic Ca^{2+} dynamics experiments were performed at the spinning disk fluorescence microscope (see above).

CMs were loaded with FURA-2AM with the same modalities used for FLUO-4AM. Experiments were performed at the microscope Olympus IX-70.

TMRM imaging

TMRM is a fluorescent dye typically used in the study of mitochondrial physiology that, when excited at 548nm, emits red light at 573nm. TMRM is a lipophilic cation that selectively accumulates in the negatively polarized mitochondria.
For the live imaging, TMRM was diluted at the concentration of 1 nM in neonatal CMs imaging solution (see *Table 1*) containing cyclosporin H (CsH, 2 μM, Sigma). Cells were

loaded with this solution for 30 minutes at 37°C, and then washed and maintained in HBSS-CsH solution. Cyclosporin H is an inhibitor of plasmalemma pumps (MDR, Multi Drug Resistance pumps), used to avoid active extrusion of TMRM by the cells.
The microscope used for this experiment was Olympus IX-81, equipped with a 60X objective, 1.4 NA. Images were recorded in time lapse series every 30 second with 50 ms exposure/frame. After 5 minutes from the beginning of the acquisition, cells were treated with Oligomycin (2.5 μg/mL, Sigma). Oligomycin is an ATP synthase inhibitor, and is used as mitochondrial respiration uncoupler. After 40 minutes of oligomycin, cells were treated with FCCP (2 μM, Sigma), a ionophore that causes proton leakage, loss of membrane potential and subsequent extrusion of TMRM from mitochondria. Analysis of fluorescence were performed by using the software Image J.

ROS live imaging

To determine mitochondrial Reactive Oxygen Species (ROS) production, we used the mitochondrial-specific probe pEGFP-N1-mt-ro1GFP (commonly known as roGFP1)[232]. The probe was introduced by transfection in neonatal CMs, which express it stably after three days, day of the experiment. RoGFP1 is a is a redox biosensitive sensor in which two cysteines were introduced in the β barrel structure of GFP, and their oxidized state (thiole or disulphide bridge) determines the different fluorescent properties showed by the protein under different conditions. Technically, roGFP1 provides an indirect measurement of ROS, since it is a sensor for GSH/GSSG ratio (glutathione, in its reduced and oxidized form, respectively), which is classically referred as an index of mitochondrial redox status, and therefore ROS production. RoGFP1 is a ratiometric probe, that has two excitation peaks (at 400 nm and 480 nm) and one emission peak (510 nm): oxidation of the cysteines residues in roGFP1 results in an increase in excitation at 400 nm, reduction of the cysteines favours excitation at 480 nm. Thus, the ratio between 510 nm emission and excitation at 400 nm and 480 nm reveals the relative amount of reduced and oxidized roGFP1, which reflects the redox state of the probe's environment.
For the live imaging experiment, cells were transfected with the plasmid encoding for roGFP1 on the first day of culture. The following day, cells were infected with MCU overexpressing or silencing virus, and from the following day were ready for the experiment. To assess with roGFP1 the mitochondrial ROS in NCMS at baseline, we

used the microscope Olympus IX-81, equipped with Nikon objective 60X. For roGFP1 imaging we used 535 nm emission and 400/480 excitation filters. Images were recorded every second with an exposure time of 30 ms. Each experiment lasted approximately one minute.

Image analysis

Off-line image analysis was performed with the dedicate software *ImageJ*.
For live imaging experiments, ROIs (Regions of Interest) were manually drawn to select the cytosol or the mitochondrial area. In both cases nuclei were excluded from the ROI.
In FRET experiments, CFP and YFP channels were evaluated separately and each channel was background subtracted selecting as background an ROI without transfected cells. Ca^{2+} levels were evaluated as ratio R= YFP/CFP. In the case of single wavelength sensors, a ROI was selected and fluorescence (F) was monitored over time, with respects to the basal level of fluorescence of the ROI (F_0) and analyzed as a relative intensity signal F/F_0.
In TMRM experiments, different ROIs were traced along mitochondria throughout the cells, and the intensity of the signals were compared to the background.
In roGFP1 experiments, ROIs were traced along the cells, and for each canal (emission and excitation) background was subtracted. Then, the ratio between the emission elicited by 400 nm excitation and the emission elicited by 490 nm excitation was calculated.
For WB analysis, a semi-quantitative evaluation of the relative protein content was performed using the ImageJ plug-in "*Gels*" for densitometry that allows to evaluate the optical density of protein bands in the photographic films. In every experiment, values were normalized to the housekeeping protein.

Statistical analysis

For data analysis, Excel® and GraphPad Prism® were used. Data fitting was performed with Clampfit® (version 10.2). Least squares was used as minimization method and the coefficient of determination, R^2, was considered to evaluate the goodness of fit.
To describe distributions, the mean and the standard error of the mean were considered. For comparisons between two distributions, the t-test was used. For comparisons between more than two distributions, the one-way anova and the Bonferroni correction were used.

P-values were considered statistically significant, when included between 0.05 and 0.01 (*), highly significant when lower than 0.01 (**).

Bioinformatics analyses

To identify the possible microRNAs (miRs) involved in MCU regulation, a bioinformatics research was performed with the collaboration of the group of Dr. Daniele Catalucci (Humanitas Research Center, Rozzano, Milan). The computational algorithm chosen for this purpose target prediction was PITA (Probability of Interaction by Target Accessibility): this algorithm is based on the target accessibility that is strictly connected to the secondary structure of 3'UTR region. In fact, the mRNA structure is a critical regulator of target recognition, by thermodynamically favoring or disfavoring the interaction[191]. PITA first predicts targets using complementarity analysis within seed regions and then compares the free energy gained from the formation of miR-target complex and the energetic cost to un-pair the target and make it accessible to the miR.
Practically, the murine MCU 3'UTR was uploaded into public PITA database (http://genie.weizmann.ac.il/pubs/mir07/mir07_data.html) and scanned for microRNA binding sites.

Table 1. Reagents

All the following solutions were sterilized by 0.22 μm filtration.

ADS Buffer

Component	Concentration
NaCl	106 mM
Hepes	20 mM
Na_2HPO_4	0.8 mM
KCl	5.3 mM
$MgSO_4 \cdot 7H_2O$	0.4 mM
Glucose	5 mM
	pH 7.4

Digestion Buffer

Component	Concentration
Collagenase A (Roche)	0.45 mg/mL
Pancreatin (SIGMA-Aldrich)	1.2 mg/mL
	in ADS Buffer

First Day Medium ("New Protocol")

Component	Concentration (v:v)
MEM	88.8%
Fetal Bovine Serum (FBS, Gibco)	10%
Non-Essential Amino Acids (NEAA, Gibco)	0.1%
Pen/Strep (Gibco)	1%
BrdU (100 μM in DMSO, SIGMA-Aldrich)	0.1%

Second Day Medium ("New Protocol")

Component	Concentration
MEM	98.8% v:v
Insulin-Transferrin-Selenite (ITS, Gibco)	0.1% v:v
Non-Essential Amino Acids (NEAA, Gibco)	0.1% v:v
Pen/Strep (Gibco)	1%

First day medium ("Standard protocol")

Component	Concentration (v:v)
DMEM 25 mM-Hepes (Gibco)	67 %
M-199 (Gibco)	17.5%
Horse Serum (Gibco)	10%
Newborn Calf Serum (Gibco)	5 %
L-Glutamine (200 mM) (Gibco)	1%
Pen/Strep (Gibco)	1%

Second day medium ("Standard protocol")

Component	Concentration (v:v)
DMEM 25 mM-Hepes (Gibco)	75 %
M-199 (Gibco)	17 %
Horse Serum (Gibco)	5%
Newborn Calf Serum (Gibco)	0.5 %
L-Glutamine (200 mM) (Gibco)	1%
Pen/Strep (Gibco)	1%

Neonatal Cardiomyocytes Imaging Solution

Component	Concentration
NaCl	125 mM
KCl	5 mM
Na_3PO_4	1 mM
$MgSO_4$	1 mM
Glucose	5.5 mM
Hepes	20 mM
$CaCl_2$	1.8 mM

Perfusion Buffer

Component	Concentration
NaCl	125 mM
KCl	5 mM
$NaHCO_3$	20 mM
Na_3PO_4	1 mM
Glucose	0.2&
$MgCl_2 \cdot 6\ H_2O$	1.7 mM
Butanedione (BND, Sigma)	20 mM

HEK-293T Standard Medium

Component	Concentration (v:v)
DMEM	89%
FBS	10%
Pen/Strep (Gibco)	1%

Retro-transcription "preparation mix"

Component	Quantity
RNA	400 ng in 11.5 µL H_2O
dNTPs (10mM)	1 µL
Random Primers mix (3µg/µL)	1 µL

Retro-transcription "final mix"

Component	Quantity
"preparation mix"	13.5 µL
Buffer (5X)	4 µL
DTT (1M)	1 µL
RNase out	1 µL
Reverse Transcriptase	0.5 µL
RNase-free H_2O	30 µL

PBS 1X

Component	Concentration
NaCl	137 mM
KCl	27 mM
KH_2PO_4	15 mM
$Na_2HPO_4 \cdot 2H_2O$	9 mM

RIPA Buffer

Component	Concentration
Tris Base	65 mM
NaCl	150 mM
Sodium Deoxycholate	0.025%
NP-40	1% v:v
EDTA	1 mM
Anti-phosphatases (Roche)	5X
Anti-proteases (Roche)	50X

Lysis Buffer

Component	Concentration
Tris Base	50 mM
NaCl	150 mM
$MgCl_2$	10 m
DTT	0.5 mM
EDTA	1 mM
Glycerol	10% v:v
SDS 10%	2% v:v
Triton X-100	1% v:v
Anti-phosphatases (Roche)	5X
Anti-proteases (Roche)	50X

Loading Buffer

Component	Concentration
DTT	50 mM
Sample Buffer (4X)	1X
SDS 1%	to volume

Fixing Solution

Component	Concentration (v:v)
H_2O	45%
Methanol	45%
Acetic Acid	10%

Destaining Solution

Component	Concentration (v:v)
H_2O	88%
Methanol	5%
Acetic Acid	7%

TTBS 0.1%

Component	Concentration
Tris Base – HCl (pH 7.6)	50 mM
NaCl	150 mM
Tween20	0.1% v:v

Transfer Buffer

Component	Concentration
NuPAGE Transfer Buffer (20X) (Invitrogen)	1X
Methanol	20% v:v
NuPAGE Antioxidant (Invitrogen)	0.05% v:v
H_2O	75% v:v

Red Ponceau

Component	Concentration (v:v)
Red Ponceau (Sigma)	0.5%
Acetic Acid	1%
H_2O	98.5%

Elvanol

Component	Quantity
PBS 1X	70 mL
Polyvinyl alcohol (Sigma)	10 g
Glycerol	30 mL
NaN_3	1 mL

Table 2. Primers

GENE / SPECIES	FORWARD SEQUENCE	REVERSE SEQUENCE
MCU (Hsa)	5'-CACACAGTTTGGCATTTTGG-3'	5'-CGTGACTTTTTGGCTCCTTT-3'
MCU (Mmu)	5'- AAAGGAGCCAAAAAGTCACG-3'	5'-AACGGATCTGTAGCCTCAGCAAGG-3'
MCUb (Hsa)	5'-GGCCTTCCCTTGGTAACACT-3'	5'-GTTGCCATCTGCTGTGAAGA-3'
MCUb (Mmu)	5'-AGTTACCTTCTTTCCTGTCGTTTGCG-3'	5'-CAGGGATTCTGTAGCCTCAGCAAGG-3'
MICU1 (Hsa)	5'-ATCAGTGAGCCTGGTGAAGC-3'	5'-ATGAGCCCACATTCTCCAAG-3'
MICU1 (Mmu)	5'-GTCGAACTCTCGGACCATGT-3'	5'-GTGCCTAAGGTGCAGGAGGTG-3'
MICU2 (Hsa)	5'-GGCAGTTTTACAGTCTCCGC-3'	5'--AAGAGGAAGTCTCGTGGTGTC-3'
MICU2 (Mmu)	5'-TGGAGCACGACGACGGAGAGTA-3'	5'-GCCAGCTTCTTGACCAGTGT-3'
MCUR1 (Hsa)	5'-GGACTTTGGTCACTTCATCCATTA-3'	5'- GGACTTTGGTCACTTCATCCATTA-3'
MCUR1 (Mmu)	5'-AGTTTTCAGCCCTCAGAGCAG-3'	5'-GGACTTTGGTCACTTCATCCATCA-3'
EMRE (Hsa/Mmu)	5'-TGTCGGGACACTCATTAGCA-3'	5'-GCTGATAGGGAAGGCAGAGA-3'
TOM20 (Hsa)	5'-TATGCGGGGCCCTTTTCATT-3'	5'-TCAGGTAACTTGGAAAGCCCA-3'
TOM20 (Mmu)	5'-CGATCGGTCGGAGCTAACC-3'	5'-TCAGGTAACTTGGAAAGCCCA-3'
MYH6 (Mmu)	5'-CGCATCAAGGAGCTCACC-3'	5'-CCTGCAGCCGCATTAAGT-3'
MYH6 (Hsa)	5'-CTCAAGCTCATGGCCACTCT-3'	5'-GCCTCCTTTGCTTTTACCACT-3'
MYH7 (Mmu)	5'-GCATCAAGGAGCTCACC-3'	5'-CTGCAGCCGCAGTAGGTT-3'
MYH7 (Hsa)	5'-ACACCCTGACTAAGGCCAAA-3'	5'-GTCCATGCGCACCTTCTT-3'
NPPA (Mmu)	5'- GTCAGTCGTTTGGGCTGTAAC-3'	5'-AGACCCAGGCAGAGTCAGAA-3'
NPPA (Hsa)	5'-CAGGATGGACAGGATTGGAG-3'	5'-TCCTCCCTGGCTGTTATCTTC-3'
NPPB (Mmu)	5'-CACAGATCTGATGGATTTCAAGA-3'	5'-CTCATCTTCTACCGGCATC-3'
NPPB (Hsa)	5'- GATGGTGCAAGGGTCTGG-3'	5'-TAATGCCGCCTCAGCACT-3'
ACTA1 (Mmu)	5'-CGGGAGAAGATGACTCAAA-3'	5'-GTAGTACGGCCGGAAGCATA-3'
ACTA1 (Hsa)	5'-GGACTTCGAGAACGAGATGG-3'	5'-CTGGCAGCTCGTAGCTCTTT-3'

Table 3. Plasmids

Plasmids used

Plasmid name	Function and employment
4mt D3-CPV	Mitochondrial Ca^{2+} measurement
D3-CPV	Cytosolic Ca^{2+} measurement
2mt-GCaMP6s	Mitochondrial Ca^{2+} measurement
MCU-flag	Overexpression of MCU
pZacf-U6-MCU-ZsGreen	Downregulation of MCU
GFP-NFATc3	Expression of fluorescent NFATc3
N1-mt-ro1GFP	Mitochondrial ROS measurement
EmGFP-miR-1	Expression of miR-1
EmGFP-miR-199	Expression of miR-199

Ca^{2+} sensors of the CaMeleon family were kindly provided by Prof. Tullio Pozzan. GCaMP sensors, as well as MCU plasmids were kindly provided by Prof. Rosario Rizzuto. pEGFP-N1-mt-ro1GFP was a gift from S. James Remington. GFP-NFATc3 was a gift from Prof. Stefano Schiaffino.

Table 4. Antibodies

Primary antibodies

Protein	Company	Dilution	Host Species	Application
Actin	SIGMA A5060	1:2000	Rabbit	WB
α-actinin	SIGMA A7732	1:200	Mouse	IF
MCU	SIGMA HPA016480	1:100 ; 1:1000	Rabbit	IF; WB
MCUb	Abgent AP12355b	1:1000	Rabbit	WB
MICU-1	SIGMA HPA037480	1:1000	Rabbit	WB
MICU-2	Abcam AB101465	1:1000	Rabbit	WB
Tom20	Santa Cruz sc-11415	1:400 ; 1:10000	Rabbit	IF WB
SERCA-2A	Santa Cruz sc-8095	1:2000	Goat	WB
RyR2	SIGMA HPA020028	1:100	Rabbit	IF
Flag	SIGMA F7425	1:200	Rabbit	IF
Dystrophin	Abcam AB15277	1:200	Rabbit	IF
Cleaved-Caspase 3	Cell Signaling 9661	1:200	Rabbit	IF
phospho-Akt (ser473)	Cell Signaling 9271	1:1000	Rabbit	WB
total Akt	Cell Signaling 9272	1:1000	Rabbit	WB
phospho-GSK3β (ser9)	Cell Signaling 9336	1:1000	Rabbit	WB
total-GSK3β	Cell Signaling 9310	1:1000	Rabbit	WB

6. PhD COURSE ACTIVITIES

6.1 List of manuscripts

1. Zaglia T*, Ceriotti P*, **Campo A*,** Borile G*, Armani A, Carullo P, Prando V, Coppini R, Vida V, Stølen TO, Ulrik W, Cerbai E, Stellin G, Faggian G, De Stefani D, Sandri M, Rizzuto R, Di Lisa F, Pozzan T, Catalucci D and Mongillo M (2017). Content of mitochondrial calcium uniporter (MCU) in cardiomyocytes is regulated by microRNA-1 in physiologic and pathologic hypertrophy. Proceedings of the National Academy of Sciences, 2017: p. 201708772.

2. **Campo A**, Borile G, Carullo P, Pesce P, Di Lisa F, Sandri M, Rizzuto R, De Stefani D, Da Costa Martins P, Catalucci D, Zaglia T*, Mongillo M*. Role of the Mitochondrial Ca^{2+} Uniporter (MCU) in cardiomyocyte adaptation to hypertrophic stimuli. (in preparation)

3. Prando V, Pianca N, Di Bona A, Franzoso M, **Campo A**, Incensi A, Donadio V, Scorrano L, Carelli V, Mongillo M* and Zaglia T*. Role of the mitochondrial protein Opa1 in the regulation of cardiac sympathetic neurons physiology. (in preparation)

6.2 Congresses attended

1. Zaglia T*, Ceriotti P*, **Campo A*,** Borile G*, Armani A, Carullo P, Prando V, Coppini R, Vida V, Stølen TO, Ulrik W, Cerbai E, Stellin G, Faggian G, De Stefani D, Sandri M, Rizzuto R, Di Lisa F, Pozzan T, Catalucci D and Mongillo M. The content of mitochondrial calcium uniporter (MCU) in cardiomyocytes is dynamically regulated by miR-1 in physiologic and pathologic cardiac hypertrophy. ESC Basic Science Summer School (June 18-22 2017, Nice, France). International, Poster.

2. Zaglia T*, Ceriotti P*, **Campo A*,** Borile G*, Armani A, Carullo P, Prando V, Coppini R, Vida V, Stølen TO, Ulrik W, Cerbai E, Stellin G, Faggian G, De Stefani D, Sandri M, Rizzuto R, Di Lisa F, Pozzan T, Catalucci D and Mongillo M. The content of mitochondrial calcium uniporter (MCU) in cardiomyocytes is dynamically regulated by

miR-1 in physiologic and pathologic cardiac hypertrophy. International Society for Heart Research (ISHR) 34th european meeting (July 24-27 2017, Hamburg, Germany). International, Poster.

3. **Campo A**, Borile G, Carullo P, Pesce P, Di Lisa F, Sandri M, Rizzuto R, De Stefani D, Da Costa Martins P, Catalucci D, Zaglia T*, Mongillo M*. Role of the Mitochondrial Ca^{2+} Uniporter (MCU) in cardiomyocyte adaptation to hypertrophic stimuli. VIMM Annual Retreat (February 17-18 2017, Preganziol, Italy). Poster.

4. Zaglia T*****, Ceriotti P*****, **Campo A*,** Borile G*****, Armani A, Carullo P, Prando V, Coppini R, Vida V, Stølen TO, Ulrik W, Cerbai E, Stellin G, Faggian G, De Stefani D, Sandri M, Rizzuto R, Di Lisa F, Pozzan T, Catalucci D and Mongillo M. The content of mitochondrial calcium uniporter (MCU) in cardiomyocytes is dynamically regulated by miR-1 in physiologic and pathologic cardiac hypertrophy. ABCD congress 2017 (September 21-23 2017, Bologna, Italy). International, Poster. **Travel grant.**

5. Zaglia T*****, Ceriotti P*****, **Campo A*,** Borile G*****, Armani A, Carullo P, Prando V, Coppini R, Vida V, Stølen TO, Ulrik W, Cerbai E, Stellin G, Faggian G, De Stefani D, Sandri M, Rizzuto R, Di Lisa F, Pozzan T, Catalucci D and Mongillo M. (2016) MicroRNA-1 dependent regulation of Mitochondrial Calcium Uniporter (MCU) in normal and hypertrophied hearts. FCVB 2016, 4th edition of the biennial meeting in Frontiers of Cardiovascular Research (July 08-10 2016, Florence, Italy) International, Poster.

6. **Campo A.** Targeting the mechanisms of mitochondrial Ca^{2+} uptake in heart diseases. VIMM Retreat (February 19-20 2016, Ponzano Veneto, Italy). Oral Presentation. **Best Oral Presentation award.**

7. **Campo A**, Zaglia T, Carullo P, Borile G, Prando V, Terrin A, Sandri M, Di Lisa F, Catalucci D, Rizzuto R, Mongillo M. Role of the Mitochondrial Ca^{2+} Uniporter (MCU) in cardiomyocyte adaptation to hypertrophic stimuli. ABCD congress 2015 (September 17-19 2015, Bologna, Italy). International, Poster.

8. **Campo A**, Borile G, Carullo P, Pesce P, Di Lisa F, Sandri M, Rizzuto R, De Stefani D, Da Costa Martins P, Catalucci D, Zaglia T*, Mongillo M*. Role of the Mitochondrial Ca^{2+} Uniporter (MCU) in cardiomyocyte adaptation to hypertrophic stimuli. VIMM Annual Retreat (February 6-7 2015, Preganziol, Italy). Poster.

7. REFERENCES

1 Sedmera, D. & Thompson, R. P. Myocyte proliferation in the developing heart. *Developmental Dynamics* **240**, 1322-1334, doi:10.1002/dvdy.22650 (2011).

2 Badeer, H. S. BIOLOGICAL SIGNIFICANCE OF CARDIAC HYPERTROPHY. *The American journal of cardiology* **14**, 133-138 (1964).

3 Shimizu, I. & Minamino, T. Physiological and pathological cardiac hypertrophy. *Journal of Molecular and Cellular Cardiology* **97**, 245-262, doi:10.1016/j.yjmcc.2016.06.001 (2016).

4 Williams, G. S. B., Boyman, L. & Lederer, W. J. Mitochondrial calcium and the regulation of metabolism in the heart. *Journal of Molecular and Cellular Cardiology* **78**, 35-45, doi:10.1016/j.yjmcc.2014.10.019 (2015).

5 De Stefani, D., Raffaello, A., Teardo, E., Szabò, I. & Rizzuto, R. A forty-kilodalton protein of the inner membrane is the mitochondrial calcium uniporter. *Nature* **476**, 336-340, doi:10.1038/nature10230 (2011).

6 Baughman, J. M. *et al.* Integrative genomics identifies MCU as an essential component of the mitochondrial calcium uniporter. *Nature* **476**, 341-345, doi:10.1038/nature10234 (2011).

7 Pan, X. *et al.* The physiological role of mitochondrial calcium revealed by mice lacking the mitochondrial calcium uniporter. *Nature Cell Biology* **15**, 1464-1472, doi:10.1038/ncb2868 (2013).

8 Rasmussen, T. P. *et al.* Inhibition of MCU forces extramitochondrial adaptations governing physiological and pathological stress responses in heart. *Proceedings of the National Academy of Sciences* **112**, 9129-9134, doi:10.1073/pnas.1504705112 (2015).

9 Kwong, Jennifer Q. *et al.* The Mitochondrial Calcium Uniporter Selectively Matches Metabolic Output to Acute Contractile Stress in the Heart. *Cell Reports* **12**, 15-22, doi:10.1016/j.celrep.2015.06.002 (2015).

10 Luongo, Timothy S. *et al.* The Mitochondrial Calcium Uniporter Matches Energetic Supply with Cardiac Workload during Stress and Modulates Permeability Transition. *Cell Reports* **12**, 23-34, doi:10.1016/j.celrep.2015.06.017 (2015).

11 Wu, Y. *et al.* The mitochondrial uniporter controls fight or flight heart rate increases. *Nature Communications* **6**, 6081, doi:10.1038/ncomms7081 (2015).

12 Small, E. M. & Olson, E. N. Pervasive roles of microRNAs in cardiovascular biology. *Nature* **469**, 336-342, doi:10.1038/nature09783 (2011).

13 Sayed, D., Hong, C., Chen, I. Y., Lypowy, J. & Abdellatif, M. MicroRNAs Play an Essential Role in the Development of Cardiac Hypertrophy. *Circulation Research* **100**, 416-424, doi:10.1161/01.res.0000257913.42552.23 (2007).

14 Ikeda, S. *et al.* MicroRNA-1 Negatively Regulates Expression of the Hypertrophy-Associated Calmodulin and Mef2a Genes. *Molecular and Cellular Biology* **29**, 2193-2204, doi:10.1128/mcb.01222-08 (2009).

15 Elia, L. *et al.* Reciprocal Regulation of MicroRNA-1 and Insulin-Like Growth Factor-1 Signal Transduction Cascade in Cardiac and Skeletal Muscle in Physiological and Pathological Conditions. *Circulation* **120**, 2377-2385, doi:10.1161/circulationaha.109.879429 (2009).

16 Castaldi, A. *et al.* MicroRNA-133 modulates the beta1-adrenergic receptor transduction cascade. *Circ Res* **115**, 273-283, doi:10.1161/circresaha.115.303252 (2014).
17 Care, A. *et al.* MicroRNA-133 controls cardiac hypertrophy. *Nat Med* **13**, 613-618, doi:10.1038/nm1582 (2007).
18 Wei, Y. *et al.* Multifaceted roles of miR-1s in repressing the fetal gene program in the heart. *Cell Res* **24**, 278-292, doi:10.1038/cr.2014.12 (2014).
19 Porrello, E. R. *et al.* MiR-15 family regulates postnatal mitotic arrest of cardiomyocytes. *Circ Res* **109**, 670-679, doi:10.1161/circresaha.111.248880 (2011).
20 Stolen, T. O. *et al.* Interval training normalizes cardiomyocyte function, diastolic Ca2+ control, and SR Ca2+ release synchronicity in a mouse model of diabetic cardiomyopathy. *Circ Res* **105**, 527-536, doi:10.1161/circresaha.109.199810 (2009).
21 Lu, X. *et al.* Measuring local gradients of intramitochondrial [Ca(2+)] in cardiac myocytes during sarcoplasmic reticulum Ca(2+) release. *Circ Res* **112**, 424-431, doi:10.1161/circresaha.111.300501 (2013).
22 Drago, I., De Stefani, D., Rizzuto, R. & Pozzan, T. Mitochondrial Ca2+ uptake contributes to buffering cytoplasmic Ca2+ peaks in cardiomyocytes. *Proceedings of the National Academy of Sciences of the United States of America* **109**, 12986-12991, doi:10.1073/pnas.1210718109 (2012).
23 Robert, V. *et al.* Beat-to-beat oscillations of mitochondrial [Ca2+] in cardiac cells. *Embo j* **20**, 4998-5007, doi:10.1093/emboj/20.17.4998 (2001).
24 Zaglia, T. *et al.* Cardiac sympathetic neurons provide trophic signal to the heart via beta2-adrenoceptor-dependent regulation of proteolysis. *Cardiovasc Res* **97**, 240-250, doi:10.1093/cvr/cvs320 (2013).
25 Kumarswamy, R. *et al.* SERCA2a gene therapy restores microRNA-1 expression in heart failure via an Akt/FoxO3A-dependent pathway. *Eur Heart J* **33**, 1067-1075, doi:10.1093/eurheartj/ehs043 (2012).
26 Sugden, P. H., Fuller, S. J., Weiss, S. C. & Clerk, A. Glycogen synthase kinase 3 (GSK3) in the heart: a point of integration in hypertrophic signalling and a therapeutic target? A critical analysis. *British Journal of Pharmacology* **153**, S137-S153, doi:10.1038/sj.bjp.0707659 (2009).
27 Anderson, M. E., Brown, J. H. & Bers, D. M. CaMKII in myocardial hypertrophy and heart failure. *Journal of Molecular and Cellular Cardiology* **51**, 468-473, doi:10.1016/j.yjmcc.2011.01.012 (2011).
28 Mongillo, M. & Marks, A. R. Models of heart failure progression: Ca2+ dysregulation. *Drug Discovery Today: Disease Models* **4**, 191-196, doi:10.1016/j.ddmod.2007.06.005 (2007).
29 Anmann, T. *et al.* Formation of highly organized intracellular structure and energy metabolism in cardiac muscle cells during postnatal development of rat heart. *Biochimica et Biophysica Acta (BBA) - Bioenergetics* **1837**, 1350-1361, doi:10.1016/j.bbabio.2014.03.015 (2014).
30 Louch, W. E., Koivumäki, J. T. & Tavi, P. Calcium signalling in developing cardiomyocytes: implications for model systems and disease. *The Journal of Physiology* **593**, 1047-1063, doi:10.1113/jphysiol.2014.274712 (2015).
31 Nielsen, M. S. Myocyte-fibroblast interactions--risky connections. *Heart Rhythm* **6**, 1650-1651, doi:10.1016/j.hrthm.2009.08.025 (2009).
32 Santiago, J. J. *et al.* Cardiac fibroblast to myofibroblast differentiation in vivo and in vitro: expression of focal adhesion components in neonatal and adult rat

ventricular myofibroblasts. *Developmental dynamics : an official publication of the American Association of Anatomists* **239**, 1573-1584, doi:10.1002/dvdy.22280 (2010).

33 Xie, Y. *et al.* Effects of fibroblast-myocyte coupling on cardiac conduction and vulnerability to reentry: A computational study. *Heart rhythm* **6**, 1641-1649, doi:10.1016/j.hrthm.2009.08.003 (2009).

34 Zhang, X. *et al.* Cardiomyocyte differentiation induced in cardiac progenitor cells by cardiac fibroblast-conditioned medium. *Experimental biology and medicine (Maywood, N.J.)* **239**, 628-637, doi:10.1177/1535370214525323 (2014).

35 Stolen, T. O. *et al.* Interval Training Normalizes Cardiomyocyte Function, Diastolic Ca2+ Control, and SR Ca2+ Release Synchronicity in a Mouse Model of Diabetic Cardiomyopathy. *Circulation Research* **105**, 527-U547, doi:10.1161/Circresaha.109.199810 (2009).

36 Boyden, P. A., Hirose, M. & Dun, W. Cardiac Purkinje cells. *Heart Rhythm* **7**, 127-135, doi:10.1016/j.hrthm.2009.09.017 (2010).

37 Bailey, J. C., Lathrop, D. A. & Pippenger, D. L. Differences between proximal left and right bundle branch block action potential durations and refractoriness in the dog heart. *Circ Res* **40**, 464-468 (1977).

38 Goldberger, A. L., Rigney, D. R. & West, B. J. Chaos and fractals in human physiology. *Scientific American* **262**, 42-49 (1990).

39 Dobrzynski, H. *et al.* Structure, function and clinical relevance of the cardiac conduction system, including the atrioventricular ring and outflow tract tissues. *Pharmacol Ther* **139**, 260-288, doi:10.1016/j.pharmthera.2013.04.010 (2013).

40 Page, E. Quantitative ultrastructural analysis in cardiac membrane physiology. *Am J Physiol* **235**, C147-158 (1978).

41 Williams, G. S., Boyman, L., Chikando, A. C., Khairallah, R. J. & Lederer, W. J. Mitochondrial calcium uptake. *Proceedings of the National Academy of Sciences of the United States of America* **110**, 10479-10486, doi:10.1073/pnas.1300410110 (2013).

42 Morita, H., Seidman, J. & Seidman, C. E. Genetic causes of human heart failure. *J Clin Invest* **115**, 518-526, doi:10.1172/jci24351 (2005).

43 Bers, D. M. Cardiac sarcoplasmic reticulum calcium leak: basis and roles in cardiac dysfunction. *Annu Rev Physiol* **76**, 107-127, doi:10.1146/annurev-physiol-020911-153308 (2014).

44 Bers, D. M. Cardiac excitation-contraction coupling. *Nature* **415**, 198-205, doi:10.1038/415198a (2002).

45 Fabiato, A. Calcium-induced release of calcium from the cardiac sarcoplasmic reticulum. *Am J Physiol* **245**, C1-14 (1983).

46 Cheng, H., Lederer, W. J. & Cannell, M. B. Calcium sparks: elementary events underlying excitation-contraction coupling in heart muscle. *Science* **262**, 740-744 (1993).

47 Lehnart, S. E. *et al.* Stabilization of cardiac ryanodine receptor prevents intracellular calcium leak and arrhythmias. *Proceedings of the National Academy of Sciences of the United States of America* **103**, 7906-7910, doi:10.1073/pnas.0602133103 (2006).

48 Wehrens, X. H. *et al.* FKBP12.6 deficiency and defective calcium release channel (ryanodine receptor) function linked to exercise-induced sudden cardiac death. *Cell* **113**, 829-840 (2003).

49 Lehnart, S. E. *et al.* Sudden death in familial polymorphic ventricular tachycardia associated with calcium release channel (ryanodine receptor) leak. *Circulation* **109**, 3208-3214, doi:10.1161/01.cir.0000132472.98675.ec (2004).

50 Huxley, H. E. The mechanism of muscular contraction. *Science* **164**, 1356-1365 (1969).

51 Egger, M. & Niggli, E. Regulatory function of Na-Ca exchange in the heart: milestones and outlook. *The Journal of membrane biology* **168**, 107-130 (1999).

52 Ferrari, R., Ceconi, C. & Guardigli, G. *Pathophysiological role of heart rate: from ischaemia to left ventricular dysfunction*. Vol. 10 (2008).

53 Akar, F. G. & O'Rourke, B. Mitochondria are sources of metabolic sink and arrhythmias. *Pharmacol Ther* **131**, 287-294, doi:10.1016/j.pharmthera.2011.04.005 (2011).

54 Brown, D. A. & O'Rourke, B. Cardiac mitochondria and arrhythmias. *Cardiovasc Res* **88**, 241-249, doi:10.1093/cvr/cvq231 (2010).

55 Kohlhaas, M. *et al.* Elevated cytosolic Na+ increases mitochondrial formation of reactive oxygen species in failing cardiac myocytes. *Circulation* **121**, 1606-1613, doi:10.1161/circulationaha.109.914911 (2010).

56 Rizzuto, R. Calcium mobilization from mitochondria in synaptic transmitter release. *The Journal of cell biology* **163**, 441-443, doi:10.1083/jcb.200309111 (2003).

57 Dorn, G. W., 2nd & Scorrano, L. Two close, too close: sarcoplasmic reticulum-mitochondrial crosstalk and cardiomyocyte fate. *Circ Res* **107**, 689-699, doi:10.1161/circresaha.110.225714 (2010).

58 Deluca, H. F. & Engstrom, G. W. Calcium uptake by rat kidney mitochondria. *Proceedings of the National Academy of Sciences of the United States of America* **47**, 1744-1750 (1961).

59 Pradhan, R. K., Qi, F., Beard, D. A. & Dash, R. K. Characterization of membrane potential dependency of mitochondrial Ca2+ uptake by an improved biophysical model of mitochondrial Ca2+ uniporter. *PLoS One* **5**, e13278, doi:10.1371/journal.pone.0013278 (2010).

60 Kamer, K. J. & Mootha, V. K. The molecular era of the mitochondrial calcium uniporter. *Nature Reviews Molecular Cell Biology* **16**, 545-553, doi:10.1038/nrm4039 (2015).

61 Perocchi, F. *et al.* MICU1 encodes a mitochondrial EF hand protein required for Ca2+ uptake. *Nature* **467**, 291-296, doi:10.1038/nature09358 (2010).

62 Mallilankaraman, K. *et al.* MCUR1 is an essential component of mitochondrial Ca2+ uptake that regulates cellular metabolism. *Nature Cell Biology* **14**, 1336-1343, doi:10.1038/ncb2622 (2012).

63 Plovanich, M. *et al.* MICU2, a paralog of MICU1, resides within the mitochondrial uniporter complex to regulate calcium handling. *PLoS One* **8**, e55785, doi:10.1371/journal.pone.0055785 (2013).

64 Sancak, Y. *et al.* EMRE Is an Essential Component of the Mitochondrial Calcium Uniporter Complex. *Science* **342**, 1379-1382, doi:10.1126/science.1242993 (2013).

65 Raffaello, A. *et al.* The mitochondrial calcium uniporter is a multimer that can include a dominant-negative pore-forming subunit. *The EMBO Journal* **32**, 2362-2376, doi:10.1038/emboj.2013.157 (2013).

66 Hoffman, N. E. *et al.* SLC25A23 augments mitochondrial Ca(2)(+) uptake, interacts with MCU, and induces oxidative stress-mediated cell death. *Molecular biology of the cell* **25**, 936-947, doi:10.1091/mbc.E13-08-0502 (2014).

67 Marchi, S. & Pinton, P. The mitochondrial calcium uniporter complex: molecular components, structure and physiopathological implications. *J Physiol* **592**, 829-839, doi:10.1113/jphysiol.2013.268235 (2014).

68 Lee, Y. *et al.* Structure and function of the N-terminal domain of the human mitochondrial calcium uniporter. *EMBO reports* **16**, 1318-1333, doi:10.15252/embr.201540436 (2015).

69 Oxenoid, K. *et al.* Architecture of the mitochondrial calcium uniporter. *Nature* **533**, 269-273, doi:10.1038/nature17656 (2016).

70 Patron, M. *et al.* MICU1 and MICU2 Finely Tune the Mitochondrial Ca2+ Uniporter by Exerting Opposite Effects on MCU Activity. *Molecular Cell* **53**, 726-737, doi:10.1016/j.molcel.2014.01.013 (2014).

71 Vais, H. *et al.* EMRE Is a Matrix Ca(2+) Sensor that Governs Gatekeeping of the Mitochondrial Ca(2+) Uniporter. *Cell Rep* **14**, 403-410, doi:10.1016/j.celrep.2015.12.054 (2016).

72 Tomar, D. *et al.* MCUR1 Is a Scaffold Factor for the MCU Complex Function and Promotes Mitochondrial Bioenergetics. *Cell Reports* **15**, 1673-1685, doi:10.1016/j.celrep.2016.04.050 (2016).

73 Paupe, V., Prudent, J., Dassa, Emmanuel P., Rendon, Olga Z. & Shoubridge, Eric A. CCDC90A (MCUR1) Is a Cytochrome c Oxidase Assembly Factor and Not a Regulator of the Mitochondrial Calcium Uniporter. *Cell Metabolism* **21**, 109-116, doi:10.1016/j.cmet.2014.12.004 (2015).

74 Fieni, F., Lee, S. B., Jan, Y. N. & Kirichok, Y. Activity of the mitochondrial calcium uniporter varies greatly between tissues. *Nature communications* **3**, 1317-1317, doi:10.1038/ncomms2325 (2012).

75 Holmström, K. M. *et al.* Assessment of cardiac function in mice lacking the mitochondrial calcium uniporter. *Journal of Molecular and Cellular Cardiology* **85**, 178-182, doi:10.1016/j.yjmcc.2015.05.022 (2015).

76 Oka, T. Cardiac-Specific Deletion of Gata4 Reveals Its Requirement for Hypertrophy, Compensation, and Myocyte Viability. *Circulation Research* **98**, 837-845, doi:10.1161/01.RES.0000215985.18538.c4 (2006).

77 Antony, A. N. *et al.* MICU1 regulation of mitochondrial Ca2+ uptake dictates survival and tissue regeneration. *Nature Communications* **7**, 10955, doi:10.1038/ncomms10955 (2016).

78 Liu, J. C. *et al.* MICU1 Serves as a Molecular Gatekeeper to Prevent In Vivo Mitochondrial Calcium Overload. *Cell Reports* **16**, 1561-1573, doi:10.1016/j.celrep.2016.07.011 (2016).

79 Logan, C. V. *et al.* Loss-of-function mutations in MICU1 cause a brain and muscle disorder linked to primary alterations in mitochondrial calcium signaling. *Nature Genetics* **46**, 188-193, doi:10.1038/ng.2851 (2013).

80 Bohovych, I. & Khalimonchuk, O. Sending Out an SOS: Mitochondria as a Signaling Hub. *Frontiers in Cell and Developmental Biology* **4**, doi:10.3389/fcell.2016.00109 (2016).

81 E., L. G., Stefano, S., David, S., Paul, B. & Margaret, B. Developmental regulation of myosin gene expression in mouse cardiac muscle. *The Journal of cell biology* **111**, 2427-2436 (1990).

82 Bass, A., Stejskalová, M., Stieglerová, A., Ostádal, B. & Samánek, M. Ontogenetic development of energy-supplying enzymes in rat and guinea-pig heart. *Physiol Res* **50**, 237-245 (2001).

83 Piquereau, J. *et al.* Postnatal development of mouse heart: formation of energetic microdomains. *The Journal of Physiology* **588**, 2443-2454, doi:10.1113/jphysiol.2010.189670 (2010).

84 Hoerter, J. A., Kuznetsov, A. & Ventura-Clapier, R. Functional development of the creatine kinase system in perinatal rabbit heart. *Circ Res* **69**, 665-676 (1991).

85 Seki, S. Fetal and postnatal development of Ca2+ transients and Ca2+ sparks in rat cardiomyocytes. *Cardiovascular Research* **58**, 535-548, doi:10.1016/s0008-6363(03)00255-4 (2003).

86 Carafoli, E., Garcia-Martin, E. & Guerini, D. The plasma membrane calcium pump: recent developments and future perspectives. *Experientia* **52**, 1091-1100 (1996).

87 Carafoli, E. Calcium pump of the plasma membrane. *Physiol Rev* **71**, 129-153 (1991).

88 Eghbali, M. *et al.* Molecular and functional signature of heart hypertrophy during pregnancy. *Circ Res* **96**, 1208-1216, doi:10.1161/01.res.0000170652.71414.16 (2005).

89 Winsor, T. & Beckner, G. Hypertrophy of the heart; electrocardiographic distinction between physiologic and pathologic enlargement. *California medicine* **82**, 151-158 (1955).

90 Maillet, M., van Berlo, J. H. & Molkentin, J. D. Molecular basis of physiological heart growth: fundamental concepts and new players. *Nature Reviews Molecular Cell Biology* **14**, 38-48, doi:10.1038/nrm3495 (2012).

91 Sugishita, Y., Koseki, S., Matsuda, M., Yamaguchi, T. & Ito, I. Myocardial mechanics of athletic hearts in comparison with diseased hearts. *Am Heart J* **105**, 273-280 (1983).

92 Bernardo, B. C., Weeks, K. L., Pretorius, L. & McMullen, J. R. Molecular distinction between physiological and pathological cardiac hypertrophy: Experimental findings and therapeutic strategies. *Pharmacology & Therapeutics* **128**, 191-227, doi:10.1016/j.pharmthera.2010.04.005 (2010).

93 Pluim, B. M., Zwinderman, A. H., van der Laarse, A. & van der Wall, E. E. The athlete's heart. A meta-analysis of cardiac structure and function. *Circulation* **101**, 336-344 (2000).

94 Sarquella-Brugada, G. *et al.* Genetics of sudden cardiac death in children and young athletes. *Cardiology in the Young* **23**, 159-173, doi:10.1017/s1047951112001138 (2012).

95 Patten, I. S. *et al.* Cardiac angiogenic imbalance leads to peripartum cardiomyopathy. *Nature* **485**, 333-338, doi:10.1038/nature11040 (2012).

96 Laughlin, M. H., Bowles, D. K. & Duncker, D. J. The coronary circulation in exercise training. *American Journal of Physiology - Heart and Circulatory Physiology* **302**, H10-H23, doi:10.1152/ajpheart.00574.2011 (2012).

97 Abel, E. D. & Doenst, T. Mitochondrial adaptations to physiological vs. pathological cardiac hypertrophy. *Cardiovascular Research* **90**, 234-242, doi:10.1093/cvr/cvr015 (2011).

98 Gertz, E. W., Wisneski, J. A., Stanley, W. C. & Neese, R. A. Myocardial substrate utilization during exercise in humans. Dual carbon-labeled carbohydrate isotope experiments. *J Clin Invest* **82**, 2017-2025, doi:10.1172/jci113822 (1988).

99 Braz, J. C. *et al.* Targeted inhibition of p38 MAPK promotes hypertrophic cardiomyopathy through upregulation of calcineurin-NFAT signaling. *J Clin Invest* **111**, 1475-1486, doi:10.1172/jci17295 (2003).

100 Aoyagi, T. & Matsui, T. Phosphoinositide-3 kinase signaling in cardiac hypertrophy and heart failure. *Current pharmaceutical design* **17**, 1818-1824 (2011).
101 Soesanto, W. *et al.* mTOR is a critical regulator of cardiac hypertrophy in Spontaneously Hypertensive Rats. *Hypertension* **54**, 1321-1327, doi:10.1161/HYPERTENSIONAHA.109.138818 (2009).
102 Boström, P. *et al.* C/EBPβ controls exercise-induced cardiac growth and protects against pathological cardiac remodeling. *Cell* **143**, 1072-1083, doi:10.1016/j.cell.2010.11.036 (2010).
103 Kehat, I. *et al.* Extracellular Signal-Regulated Kinases 1 and 2 Regulate the Balance Between Eccentric and Concentric Cardiac Growth. *Circulation Research* **108**, 176-183, doi:10.1161/circresaha.110.231514 (2010).
104 Kehat, I. & Molkentin, J. D. Extracellular signal-regulated kinase 1/2 (ERK1/2) signaling in cardiac hypertrophy. *Ann N Y Acad Sci* **1188**, 96-102, doi:10.1111/j.1749-6632.2009.05088.x (2010).
105 Feldman, M. D. *et al.* Deficient production of cyclic AMP: pharmacologic evidence of an important cause of contractile dysfunction in patients with end-stage heart failure. *Circulation* **75**, 331-339 (1987).
106 Hasenfuss, G. Alterations of calcium-regulatory proteins in heart failure. *Cardiovasc Res* **37**, 279-289 (1998).
107 Schwinger, R. H. *et al.* Reduced Ca(2+)-sensitivity of SERCA 2a in failing human myocardium due to reduced serin-16 phospholamban phosphorylation. *J Mol Cell Cardiol* **31**, 479-491 (1999).
108 Respress, J. L. *et al.* Long-term simulated microgravity causes cardiac RyR2 phosphorylation and arrhythmias in mice. *International Journal of Cardiology* **176**, 994-1000, doi:10.1016/j.ijcard.2014.08.138 (2014).
109 Dobrev, D. & Wehrens, X. H. T. Role of RyR2 Phosphorylation in Heart Failure and Arrhythmias: Controversies Around Ryanodine Receptor Phosphorylation in Cardiac Disease. *Circulation Research* **114**, 1311-1319, doi:10.1161/circresaha.114.300568 (2014).
110 Houser, S. R. Role of RyR2 Phosphorylation in Heart Failure and Arrhythmias: Protein Kinase A-Mediated Hyperphosphorylation of the Ryanodine Receptor at Serine 2808 Does Not Alter Cardiac Contractility or Cause Heart Failure and Arrhythmias. *Circulation Research* **114**, 1320-1327, doi:10.1161/circresaha.114.300569 (2014).
111 Luo, M. & Anderson, M. E. Mechanisms of Altered Ca2+Handling in Heart Failure. *Circulation Research* **113**, 690-708, doi:10.1161/circresaha.113.301651 (2013).
112 Crossman, D. J., Ruygrok, P. N., Soeller, C. & Cannell, M. B. Changes in the organization of excitation-contraction coupling structures in failing human heart. *PLoS One* **6**, e17901, doi:10.1371/journal.pone.0017901 (2011).
113 Taegtmeyer, H. Switching Metabolic Genes to Build a Better Heart. *Circulation* **106**, 2043-2045, doi:10.1161/01.cir.0000036760.42319.3f (2002).
114 Akki, A., Smith, K. & Seymour, A.-M. L. Compensated cardiac hypertrophy is characterised by a decline in palmitate oxidation. *Molecular and Cellular Biochemistry* **311**, 215-224, doi:10.1007/s11010-008-9711-y (2008).
115 Lydell, C. P. *et al.* Pyruvate dehydrogenase and the regulation of glucose oxidation in hypertrophied rat hearts. *Cardiovasc Res* **53**, 841-851 (2002).
116 Friehs, I. *et al.* Vascular endothelial growth factor delays onset of failure in pressure–overload hypertrophy through matrix metalloproteinase activation and

angiogenesis. *Basic Research in Cardiology* **101**, 204-213, doi:10.1007/s00395-005-0581-0 (2005).

117 Fowler, E. D. *et al.* Decreased creatine kinase is linked to diastolic dysfunction in rats with right heart failure induced by pulmonary artery hypertension. *Journal of Molecular and Cellular Cardiology* **86**, 1-8, doi:10.1016/j.yjmcc.2015.06.016 (2015).

118 Shiojima, I. Disruption of coordinated cardiac hypertrophy and angiogenesis contributes to the transition to heart failure. *Journal of Clinical Investigation* **115**, 2108-2118, doi:10.1172/jci24682 (2005).

119 Izumiya, Y. *et al.* Vascular Endothelial Growth Factor Blockade Promotes the Transition From Compensatory Cardiac Hypertrophy to Failure in Response to Pressure Overload. *Hypertension* **47**, 887-893, doi:10.1161/01.hyp.0000215207.54689.31 (2006).

120 Brown, R. D., Ambler, S. K., Mitchell, M. D. & Long, C. S. THE CARDIAC FIBROBLAST: Therapeutic Target in Myocardial Remodeling and Failure. *Annual Review of Pharmacology and Toxicology* **45**, 657-687, doi:10.1146/annurev.pharmtox.45.120403.095802 (2005).

121 Berk, B. C., Fujiwara, K. & Lehoux, S. ECM remodeling in hypertensive heart disease. *The Journal of Clinical Investigation* **117**, 568-575, doi:10.1172/JCI31044 (2007).

122 Gonzalez, G. E. *et al.* Deletion of interleukin-6 prevents cardiac inflammation, fibrosis and dysfunction without affecting blood pressure in angiotensin II-high salt-induced hypertension. *Journal of hypertension* **33**, 144-152, doi:10.1097/hjh.0000000000000358 (2015).

123 Mann, D. L. The emerging role of innate immunity in the heart and vascular system: for whom the cell tolls. *Circ Res* **108**, 1133-1145, doi:10.1161/circresaha.110.226936 (2011).

124 Mann, D. L. Inflammatory mediators and the failing heart: past, present, and the foreseeable future. *Circ Res* **91**, 988-998 (2002).

125 Du, X.-J. Distinct Role of Adrenoceptor Subtypes in Cardiac Adaptation to Chronic Pressure Overload. *Clinical and Experimental Pharmacology and Physiology* **35**, 355-360, doi:10.1111/j.1440-1681.2007.04871.x (2008).

126 Engelhardt, S., Hein, L., Wiesmann, F. & Lohse, M. J. Progressive hypertrophy and heart failure in beta1-adrenergic receptor transgenic mice. *Proceedings of the National Academy of Sciences of the United States of America* **96**, 7059-7064 (1999).

127 Bristow, M. R. beta-adrenergic receptor blockade in chronic heart failure. *Circulation* **101**, 558-569 (2000).

128 Kiriazis, H. *et al.* Knockout of β1- and β2-adrenoceptors attenuates pressure overload-induced cardiac hypertrophy and fibrosis. *British Journal of Pharmacology* **153**, 684-692, doi:10.1038/sj.bjp.0707622 (2008).

129 Bowling, N. *et al.* Increased protein kinase C activity and expression of Ca2+-sensitive isoforms in the failing human heart. *Circulation* **99**, 384-391 (1999).

130 Braz, J. C. *et al.* PKC-α regulates cardiac contractility and propensity toward heart failure. *Nature Medicine* **10**, 248-254, doi:10.1038/nm1000 (2004).

131 Bowman, J. C. *et al.* Expression of protein kinase C beta in the heart causes hypertrophy in adult mice and sudden death in neonates. *Journal of Clinical Investigation* **100**, 2189-2195, doi:10.1172/jci119755 (1997).

132 Haq, S. *et al.* Differential activation of signal transduction pathways in human hearts with hypertrophy versus advanced heart failure. *Circulation* **103**, 670-677 (2001).

133 Sussman, M. A. *et al.* Prevention of cardiac hypertrophy in mice by calcineurin inhibition. *Science* **281**, 1690-1693 (1998).

134 Zhang, T. The deltaC Isoform of CaMKII Is Activated in Cardiac Hypertrophy and Induces Dilated Cardiomyopathy and Heart Failure. *Circulation Research* **92**, 912-919, doi:10.1161/01.res.0000069686.31472.c5 (2003).

135 Westenbrink, B. D. *et al.* Mitochondrial Reprogramming Induced by CaMKII Mediates Hypertrophy Decompensation. *Circulation Research* **116**, e28-e39, doi:10.1161/circresaha.116.304682 (2015).

136 Kreusser, M. M. *et al.* Cardiac CaM Kinase II Genes δ and γ Contribute to Adverse Remodeling but Redundantly Inhibit Calcineurin-Induced Myocardial HypertrophyCLINICAL PERSPECTIVE. *Circulation* **130**, 1262-1273, doi:10.1161/circulationaha.114.006185 (2014).

137 Tham, Y. K., Bernardo, B. C., Ooi, J. Y. Y., Weeks, K. L. & McMullen, J. R. Pathophysiology of cardiac hypertrophy and heart failure: signaling pathways and novel therapeutic targets. *Archives of Toxicology* **89**, 1401-1438, doi:10.1007/s00204-015-1477-x (2015).

138 McMullen, J. R. *et al.* Protective effects of exercise and phosphoinositide 3-kinase(p110) signaling in dilated and hypertrophic cardiomyopathy. *Proceedings of the National Academy of Sciences* **104**, 612-617, doi:10.1073/pnas.0606663104 (2007).

139 Lin, Z. *et al.* Pi3kcb Links Hippo-YAP and PI3K-AKT Signaling Pathways to Promote Cardiomyocyte Proliferation and Survival. *Circulation Research* **116**, 35-45, doi:10.1161/circresaha.115.304457 (2014).

140 Zsebo, K. *et al.* Long-Term Effects of AAV1/SERCA2a Gene Transfer in Patients With Severe Heart FailureNovelty and Significance. *Circulation Research* **114**, 101-108, doi:10.1161/circresaha.113.302421 (2014).

141 Raake, P. W. *et al.* G Protein-Coupled Receptor Kinase 2 Ablation in Cardiac Myocytes Before or After Myocardial Infarction Prevents Heart Failure. *Circulation Research* **103**, 413-422, doi:10.1161/circresaha.107.168336 (2008).

142 Aiello, L. P. Inhibition of PKC by Oral Administration of Ruboxistaurin Is Well Tolerated and Ameliorates Diabetes-Induced Retinal Hemodynamic Abnormalities in Patients. *Investigative Ophthalmology & Visual Science* **47**, 86-92, doi:10.1167/iovs.05-0757 (2006).

143 Santulli, G., Xie, W., Reiken, S. R. & Marks, A. R. Mitochondrial calcium overload is a key determinant in heart failure. *Proceedings of the National Academy of Sciences* **112**, 11389-11394, doi:10.1073/pnas.1513047112 (2015).

144 Kindo, M. *et al.* Pressure overload-induced mild cardiac hypertrophy reduces left ventricular transmural differences in mitochondrial respiratory chain activity and increases oxidative stress. *Frontiers in Physiology* **3**, doi:10.3389/fphys.2012.00332 (2012).

145 Rosca, M. G. & Hoppel, C. L. Mitochondria in heart failure. *Cardiovascular Research* **88**, 40-50, doi:10.1093/cvr/cvq240 (2010).

146 Rosca, M. G., Tandler, B. & Hoppel, C. L. Mitochondria in cardiac hypertrophy and heart failure. *Journal of Molecular and Cellular Cardiology* **55**, 31-41, doi:10.1016/j.yjmcc.2012.09.002 (2013).

147 Taegtmeyer, H. & Overturf, M. L. Effects of moderate hypertension on cardiac function and metabolism in the rabbit. *Hypertension* **11**, 416-426 (1988).

148 Taegtmeyer, H., Golfman, L., Sharma, S., Razeghi, P. & van Arsdall, M. Linking gene expression to function: metabolic flexibility in the normal and diseased heart. *Ann N Y Acad Sci* **1015**, 202-213, doi:10.1196/annals.1302.017 (2004).

149 Bishop, S. P. & Altschuld, R. A. Increased glycolytic metabolism in cardiac hypertrophy and congestive failure. *The American journal of physiology* **218**, 153-159 (1970).

150 Taegtmeyer, H., Sen, S. & Vela, D. Return to the fetal gene program. *Annals of the New York Academy of Sciences* **1188**, 191-198, doi:10.1111/j.1749-6632.2009.05100.x (2010).

151 Taegtmeyer, H., Sen, S. & Vela, D. Return to the fetal gene program: a suggested metabolic link to gene expression in the heart. *Ann N Y Acad Sci* **1188**, 191-198, doi:10.1111/j.1749-6632.2009.05100.x (2010).

152 Sambandam, N., Lopaschuk, G. D., Brownsey, R. W. & Allard, M. F. Energy metabolism in the hypertrophied heart. *Heart Fail Rev* **7**, 161-173 (2002).

153 Allard, M. F., Schonekess, B. O., Henning, S. L., English, D. R. & Lopaschuk, G. D. Contribution of oxidative metabolism and glycolysis to ATP production in hypertrophied hearts. *The American journal of physiology* **267**, H742-750 (1994).

154 Hue, L. & Taegtmeyer, H. The Randle cycle revisited: a new head for an old hat. *American journal of physiology. Endocrinology and metabolism* **297**, E578-591, doi:10.1152/ajpendo.00093.2009 (2009).

155 Sorokina, N. *et al.* Recruitment of compensatory pathways to sustain oxidative flux with reduced carnitine palmitoyltransferase I activity characterizes inefficiency in energy metabolism in hypertrophied hearts. *Circulation* **115**, 2033-2041, doi:10.1161/circulationaha.106.668665 (2007).

156 Martin, M. A. *et al.* Myocardial carnitine and carnitine palmitoyltransferase deficiencies in patients with severe heart failure. *Biochimica et biophysica acta* **1502**, 330-336 (2000).

157 Graham, B. H. *et al.* A mouse model for mitochondrial myopathy and cardiomyopathy resulting from a deficiency in the heart/muscle isoform of the adenine nucleotide translocator. *Nat Genet* **16**, 226-234, doi:10.1038/ng0797-226 (1997).

158 Walther, T. *et al.* Accelerated mitochondrial adenosine diphosphate/adenosine triphosphate transport improves hypertension-induced heart disease. *Circulation* **115**, 333-344, doi:10.1161/circulationaha.106.643296 (2007).

159 Ingwall, J. S. & Weiss, R. G. Is the failing heart energy starved? On using chemical energy to support cardiac function. *Circ Res* **95**, 135-145, doi:10.1161/01.RES.0000137170.41939.d9 (2004).

160 Neubauer, S. The failing heart--an engine out of fuel. *The New England journal of medicine* **356**, 1140-1151, doi:10.1056/NEJMra063052 (2007).

161 Santulli, G. e. in *Advances in Experimental Medicine and Biology* Vol. 982 (Springer International Publishing AG 2017, 2017).

162 Wu, Z. *et al.* Mechanisms controlling mitochondrial biogenesis and respiration through the thermogenic coactivator PGC-1. *Cell* **98**, 115-124, doi:10.1016/s0092-8674(00)80611-x (1999).

163 Puigserver, P. *et al.* A cold-inducible coactivator of nuclear receptors linked to adaptive thermogenesis. *Cell* **92**, 829-839 (1998).

164 Esterbauer, H., Oberkofler, H., Krempler, F. & Patsch, W. Human peroxisome proliferator activated receptor gamma coactivator 1 (PPARGC1) gene: cDNA sequence, genomic organization, chromosomal localization, and tissue expression. *Genomics* **62**, 98-102, doi:10.1006/geno.1999.5977 (1999).

165 Arany, Z. *et al.* Transverse aortic constriction leads to accelerated heart failure in mice lacking PPAR-gamma coactivator 1alpha. *Proceedings of the National Academy of Sciences of the United States of America* **103**, 10086-10091, doi:10.1073/pnas.0603615103 (2006).

166 Riehle, C. *et al.* PGC-1beta deficiency accelerates the transition to heart failure in pressure overload hypertrophy. *Circ Res* **109**, 783-793, doi:10.1161/circresaha.111.243964 (2011).

167 Garnier, A. *et al.* Depressed mitochondrial transcription factors and oxidative capacity in rat failing cardiac and skeletal muscles. *J Physiol* **551**, 491-501, doi:10.1113/jphysiol.2003.045104 (2003).

168 Osterholt, M., Nguyen, T. D., Schwarzer, M. & Doenst, T. Alterations in mitochondrial function in cardiac hypertrophy and heart failure. *Heart Failure Reviews* **18**, 645-656, doi:10.1007/s10741-012-9346-7 (2012).

169 Hirotani, S. *et al.* Involvement of nuclear factor-kappaB and apoptosis signal-regulating kinase 1 in G-protein-coupled receptor agonist-induced cardiomyocyte hypertrophy. *Circulation* **105**, 509-515 (2002).

170 Pimentel, D. R. *et al.* Reactive oxygen species mediate amplitude-dependent hypertrophic and apoptotic responses to mechanical stretch in cardiac myocytes. *Circ Res* **89**, 453-460 (2001).

171 Nakamura, K. *et al.* Inhibitory effects of antioxidants on neonatal rat cardiac myocyte hypertrophy induced by tumor necrosis factor-alpha and angiotensin II. *Circulation* **98**, 794-799 (1998).

172 Xie, Z. *et al.* Intracellular reactive oxygen species mediate the linkage of Na+/K+-ATPase to hypertrophy and its marker genes in cardiac myocytes. *The Journal of biological chemistry* **274**, 19323-19328 (1999).

173 Dhalla, A. K. & Singal, P. K. Antioxidant changes in hypertrophied and failing guinea pig hearts. *The American journal of physiology* **266**, H1280-1285 (1994).

174 Kuroda, J. *et al.* NADPH oxidase 4 (Nox4) is a major source of oxidative stress in the failing heart. *Proceedings of the National Academy of Sciences of the United States of America* **107**, 15565-15570, doi:10.1073/pnas.1002178107 (2010).

175 Ago, T. *et al.* Upregulation of Nox4 by hypertrophic stimuli promotes apoptosis and mitochondrial dysfunction in cardiac myocytes. *Circ Res* **106**, 1253-1264, doi:10.1161/circresaha.109.213116 (2010).

176 Bauersachs, J. Aldosterone antagonism in heart failure: improvement of cardiac remodelling, endothelial dysfunction and platelet activation. *European journal of clinical investigation* **34**, 649-652, doi:10.1111/j.1365-2362.2004.01400.x (2004).

177 Adiga, I. K. & Nair, R. R. Multiple signaling pathways coordinately mediate reactive oxygen species dependent cardiomyocyte hypertrophy. *Cell biochemistry and function* **26**, 346-351, doi:10.1002/cbf.1449 (2008).

178 Zhang, W., Elimban, V., Nijjar, M. S., Gupta, S. K. & Dhalla, N. S. Role of mitogen-activated protein kinase in cardiac hypertrophy and heart failure. *Experimental & Clinical Cardiology* **8**, 173-183 (2003).

179 Liang, Q. & Molkentin, J. D. Redefining the roles of p38 and JNK signaling in cardiac hypertrophy: dichotomy between cultured myocytes and animal models. *J Mol Cell Cardiol* **35**, 1385-1394 (2003).

180 Li, H. L. *et al.* Epigallocathechin-3 gallate inhibits cardiac hypertrophy through blocking reactive oxidative species-dependent and -independent signal pathways. *Free radical biology & medicine* **40**, 1756-1775 (2006).

181 Cai, J. *et al.* Crocetin protects against cardiac hypertrophy by blocking MEK-ERK1/2 signalling pathway. *Journal of cellular and molecular medicine* **13**, 909-925, doi:10.1111/j.1582-4934.2008.00620.x (2009).

182 Zhang, L., Zhang, Z., Guo, H. & Wang, Y. Na+/K+-ATPase-mediated signal transduction and Na+/K+-ATPase regulation. *Fundamental & Clinical Pharmacology* **22**, 615-621, doi:10.1111/j.1472-8206.2008.00620.x (2008).

183 Guo, J., Gertsberg, Z., Ozgen, N. & Steinberg, S. F. p66Shc links alpha1-adrenergic receptors to a reactive oxygen species-dependent AKT-FOXO3A phosphorylation pathway in cardiomyocytes. *Circ Res* **104**, 660-669, doi:10.1161/circresaha.108.186288 (2009).

184 Zou, X. J., Yang, L. & Yao, S. L. Propofol depresses angiotensin II-induced cardiomyocyte hypertrophy in vitro. *Experimental biology and medicine (Maywood, N.J.)* **233**, 200-208, doi:10.3181/0707-rm-206 (2008).

185 Frey, N., McKinsey, T. A. & Olson, E. N. Decoding calcium signals involved in cardiac growth and function. *Nat Med* **6**, 1221-1227, doi:10.1038/81321 (2000).

186 Izem-Meziane, M. *et al.* Catecholamine-induced cardiac mitochondrial dysfunction and mPTP opening: protective effect of curcumin. *American journal of physiology. Heart and circulatory physiology* **302**, H665-674, doi:10.1152/ajpheart.00467.2011 (2012).

187 Viola, H. M. & Hool, L. C. Targeting calcium and the mitochondria in prevention of pathology in the heart. *Current drug targets* **12**, 748-760 (2011).

188 Zaglia, T. *et al.* Content of mitochondrial calcium uniporter (MCU) in cardiomyocytes is regulated by microRNA-1 in physiologic and pathologic hypertrophy. *Proceedings of the National Academy of Sciences*, 201708772, doi:10.1073/pnas.1708772114 (2017).

189 Marchi, S. *et al.* Downregulation of the Mitochondrial Calcium Uniporter by Cancer-Related miR-25. *Current Biology* **23**, 58-63, doi:10.1016/j.cub.2012.11.026 (2013).

190 Mitchelson, K. R. Roles of the canonical myomiRs miR-1, -133 and -206 in cell development and disease. *World Journal of Biological Chemistry* **6**, 162, doi:10.4331/wjbc.v6.i3.162 (2015).

191 Kertesz, M., Iovino, N., Unnerstall, U., Gaul, U. & Segal, E. The role of site accessibility in microRNA target recognition. *Nature Genetics* **39**, 1278-1284, doi:10.1038/ng2135 (2007).

192 Latronico, M. V. G., Catalucci, D. & Condorelli, G. Emerging Role of MicroRNAs in Cardiovascular Biology. *Circulation Research* **101**, 1225-1236, doi:10.1161/circresaha.107.163147 (2007).

193 Zhao, Y., Samal, E. & Srivastava, D. Serum response factor regulates a muscle-specific microRNA that targets Hand2 during cardiogenesis. *Nature* **436**, 214-220, doi:10.1038/nature03817 (2005).

194 Callis, T. E. *et al.* MicroRNA-208a is a regulator of cardiac hypertrophy and conduction in mice. *Journal of Clinical Investigation* **119**, 2772-2786, doi:10.1172/JCI36154 (2009).

195 Callis, T. E. & Wang, D. Z. Taking microRNAs to heart. *Trends Mol Med* **14**, 254-260, doi:10.1016/j.molmed.2008.03.006 (2008).

196 Terentyev, D. *et al.* miR-1 Overexpression Enhances Ca2+ Release and Promotes Cardiac Arrhythmogenesis by Targeting PP2A Regulatory Subunit B56 alpha and Causing CaMKII-Dependent Hyperphosphorylation of RyR2. *Circulation Research* **104**, 514-521, doi:10.1161/Circresaha.108.181651 (2009).

197 Tritsch, E. *et al.* An SRF/miR-1 axis regulates NCX1 and Annexin A5 protein levels in the normal and failing heart. *Cardiovascular Research* **98**, 372-380, doi:10.1093/cvr/cvt042 (2013).

198 Lyons, G. E., Schiaffino, S., Sassoon, D., Barton, P. & Buckingham, M. Developmental regulation of myosin gene expression in mouse cardiac muscle. *J Cell Biol* **111**, 2427-2436 (1990).

199 Anmann, T. *et al.* Formation of highly organized intracellular structure and energy metabolism in cardiac muscle cells during postnatal development of rat heart. *Bba-Bioenergetics* **1837**, 1350-1361, doi:10.1016/j.bbabio.2014.03.015 (2014).

200 Piquereau, J. *et al.* Postnatal development of mouse heart: formation of energetic microdomains. *J Physiol-London* **588**, 2443-2454, doi:10.1113/jphysiol.2010.189670 (2010).

201 Ikeda, S. *et al.* MicroRNA-1 negatively regulates expression of the hypertrophy-associated calmodulin and Mef2a genes. *Mol Cell Biol* **29**, 2193-2204, doi:10.1128/MCB.01222-08 [pii] (2009).

202 Knezevic, I. *et al.* A novel cardiomyocyte-enriched microRNA, miR-378, targets insulin-like growth factor 1 receptor: implications in postnatal cardiac remodeling and cell survival. *J Biol Chem* **287**, 12913-12926, doi:10.1074/jbc.M111.331751 [pii] (2012).

203 Goss, R. J. Hypertrophy versus hyperplasia. *Science.* **153**, 1615-1620. (1966).

204 Nadal-Ginard, B., Kajstura, J., Leri, A. & Anversa, P. Myocyte death, growth, and regeneration in cardiac hypertrophy and failure. *Circ Res.* **92**, 139-150. (2003).

205 Rumyantsev, P. P. Interrelations of the proliferation and differentiation processes during cardiact myogenesis and regeneration. *Int Rev Cytol.* **51**, 186-273. (1977).

206 Tuomainen, T. & Tavi, P. The role of cardiac energy metabolism in cardiac hypertrophy and failure. *Experimental Cell Research*, doi:10.1016/j.yexcr.2017.03.052 (2017).

207 Rockman, H. A. *et al.* Segregation of atrial-specific and inducible expression of an atrial natriuretic factor transgene in an in vivo murine model of cardiac hypertrophy. *Proc Natl Acad Sci U S A* **88**, 8277-8281 (1991).

208 Lu, X. *et al.* Measuring Local Gradients of Intramitochondrial [Ca2+] in Cardiac Myocytes During Sarcoplasmic Reticulum Ca2+ReleaseNovelty and Significance. *Circulation Research* **112**, 424-431, doi:10.1161/circresaha.111.300501 (2013).

209 Robert, V. *et al.* Beat-to-beat oscillations of mitochondrial [Ca2+] in cardiac cells. *Embo J.* **20**, 4998-5007. (2001).

210 Drago, I., De Stefani, D., Rizzuto, R. & Pozzan, T. Mitochondrial Ca2+ uptake contributes to buffering cytoplasmic Ca2+ peaks in cardiomyocytes. *Proc Natl Acad Sci U S A.* **109**, 12986-12991. doi: 12910.11073/pnas.1210718109. Epub 1210712012 Jul 1210718120. (2012).

211 Ambardekar, A. V. & Buttrick, P. M. Reverse Remodeling With Left Ventricular Assist Devices: A Review of Clinical, Cellular, and Molecular Effects. *Circulation: Heart Failure* **4**, 224-233, doi:10.1161/circheartfailure.110.959684 (2011).

212 Wilkins, B. J. Calcineurin/NFAT Coupling Participates in Pathological, but not Physiological, Cardiac Hypertrophy. *Circulation Research* **94**, 110-118, doi:10.1161/01.res.0000109415.17511.18 (2004).

213 Zhang, W. *et al.* β-Adrenergic Receptor-PI3K Signaling Crosstalk in Mouse Heart: Elucidation of Immediate Downstream Signaling Cascades. *PLoS ONE* **6**, e26581, doi:10.1371/journal.pone.0026581 (2011).

214 Erickson, J. R. *et al.* A Dynamic Pathway for Calcium-Independent Activation of CaMKII by Methionine Oxidation. *Cell* **133**, 462-474, doi:10.1016/j.cell.2008.02.048 (2008).

215 Erickson, J. R. Mechanisms of CaMKII Activation in the Heart. *Frontiers in Pharmacology* **5**, doi:10.3389/fphar.2014.00059 (2014).

216 Yang, H. T. *et al.* The ryanodine receptor modulates the spontaneous beating rate of cardiomyocytes during development. *Proceedings of the National Academy of Sciences of the United States of America* **99**, 9225-9230, doi:10.1073/pnas.142651999 (2002).

217 Bish, L. T. *et al.* Adeno-associated virus (AAV) serotype 9 provides global cardiac gene transfer superior to AAV1, AAV6, AAV7, and AAV8 in the mouse and rat. *Human gene therapy* **19**, 1359-1368, doi:10.1089/hum.2008.123 (2008).

218 Rose, T., Goltstein, P. M., Portugues, R. & Griesbeck, O. Putting a finishing touch on GECIs. *Front Mol Neurosci* **7**, 88, doi:10.3389/fnmol.2014.00088 (2014).

219 Akerboom, J. *et al.* Genetically encoded calcium indicators for multi-color neural activity imaging and combination with optogenetics. *Frontiers in molecular neuroscience* **6**, 2, doi:10.3389/fnmol.2013.00002 (2013).

220 Kotlikoff, M. I. Genetically encoded Ca2+ indicators: using genetics and molecular design to understand complex physiology. *J Physiol* **578**, 55-67, doi:10.1113/jphysiol.2006.120212 (2007).

221 Miyawaki, A., Griesbeck, O., Heim, R. & Tsien, R. Y. Dynamic and quantitative Ca2+ measurements using improved cameleons. *Proceedings of the National Academy of Sciences of the United States of America* **96**, 2135-2140 (1999).

222 Heim, R. & Tsien, R. Y. Engineering green fluorescent protein for improved brightness, longer wavelengths and fluorescence resonance energy transfer. *Curr Biol* **6**, 178-182 (1996).

223 McCombs, J. E. & Palmer, A. E. Measuring calcium dynamics in living cells with genetically encodable calcium indicators. *Methods* **46**, 152-159, doi:10.1016/j.ymeth.2008.09.015 S1046-2023(08)00166-7 [pii] (2008).

224 Griffiths, E. J., Balaska, D. & Cheng, W. H. The ups and downs of mitochondrial calcium signalling in the heart. *Biochim Biophys Acta* **1797**, 856-864, doi:10.1016/j.bbabio.2010.02.022 (2010).

225 O'Rourke, B. & Blatter, L. A. Mitochondrial Ca2+ uptake: tortoise or hare? *J Mol Cell Cardiol* **46**, 767-774, doi:10.1016/j.yjmcc.2008.12.011 (2009).

226 Miyawaki, A. *et al.* Fluorescent indicators for Ca2+ based on green fluorescent proteins and calmodulin. *Nature* **388**, 882-887, doi:10.1038/42264 (1997).

227 Palmer, A. E. & Tsien, R. Y. Measuring calcium signaling using genetically targetable fluorescent indicators. *Nat Protoc* **1**, 1057-1065, doi:10.1038/nprot.2006.172 (2006).

228 Greotti, E., Wong, A., Pozzan, T., Pendin, D. & Pizzo, P. Characterization of the ER-Targeted Low Affinity Ca2+ Probe D4ER. *Sensors* **16**, 1419, doi:10.3390/s16091419 (2016).

229 Nagai, T., Yamada, S., Tominaga, T., Ichikawa, M. & Miyawaki, A. Expanded dynamic range of fluorescent indicators for Ca(2+) by circularly permuted yellow fluorescent proteins. *Proceedings of the National Academy of Sciences of the United States of America* **101**, 10554-10559, doi:10.1073/pnas.0400417101 (2004).

230 Akerboom, J. *et al.* Optimization of a GCaMP calcium indicator for neural activity imaging. *The Journal of neuroscience : the official journal of the Society for Neuroscience* **32**, 13819-13840, doi:10.1523/jneurosci.2601-12.2012 (2012).

231 Chen, T. W. *et al.* Ultrasensitive fluorescent proteins for imaging neuronal activity. *Nature* **499**, 295-300, doi:10.1038/nature12354 (2013).

232 Hanson, G. T. *et al.* Investigating Mitochondrial Redox Potential with Redox-sensitive Green Fluorescent Protein Indicators. *Journal of Biological Chemistry* **279**, 13044-13053, doi:10.1074/jbc.M312846200 (2004).

8. APPENDIX

In the following pages, you can find attached the paper "Content of mitochondrial calcium uniporter (MCU) in cardiomyocytes is regulated by microRNA-1 in physiologic and pathologic hypertrophy", in which I am co-first author[188].

Content of mitochondrial calcium uniporter (MCU) in cardiomyocytes is regulated by microRNA-1 in physiologic and pathologic hypertrophy

Tania Zaglia[a,b,c,1], Paola Ceriotti[d,e,1], Antonio Campo[b,c,1], Giulia Borile[b,c,1], Andrea Armani[c], Pierluigi Carullo[d,e], Valentina Prando[b,c], Raffaele Coppini[f], Vladimiro Vida[a], Tomas O. Stølen[g], Wisløff Ulrik[g,h], Elisabetta Cerbai[f], Giovanni Stellin[a], Giuseppe Faggian[i], Diego De Stefani[b], Marco Sandri[b,c,j], Rosario Rizzuto[b], Fabio Di Lisa[b], Tullio Pozzan[b,c,j,2,3], Daniele Catalucci[d,e,2,3], and Marco Mongillo[b,c,j,2,3]

[a]Department of Cardiac, Thoracic and Vascular Sciences, University of Padua Medical School, 35128 Padua, Italy; [b]Department of Biomedical Sciences, University of Padua, 35131 Padua, Italy; [c]Venetian Institute of Molecular Medicine, 35129 Padua, Italy; [d]Humanitas Clinical and Research Center, Rozzano, 20089 Milan, Italy; [e]National Research Council Institute of Genetic and Biomedical Research–Unità Operativa di Supporto Milan, 20089 Rozzano, Milan, Italy; [f]Division of Pharmacology, Department "NeuroFarBa," University of Florence, 50139 Florence, Italy; [g]K. G. Jebsen Center of Exercise in Medicine at Department of Circulation and Medical Imaging, Faculty of Medicine and Health Sciences, Norwegian University of Science and Technology, 7491 Trondheim, Norway; [h]School of Human Movement and Nutrition Sciences, The University of Queensland, Brisbane, QLD, 4072 Australia; [i]Division of Cardiac Surgery, University Hospital of Verona, 37126 Verona, Italy; and [j]Padua Section, National Research Council Institute of Neuroscience, 35131 Padua, Italy

Contributed by Tullio Pozzan, September 5, 2017 (sent for review May 31, 2017; reviewed by Paula Da Costa Martins and John W. Elrod)

The mitochondrial Ca^{2+} uniporter complex (MCUC) is a multimeric ion channel which, by tuning Ca^{2+} influx into the mitochondrial matrix, finely regulates metabolic energy production. In the heart, this dynamic control of mitochondrial Ca^{2+} uptake is fundamental for cardiomyocytes to adapt to either physiologic or pathologic stresses. Mitochondrial calcium uniporter (MCU), which is the core channel subunit of MCUC, has been shown to play a critical role in the response to β-adrenoreceptor stimulation occurring during acute exercise. The molecular mechanisms underlying the regulation of MCU, in conditions requiring chronic increase in energy production, such as physiologic or pathologic cardiac growth, remain elusive. Here, we show that microRNA-1 (miR-1), a member of the muscle-specific microRNA (myomiR) family, is responsible for direct and selective targeting of MCU and inhibition of its translation, thereby affecting the capacity of the mitochondrial Ca^{2+} uptake machinery. Consistent with the role of miR-1 in heart development and cardiomyocyte hypertrophic remodeling, we additionally found that MCU levels are inversely related with the myomiR content, in murine and, remarkably, human hearts from both physiologic (i.e., postnatal development and exercise) and pathologic (i.e., pressure overload) myocardial hypertrophy. Interestingly, the persistent activation of β-adrenoreceptors is likely one of the upstream repressors of miR-1 as treatment with β-blockers in pressure-overloaded mouse hearts prevented its down-regulation and the consequent increase in MCU content. Altogether, these findings identify the miR-1/MCU axis as a factor in the dynamic adaptation of cardiac cells to hypertrophy.

microRNA | mitochondrial calcium uniporter | heart | myocardial hypertrophy | cardiomyocyte calcium

From birth, throughout the entire lifespan, the healthy myocardium is constituted by an almost fixed number of cardiomyocytes (1). Postnatal heart growth occurs by cardiomyocyte hypertrophy, a process which brings the cell to the adult phenotype, through a dramatic structural, functional, and metabolic maturation. Once fully developed, the heart continuously adapts both its performance and cardiomyocyte structure, in response to the varying requests of the organism as elicited by changes in intrinsic and environmental conditions (2). While acute stresses operate mostly through reversible modulation of contractility, cardiomyocytes subjected to prolonged increase in workload experience a complex structural remodeling, which stimulates their further growth necessary to sustain the chronic elevation of mechanical load. In common with postnatal heart development, hypertrophic remodeling of adult cardiomyocyte requires the cell to enhance ATP production, whose adequate supply determines whether cardiac hypertrophy would evolve toward a fully adaptive (physiologic) or a maladaptive (pathologic) response, this latter being a major cause of heart failure (3). Mitochondria are the cardiomyocyte powerhouse, and $[Ca^{2+}]$ operates as a primary dynamic regulator of ATP production, by modulating both pyruvate dehydrogenase, the main glucose oxidation gatekeeper, and other enzymatic key players of the TCA cycle (isocitrate dehydrogenase and 2-oxoglutarate dehydrogenase) in the mitochondrial matrix (4), as well as ATP synthase (5). In heart cells, Ca^{2+} influx into the mitochondrial matrix occurs during cytosolic Ca^{2+} fluctuations in systole and is mediated by the recently identified mitochondrial Ca^{2+} uniporter complex (MCUC) (4, 5). This multimolecular structure, localized in the inner mitochondrial membrane, is formed by core channel-forming subunits, namely mitochondrial calcium uniporter (MCU) (6, 7), its paralog MCUb (8), and essential MCU regulator (EMRE) (9),

Significance

Mitochondrial calcium uniporter (MCU) is the core channel subunit of the mitochondrial Ca^{2+} uniporter complex (MCUC) and contributes to the regulation of ATP production. Here, we identify that the adaptive and maladaptive remodeling occurring in rodent and human cardiomyocytes is associated with changes in MCU content, which are inversely correlated with those of its regulator microRNA-1 (miR-1). The present study thus defines the molecular mechanism by which MCU content and, consequently, mitochondrial Ca^{2+} uptake are directly modified by alteration of miR-1, a key regulator affecting physiological and pathological heart growth. These findings provide evidence for the miR-1/MCU axis as a potential target for the development of novel therapeutic approaches.

Author contributions: T.Z., D.C., and M.M. designed research; T.Z., P. Ceriotti, A.C., G.B., A.A., P. Carullo, V.P., T.O.S., W.U., and D.D.S. performed research; R.C., V.V., E.C., G.S., and G.F. contributed new reagents/analytic tools; T.Z., P. Ceriotti, A.C., G.B., T.O.S., W.U., D.D.S., M.S., R.R., T.P., D.C., and M.M. analyzed data; T.Z., F.D.L., T.P., D.C., and M.M. wrote the paper; and R.C., V.V., E.C., M.S., and R.R. interpreted data.

Reviewers: P.D.C.M., University of Maastricht; and J.W.E., Temple University.

The authors declare no conflict of interest.

[1]T.Z., P. Ceriotti, A.C., and G.B. contributed equally to this work.

[2]T.P., D.C., and M.M. contributed equally to this work.

[3]To whom correspondence may be addressed. Email: tullio.pozzan@unipd.it, daniele.catalucci@cnr.it, or marco.mongillo@unipd.it.

This article contains supporting information online at www.pnas.org/lookup/suppl/doi:10.1073/pnas.1708772114/-/DCSupplemental.

which determine channel conductance. Additional subunits, such as the Ca^{2+}-sensitive interactors Mitochondrial calcium uptake 1 (MICU1) (10–12) and MICU2 (13, 14), regulate, on the other hand, channel gating (ref. 15; for a review, see refs. 16 and 17). While the exact composition of the MCUC in intact cells is still debated, the multiple variants of pore-forming subunits, each with specific impact on the channel properties (e.g., MCUb is an inhibitor of the mitochondrial Ca^{2+} current), indicate that the molecular architecture of the MCUC may influence the capacity of the mitochondrion to take up Ca^{2+} and therefore regulate ATP production. In the heart, mitochondrial Ca^{2+} uptake is fundamental in the acute modulation of cardiac contractility during the fight-or-flight response triggered by β-adrenergic (β-AR) receptor activation. Consistently, deletion of MCU in mice impairs exercise capacity (18), and reduction of functioning MCU channels in sinoatrial node cells or ventricular cardiomyocytes blunts the chronotropic or contractile response, respectively, to β-AR stimulation (19–22). At present, the transcriptional regulation of genes encoding the MCUC subunits is poorly understood, and whether changes in the expression of mitochondrial uniporter proteins take place during cardiac diseases has not been addressed. In intestinal epithelial cells, protein levels of MCU are regulated by the microRNA-25 (miR-25), and alterations in the miR-25/MCU axis are implicated in tumorigenesis (23). This evidence highlights that posttranslational modulation of MCUC protein levels, by microRNAs (miRs), may impact on cell trophism, reflected on the proliferative phenotype in epithelial cells. However, the comprehensive mechanisms underlying the miR role in MCU regulation in the heart remain elusive. MicroRNAs are small, noncoding RNA sequences (18 to 25 nt) capable of finely tuning the expression of a variety of genes, by interfering with either the mRNA stability or translation of target mRNA (24). Among the few thousand different miRs identified so far, the miR-1/miR-133/miR-206 cluster, belonging to the same transcriptional units, have been largely recognized for their central regulatory role in muscle biology and are part of the so-called "myomiRs," for their muscle-specific expression (25). Posttranslational control of protein expression by miRs has been shown to accompany the profound changes of cardiomyocytes during postnatal development and to allow the fully developed myocardium to grow, in response to intrinsic or extrinsic hypertrophic stimuli (26). Here, in light of the housekeeping function of metabolic adaptation during cardiomyocyte remodeling, we sought to determine whether myomiRs, involved in myocardial hypertrophy, could regulate the protein level of MCUC subunits, thus impinging on the molecular architecture and function of the uniporter complex. By combining bioinformatics and cellular biology, we demonstrate that miR-1 selectively represses, at the posttranscriptional level, the pore-forming subunit MCU. In addition, by analyzing murine and human heart samples from a diverse set of physiologic and pathologic

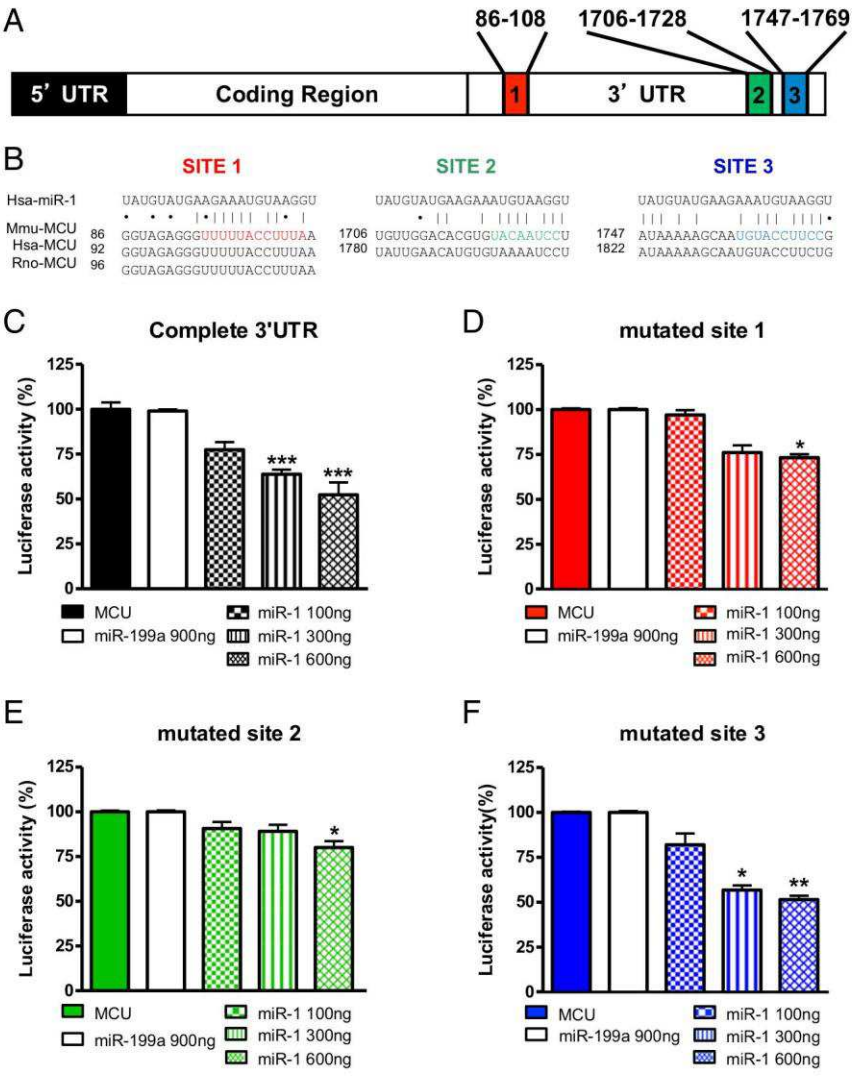

Fig. 1. Bioinformatic prediction and luciferase validation of miR-1 targeting of MCU mRNA. (*A*) Predicted interaction sites between miR-1 and the murine MCU 3′ UTR region, revealing the three seed regions labeled 1 to 3. (*B*) Alignment of the miR-1 sequence with the seed regions in *A*, in mouse (Mmu), human (Hsa), and rat (Rno), showing that the seed region 1 is conserved among all these species. In the alignment, dots represent wobble pairs, and lines represent base pairing. (*C–F*) Assessment of the effects of increasing doses of miR-1 on the bioluminescence of HEK293T cells transfected with a plasmid encoding Luciferase-flanking: (C) full-length MCU 3′ UTR, (*D*) site 1 mutant MCU 3′ UTR, (*E*) site 2 mutant MCU 3′ UTR, (*F*) site 3 mutant MCU 3′ UTR. The noninteracting miR-199a was used as negative control. Luminescence values are normalized to those detected in cells transfected with the Luc construct, but not treated with miR. (*$P < 0.05$; **$P < 0.01$; ***$P < 0.001$; $n = 6$ independent experiments.)

conditions, we show that changes in miR-1 expression, associated with physiological and pathological heart growth, are mirrored by variation in MCU content which presumably modifies the stoichiometry of the MCUC subunits and the overall function of the mitochondrial Ca^{2+} handling machinery.

Results

MCU Is a Predicted Target of the MyomiR miR-1. To determine the potential role of miRs in cardiac MCU regulation, we performed a bioinformatic search using the probability of interaction by target accessibility (PITA) algorithm (27). Among the microRNAs predicted to target the MCU 3′ untranslated region (UTR), we were intrigued by miR-1 and miR-206 as they belong to the family of the so-called myomiRs. MiR-1 is the most abundant miR in the heart, is highly conserved among species (Fig. S1*A*), and has previously been shown to regulate proteins involved in heart development and cardiomyocyte homeostasis (28). MiR-206, on the other hand, is a skeletal muscle-specific microRNA (29) expressed at almost negligible levels in the heart. Interestingly, no targeting sites on the MCU mRNA were predicted for miR-133, which is coexpressed together with miR-1 by the same transcriptional unit (30, 31) (Fig. S1*B*). We thus focused on miR-1, which was found to potentially anneal with MCU mRNA in three putative sites, localized at the beginning [mouse (Mmu), 86 to 108; human (Hsa), 92 to 114 (site 1)] and the end [Mmu, 1,706 to 1,728 and 1,747 to 1,769; Hsa, 1,780 to 1,802 and 1,822 to 1,844 (sites 2 and 3, respectively)] of the 3′ UTR (Fig. 1*A*). Notably, interaction site 1 is predicted also in the rat (Rno) (96 to 118), suggesting strong evolutionary conservation (Fig. 1*B* and Fig. S1*C*). Given that mitochondrial Ca^{2+} uptake depends on the molecular architecture of the uniporter complex, we additionally searched whether miR-1 could potentially target other constituents of the complex. Interestingly, no targeting sites were found for MCUb, MICU2, and EMRE, and just a very weak-scored site resulted for the 3′ UTR of the gatekeeper protein MICU1 (Fig. S1*D*). We thus decided to keep our focus on the potential posttranscriptional regulation of the pore-forming subunit MCU by miR-1, whose mechanism appears evolutionarily conserved from rodents to humans.

MiR-1 Represses MCU Translation and Reduces Mitochondrial Ca^{2+} Uptake in Cardiomyocytes. To validate the in silico prediction, we developed a luciferase assay in which the Luc gene, fused to the MCU 3′ UTR (psiCHECK-3′UTR-MCU), was transfected into HEK293T cells coexpressing miR-1 at increasing copy number. Consistent with the bioinformatic predictions, expression of miR-1 caused a dose-dependent reduction in luciferase activity while no effects were detected in cells transfected with the MCU-unrelated miR-199a, which served as negative control (Fig. 1*C*). To further our molecular insight, we constructed three

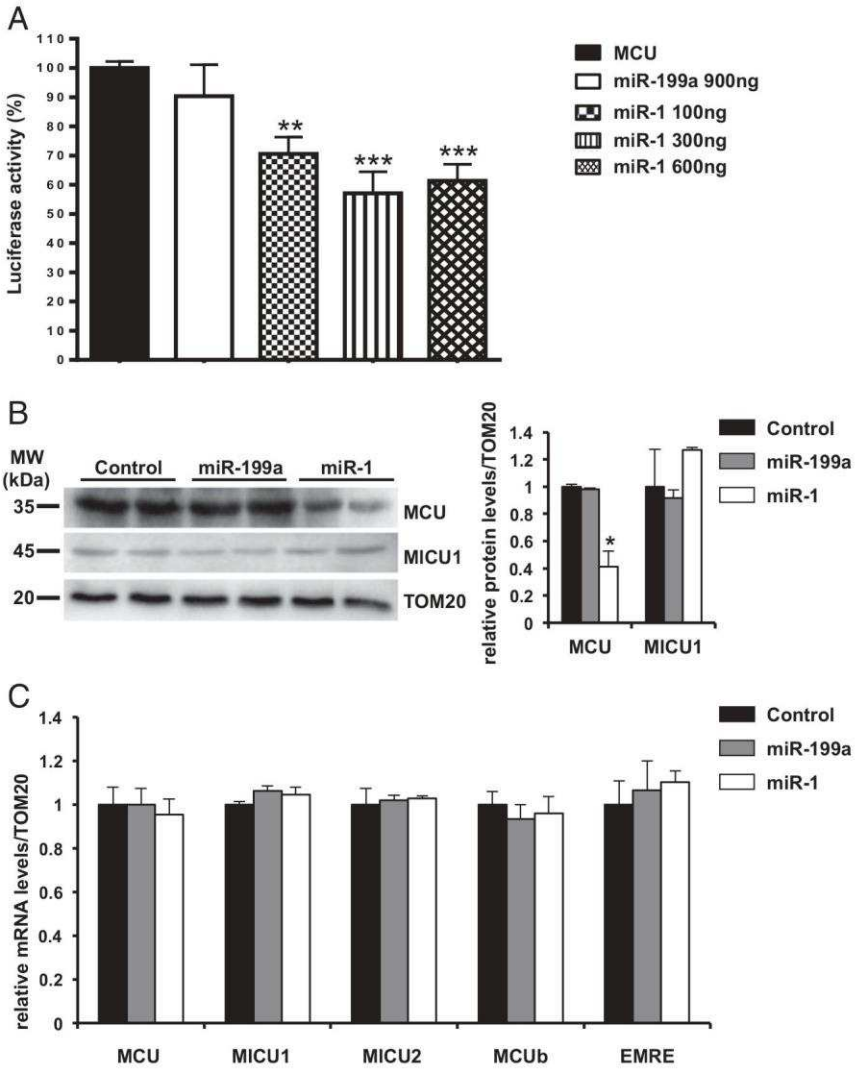

Fig. 2. In vitro regulation of MCU by miR-1 in HL1 cardiomyocytes. (*A*) Assessment of the effects of increasing doses of miR-1 on the bioluminescence of HL1 cardiomyocytes transfected with a plasmid encoding Luciferase-flanking full-length MCU 3′ UTR. The noninteracting miR-199 was used as negative control. Luminescence values are normalized to those detected in cells transfected with the Luc construct, but not treated with miR. (**$P < 0.01$; ***$P < 0.001$; $n = 6$ independent experiments). (*B*) Western blotting on protein extracts from control, miR-199a, and miR-1 overexpressing HL1 cardiomyocytes (*Left*). TOM20 was used as mitochondrial protein loading control. Densitometry (*Right*) shows a significant decrease in MCU protein content in miR-1 overexpressing cells. (*$P < 0.05$; $n = 6$ samples for each study group). (*C*) RTqPCR analysis on extracts from control, miR-199, or miR-1 overexpressing HL1 cardiomyocytes. MCU mRNA levels were not affected by miR-1 expression ($n = 6$ samples for each group.) In *B* and *C*, miR-199a overexpression was performed as control.

mutant vectors (psi-CHECK.3′UTR-MCU-mut), each harboring individual site-specific mutations to selectively ablate the predicted base pairing of miR-1 with its seed sequences in the 3′ UTR-MCU sites. Notably, mutations of either site 1 or site 2 significantly blunted miR-1–dependent repression of luciferase activity (Fig. 1 *D* and *E*) while no effects were obtained when site 3 was mutated (Fig. 1*F*). Collectively, these data demonstrate that miR-1 functionally interacts with the MCU 3′ UTR, by specifically targeting both site 1 and site 2.

Interestingly, miR-1 targeting of MCU was confirmed by luciferase assay in HL-1 cardiomyocytes (Fig. 2*A*). In such cardiac cell lines, overexpression of miR-1 caused a marked reduction in MCU protein content, with no changes in the weakly predicted target MICU1, thus demonstrating that miR-1 is a selective negative regulator of MCU (Fig. 2*B*). In addition, such an effect was not accompanied by changes in mRNA levels (Fig. 2*C*), indicating that miR-1 operates exclusively at the translational level, with no effects on mRNA stability. To functionally probe the effect of miR-1 on mitochondrial Ca^{2+} uptake, we monitored Ca^{2+} dynamics using fluorescence imaging in neonatal rat cardiomyocytes transfected with the cytosolic or mitochondrial sensors CaMeleon D3cpV or 4mt-D3cpV, respectively. In cultured cardiomyocytes, electrical pacing triggered rapid oscillations in cytoplasmic Ca^{2+} (Fig. S2), which caused its entry into the mitochondrial matrix. Consistent with the effects of miR-1 on MCU, its overexpression significantly reduced the amplitude of the steady-state mitochondrial Ca^{2+} level during pacing (controls: $\Delta R/R_0 = 42 \pm 3\%$ vs. miR-1: $\Delta R/R_0 = 27 \pm 3\%$) (Fig. 3 *A*–*C*), with no significant effects on cytoplasmic Ca^{2+} dynamics (32, 33) (Fig. 3 *D* and *E*). Altogether, these data support that, by reducing MCU levels, miR-1 directly affects the maximal capacity of mitochondria to take up Ca^{2+} during contraction. These results broaden the list of functions attributed to miR-1, extending its impact beyond the regulation of the hypertrophic gene program and excitation–contraction coupling, to include metabolism and ATP production, altogether processes deemed to change simultaneously during hypertrophic adaptation of cardiomyocytes. On this basis, we next investigated the possibility that MCU levels may be modulated in hypertrophic conditions previously associated to changes in miR-1, elicited in response to either intrinsic or extrinsic factors, including (*i*) postnatal development, (*ii*) moderate exercise, and (*iii*) pressure overload.

To test these hypotheses, we used molecular biology and biochemistry approaches to compare the miR-1 and MCU levels in a collection of tissue samples from human and experimental hearts before and after the onset of cardiac hypertrophy.

The miR-1/MCU Axis During Postnatal Cardiac Growth. Hypertrophic heart growth occurs throughout postnatal development to maintain cardiac size and performance adequate to the increasing perfusional demand of the body. In parallel to the increase in cell dimensions, postnatal cardiomyocyte growth is underlain by pronounced reshaping of the cellular architecture (34, 35). Such remodeling includes maturation of the sarcoplasmic reticulum (SR) and, remarkably, redistribution of mitochondria into the confines of the high-Ca^{2+} microdomains generated, during contraction, at the interface with the SR (35, 36). Whether the intrinsic properties of the Ca^{2+} uniporter complex adapt to the modified mitochondrial environment, along with cardiomyocyte maturation, has not been investigated. It has been demonstrated (37, 38), and confirmed by us, that miR-1 levels increase during postnatal cardiac growth (Fig. 4*A*). In line with the role of miR-1 on MCU translation, mitochondrial MCU protein density decreased in adult hearts, compared with neonatal hearts [3 mo vs. 7-day-old (P7) mice] (Fig. 4*B*), with no changes in its mRNA level (Fig. 4*C*). Notably, we did not observe significant changes in the transcriptional levels of the other MCUC components, with the exception of MCUb, whose

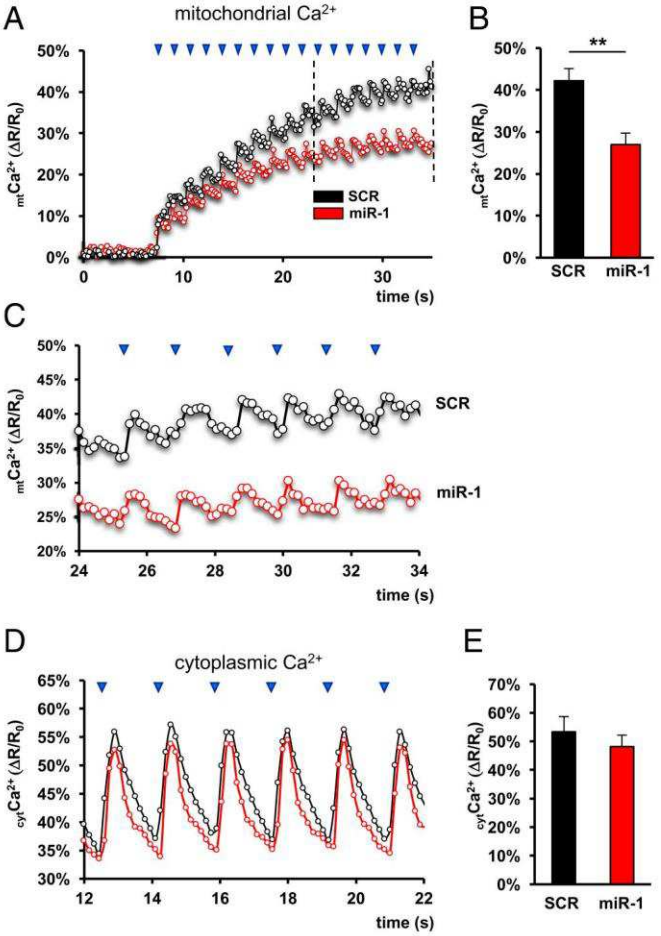

Fig. 3. MiR-1 overexpression reduces mitochondrial Ca^{2+} uptake in cultured neonatal cardiomyocytes. (*A*) Representative traces of mitochondrial Ca^{2+} uptake, measured with 4mt-D3cpV, in control (black trace) and miR-1 overexpressing (red trace) neonatal cardiomyocytes, electrically paced with field stimulation, at rates highlighted by the arrowheads. (*B*) Amplitude of the average mitochondrial Ca^{2+} level at steady state, in control [scramble (SCR)] and miR-1 overexpressing cardiomyocytes (**$P < 0.01$, n = 40 cardiomyocytes per group). (*C*) Magnification of the traces in *A*, showing mitochondrial Ca^{2+} uptake at steady-state level. (*D*) Representative traces of cytosolic Ca^{2+} transients, measured with D3CPV, in control (black trace) and miR-1 overexpressing (red trace) neonatal cardiomyocytes, electrically paced with field stimulation. Statistics of the amplitude (*E*) of Ca^{2+} oscillations in miR-1 overexpressing and control cells (n = 40 cardiomyocytes per group.)

expression significantly increased during postnatal development (Fig. 4*C*). Remarkably, the reciprocal changes in miR-1 and MCU protein levels were similar during postnatal cardiac development in humans, as shown by the comparison of miR-1 and MCU levels in ventricular biopsies from neonatal and adult human hearts (Fig. 4 *D* and *E*). Additionally, no changes in the expression of other human genes encoding the members of the uniporter complex, including MCUb, were detected (Fig. 4*F*). Taken together, these data demonstrate that changes in the molecular composition of the mitochondrial Ca^{2+} uptake complex, likely driven by the miR-1/MCU axis, take part in the plethora of structural and functional modifications of postnatal cardiomyocyte maturation.

The miR-1/MCU Axis in Physiologic and Pathologic Cardiac Hypertrophy. Being an example of postmitotic tissue, the adult myocardium is incapable of repairing tissue damage through cell division (39–41). Nevertheless, abundant clinical and preclinical evidence has

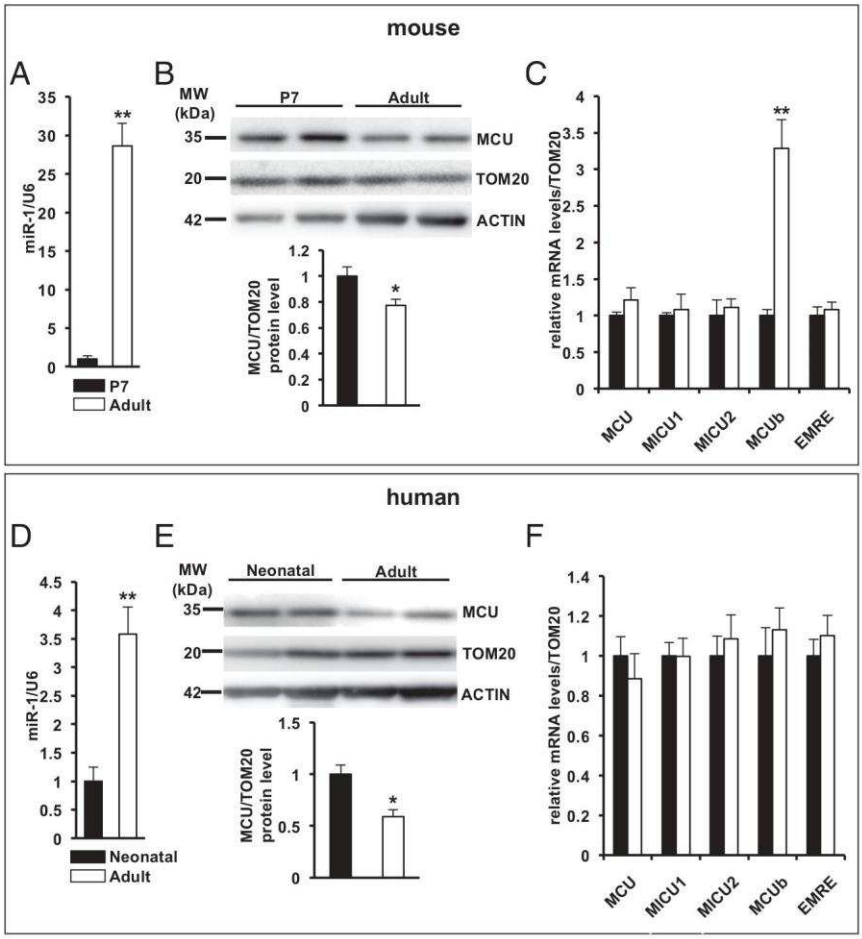

Fig. 4. Changes in mitochondrial MCU density during postnatal growth in mouse and human hearts. (*A*) MiR-1 expression was compared, by RTqPCR analysis, on extracts from neonatal (P7) vs. adult (3 mo) mouse hearts ($n = 6$ mouse samples for each study group; $^{**}P < 0.01$). (*B*, *Upper*) Western blotting on protein extracts from P7 and adult mouse hearts and (*Lower*) relative densitometry showing a significant decrease in MCU protein content during postnatal heart development ($n = 6$ hearts for each study group; $^{*}P < 0.05$). (*C*) RTqPCR analysis of the molecular components of the MCUC in extracts from P7 and adult mouse hearts ($n = 6$ hearts for each group; $^{**}P < 0.01$. (*D*) RTqPCR analysis of miR-1 expression in extracts from neonatal vs. adult human heart samples ($n = 4$ neonatal and five adult human heart samples; $^{**}P < 0.01$). (*E*, *Upper*) Western blotting and (*Lower*) relative densitometry and (*F*) RTqPCR on extracts from human heart samples showing mitochondrial MCU density and the expression levels of the molecular components of the uniporter complex in neonatal vs. adult subjects ($n = 6$ neonatal and four adult heart samples; $^{*}P < 0.05$). In both *B* and *E*, immunoreactivity for TOM20 was used as mitochondrial protein loading control while that for actin was used as a whole-cell protein loading control.

demonstrated that, on the contrary, the heart is indeed highly dynamic and that fully developed cardiomyocytes can grow further in response to stresses, such as increased mechanical workload. Differences in the nature, intensity, and duration of the hypertrophying stimuli determine whether cardiac remodeling would progress toward either the so-called "physiologic" (i.e., in the athletic heart) or "pathologic" (i.e., in pressure overload) hypertrophy, the latter resulting, with time, in cardiac dysfunction, heart failure, and death. Although the cellular and clinical phenotypes of the two conditions are very different, the common tenet is that, in the initial phases, they share the same adaptive mechanisms, including increased sarcomeric deposition and enhanced/preserved contractility, both of which require increased ATP supply (42). It follows that the regulation of mitochondrial function is a critical process for ATP production to match energetic demand during cell growth. With the notion that miR-1 is a repressor of the hypertrophic gene program (26, 37), and based on our data showing the effect of miR-1 on the MCU levels, we analyzed in murine and human hearts whether distinctive changes in the uniporter architecture may depend on physiologic vs. pathologic stimuli. To this end, two groups of mice were subjected to chronic running exercise and aortic coarctation, respectively.

The exercise protocol consisted of repeated running bouts of 1 h/d for eight consecutive weeks (43), which caused an elevation in the maximal oxygen consumption (VO_{2max}), consistent with an increase in contractile performance, and accompanied, as expected, by a slight elevation in cardiac mass (heart weight/body weight),(exercise, $5.5 \pm 0.3 \times 10^{-3}$ vs. sedentary, $4.6 \pm 0.2 \times 10^{-3}$) and cardiomyocyte cross-sectional area (cardiomyocyte areas) (exercise, $231 \pm 6\ \mu m^2$ vs. sedentary, $201 \pm 5\ \mu m^2$) (Fig. 5 *A–D*). Exercised heart did not display changes in myocardial histology or reactivation of the fetal gene program (Fig. 5*E* and Fig. S3*A*). In striking difference with the skeletal muscle, exercise-dependent mitochondrial biogenesis was negligible in the heart. As previously demonstrated, miR-1 expression decreased in extracts from exercised hearts (Fig. 5*F*), and, in agreement with our findings (above), MCU protein levels increased (Fig. 5*G*). No changes in the transcriptional level of the other members of the MCUC were observed (Fig. 5*H*).

We thus analyzed the uniporter complex biochemistry in hearts harvested 1 wk after the induction of ventricular pressure overload following transaortic constriction (TAC) surgery. This condition corresponds to the initial, compensatory response to a hypertrophying stimulus and, in fact, elicits a modest cardiomyocyte growth with no contractile failure, and only limited signs of tissue damage (focal fibrosis) (Fig. 6 *A–E*). Contrary to exercise hypertrophy, TAC hearts showed a significant increase in the expression levels of stress markers (Fig. S3*B*). The changes in miR-1 and MCU were similar to those observed in hearts from exercised mice, with decreased miR-1 (Fig. 6*F*) and, accordingly, increased MCU content (Fig. 6*G*). These results suggest that, regardless of the nature of the hypertrophic stimulus (physiologic or pathologic), the initial cardiomyocyte adaptation to increased heart work is characterized by similar enhancement in the availability of uniporter-forming MCU molecules. Interestingly, while the transcriptional level of the MCU-related partners did not vary after exercise, in TAC hearts, mRNA of the pore-inhibiting subunit MCUb was doubled compared with sham operated mice (Fig. 6*H*). To determine whether the reciprocal miR-1 and MCU modulation occurred in a clinically relevant model

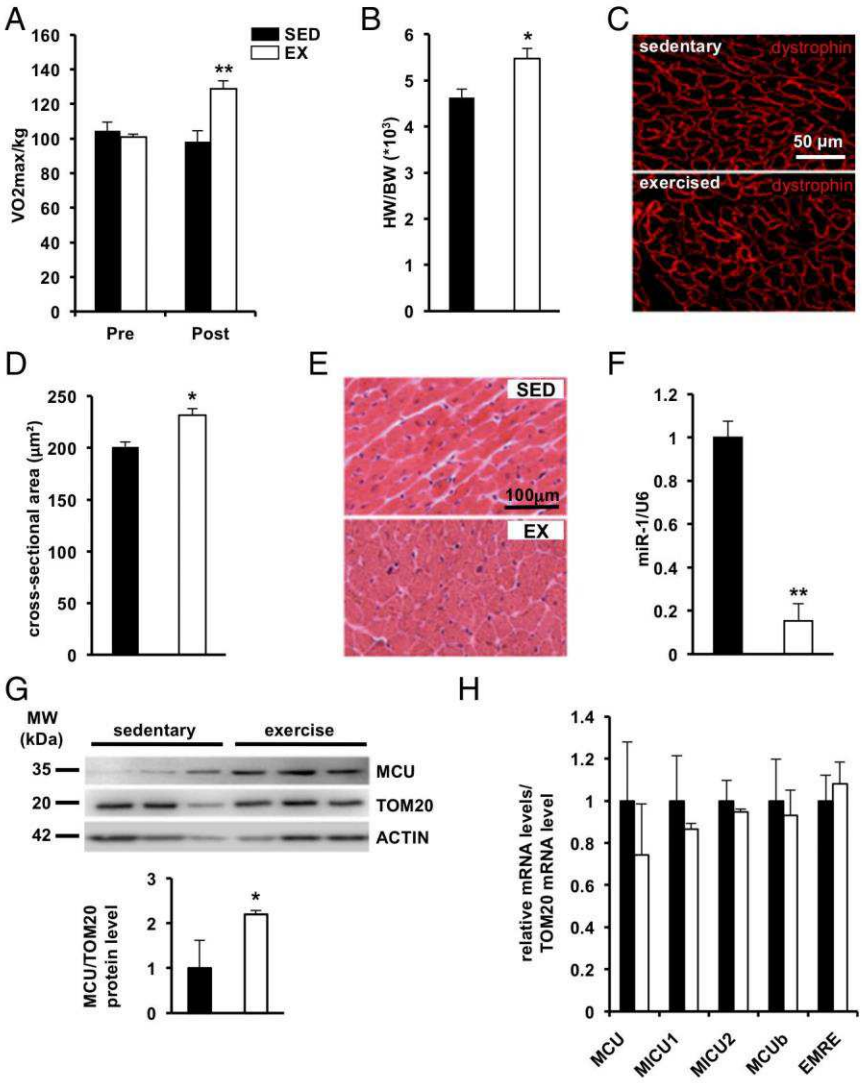

Fig. 5. Mitochondrial MCU protein density increases in exercise-induced cardiac hypertrophy. (*A*) Maximal oxygen uptake (VO_{2max}) from the sedentary (SED) and exercised (EX) mouse cohort before (pre) and after (post) the 8-wk high intensity exercise training protocol ($n = 6$ mice for each study group; $^{**}P < 0.01$). (*B*) Evaluation of heart weight to body weight ratio (HW/BW) in sedentary and 8-wk-exercised mice ($n = 6$ mice for each group; $^{*}P < 0.05$). (*C*) Confocal immunofluorescence analysis of heart sections from sedentary and exercised mice, stained with an antibody to dystrophin. Images are details from the left ventricle. (*D*) Evaluation of left ventricular cardiomyocyte cross-sectional areas in sedentary vs. exercised mouse hearts ($n = 500$ cardiomyocytes for each group; $^{*}P < 0.05$). (*E*) Hematoxylin/eosin staining of heart sections from sedentary and exercised mice. Images are details from the left ventricle, showing the integrity of the myocardium. (*F*) MiR-1 expression was compared, by RTqPCR analysis, on left ventricular heart extracts from sedentary vs. exercised mice ($n = 6$ hearts for each study group; $^{**}P < 0.01$). (*G*, *Upper*) Western blotting on heart extracts from sedentary and exercised mice, and (*Lower*) relative densitometry showing a significant increase in mitochondrial MCU protein content ($n = 6$ hearts for each study group; $^{*}P < 0.05$). Immunoreactivity for TOM20 was used as mitochondrial protein loading control while that for actin was used as a whole-cell protein loading control. (*H*) RTqPCR on extracts from sedentary vs. exercised hearts showing the expression levels of the members of the uniporter complex ($n = 6$ hearts for each study group.)

of cardiac hypertrophy, we analyzed human heart biopsies obtained from healthy subjects and patients (age, 59 ± 13 y) with myocardial hypertrophy due to aortic stenosis. This latter patient cohort had conserved ejection fraction (EF) (>55%), and the expression of the fetal gene program only trended to be elevated (Fig. S4). Similar to the data obtained in the animal model, miR-1 level was generally decreased (Fig. 7*A*), and, consistently, MCU content was augmented (Fig. 7*B*). Congruous with the results obtained in postnatal development of human hearts, no changes in the expression level of the other MCUC genes were detected (Fig. 7*C*).

The β-Adrenergic Receptor System Participates to Control the miR-1/MCU Axis. Taken altogether, the results presented above demonstrate that reciprocal fluctuations of the miR-1 and MCU levels occur during physiologic (i.e., postnatal and exercise) and pathologic (i.e., pressure overload) cardiac hypertrophy, in both experimental models and human hearts. Given that similar changes in the miR1/MCU axis occur, in the fully developed heart, upon exercise and in the initial phases of pathologic hypertrophy (Fig. 8*A*), we made the hypothesis that a common regulatory mechanism may exist. We thus focused on the cardiac β-AR system, which is the primary physiologic mechanism engaged in response to increased heart load, a condition in common between exercise and TAC-induced pressure overload. Activation of β-AR signaling leads to enhancement of cytosolic Ca^{2+} oscillations and mitochondrial Ca^{2+} uptake (44–46) and is involved in the parallel activation of pathways controlling cell growth, such as the Akt-FOXO cascade (47). Interestingly, miR-1 expression has been shown to depend on FOXO3a (48), suggesting that, in conditions of chronic β-AR activation, the blockade of FOXO3a nuclear translocation may inhibit miR-1 increase and, consequently, its repression of MCU translation. On these bases, we treated mice who had undergone TAC, a condition associated with increased cardiac sympathetic neuron activity, with the β1-blocker metoprolol. The efficacy of the treatment was confirmed by the inhibition of the TAC-induced reactivation of fetal genes (Fig. S5). Interestingly, metoprolol treatment was not accompanied by miR-1 repression (Fig. 8*B*), and, accordingly, this prevented the increase in MCU protein content, which occurred in vehicle-treated TAC mice (Fig. 8*C*). In addition, metoprolol treatment blunted the induction of MCUb transcription, presumably through an miR-1–independent mechanism, as the MCUb transcript is not targeted by miR-1 (Fig. 8*D*).

Discussion

Matching energy production and cellular metabolic request is essential in cardiomyocytes, which are high energy-consuming cells, subjected to variable ATP consumption rates mainly depending on

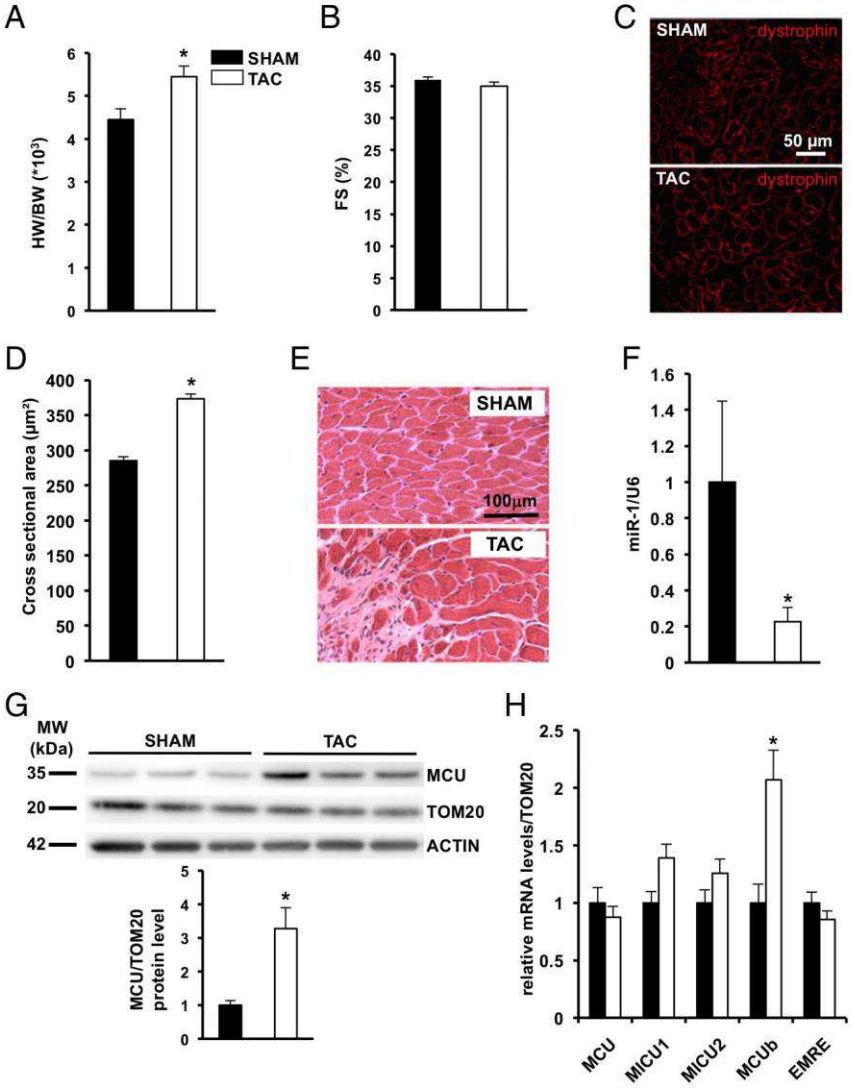

Fig. 6. Mitochondrial MCU protein density increases during pressure overload-induced cardiac hypertrophy in mouse hearts. (*A*) HW/BW and (*B*) fractional shortening (FS) in 1-wk sham-operated and TAC mice ($n = 6$ mice for each group; $^*P < 0.05$). (*C*) Confocal immunofluorescence analysis on heart sections from 1-wk sham-operated and TAC mice, stained with an antibody to dystrophin. Images are details from the left ventricle. (*D*) Evaluation of left ventricular cardiomyocyte cross-sectional areas in sham-operated vs. TAC mouse hearts ($n = 500$ cardiomyocytes for each group; $^*P < 0.05$). (*E*) Hematoxylin/eosin staining of heart sections from sham-operated and TAC mice. Images are details from the left ventricle. (*F*) MiR-1 expression level was compared, by RTqPCR analysis, on heart extracts from sham-operated vs. TAC mice ($n = 6$ hearts for each study group; $^*P < 0.05$). (*G*, *Upper*) Western blotting on heart extracts from sham-operated and TAC mice and (*Lower*) relative densitometry showing a significant increase in mitochondrial MCU protein content, in TAC hearts ($n = 6$ hearts for each study group; $^*P < 0.05$). Immunoreactivity for TOM20 was used as mitochondrial protein loading control while that for actin was used as a whole-cell protein loading control. (*H*) RTqPCR on extracts from sham vs. TAC hearts showing the expression levels of the members of the uniporter complex. The graph displays a significant increase in expression level of MCUb ($n = 6$ hearts for each study group, $^*P < 0.05$.)

cardiac contractile load. Intracellular Ca^{2+} is a central mediator of contraction/metabolism coupling as, during the same heart cycle, it modulates contraction on one hand and enters mitochondria-stimulating ATP production on the other. The identification of the molecular components underlying the well-characterized capacity of mitochondria to take up Ca^{2+} has started only recently with the discovery of the pore-forming subunit MCU (6, 7), followed by rapid progress leading to the picture of a multimolecular mitochondrial uniporter complex, including a multimeric pore subunit (MCU, MCUb, EMRE) and a number of associated regulatory proteins (MICU1, MICU2, MCUR1) (8–14).

Given that the heart is continuously subjected to acute and chronic inputs, resulting, respectively, in enhancement of contractility or stimulation of cell growth, both of which are associated with increased energy demand, one would expect modulation of the mitochondrial Ca^{2+} uptake machinery to be a central need for adequate metabolic adaptation. However, the studies focusing on cardiac MCUC (and, in particular, MCU) failed to produce a consensus view on its role in heart physiology and pathology. As a result, the current knowledge on the mechanisms of regulation of the individual MCUC components in heart cells remains elusive, and signaling pathways specifically controlling MCU expression at the transcriptional or posttranscriptional levels have scarcely been investigated.

Here, we focused on microRNAs, which have been shown to operate parallel control on the expression level of a number of proteins and to associate with structural and functional cardiomyocyte remodeling. Interestingly, in the highly proliferative epithelial cells, MCU is targeted by miR-25, and such regulation is involved in cell division and tumor development. MiR-25 is also expressed in the heart (49, 50), but we did not observe significant changes in its expression levels, in the experimental models analyzed, suggesting that, in the cardiac context, the dynamic modulation of MCU is not triggered by miR-25. This evidence prompted us to investigate whether regulation of MCU, in cardiomyocytes, could be operated by myomiRs and be involved in cell growth, which occurs through hypertrophy, congruously with the cell type. The first finding of our study shows that, in the heart, miR-1 selectively targets MCU and negatively regulates its expression, through interference with protein translation. MiR-1 is a well-characterized cardiac miR whose expression is tightly controlled since early stages of cardiogenesis by transcriptional activators, such as SRF, MyoD, and MEF2 (25, 29, 51, 52). In the adult heart, the expression of this myomiR is causally associated with the dynamicity of cardiac function and signaling pathways, such as the insulin-like growth factor-1/Akt axis, which modulates miR-1 transcription via Foxo3a (48). MiR-1 repression has been demonstrated to ignite cardiomyocyte hypertrophy by modulating the levels of several targets, including

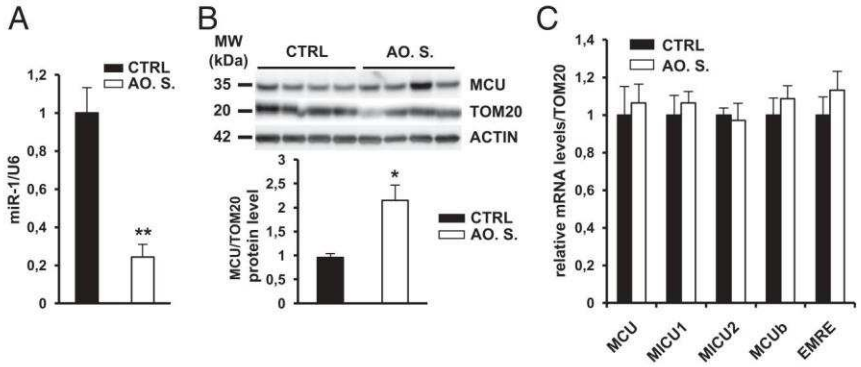

Fig. 7. Mitochondrial MCU protein density increases during pressure overload-induced cardiac hypertrophy in human hearts. (*A*) MiR-1 level assessed by RTqPCR in heart samples from healthy subjects (CTRL) and patients affected by aortic stenosis (Ao.S.) ($n = 5$ control and 6 Ao.S. hearts; $^{**}P < 0.01$). (*B*) Western blotting on extracts from human heart samples from healthy subjects (CTRL) and patients affected by aortic stenosis (Ao.S.), and relative densitometry showing a significant increase in mitochondrial MCU protein content, in hypertrophic hearts ($n = 5$ CTRL and 6 Ao.S. hearts; $^{*}P < 0.05$). Immunoreactivity for TOM20 was used as mitochondrial protein loading control, while that for actin was used as a whole-cell protein loading control. (*C*) RTqPCR on extracts from control and Ao.S. hearts showing the expression levels of the members of the uniporter complex ($n = 4$ heart samples for each study group.)

structural proteins, transcription factors, ion channels, and pumps, but not any member of the Ca^{2+} uniporter complex or other regulators of ATP production.

The effect of miR-1 expression on mitochondrial Ca^{2+} dynamics, driven by the changes in MCU levels, were characterized in vitro with live cell imaging, and, consistent with previous data, our results show that, during cardiomyocyte pacing, mitochondrial Ca^{2+} reaches a stable level, which parallels the pacing rate, with regular systolic fluctuations. Consistent with the biophysical modeling of mitochondrial Ca^{2+} uptake, by reducing the MCU copy number, miR-1 would decrease the capacity of Ca^{2+} transport, lowering the equilibrium level between mitochondrial Ca^{2+} entry and release. Our data show that miR-1–dependent regulation is highly specific as it only targets the pore-forming subunit (MCU) among the MCUC members. While this does not exclude that expression of the other complex members is regulated by parallel mechanisms, possibly including other miRs, the target selectivity of miR-1 for MCU may impact on the uniporter complex architecture (i.e., altered stoichiometry between MCU and the channel inhibitor MCUb).

Given the molecular and cellular evidence of miR-1 targeting MCU, we explored the state of the miR-1/MCU axis in three different conditions associated with cardiomyocyte hypertrophy and increased energy requirements, in which changes in miR-1 have previously been observed, including postnatal development, chronic exercise, and the early phases of pressure overload. In all such conditions, MCU levels mirrored miR-1 variations, suggesting that the miR-1/MCU axis of regulation identified with the in vitro analyses is operational in the intact mouse heart.

Although both postnatal and exercise-induced cell growth fall into the broad definition of physiologic hypertrophy, the two processes are very distinct as they occur in cardiomyocytes at different maturation stage (immature vs. fully differentiated cells), and they are driven by specific sets of upstream stimuli. Remarkably, miR-1 expression and, consequently, MCU content change in the opposite direction when postnatal heart growth is compared with exercise hypertrophy of the adult heart.

During postnatal maturation, cardiomyocyte mitochondria, which are distributed throughout the cytoplasm in immature cells, redistribute along well-aligned sarcomeres and come into regular contact with Ca^{2+}-release sites of the SR (53). The tethering of mitochondria close to the SR exposes them to a microdomain of a pronounced cytoplasm/matrix Ca^{2+} concentration gradient (54, 55). This may on the one hand facilitate Ca^{2+} uptake but, on the other, puts the cell at risk for mitochondrial Ca^{2+} overload. Remarkably, during the first weeks of cellular maturation, miR-1 up-regulation, by lowering MCU content, may be regarded as a protective mechanism against mitochondrial Ca^{2+} overload, further amplified by the increase in the inhibitory MCUb transcription.

In exercise-dependent cell growth, as well as in the initial compensated phase of pressure overload-dependent hypertrophy, the increase in mitochondrial MCU density is a likely mechanism to elevate the average Ca^{2+} in the matrix and, subsequently, ATP production, which is likely required to sustain cell growth. It might be surprising to observe similar behavior of the miR-1/MCU axis in these two very different conditions (athletic vs. pressure-overloaded heart), and this prompted the hypothesis that a common denominator may act as upstream regulator of the miR-1/MCU signaling pathway. In support of this, miR-1 expression has been suggested to depend on the β-AR/Akt/FOXO pathway (48, 56). Consistently, our data show that, in the murine TAC model, pharmacologic interference with β-AR blunted the increase in MCU content. Given the complex and not entirely uncovered role of β-ARs in pathologic hypertrophy, further studies will be required to understand how β-AR signaling may affect MCUC components and whether miR-1–dependent modulation of MCU has a role in the progression of hypertrophy from the compensated (adaptive) to the decompensated (maladaptive) phase.

Remarkably, the reciprocal changes in miR-1 and MCU levels, observed in the experimental models, were replicated when analyzing healthy neonatal vs. adult biopsies, as well as normal vs. hypertrophic human biopsies. One notable difference is that while, in the mouse, an miR-1–dependent increase in MCU protein levels was accompanied by increased transcription of the inhibitory subunit MCUb, such regulation was not detected in human hearts. Interestingly, Luongo et al. (57) detected increased expression of NCLX (the main mitochondrial Ca^{2+} extrusion route) and MICU1, a negative regulator of MCU activity, in failing human heart samples. A conjectural comparison between these data may be that, during myocardial hypertrophy, transcriptional control of MCUC components participates in tuning mitochondrial Ca^{2+} exchange and preventing overload and occurs with species-specific mechanisms, which may relate to the distinct kinetics of mitochondrial Ca^{2+} exchange, depending on different duration and repetition rates of Ca^{2+} oscillations in human vs. murine hearts.

Altogether, our data support that modulation of MCU takes place during physiologic and pathologic remodeling in human hearts and, in combination with the evidence accrued by molecular and cellular analyses in vitro, suggest that posttranscriptional

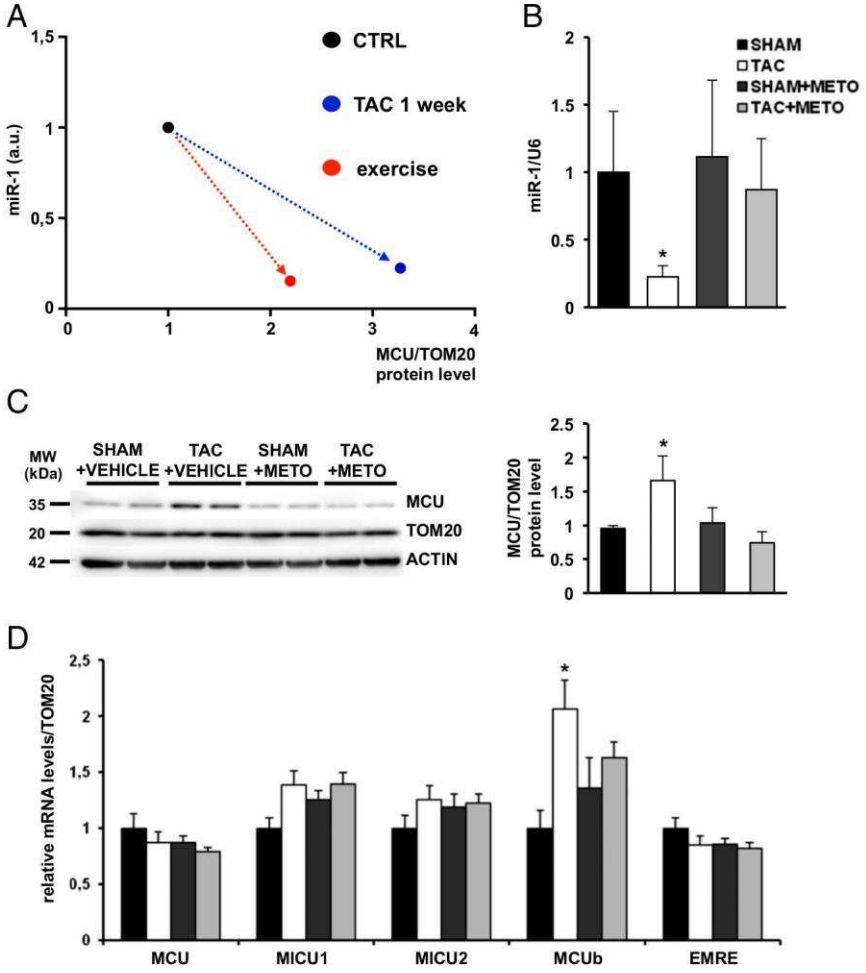

Fig. 8. The β1-AR blocker metoprolol (METO) counteracts changes in the miR-1/MCU axis during pathologic cardiac hypertrophy. (*A*) Representative graph summarizing the variations of the miR1/MCU axis in exercise and pressure-overload heart hypertrophy, in experimental models. (*B*) RTqPCR analysis on heart extracts from sham-operated vs. TAC mice, either treated with the β1-receptor blocker metoprolol or with a vehicle control, to determine the expression level of miR-1 ($n = 6$ hearts for each study group; $^*P < 0.05$). (*C*, *Left*) Western blotting on heart extracts from 1-wk sham-operated and TAC mice treated with metoprolol or vehicle and (*Right*) relative densitometry showing that metoprolol blunted TAC-dependent mitochondrial MCU increase ($n = 6$ hearts for each study group; $^*P < 0.05$). Immunoreactivity for TOM20 was used as a mitochondrial protein loading control while that for actin was used as a whole-cell protein loading control. (*D*) RTqPCR on extracts from sham-operated and TAC hearts, in both the metoprolol-treated or vehicle-treated groups, assessing the expression levels of the members of the uniporter complex. Note that metoprolol treatment blunted TAC-dependent MCUb transcriptional induction ($n = 6$ hearts for each group; $^*P < 0.05$.)

mechanisms mediated by miR-1 may play a role. Given that miRs are well-suited therapeutic targets, as they can easily be mimicked or antagonized pharmacologically (miR mimics or antagomiRs, respectively), even with target selectivity, our identification of the miR-1/MCU axis and its involvement in myocardial hypertrophy may lay the groundwork for refined therapeutic approaches.

Methods

Patients Selection and Use of Human Samples. Patients with aortic stenosis who underwent aortic valve replacement were recruited retrospectively from the biobank of the University Hospital of Verona, Division of Cardiac Surgery, Verona, Italy. Approval for studies on human tissue samples was obtained from the Ethical Committee of the University Hospital of Verona. Each patient gave written informed consent. Septal specimens were collected from five healthy donor hearts rejected for transplantation and included as controls [experimental protocols approved by the ethical committee of Careggi University-Hospital (2006/0024713; renewed May 2009)]. Neonatal heart biopsies were obtained as routine procedure during cardiac surgery for correction of nonhypertrophying congenital cardiomyopathies in patients from 4 to 48 mo. This procedure was communicated to the Nucleo di Valutazione della Ricerca Clinica, Az. Ospedaliera di Padova, for approval. All samples were anonymous to the investigators, and no details on the anagraphical and clinical data were available to the researchers. Samples were used in accordance with the directives of the National Committee of Bioethics and the Recommendation R(06)I on Research on Biological Materials of Human Origin of the European Commission (15/03/2006).

Animal Models. Here, we used neonatal and adult CD1 and C57BL/6J mice (all from Charles River) and neonatal Sprague–Dawley rats. All experimental procedures were performed according to institutional guidelines in compliance with national (4D.L. N.116, G.U., suppl. 40, 18-2-1992) and international law and policies [EEC Council-Directive 86/609, OJ L 358,1,12-12-1987; NIH *Guide for the Care and Use of Laboratory Animals* (58), US National Research Council-1996 and new directive 2010/63/EU].

Target Prediction. The murine MCU 3′ UTR was uploaded into the public PITA database (https://genie.weizmann.ac.il/pubs/mir07/mir07_data.html) and scanned for microRNA binding sites.

Luciferase Assay. The murine MCU 3′ UTR was cloned into the psiCHECK-TM2 vector (Promega) using the In-fusion HD Cloning Plus kit (Clontech). Details are given in *SI Methods*.

Western Blotting. This analysis was performed on extracts from the dissected left ventricle, as detailed in ref. 59. Antibodies used for Western blotting (WB) analysis are listed in Table S1.

Real-Time qPCR. Real-time qPCR (RTqPCR) analysis was performed on extracts from the dissected left ventricle, as previously described in ref. 59. The primers used in this study are summarized in Table S2.

Statistical Analysis. All data are expressed as the mean ± SEM. Comparison between experimental groups was made by using an unpaired ANOVA test, and comparison between multiple groups was performed using the Kruskal–Wallis test. $P < 0.05$ was considered statistically significant.

The remainder of the experimental methods are described in detail in *SI Methods*.

ACKNOWLEDGMENTS. We thank Prof. Paolo Bernardi for critical discussion, Dr. Nicola Pianca for technical assistance, Dr. Maddalena Tessari for the clinical information related to AoS patients, Dr. Anna Chiara Frigo for advice on statistical analysis, and Ms. Margherita Zorzut for support. This work was supported by the following grants: European Community Seventh Framework

Program FP7/2007-2013 under Grant Agreement HEALTH-F2-2009-241526, EUTrigTreat, and Telethon-Italy (GGP11224) (to M.M.); the Italian Ministry of University and Research Fondo per gli Investimenti della Ricerca di Base (FIRB)–Futuro in Ricerca (RBFR12I3KA) (to D.C.); Fondazione Cariparo "Mitochondrial Ca2+ uptake and cardiac pathophysiology" (to F.D.L.); and the European Union (European Research Council mitoCalcium, 294777) (to R.R.).

1. Sedmera D, Thompson RP (2011) Myocyte proliferation in the developing heart. *Dev Dyn* 240:1322–1334.
2. Badeer HS (1964) The stimulus to hypertrophy of the myocardium. *Circulation* 30: 128–136.
3. Shimizu I, Minamino T (2016) Physiological and pathological cardiac hypertrophy. *J Mol Cell Cardiol* 97:245–262.
4. Williams GS, Boyman L, Lederer WJ (2015) Mitochondrial calcium and the regulation of metabolism in the heart. *J Mol Cell Cardiol* 78:35–45.
5. Territo PR, Mootha VK, French SA, Balaban RS (2000) Ca(2+) activation of heart mitochondrial oxidative phosphorylation: Role of the F(0)/F(1)-ATPase. *Am J Physiol Cell Physiol* 278:C423–C435.
6. De Stefani D, Raffaello A, Teardo E, Szabò I, Rizzuto R (2011) A forty-kilodalton protein of the inner membrane is the mitochondrial calcium uniporter. *Nature* 476: 336–340.
7. Baughman JM, et al. (2011) Integrative genomics identifies MCU as an essential component of the mitochondrial calcium uniporter. *Nature* 476:341–345.
8. Raffaello A, et al. (2013) The mitochondrial calcium uniporter is a multimer that can include a dominant-negative pore-forming subunit. *EMBO J* 32:2362–2376.
9. Sancak Y, et al. (2013) EMRE is an essential component of the mitochondrial calcium uniporter complex. *Science* 342:1379–1382.
10. Csordás G, et al. (2013) MICU1 controls both the threshold and cooperative activation of the mitochondrial Ca^{2+} uniporter. *Cell Metab* 17:976–987.
11. Perocchi F, et al. (2010) MICU1 encodes a mitochondrial EF hand protein required for Ca(2+) uptake. *Nature* 467:291–296.
12. Mallilankaraman K, et al. (2012) MICU1 is an essential gatekeeper for MCU-mediated mitochondrial Ca(2+) uptake that regulates cell survival. *Cell* 151:630–644.
13. Patron M, et al. (2014) MICU1 and MICU2 finely tune the mitochondrial Ca2+ uniporter by exerting opposite effects on MCU activity. *Mol Cell* 53:726–737.
14. Plovanich M, et al. (2013) MICU2, a paralog of MICU1, resides within the mitochondrial uniporter complex to regulate calcium handling. *PLoS One* 8:e55785.
15. De Stefani D, Patron M, Rizzuto R (2015) Structure and function of the mitochondrial calcium uniporter complex. *Biochim Biophys Acta* 1853:2006–2011.
16. De Stefani D, Rizzuto R, Pozzan T (2016) Enjoy the trip: Calcium in mitochondria back and forth. *Annu Rev Biochem* 85:161–192.
17. Pendin D, Greotti E, Pozzan T (2014) The elusive importance of being a mitochondrial Ca(2+) uniporter. *Cell Calcium* 55:139–145.
18. Pan X, et al. (2013) The physiological role of mitochondrial calcium revealed by mice lacking the mitochondrial calcium uniporter. *Nat Cell Biol* 15:1464–1472.
19. Rasmussen TP, et al. (2015) Inhibition of MCU forces extramitochondrial adaptations governing physiological and pathological stress responses in heart. *Proc Natl Acad Sci USA* 112:9129–9134.
20. Kwong JQ, et al. (2015) The mitochondrial calcium uniporter selectively matches metabolic output to acute contractile stress in the heart. *Cell Rep* 12:15–22.
21. Luongo TS, et al. (2015) The mitochondrial calcium uniporter matches energetic supply with cardiac workload during stress and modulates permeability transition. *Cell Rep* 12:23–34.
22. Wu Y, et al. (2015) The mitochondrial uniporter controls fight or flight heart rate increases. *Nat Commun* 6:6081.
23. Marchi S, et al. (2013) Downregulation of the mitochondrial calcium uniporter by cancer-related miR-25. *Curr Biol* 23:58–63.
24. Small EM, Olson EN (2011) Pervasive roles of microRNAs in cardiovascular biology. *Nature* 469:336–342.
25. Mitchelson KR, Qin WY (2015) Roles of the canonical myomiRs miR-1, -133 and -206 in cell development and disease. *World J Biol Chem* 6:162–208.
26. Sayed D, Hong C, Chen IY, Lypowy J, Abdellatif M (2007) MicroRNAs play an essential role in the development of cardiac hypertrophy. *Circ Res* 100:416–424.
27. Kertesz M, Iovino N, Unnerstall U, Gaul U, Segal E (2007) The role of site accessibility in microRNA target recognition. *Nat Genet* 39:1278–1284.
28. Latronico MVG, Catalucci D, Condorelli G (2007) Emerging role of microRNAs in cardiovascular biology. *Circ Res* 101:1225–1236.
29. Zhao Y, Samal E, Srivastava D (2005) Serum response factor regulates a muscle-specific microRNA that targets Hand2 during cardiogenesis. *Nature* 436:214–220.
30. Callis TE, et al. (2009) MicroRNA-208a is a regulator of cardiac hypertrophy and conduction in mice. *J Clin Invest* 119:2772–2786.
31. Callis TE, Wang DZ (2008) Taking microRNAs to heart. *Trends Mol Med* 14:254–260.
32. Terentyev D, et al. (2009) miR-1 overexpression enhances Ca(2+) release and promotes cardiac arrhythmogenesis by targeting PP2A regulatory subunit B56alpha and causing CaMKII-dependent hyperphosphorylation of RyR2. *Circ Res* 104:514–521.
33. Tritsch E, et al. (2013) An SRF/miR-1 axis regulates NCX1 and annexin A5 protein levels in the normal and failing heart. *Cardiovasc Res* 98:372–380.
34. Lyons GE, Schiaffino S, Sassoon D, Barton P, Buckingham M (1990) Developmental regulation of myosin gene expression in mouse cardiac muscle. *J Cell Biol* 111: 2427–2436.
35. Anmann T, et al. (2014) Formation of highly organized intracellular structure and energy metabolism in cardiac muscle cells during postnatal development of rat heart. *Biochim Biophys Acta* 1837:1350–1361.
36. Piquereau J, et al. (2010) Postnatal development of mouse heart: Formation of energetic microdomains. *J Physiol* 588:2443–2454.
37. Ikeda S, et al. (2009) MicroRNA-1 negatively regulates expression of the hypertrophy-associated calmodulin and Mef2a genes. *Mol Cell Biol* 29:2193–2204.
38. Knezevic I, et al. (2012) A novel cardiomyocyte-enriched microRNA, miR-378, targets insulin-like growth factor 1 receptor: Implications in postnatal cardiac remodeling and cell survival. *J Biol Chem* 287:12913–12926.
39. Goss RJ (1966) Hypertrophy versus hyperplasia. *Science* 153:1615–1620.
40. Nadal-Ginard B, Kajstura J, Leri A, Anversa P (2003) Myocyte death, growth, and regeneration in cardiac hypertrophy and failure. *Circ Res* 92:139–150.
41. Rumyantsev PP (1977) Interrelations of the proliferation and differentiation processes during cardiact myogenesis and regeneration. *Int Rev Cytol* 51:186–273.
42. Tuomainen T, Tavi P (March 24, 2017) The role of cardiac energy metabolism in cardiac hypertrophy and failure. *Exp Cell Res*, 10.1016/j.yexcr.2017.03.052.
43. Stølen TO, et al. (2009) Interval training normalizes cardiomyocyte function, diastolic Ca2+ control, and SR Ca2+ release synchronicity in a mouse model of diabetic cardiomyopathy. *Circ Res* 105:527–536.
44. Lu X, et al. (2013) Measuring local gradients of intramitochondrial [Ca(2+)] in cardiac myocytes during sarcoplasmic reticulum Ca(2+) release. *Circ Res* 112:424–431.
45. Robert V, et al. (2001) Beat-to-beat oscillations of mitochondrial [Ca2+] in cardiac cells. *EMBO J* 20:4998–5007.
46. Drago I, De Stefani D, Rizzuto R, Pozzan T (2012) Mitochondrial Ca2+ uptake contributes to buffering cytoplasmic Ca2+ peaks in cardiomyocytes. *Proc Natl Acad Sci USA* 109:12986–12991.
47. Zaglia T, et al. (2013) Cardiac sympathetic neurons provide trophic signal to the heart via β2-adrenoceptor-dependent regulation of proteolysis. *Cardiovasc Res* 97:240–250.
48. Elia L, et al. (2009) Reciprocal regulation of microRNA-1 and insulin-like growth factor-1 signal transduction cascade in cardiac and skeletal muscle in physiological and pathological conditions. *Circulation* 120:2377–2385.
49. Wahlquist C, et al. (2014) Inhibition of miR-25 improves cardiac contractility in the failing heart. *Nature* 508:531–535.
50. Dirkx E, et al. (2013) Nfat and miR-25 cooperate to reactivate the transcription factor Hand2 in heart failure. *Nat Cell Biol* 15:1282–1293.
51. Liu N, et al. (2007) An intragenic MEF2-dependent enhancer directs muscle-specific expression of microRNAs 1 and 133. *Proc Natl Acad Sci USA* 104:20844–20849.
52. Liu N, Olson EN (2010) MicroRNA regulatory networks in cardiovascular development. *Dev Cell* 18:510–525.
53. Griffiths EJ, Balaska D, Cheng WHY (2010) The ups and downs of mitochondrial calcium signalling in the heart. *Biochim Biophys Acta* 1797:856–864.
54. Rizzuto R, et al. (1998) Close contacts with the endoplasmic reticulum as determinants of mitochondrial Ca2+ responses. *Science* 280:1763–1766.
55. De La Fuente S, et al. (2016) Strategic positioning and biased activity of the mitochondrial calcium uniporter in cardiac muscle. *J Biol Chem* 291:23343–23362.
56. Kumarswamy R, et al. (2012) SERCA2a gene therapy restores microRNA-1 expression in heart failure via an Akt/FoxO3A-dependent pathway. *Eur Heart J* 33:1067–1075.
57. Luongo TS, et al. (2017) The mitochondrial Na+/Ca2+ exchanger is essential for Ca2+ homeostasis and viability. *Nature* 545:93–97.
58. National Research Council (2011) *Guide for the Care and Use of Laboratory Animals* (National Academies Press, Washington, DC), 8th Ed.
59. Zaglia T, et al. (2014) Atrogin-1 deficiency promotes cardiomyopathy and premature death via impaired autophagy. *J Clin Invest* 124:2410–2424.
60. Rusconi F, et al. (2016) Peptidomimetic targeting of Cavβ2 overcomes dysregulation of the L-type calcium channel density and recovers cardiac function. *Circulation* 134: 534–546.
61. Castaldi A, et al. (2014) MicroRNA-133 modulates the β1-adrenergic receptor transduction cascade. *Circ Res* 115:273–283.

Supporting Information

Zaglia et al. 10.1073/pnas.1708772114

SI Methods

HL-1 Cells. Cells were kindly provided by W. Claycomb, Louisiana State University Medical Center, New Orleans. Cells were cultured as previously described (60). Briefly, 5×10^5 HL-1 cells were transfected with pcDNA6.2-GW/EmGFP-miR-1 or pcDNA6.2-GW/EmGFP-miR-199. Forty-eight hours posttransfection, cells were collected and analyzed.

Luciferase Assay. The murine MCU 3′ UTR was cloned into the psiCHECK-TM2 vector (Promega) using the In-fusion HD Cloning Plus kit (Clontech). The miR-1 mature sequence was cloned in the pcDNA6.2-GW/EmGFP-miR vector according to the manufacturer's procedure (Invitrogen). Then, 1.5×10^5 HEK293T or HL1 cells were cotransfected with psiCHECK-3′UTR-MCU and pcDNA6.2-GW/EmGFP-miR-1. Forty-eight hours after transfection, the luciferase activity was detected using a luminometer (Synergy 4; BioTek). To further confirm the specific targeting of the 3′ UTR of MCU, site-directed mutagenesis was performed at predicted sites using the QuikChange Site-Directed Mutagenesis Kit (Stratagene) following the manufacturer's instructions.

Primary Cultures of Neonatal Rat Cardiomyocytes. Hearts from P1 to P3 Sprague–Dawley rats were minced in ADS (5 mM glucose, 106 mM NaCl, 5.3 mM KCl, 20 mM Hepes, 0.8 mM Na_2HPO_4, and 0.4 mM $MgSO_4$, pH 7.4) and enzymatically dissociated with collagenase A (0.4 mg/mL) (Roche) and pancreatine (1.2 mg/mL) (SIGMA-Aldrich). Cells were plated on laminin-coated coverslips (1.8 μg/100 mm^2; BD) at a density of 470 cells per square millimeter and maintained in standard culture medium, as previously described in ref. 61.

Ca^{2+} Imaging on Cultured Cardiomyocytes. Neonatal cardiomyocytes were transfected, before seeding, with the appropriate Ca^{2+} sensor using Lipofectamine 2000 (Life Technologies), as recommended by the manufacturer. Ca^{2+} imaging experiments were performed 48 h after transfection. Cells were transferred to the imaging chamber and maintained in Hepes-buffered saline solution (125 mmol/L NaCl, 5 mmol/L KCl, 1 mmol/L Na_3PO_4, 1 mmol/L $MgSO_4$, 5.5 mmol/L glucose, 1.8 mmol/L $CaCl_2$, 20 mmol/L Hepes, pH 7.4) at room temperature. Cells were paced with 5-ms pulses at 0.5 Hz, delivered by a programmable field stimulator (Warner Instruments). FRET experiments were performed with an inverted Olympus IX50 microscope coupled to a CCD camera (Sensicam QE; PCO) and a custom-built beam splitter optical device (F. Mammano; Venetian Institute of Molecular Medicine). Fluorescence resonance energy transfer (FRET) changes were measured as changes in the 480 nm/535 nm fluorescence emission intensities upon excitation at 430 nm, which were analyzed with ImageJ (W. Rasband, National Institutes of Health, Bethesda). For cytosolic Ca^{2+} measurement, cells were incubated in a 10-μM solution of Fluo-4 AM (Invitrogen) for 20 min at room temperature and washed in dye-free modified Tyrode solution for 15 min, before imaging, with excitation at 488 nm and emission at 525 nm.

Chronic Exercise Training. Adult (3 mo) C57BL/6J mice (all from Charles River) were trained on a treadmill chamber (Harvard Apparatus) for 60 min/d, 5 d/wk, for eight consecutive weeks. In detail, after acclimation to the treadmill, mice started to warm up at 10 cm/s, increasing the running speed with 2 cm/s every 2 min until 18 cm/s was reached. Afterward, high-intensity aerobic interval training was performed, alternating between 4 min of maximal speed and 2 min of slow speed for a total of 10 repetitions. To determine maximal oxygen uptake (VO_{2max}), mice ran a ramp protocol until exhaustion on a customized treadmill in a metabolic chamber. Previous reports demonstrated the efficacy and relevance of this exercise regime by both clinical trials and experimental studies (modified from ref. 43).

Transversal Aortic Coarctation in Adult Mice. Adult C57BL/6J male mice (Charles River) were subjected to TAC following the procedure described in ref. 61. A control group of sham-operated mice was also set up. Animals were killed 1 wk after surgery, the hearts were removed, and chambers were dissected and used for molecular, biochemical, and histological analyses.

Mouse Echocardiography. Heart performance was evaluated before mice were killed as previously described in ref. 59.

Heart Processing and Immunofluorescence Analysis. Mouse hearts were harvested and processed, as previously described. Ten-micrometer heart cryosections were used for standard histological and immunofluorescence analyses, using the protocols previously described in ref. 59. The primary antibodies used in immunofluorescence (IF) analysis are listened in Table S1. Alexafluor-488 and Cy3-conjugated secondary antibodies, all from The Jackson Laboratory, were used to detect primary antibodies.

Morphometric Evaluation of Cardiomyocyte Cross-Sectional Areas. Images of 12 randomly chosen fields (320 × 320 μm) from the left ventricular wall were acquired at the confocal microscope (LSM5; Leica) in cryosections from exercised, TAC, and relative control hearts, processed with anti-dystrophin IF. The cross-sectional areas of cardiomyocytes were calculated using ImageJ.

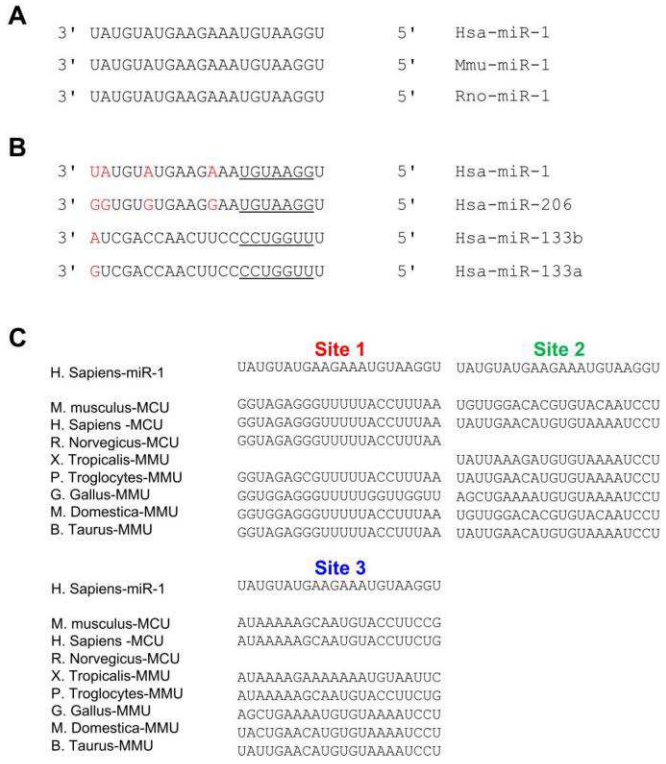

D

MCUC members	miR-1
MCU	Predicted
MCUb	NO
EMRE	NO
MICU1	Predicted (weakly)
MICU2	NO

Fig. S1. MyomiRs and target prediction for the MCU complex. (*A*) miR-1 sequence similarities among different species (Hsa, human; Mmu, mouse; Rno, rat). (*B*) miR-1/133/206 sequence similarities. (*C*) MCU seed-sequence similarities among different species. (*D*) Bioinformatics analysis was performed to determine whether miR-1 targets other members of the MCUC.

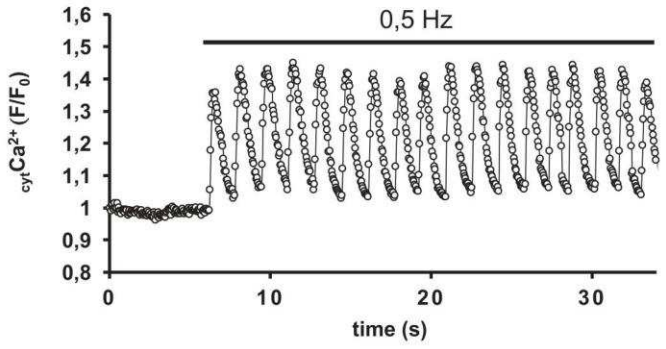

Fig. S2. Cytosolic Ca^{2+} transients in cultured neonatal cardiomyocytes. Representative trace of cytosolic Ca^{2+} transients in control cardiomyocytes, loaded with the fluorescent Ca^{2+} dye Fluo-4 (2.5 μM) and electrically paced with field stimulation at 0.5 Hz.

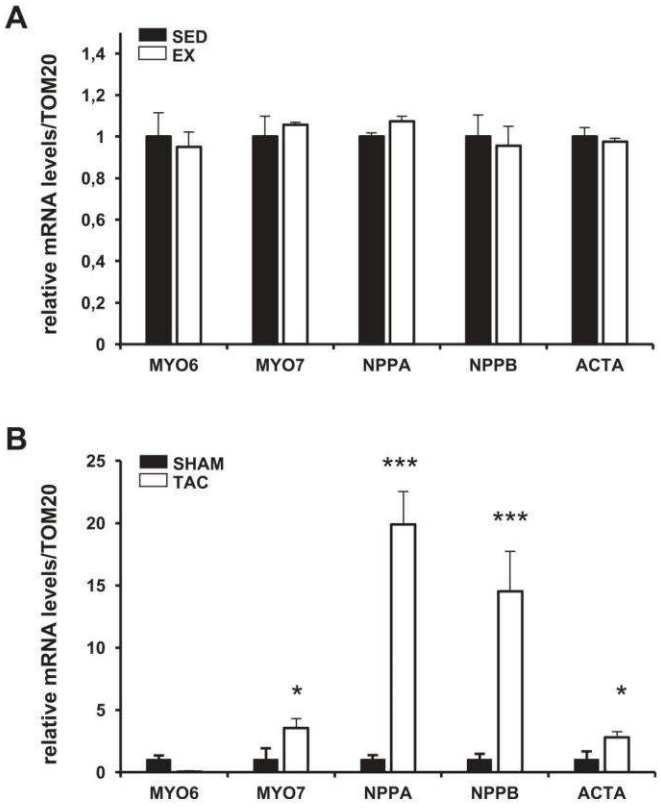

Fig. S3. Stress markers in exercised and TAC mouse hearts. (*A*) RTqPCR analysis on extracts from sedentary (SED) and exercised (EX) mouse hearts to assess the transcriptional levels of fetal genes ($n = 6$ hearts for each group). (*B*) RTqPCR analysis on extracts from 1-wk sham-operated and TAC mouse hearts to assess the transcriptional levels of fetal genes ($n = 6$ hearts for each group; $^{***}P < 0.001$; $^{*}P < 0.05$).

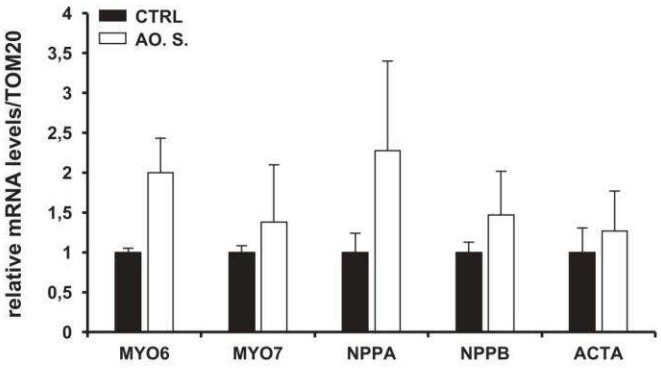

Fig. S4. Stress markers in hypertrophic human hearts. RTqPCR analysis on cardiac extracts from patients affected by aortic stenosis to assess the transcriptional levels of fetal genes ($n = 6$ hearts for each group).

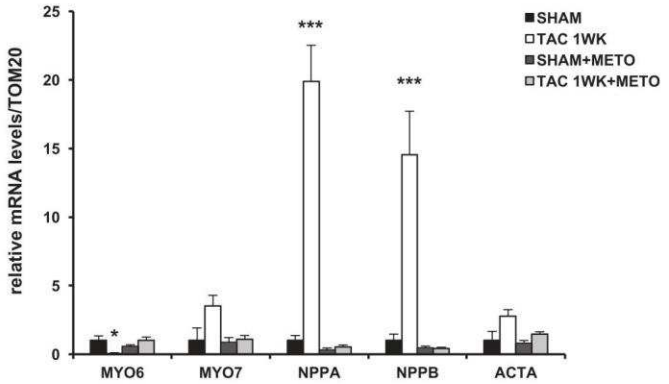

Fig. S5. Stress markers in TAC mouse hearts during treatment with the β-blocker metoprolol. RTqPCR analysis on extracts from 1-wk sham-operated and TAC mouse hearts, either treated with the β1-receptor blocker metoprolol or with a vehicle control, to determine the expression level of fetal genes ($n = 6$ hearts for each group; $^{***}P < 0.001$; $^{*}P < 0.05$).

Table S1. Antibodies and respective applications and experimental conditions used in the study

Antigen	Company	Dilution	Host species	Application
Actin	SIGMA A 5060	1:2,500	Rabbit	WB
Dystrophin	Abcam ab15277	1:200	Rabbit	IF
MCU	SIGMA HPA016480	1:1,000	Rabbit	WB
MICU-1	SIGMA HPA037480	1:1,000	Rabbit	WB
Tom20	Santa Cruz sc-11415	1:10,000	Rabbit	WB

Table S2. Primers used for RT-qPCR analysis in both mouse and human extracts

Gene name/species	Forward sequence	Reverse sequence
MCU (Hsa)	5′-CACACAGTTTGGCATTTTGG-3′	5′-CGTGACTTTTTGGCTCCTTT-3′
MCU (Mmu)	5′-AAAGGAGCCAAAAAGTCACG-3′	5′-AACGGATCTGTAGCCTCAGCAAGG-3′
MCUb (Hsa)	5′-GGCCTTCCCTTGGTAACACT-3′	5′-GTTGCCATCTGCTGTGAAGA-3′
MCUb (Mmu)	5′-AGTTACCTTCTTTCCTGTCGTTTGCG-3′	5′-CAGGGATTCTGTAGCCTCAGCAAGG-3′
MICU1 (Hsa)	5′-ATCAGTGAGCCTGGTGAAGC-3′	5′-ATGAGCCCACATTCTCCAAG-3′
MICU1 (Mmu)	5′-GTCGAACTCTCGGACCATGT-3′	5′-GTGCCTAAGGTGCAGGAGGTG-3′
MICU2 (Hsa)	5′-GGCAGTTTTACAGTCTCCGC-3′	5′-AAGAGGAAGTCTCGTGGTGTC-3′
MICU2 (Mmu)	5′-TGGAGCACGACGACGGAGAGTA-3′	5′-GCCAGCTTCTTGACCAGTGT-3′
MCUR1 (Hsa)	5′-GGACTTTGGTCACTTCATCCATTA-3′	5′-GGACTTTGGTCACTTCATCCATTA-3′
MCUR1 (Mmu)	5′-AGTTTTCAGCCCTCAGAGCAG-3′	5′-GGACTTTGGTCACTTCATCCATCA-3′
EMRE (Hsa/Mmu)	5′-TGTCGGGACACTCATTAGCA-3′	5′-GCTGATAGGGAAGGCAGAGA-3′
TOM20 (Hsa)	5′-TATGCGGGGCCCTTTTCATT-3′	5′-TCAGGTAACTTGGAAAGCCCA-3′
TOM20 (Mmu)	5′-CGATCGGTCGGAGCTAACC-3′	5′-TCAGGTAACTTGGAAAGCCCA-3′
MYH6 (Mmu)	5′-CGCATCAAGGAGCTCACC-3′	5′-CCTGCAGCCGCATTAAGT-3′
MYH6 (Hsa)	5′-CTCAAGCTCATGGCCACTCT-3′	5′-GCCTCCTTTGCTTTTACCACT-3′
MYH7 (Mmu)	5′-GCATCAAGGAGCTCACC-3′	5′-CTGCAGCCGCAGTAGGTT-3′
MYH7 (Hsa)	5′-ACACCCTGACTAAGGCCAAA-3′	5′-GTCCATGCGCACCTTCTT-3′
NPPA (Mmu)	5′-GTCAGTCGTTTGGGCTGTAAC-3′	5′-AGACCCAGGCAGAGTCAGAA-3′
NPPA (Hsa)	5′-CAGGATGGACAGGATTGGAG-3′	5′-TCCTCCCTGGCTGTTATCTTC-3′
NPPB (Mmu)	5′-CACAGATCTGATGGATTTCAAGA-3′	5′-CTCATCTTCTACCGGCATC-3′
NPPB (Hsa)	5′-GATGGTGCAAGGGTCTGG-3′	5′-TAATGCCGCCTCAGCACT-3′
ACTA1 (Mmu)	5′-CGGGAGAAGATGACTCAAA-3′	5′-GTAGTACGGCCGGAAGCATA-3′
ACTA1 (Hsa)	5′-GGACTTCGAGAACGAGATGG-3′	5′-CTGGCAGCTCGTAGCTCTTT-3′

9. ACKNOWLEDGMENTS

I would like to thank my supervisors, Prof. Marco Mongillo and Dr. Tania Zaglia, who supported my work with their knowledge, passion and enthusiasm: curiosity and love for science cannot be taught, but showed through personal example day-by-day. Their scientific support in planning experiments and discussing results is inestimable, and what I learned from them is what I consider the true achievement of my PhD.

In last three years, I have had the pleasure and honour to work and grow with special people, who formed a close-knit group. All my colleagues have been a crucial part of my PhD, both for their scientific and humane contribution. In particular, I would like to thank Giulia Borile, who collaborated with me in all "MCU projects"; Valentina Prando, who was extremely helpful with *in vivo* experiments; Nicola Pianca, a true master of RTqPCR; Mauro Franzoso, whose scientific mentality is, for me, truly inspiring. I would like to express my biggest gratitude to Anna Di Bona, for great scientific (and not-scientific) discussions, Silvia Bertoli for her helpful dedication in collaborating with me in lab's life, Veronica Vita, Arianna Scalco, Lolita Dokshokova for the support. I would like to thank also Lucia Cavallo and especially Ilaria Barison, who provided a great help in the development of a *New* protocol to induce maturation of neonatal cardiomyocytes *in vitro.*

During my PhD I had the opportunity to collaborate with a number of scientists, who I could learn from. Among them, I'm extremely grateful to Pierluigi Carullo for TAC experiments, Paola Pesce for ECHO analyses, Andrea Armani for RTqPCR, Martina Semenzato for TMRM and ROS live imaging.

I would like to thank also Daniele Catalucci, Paola Ceriotti, Diego De Stefani, Cristina Mammucari, Marco Sandri.

Finally, I would like to thank the PhD school and the professors, for the many opportunities offered for scientific and personal growth.